DOKTORSAVHANDLINGAR
VID
CHALMERS TEKNISKA HÖGSKOLA
Nr 99

EXPERIMENTAL INVESTIGATIONS OF SOME TIME-DEPENDENT PHENOMENA IN THE SLOWING DOWN AND DIFFUSION OF NEUTRONS

BY

GUDMAR GROSSHÖG

GÖTEBORG 1970

EXPERIMENTAL INVESTIGATIONS OF SOME TIME-DEPENDENT PHENOMENA IN THE SLOWING DOWN AND DIFFUSION OF NEUTRONS

BY

GUDMAR GROSSHÖG

AKADEMISK AVHANDLING

SOM MED TILLSTÅND AV SEKTIONEN FÖR TEKNISK FYSIK
VID CHALMERS TEKNISKA HÖGSKOLA
FRAMLÄGGES TILL OFFENTLIG GRANSKNING
FÖR VINNANDE AV TEKNISK DOKTORSGRAD
MÅNDAGEN DEN 11 MAJ 1970 KL 10 Å HÖRSAL A,
INSTITUTIONSBYGGNADEN FÖR FYSIK
VID CHALMERS TEKNISKA HÖGSKOLA,
GIBRALTARGATAN 5 B, GÖTEBORG

GÖTEBORG
ELANDERS BOKTRYCKERI AKTIEBOLAG
1970

DOKTORSAVHANDLINGAR
VID
CHALMERS TEKNISKA HÖGSKOLA

EXPERIMENTAL INVESTIGATIONS OF SOME TIME-DEPENDENT PHENOMENA IN THE SLOWING DOWN AND DIFFUSION OF NEUTRONS

BY

GUDMAR GROSSHÖG

GÖTEBORG
ELANDERS BOKTRYCKERI AKTIEBOLAG
1970

To

Ulla Britt
Stefan
Ann Christine

List of papers

A. Measurement of the slowing-down time of Ra-Be neutrons in water, Arkiv Fysik *27*, 215 (1964).

B. A system for simultaneous measurement of the amplitude and time distribution for pulses from up to four detectors, CTH-RF-10 (1967).

C. Determination of neutron decay constants using simultaneous pulse height and time analysis, CTH-RF-16 (1968).

D. Deadtime corrections in a two-parameter system containing four detectors, Proc. of Ispra Nuclear Electronics symposium, Ispra 1969.

E_1. The pulsed neutron method applied to the interaction between two moderators, CTH-RF-17 (1969).

E_2. The pulsed neutron method applied to the interaction between moderators, J. Nucl. Energy (in press).

F. Measurement of the neutronic interaction between two cylindrical moderators, CTH-RF-18 (1969).

G. An experimental study of the thermal neutron field decay in a spherical moderator with a central cavity, CTH-RF-19 (1970).

1. Introduction

An understanding of the interaction between neutrons and moderators is of great importance in the development of nuclear reactors. The first experimental study of this process was undertaken by Fermi in 1934 shortly after the discovery of the neutron by Chadwick in 1932, but more extensive studies of the subject were not taken up until after the discovery of fission by Hahn and Strassmann in 1939 and the experimental proof of the possibility of a chain reaction in 1942.

The theoretical foundations go back to 1895. In that year Boltzmann completed his formulation of the particle diffusion problem. The linearized classical version of this formalism was first used for the description of neutron phenomena by Ornstein and Uhlbrich in 1937. Although the Boltzmann equation is well established, exact solutions can seldom be found in practical cases. This depends on the mathematical difficulties involved in handling simultaneously the seven variables of space, velocity and time, and in addition on the fact that it is not entirely clear how to represent mathematically the physical situation represented by the scattering kernel, the cross sections and the boundary conditions.

The interaction between neutrons and moderators has been treated experimentally by two different kinds of methods, namely differential measurements where the intention is to clarify the detailed interaction between the neutrons and the moderator, and integral measurements where the information is collected in a small number of fundamental parameters. A review of the developments in models and measurements can be found in e.g. Williams [1], where references to the above-mentioned works are also given.

One of the most widely used experimental methods is the pulsed neutron source method. The time behaviour of a short burst of fast neutrons injected into a moderator can be divided into three parts, the slowing-down period, the thermalization period and the diffusion period. During the slowing-down period the energy of the neutrons is

so high that the moderator atoms can be regarded as free and at rest. In a hydrogeneous moderator this period is followed after a few microseconds by the thermalization period, during which the motion and binding of the moderator atoms come into the picture. After about 15–20 microseconds an energy equilibrium is attained. The neutrons diffuse and may also reach a spatial equilibrium, asymptotically characterized in space by the Helmholtz equation and in time by a pure exponential. Measurable quantities are the decay rates during the different periods and the time dependent neutron distribution.

The basic ideas of the pulsed source method were developed during the fifties. A review covering this time period is given by von Dardel and Sjöstrand [2]. The work of the sixties is elucidated in reports from three international conferences, which were partly devoted to the subject. They are "The Brookhaven conference on neutron thermalization" [3], "Pulsed neutron research" [4], and "Neutron thermalization and reactor spectra" [5].

The pulsed neutron source method is one of a group of methods connected with the generalized dispersion law of neutron diffusion:

$$Z(-k^2, i\omega)=0 \tag{1}$$

where k is a wave number-like and ω a frequency-like parameter [6]. The dispersion law depends on the diffusion parameters and can be written, in conventional notation, as

$$\lambda=\lambda_0+DB^2-CB^4+O(B^6) \tag{2}$$

(This is eq. 2.1 of paper G.) Here λ is the decay constant in a finite moderator with the buckling B^2.

Other types of experiment can be performed by setting up other initial and boundary conditions. A "poisoning" experiment is a stationary experiment where B^2 is substituted by $(-\varkappa^2)$ and λ by α [7]. Here $\varkappa$ is the inverse relaxation length and α the product of the velocity and the absorption cross section for the added absorber.

$$\alpha=-\lambda_0+D\varkappa^2+C\varkappa^4+O(\varkappa^6) \tag{3}$$

If the decay is controlled the part of the dispersion relation corresponding to $\lambda>0$, $B^2<0$ can be measured [8] (See fig. 1). Finally, if the frequency parameter is allowed to be complex, we have the experiments involving the propagation of neutron diffusion waves [9].

Inspired by some theoretical work by Case [10], Corngold [11] has

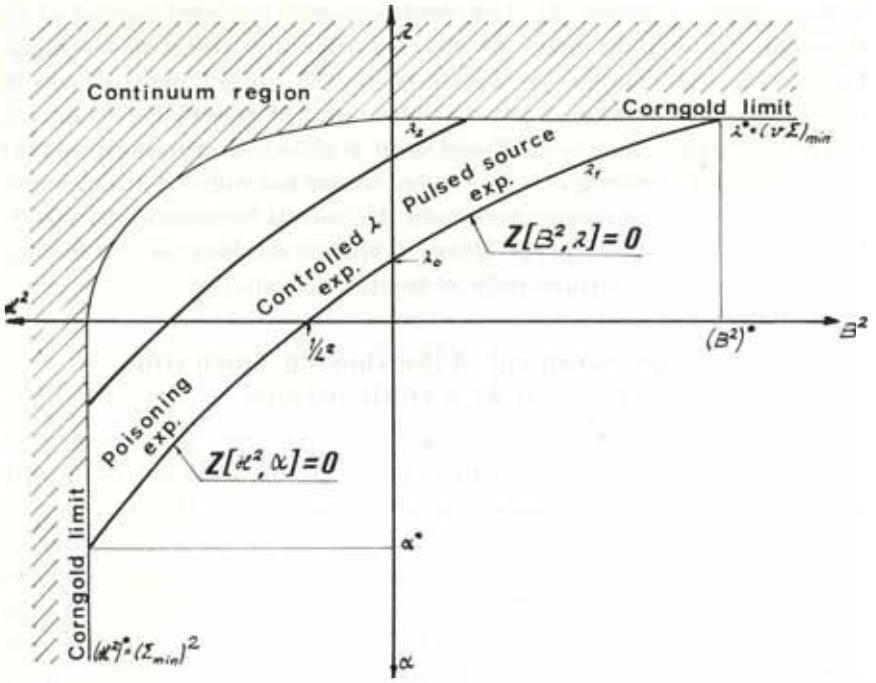

Fig. 1. The generalized dispersion law of neutron diffusion.
The stars denote the limiting values.

shown that the point spectrum of the decay constants disappears at sufficiently large values of the buckling leaving only a continuum. The maximum value of the decay constant is given by the minimum of the product of the velocity and the scattering cross section and is often called the Corngold limit. The limit is high in hydrogeneous media, but owing to the Bragg cut-off is low in crystalline media. Experimental evidence for the limit in Be was given by Fullwood *et al.* [12]. It is interesting to note that they had to follow the decay for five decades and make a comparison measurement on polyethylene with the same decay constant before they were able to establish the effect. In later work [13] the effect was shown to be caused by "trapping" of neutrons in the low energy region. A measurement of the time dependent energy distribution gave varying neutron energy spectra for bucklings higher than the Corngold limit.

The material presented in this thesis can be divided into three parts. The first part describes a measurement of the slowing-down time by

a static method (paper A). The second treats the development of an electronic system, the methods of calculation and the data handling, for precision measurements obtained by the pulsed neutron source method (papers B, C and D and some parts of papers E, F and G). In the third part (papers E, F and G) it is shown that decay constant variations and trapping effects can be caused not only by the velocity dependence of the cross sections as in the case of Be mentioned above, but also by their space dependence. A special method for eliminating this delay effect experimentally is treated in paper F.

2. A measurement of the slowing-down time in water by a static method

The purpose of the work described in paper A was to obtain an independent check of a measurement of the slowing-down time in water performed with a pulsed neutron source by Möller and Sjöstrand [14]. For H_2O there are three modes of internal vibration having energies 0.205, 0.474 and 0.488 eV. The thermal effect can therefore be expected to influence the slowing-down time at neutron energies lower than about 0.5 eV. Möller and Sjöstrand showed that a thermal effect exists at 0.2 eV, and in some earlier work [15] we confirmed the result of DeJuren [16] that the thermal effect is negligible at 0.5 eV. In the work described in paper A the precision was increased at 0.5 eV and a new measurement was performed at 0.3 eV. The result is in agreement with the conclusions of Möller and Sjöstrand and has been confirmed since by the calculation of Ghatak and Krieger [17].

3. Measuring system, numerical methods and corrections for the pulsed neutron source method

One of the important parameters in the pulsed neutron source method is the fundamental decay constant. It can be determined from the measured decay curve. Two problems arise however. At the beginning of the decay the fundamental is mixed with higher modes. At the end its behaviour is obscured by background. The higher modes may be resolved by the use of a Fourier technique [18] or partly resolved by a suitable choice of detector position. The background is directly connected with the gamma sensitivity of the detectors. In many situations the BF_3 detector has proved to be the best choice in diffusion experiments. It has an acceptable time resolu-

tion and a very low gamma sensitivity. In order to avoid time-of-flight effects, however, the detector volume must be small compared with the dimensions of the moderator. This gives a low neutron sensitivity. The provisional siting of our laboratory (an appartment house) imposes very severe restrictions on the permitted radiation level in the surroundings. We can not therefore use the full capacity of the small accelerator and this must be compensated by the highest possible neutron sensitivity in the detectors. The Li-glass scintillators chosen have not only high sensitivity but also small time-of-flight effects and a good time resolution.

The background can be suppressed by amplitude or pulse shape discrimination. We have tried both these methods but without success. Another method has therefore been adopted. The pulse amplitude distribution around the neutron peak is measured for all time intervals. The background is then subtracted by a numerical method which makes use of the difference in shape between the amplitude distribution of the background pulses and the neutron pulses. We have found that 32 intervals are needed in order to get sufficient material for subtraction of the background. If four detectors are used, a 1024 channel analyzer has only room for eight time intervals.

The problem of using a given number of intervals most effectively has been studied by Janossy [19]. However, his suggested subdivision of the measuring time is too complicated to be included in the logics of the equipment. Another sequence of time interval widths was therefore chosen, using a logarithmic time scale. It is described in paper B, and different numerical methods based on this time scale are analysed in paper C.

The basic principles of the system are described in paper B. The equipment has since been continuously improved. Since the description of these improvements in the papers following paper B is mixed with the application for each separate experiment, a summary of the most important developments will be given here.

One problem connected with the linear circuits of a system designed for the pulsed source method is that the system must be able to handle low as well as high intensities. During the neutron burst the linear amplifiers are near to overloading and therefore the recovery time must be short. In the work described in paper B a baseline restorer was incorporated in order to decrease the amplitude shift.

In connection with the work described in paper E the part of the system which handles the output from the linear amplifiers was re-

designed. The advantage of the new unit is that the interaction between the different detectors is minimized. Fast logics working on the leading edge of the amplified detector pulses activate a gate system in such a way that only the actual signal is transferred to the analog to digital converter. The new unit also opens up the possibility of exchanging the time to digital converter as only one of the four detector lines is now used. For the best working conditions four baseline restorers are needed. For economical reasons these were not included before the work described in paper F. In paper G an example is given of the flexibility of the system.

The principle behind the main part of the dead-time correction is given in paper B. A numerical check on the method is described in papers C and D. In paper C a method based on the coincidences between the detectors is described for correcting for the extrinsic dead-time, but a better method is introduced in paper D. The latter has the advantage of giving an amplitude dependent correction and it therefore also increases the accuracy of the background correction.

The data handling was performed on an IBM computer. The direct access method was used with the programs and the intermediate results stored in a disc memory. The method is practical as the data handling can easily be altered in order to match new experimental situations, but it is rather uneconomical as large amounts of data have to be transferred between the disc memory and the computer.

4. Previous and contemporary work concerning cavities in moderators

The possibility of using the pulsed neutron method to determine the buckling was proposed by Sjöstrand *et al.* [20]. Sawyer [21] used the method to study a cylindrical assembly with one concentric void in a water system. He obtained satisfactory agreement with a stationary theory for small void dimensions but noted deviations for large values. An extensive study using the same geometry has been performed by Ocasio-Cabanas [22]. The result was compared with several static models, but the agreement was bad, especially at large values of the void diameter.

Čopič *et al.* [23] have studied the effect of channels in a plexiglass system. They obtained a result that deviated widely from the theoretical predictions obtained using both the classic method of Behrens [24] and a static Monte Carlo calculation. During a study of the condi-

tions in a bore hole for oil prospecting Mills *et al.* [25] found that porosities increase the content of higher harmonics.

The first attempt to include a correction for the delay effects in the cavities was made by Page [26]. Considering the decay in the cavity as a source term he obtained good agreement with a static theory by Leslie [27].

The experiments mentioned so far were performed with hydrogeneous moderators. Graphite moderators have been studied by Deniz *et al.* [28]. They included corrections for the delay time in the cavities and indicated clearly the differences between stationary and dynamic systems. In spite of this they found systematic differences between the calculated and measured values of the radial diffusion constant which are still not explained.

Joshi *et al.* [29] made measurements on BeO but did not correct for dynamic effects. This was also the case in the work on graphite reported by Zezherun [30]. The deviations from the theory were not so large as in the hydrogeneous case. This depends on the lower values of the decay constant.

Bull [31] and Dance [32] have included the time delay effect in their analyses. They have also found experimentally variations in the asymptotic decay constant which they attributed to trapping effects. The experiments of Dance also show that the time-of-flight effect can be so strong that no fundamental pseudomode can be found.

It is interesting to compare these results with those from static sigma pile measurements. Palmedo *et al.* [33] show that the decay is not exponential in the direction parallel to plates of Al in H_2O. This behaviour has been confirmed theoretically by Williams [34].

5. Studies of the influence of cavities on the decay of the neutron field

We have approached the subject of cavities from quite a different point of view, namely the interaction between subcritical assemblies. A measurement of the interaction by Kiyose *et al.* [35] using the pulsed neutron source method gave a result very different from equivalent measurements with subcritical assemblies [36]. In paper E we show that the difference is caused by the time of flight of the neutrons in the space between the moderators and that this is a dynamic effect which depends not only on the geometry of the cavity but also on the decay rate of the system. It is further shown that the gap between

the two moderators introduces large variations in the decay constant. From a theoretical point of view there are good reasons for believing that a pure fundamental asymptotic decay constant does not exist.

The effect introduced by the inhomogeneity can be looked upon as a trapping effect. Neutrons moving in directions nearly parallel to the gap or with velocities near zero have flight times that are long in comparison with the decay of the system. Experimentally this delay effect is important in connection with the time-of-flight method for measuring the velocity distribution of neutrons.

One can also use the arguments of Corngold [11] in order to explain the effect. In the cavity the Corngold limit is zero. The cavity therefore extends the continuum in the spectrum of decay constants down to zero and a pure asymptotic exponential does not exist. The Corngold limit in hydrogeneous media is about 300,000 s^{-1}. It is therefore very difficult to establish the limit experimentally in a homogeneous moderator. However, the cavity introduces a continuum that covers all positive real decay constants and so offers the possibility of studying the influence of a continuum in hydrogeneous media.

Another way of approaching the problem is to introduce the concept of "importance". The importance of the neutrons in the gap increases as the field in the moderator decays. On the other hand an absorber placed in the cavity reduces the number of neutrons. The time-of-flight effect can therefore be eliminated by introducing a $1/v$ absorber. This idea was used in the work described in paper F in order to solve the original problem, the measurement of the static interaction between two moderators.

The delay effect can be divided into a space effect and a velocity effect. In the case of plane symmetry the space effect predominates and in a practical finite system the loss of neutrons through the cavity complicates the picture. A more well-defined experiment can be performed by using spherical symmetry. Paper F treats this case and it is shown that a strong velocity effect does exist. In addition it is shown that the same kind of time dependence as in the plane experiment occurs in this case also.

Some irregularities detected both with plane and with spherical symmetry are interesting. They cannot be explained by the quasi-stationary methods used but might be connected with the theories of diffusing neutron waves. Such effects have in fact been demonstrated [37, 38]. However, a more careful study of these topics is needed to confirm and explain the effects.

Acknowledgements

The measuring system and the methods used in this thesis were developed at the Department of Reactor Physics, Chalmers University of Technology during the last seven years. During this time several of my colleagues made considerable contributions to the work described. In this respect I should like to thank

Jan Collén	Jan Elkert
Salih Dinçer	Henry Samuelsson
Gunnar Rönnberg	Rune Persson
Rolf Bodh	Göran Svenbrandt
Lizzie Collén	Bert Thalenius
Christina Varenius	Kent Mandorff
Signe Berglund	Lennart Carlsson
	Göran Hansson

In addition I should like to thank Professor Nils Göran Sjöstrand for help, advice and criticism which was often hard, but was always constructive and stimulating.

The work was supported by the Swedish Atomic Research Council.

References

1. M. M. R. Williams, The slowing down and thermalization of neutrons, North-Holland, Amsterdam 1966.
2. G. von Dardel and N. G. Sjöstrand, Progress in Nuclear Energy, Series 1, Vol. 2, pp. 183–221, Pergamon Press, London 1959.
3. Proc. of the Brookhaven conference on neutron thermalization, BNL 719 (C-32), (1962).
4. Proc. of IAEA symp. on pulsed neutron research, Karlsruhe 1965.
5. Proc. of IAEA symp. on neutron thermalization and reactor spectra, Ann Arbor 1967.
6. M. N. Moore, Nucl. Sci. Eng. *21*, 565 (1965).
7. F. Starr and J. Koppel, ref. 3, p. 1012.
8. E. Arai and M. Küchle, Nukleonik *7*, 416 (1965).
9. R. B. Perez and R. S. Booth, ref. 4, Vol. 2, p. 701.
10. K. M. Case, Ann. Phys., *9*, 1 (1960).
11. N. Corngold, Nucl. Sci. Eng. *19*, 80 (1964).
12. R. R. Fullwood, R. E. Slovacek and E. R. Gaerttner, Nucl. Sci. Eng. *18*, 137 (1964).
13. E. R. Gaerttner, P. B. Daitch, R. R. Fullwood, R. R. Lee and R. E. Slovacek, ref. 4, Vol. I, p. 483.
14. E. Möller and N. G. Sjöstrand, Arkiv Fysik *27*, 501 (1964).
15. G. Grosshög, CTH-RF-4, (1963).
16. J. A. DeJuren, Nucl. Sci. Eng. *9*, 408 (1961).
17. A. K. Ghatak and T. J. Krieger, Nucl. Sci. Eng. *21*, 304 (1965).
18. V. M. Lopez and J. R. Beyster, Nucl. Sci. Eng. *12*, 190 (1960).
19. L. Jánossy, Theory and practice of the evaluation of measurements, Clarendon Press, Oxford 1965.
20. N. G. Sjöstrand, J. Mednis and T. Nilsson, Arkiv Fysik *15*, 471 (1959).
21. J. A. Sawyer, Thesis, N. C. State College, Raleigh 1961.
22. W. Ocasio-Cabanas, Thesis, N. C. State College, Raleigh 1968.
23. M. Čopič, T. Kalin, G. Pregl and F. Žerdin, Nucl. Sci. Eng. *19*, 74 (1964).
24. D. J. Behrens, Proc. Phys. Soc. (London) *52*, 607 (1949).
25. W. R. Mills Jr, L. S. Allen, F. Seilig and R. L. Caldwell, Nucl. Appl. *1*, 4 (1965).
26. R. W. Page, J. Nucl. Energy *21*, 403 (1967).
27. D. C. Leslie, Reactor Sci. Techn. (J. Nucl. Energy Part A/B) *16*, 1 (1962).
28. V. Deniz, J. G. LeHo and M. Sagot, Nucl. Sci. Eng. *32*, 201 (1968).
29. B. V. Joshi, V. R. Nargundkar and K. Subbaro, Nukleonik *10*, 323 (1968).
30. I. F. Zhezherun, Sov. At. Energy *24*, 1 (1968).
31. S. Bull, Thesis, Stanford University 1968.

32. K. Dance, Thesis, Stanford University 1968.
33. P. Palmedo and J. F. Conant, Nucl. Sci. Eng. *36*, 326 (1969).
34. M. M. R. Williams, Nukleonik *12*, 3 (1969).
35. R. Kiyose, Y. Shimazaki and S. Enomoto, Proc. of IAEA symp. on criticality control of fissile materials, Stockholm 1965, pp. 337–345.
36. H. K. Clark, Proc. of IAEA symp. on criticality control of fissile materials, Stockholm 1965, pp. 87–102.
37. O. C. Baldonado and R. C. Erdmann, Nucl. Sci. Eng. *37*, 59 (1969).
38. M. A. Quddus, R. G. Cochran and D. E. Emon, Nucl. Sci. Eng. *35*, 342 (1969).

Contents

GÖTEBORG
ELANDERS BOKTRYCKERI AKTIEBOLAG
1970

A

ARKIV FÖR FYSIK

UTGIVET AV

KUNGL. SVENSKA VETENSKAPSAKADEMIEN

Band 27 nr 16

GUDMAR GROSSHÖG

Measurement of the slowing-down time of Ra–Be neutrons in water

---

ALMQVIST & WIKSELL

STOCKHOLM

GÖTEBORG · UPPSALA

1964

ARKIV FÖR FYSIK Band 27 nr 16

3.64024 Communicated 22 January 1964 by G. Borelius and I. Waller

Measurement of the slowing-down time of Ra–Be neutrons in water

By Gudmar Grosshög

SUMMARY

The time for slowing down of Ra–Be neutrons to the cadmium and gadolinium cut-off energies in water has been measured with a stationary method to 1.60 ± 0.07 and 2.47 ± 0.11 μs respectively. The method uses the fact that the cut-off ratio of the total neutron population in a moderating medium is equal to the ratio between the total mean life time and the mean life time of the neutrons above cut-off. For a medium having 1/v absorption the cut-off ratio is directly related to the slowing-down time. The measurements were performed with a small BF_3 proportional counter and with filters of cadmium and gadolinium having cut-off energies at 0.5 and 0.3 eV respectively. It is shown that the correction for the flux perturbation of a gas detector can be calculated with sufficient accuracy using the P_1-approximation.

Introduction

A neutron source with the intensity Q n/s is placed in an infinite moderating medium, where it causes a neutron density $n(r, v)$. The total number of neutrons N and the number N_a of neutrons with velocity larger than v_c in the medium are then

$$N_a = \int_{v_c}^{\infty} \int_{0}^{\infty} n(r, v) 4\pi \cdot r^2 \cdot dr \cdot dv, \tag{1}$$

$$N = \int_{0}^{\infty} \int_{0}^{\infty} n(r, v) 4\pi \cdot r^2 \cdot dr \cdot dv. \tag{2}$$

A neutron balance gives us directly the mean life time of the total neutron population

$$t = \frac{N}{Q}$$

and the mean life time of the neutron population above the velocity v_c

$$t_c = \frac{N_a}{Q}.$$

Thus we can write

$$\frac{\bar{t}}{\bar{t}_c} = \frac{N}{N_a} = R, \tag{3}$$

where R is the cut-off ratio of a 1/v detector, i.e. the ratio of the integrated counting rates observed without and with a filter having a cut-off at v_c. Let us define the slowing-down time ($\bar{t}_s$) as the average time a neutron spends from birth to reaching the cut-off energy. The difference between the slowing-down time and the mean life time is due to the absorption. If the absorption cross section is 1/v dependent and has the value Σ_{a0} at the velocity v_0, a neutron balance for the neutrons above cut-off will give us

$$\bar{t}_s = \frac{N_a}{Q - N_a \cdot \Sigma_{a0} \cdot v_0} \tag{4}$$

and thus

$$\frac{\bar{t}}{\bar{t}_s} = R - 1. \tag{5}$$

This has in another way been shown by DeJuren [1], who calculated the slowing-down time to cadmium cut-off using a value of R measured by Walker [2]. The aim of Walker was, however, only to obtain a correction for the epithermal flux in connection with a source calibration. For this purpose he got a sufficiently good value without making detailed studies of the disturbance caused by the detector etc.

In this work we have measured the cadmium ratio in order to determine the slowing-down time to 0.5 eV with higher accuracy. We have also measured the gadolinium ratio in order to get a value of the slowing-down time to 0.3 eV.

Experiment

The experimental arrangement is shown in Fig. 1. The source, 99.7 mC Ra(α, n)Be, is fixed through an aluminium tube in the centre of a cylindrical aluminium tank (height 100 cm, diameter 90 cm) filled with water. The BF_3 proportional counter uses boron enriched to about 95 %, has 0.4 mm copper walls and the active dimensions 50 × 13 mm. By an aluminium tube the detector is mechanically and electrically connected to the preamplifier, which is sliding on two horizontal steel tubes. The distance be-

Table 1.

Run	Distance in cm between source and detector: from	to	in steps	Filter
0	16.0	35.5	0.5	None
1	2.3	20.0	0.1	None
2	2.4	10.6	0.2	Gd
3	2.4	9.6	0.2	Cd
4		10.0		None, Gd, Cd

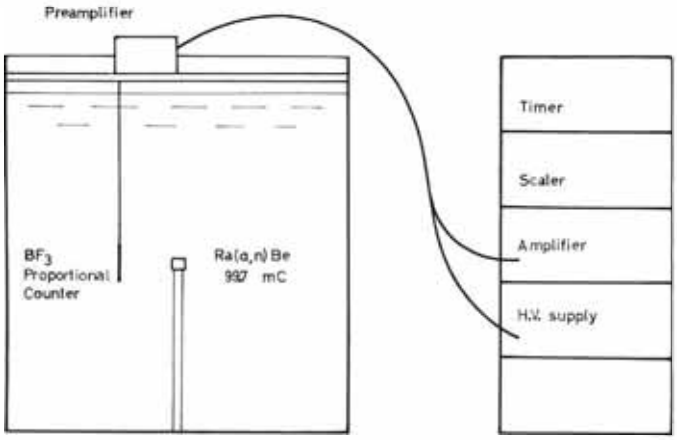

Fig. 1. Experimental arrangement.

tween detector and source is indicated on a steel scale. The cylindrical filters are made out of a 600 mg/cm² cadmium sheet and a 150 mg/cm² gadolinium sheet.

The measurement was separated into 5 runs according to Table 1. It will be shown later on that this separation is justified and that drift in the electronics between the runs will cancel. Every run took about one day. The purpose of run 0 is to determine the exponential part of the total neutron distribution. Runs 1 to 3 give the main part of the total, the epigadolinium and the epicadmium distribution. Run 4 gives a comparison between the different distributions.

Data handling

The total cut-off ratio can be written

$$R = R(a)\frac{I_t}{I_c}, \tag{6}$$

where $R(a)$ is the cut-off ratio at the radius a and

$$I_t = \frac{\int_0^\infty \int_0^\infty n(r, v) r^2 \cdot dv \cdot dr}{\int_0^\infty n(a, v)\, dv}, \tag{7}$$

$$I_c = \frac{\int_0^\infty \int_{v_c}^\infty n(r, v) r^2 \cdot dv \cdot dr}{\int_{v_c}^\infty n(a, v)\, dv}. \tag{8}$$

In order to evaluate the integrals analytically the measured distributions multiplied by the square of the radius are fitted by the following function:

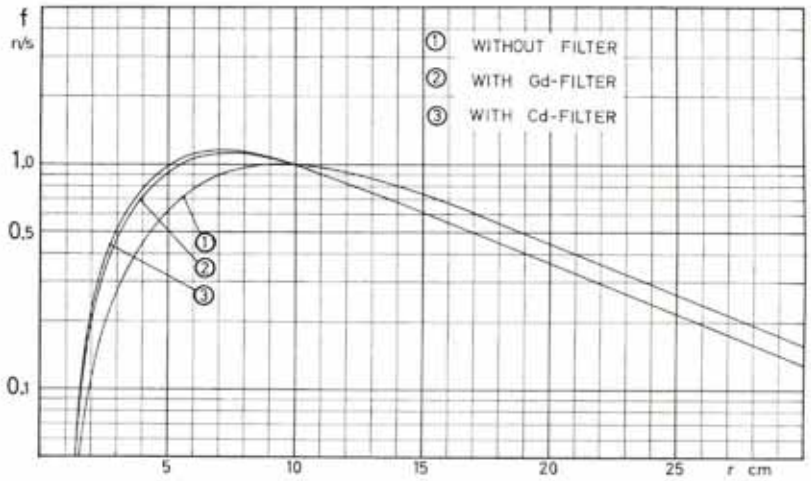

Fig. 2. The function f for the three runs. The curves have been normalized so that $f(10) = 1$.

$$f(r) = A(1 - e^{-\beta(r-c)^3})e^{-\alpha r}. \tag{9}$$

The constant α is calculated from the exponential part of the total distribution, and it is assumed that this value can be used also for the other distributions. This means that the spectrum at large distances from the source has reached an equilibrium. The constants A, β and c are obtained with the method of least squares from the data of the actual runs.

The goodness of fit is demonstrated in Figs. 3, 4 and 5 where Δf is the difference between the measured and the calculated values. It is seen that the function excellently represents the data from the measurements with filters. There is some deviation for the first values of the total distribution. The numerical difference is, however, small and the effect on the integration can be neglected. Another weakness of the function is that it gives zero for $r = c$. Also this can be neglected if the integration is taken from $r = c$ instead of $r = 0$.

Another check of the function $f(r)$ is to use it to determine the age τ. For the filter measurements

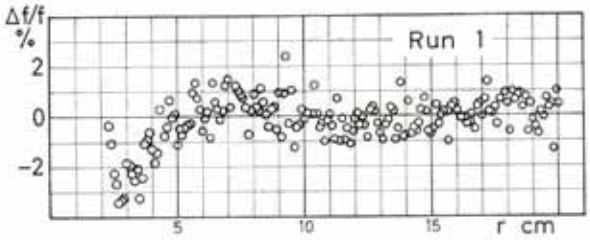

Fig. 3. The difference in per cent between the primary data and the function f for the measurement without filter.

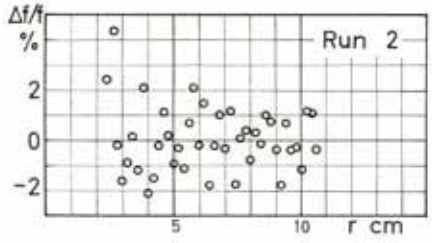

Fig. 4.

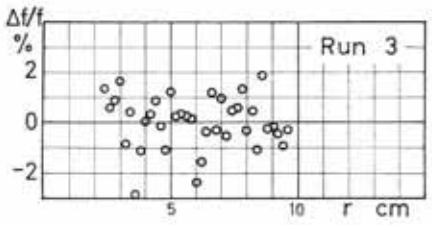

Fig. 5.

Fig. 4. The difference in per cent between the primary data and the function f for the measurement with gadolinium filter.

Fig. 5. The difference in per cent between the primary data and the function f for the measurement with cadmium filter.

$$\tau = \frac{\overline{r^2}}{6} = \frac{1}{6}\frac{\int_0^\infty f(r)\, r^2 \cdot dr}{\int_0^\infty f(r)\, dr} \tag{10}$$

and for the measurement without filter

$$\tau_{\text{thermal}} = \frac{\overline{r^2}}{6} - L^2, \tag{11}$$

where L is the thermal diffusion length. The result is

$$\tau_{\text{Cd}} = 47.4 \pm 0.7 \text{ cm}^2,$$
$$\tau_{\text{Gd}} = 48.3 \pm 0.7 \text{ cm}^2,$$
$$\tau_{\text{thermal}} = 50.7 \pm 0.6 \text{ cm}^2.$$

Table 2.

	Run 0	Run 1	Run 2	Run 3
		Filter		
Symbol	None	None	Gd	Cd
A	255 100	254 600	2444	1532
	1 800	200	10	7
α	−0.10 585			
	0.00 026			
c		0.52	0.41	0.42
		0.02	0.04	0.04
β		0.0167	0.0366	0.0406
		0.0001	0.0008	0.0010
I		17.12	17.05	17.23
		0.06	0.12	0.12
$\overline{r^2}$		350	290	285
		4	4	4
$k_s(10)$		1.0234	1.0245	1.0245
$f(10)$		68 670	819	519

L^2 is here assumed to be 7.67 cm². ANL 5800 [3] gives seven rather scattered values of the age to the indium resonance for Ra–Be neutrons. They give the mean value 49.8 cm² for the age to cadmium cut-off if we take the age between the indium resonance and the cadmium cut-off to be 0.6 cm². The agreement is rather good, but of limited value as a check of the function f because of the large deviations between the different measurements of the age to the indium resonance.

The data handling is programmed for the electronic computer FACIT EDB. The program corrects the primary data for deadtime and for the finite volume of the detector, determines the constants α, β, c and A with error limits, makes the integrations, determines $\bar{r}^2$ and the error limits of I and $\bar{r}^2$. The result of the calculation is summarized in Table 2. The figures below each value are the limits of errors.

Corrections

The primary data have been corrected according to the following list.

a. Space independent corrections:

Flux depression,
Leakage through filter.

b. Space dependent corrections:

Finite volume of the detector,
Unsymmetrical parts of the neutron distribution.

Detector perturbation, theory

The perturbation of detector foils has been investigated very much. A review of the later results can be found in reference [4]. The perturbation of BF_3 detectors is, however, sparsely treated which may be due to the fact that these detectors are not so well suited to determine neutron fluxes absolutely. The disturbance problem is, however, simpler for a gas detector than for a foil. This depends on the fact that the absorption of a foil is concentrated to a point or a thin layer, which is not the case for a gas detector. The gas detector problem can therefore be treated with elementary theories of neutron transport.

For the gas volume and the detector walls the energy independent Boltzmann equation can be written

$$\Omega \cdot \nabla\phi(r,\Omega) + \phi(r,\Omega)[\Sigma_s(r) + \Sigma_a(r)] = \phi_0(r,\Omega)[\Sigma_s(r) + \Sigma_a(r)] + \int d\Omega' \phi(r,\Omega')\Sigma_s(r,\Omega' \to \Omega) - \int d\Omega' \phi_0(r,\Omega')\Sigma_s(r,\Omega' \to \Omega). \quad (12)$$

For the medium surrounding the detector:

$$\Omega \cdot \nabla\phi(r,\Omega) + \phi(r,\Omega)[\Sigma_s(r) + \Sigma_a(r)] = \int d\Omega' \phi(r,\Omega')\Sigma_s(r,\Omega' \to \Omega). \quad (13)$$

Here $\phi_0(r,\Omega)$ is the unperturbed differential neutron flux of the angle Ω at the space point r, $\phi(r,\Omega)$ the difference between unperturbed and perturbed flux, Σ_a the absorption cross section and Σ_s the scattering cross section.

From these equations it is seen that the perturbation of the flux is equivalent to the neutron distribution that should be established around the detector if it produced neutrons with the source distribution

$$S(r, \Omega) = \phi_0(r, \Omega)[\Sigma_s(r) + \Sigma_a(r)] - \int d\Omega' \phi_0(r, \Omega')\Sigma_s(r, \Omega' \to \Omega). \tag{14}$$

The correction factor k_p can be defined

$$k_p = \frac{\overline{\phi_0(r)}}{\overline{\phi_0(r)} - \overline{\phi(r)}}, \tag{15}$$

where the mean values are taken over the gas volume. Using the P_1-approximation and assuming that $\phi_0(r,\Omega)$ is constant and isotropic over the gas volume, that $\phi(r,\Omega) \ll \phi_0(r,\Omega)$ and that the detector is cylindrical and has an infinite length we obtain

$$k_p = 1 + \frac{3}{2}[\Sigma_{a2}(R_2^2 - R_1^2) + \Sigma_{a1} R_1^2]\left[\Sigma_{tr\,2} \ln\left(\frac{R_1}{R_2}\right) + \frac{\Sigma_{tr\,3}}{\varkappa_3 R_2} \cdot \frac{K_0(\varkappa_3 R_2)}{K_1(\varkappa_3 R_2)} - \frac{1}{8}\varkappa_1^2 R_1^2\right], \tag{16}$$

where index 1, 2 and 3 indicate the gas volume, the detector wall and the surrounding medium respectively, R(cm) is the outer radius of the regions, $\Sigma_{tr}(\text{cm}^{-1})$ is the transport cross section, K_0 and K_1 are the associated Bessel functions of zeroth and first kind and $\varkappa = \sqrt{3\Sigma_{tr}\Sigma_a}$.

It can be shown that the approximation is good if

$$\varepsilon = \left|\frac{3}{2}\Sigma_{tr\,2} \ln\left(\frac{R_1}{R_2}\right)[\Sigma_{a2}(R_2^2 - R_1^2) - \Sigma_{a1} R_1^2] - \frac{1}{8}\varkappa_1^2 R_1^2\right| \ll 1. \tag{17}$$

In our case we get

$$k_p = 1.158 \quad \varepsilon = 0.002.$$

Detector perturbation, experimental

The correction factor can also be written

$$k_p = \frac{1}{1+\varepsilon}\left[1 + \frac{E}{\phi_d} K_0(\varkappa_3 R_2)\right], \tag{18}$$

where ϕ_d is the flux at R_2.

The perturbation in the outer medium is

$$\phi(r) = E K_0(\varkappa_3 r), \tag{19}$$

where E is a constant. These equations have been used to determine the correction factor experimentally. Two gold foils ($0.2 \times 150 \times 5$ mm) were placed according to Fig. 6 and were activated during one week. The foils were then cut up and the activity of the foils was determined with a NaJ(Tl) crystal and a one channel pulse height analyser. Since we measured on the gold peak, the background was low and the

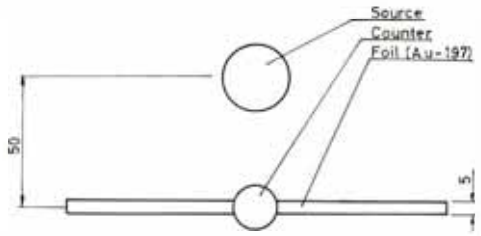

Fig. 6. The experimental arrangement at the gold activation.

influence of any impurities could be avoided. The experiment was repeated with the detector exchanged for a void, which was realized by an aluminium tube. The difference between the two measurements is plotted in Fig. 7. The Bessel function is fitted to the experimental points through the method of least squares. This gives $k_p = 1.168 \pm 0.009$, a value that is somewhat higher than the theoretical value 1.158. This can be due to the fact that the theoretical study did not include the materials at bottom and top of the detector. We have therefore chosen the experimental value as the most correct and used it in the calculation of R.

Figure 7 also gives a comparison between the P_1-approximation and the experimental result. It is seen that there is no significant disagreement between theory and experiment, indicating that higher terms give no significant contribution to the flux depression.

From equation (16) it is seen that the main part of the correction term is due to the absorption in the detector, which for neutrons above cut-off is only some per cent of the total absorption. The correction of the fast neutron flux depression is therefore about some per mille and can be neglected.

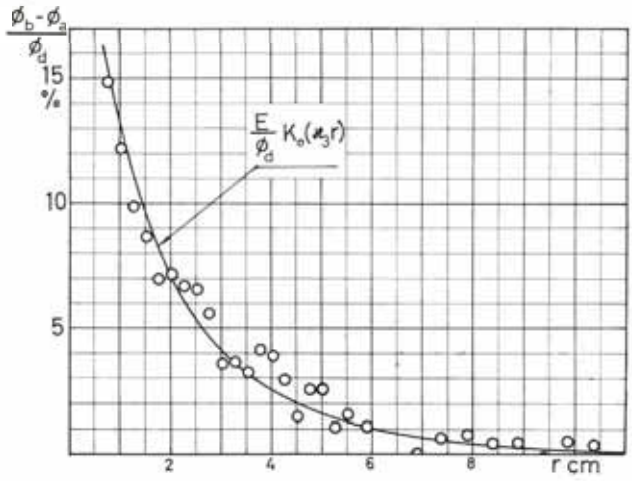

Fig. 7. The flux depression as a function of distance from the centre of the detector.

Other corrections

The fact that the detector has to be connected to the preamplifier gives a leakage of thermal neutrons through the filter. The correction was determined for the cadmium filter through simulating another identical leak and measuring with and without this leak. This gave a correction factor $k_{f\,Cd} = 1.065 \pm 0.005$. Since the cadmium and gadolinium filters are geometrically equal we can assume that the same amount of thermal neutrons leaks into the detector in both cases. This gives a correction factor for the gadolinium filter of $k_{f\,Gd} = 1.040 \pm 0.005$.

The filter leak correction is not strictly space independent since the neutron spectrum varies with the distance from the source. The difference is, however, small and can be neglected.

The finite volume of the detector gives a space dependent correction since the detector senses a mean value of the neutron distribution in the detector. The shape of the distribution in the detector changes with position and so does the ratio between the mean flux value and the flux value at the centre of the detector. Using a Taylor expansion of the flux around the detector centre (r_0) the correction factor (k_s) can be written

$$\frac{1}{k_s} = 1 + \frac{1}{\phi(r_0)}\left(\frac{d\phi}{dr}\right)_{r_0}\overline{(r-r_0)} + \frac{1}{2}\frac{1}{\phi(r_0)}\left(\frac{d^2\phi}{dr^2}\right)_{r_0}\overline{(r-r_0)^2} + \text{---}, \tag{20}$$

where r is the radius from centre of the source and the mean values are taken over the active detector volume. The flux and the derivatives can be taken from the uncorrected distributions.

Unsymmetrical parts of the flux distribution can be caused by the aluminium tube holding, the shape of the moderating medium and the shape of the source. All these effects must be very small, since the absorption rate in the aluminium tube is small, since the tank is large and since the source shape is effecting only the measurements close to the source, a region where r is small.

Results

Using 330 ± 3 mb as the 2200 m/s cross section of hydrogen we get

$$l = 2.06 \cdot 10^{-4}\ s$$

and from this

$$t_s = 2.47 \pm 0.11\ \mu s \quad \text{for gadolinium,}$$

$$t_s = 1.60 \pm 0.07\ \mu s \quad \text{for cadmium,}$$

where the error limits are calculated from the statistical fluctuations of the measurements. The water temperature was 22°C.

Possible systematic errors can be caused by

impurities in the water,

gamma radiation,

instability of the electronics.

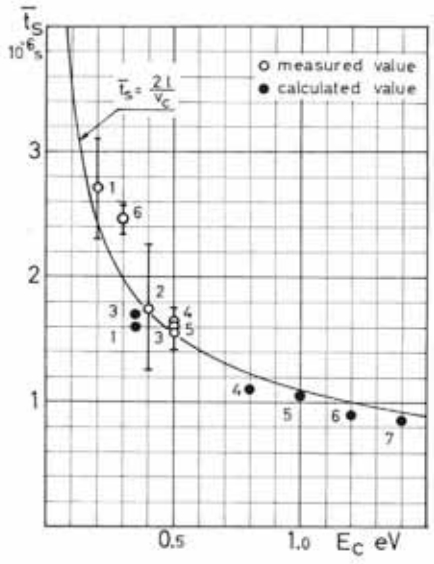

Fig. 8. The slowing-down time as a function of neutron energy. The point numbers are explained in Tables 3 and 4.

We used ordinary tap water as moderator. According to an analysis from the waterworks the total absorption cross section of the impurities did not exceed 0.30 per cent of the hydrogen cross section and was therefore neglected. Gamma pile-up was avoided through working with as low detector voltage as possible. The best part of the plateau could therefore not be used. This may have affected the stability of the electronics. However, we measured every odd number point in Figs. 3, 4 and 5 moving outwards and then every even number point when going back in each run. Any long term instabilities should therefore be seen in the figures.

The effective cut-off energies of neutron filters have been calculated by Stoughton and Halperin [5]. From their report we get the values 0.5 eV for our cadmium filter and 0.3 eV for our gadolinium filter. It is not easy to get a reliable value of the error limits. We have estimated them to less than 10 per cent.

The results are summarized in Tables 3 and 4 together with earlier experimental and theoretical results. In order to get a comparison we have plotted the most im-

Table 3.

Name	Ref.	$\bar{t}_s(\mu s)$	E_c(eV)	Point in Fig. 8
Möller, Sjöstrand	6	2.7 ±0.4	0.2	1
Profio	7	1.75±0.5	0.4	2
Walker, DeJuren	1, 2	1.54±0.13	0.5	3
Prel. result	8	1.65±0.10	0.50	4
Crouch	9	5.2	0.35	(7)
Present work		1.60±0.07	0.5	5
Present work		2.47±0.11	0.3	6

Table 4.

Name	Ref.	$\bar{t}_s(\mu s)$	E_c(eV)	Point in Fig. 8
Krieger, Federighi	10	1.6	0.35	1
Haynam, Crouch	11	5.2	0.025	(2)
Haynam, Crouch	11	1.7	0.35	3
Haynam, Crouch	11	1.1	0.8	4
Haynam, Crouch	11	1.05	1.0	5
Haynam, Crouch	11	0.9	1.2	6
Haynam, Crouch	11	0.85	1.4	7
Haynam, Crouch	11	0.8	1.6	(8)

portant values in Fig. 8 together with the result from the model of free protons at rest

$$\bar{t}_s = \frac{21}{v_c}, \tag{21}$$

where the scattering mean free path l has been taken to 0.75 cm.

In Fig. 8 we first observe that all the calculated values are lower than the results from the model of free protons. This may be due to differences in primary data and uncertainties in the calculations. Next we observe that all the measured values lie on or above the curve. Crouch's value is probably caused by time-of-flight effects in the counter. The results from pulsed measurements of Möller and Sjöstrand [6] and of Profio [7] have rather large limits of error. Walker's value has been discussed above.

The difference between the experimental results and the model of free protons can be due to the low energy effects, chemical binding and up-scattering. Chemical binding can influence our values because the vibrational frequencies of the bonds in the water molecule correspond to energies in the region of interest. Up-scattering has been investigated theoretically by Krieger and Federighi [10] who found that it can influence the slowing-down time up to about 0.4 eV.

The conclusion of this experiment is that the low energy effects are small at 0.5 eV but cannot be ignored at 0.3 eV.

ACKNOWLEDGEMENTS

The author is grateful to Professor N. G. Sjöstrand for his guidance, to Mr. H. Samuelsson for his technical assistance and to all members of the reactor physics department for their interest and help. This work has been supported by the Swedish Atomic Research Council.

Department of Reactor Physics, Chalmers University of Technology, Göteborg

REFERENCES

1. DeJuren, J. A., Slowing-down time of neutrons in water, Nuclear Sci. Eng. *9*, 408 (1961).
2. Walker, R. L., Absolute calibration of a Ra–Be neutron source, U.S. Atomic Energy Document, MDDC-414 (October 22, 1946).
3. Reactor physics constants, ANL-5800, USAEC (1963).
4. Flux perturbations measurements and calculations, Trans. Am. Nuclear Soc. *5*, Session 5, 30 (June 1962).

5. STOUGHTON, R. W., and HALPERIN, J., Effective cut-off energies for B, Cd, Gd and Sm filters, ORNL-TM-236 (July 1962).
6. MÖLLER, E., and SJÖSTRAND, N. G., The time scale of neutron slowing down in water, Nucl. Sci. Eng. *15*, 221 (1963), and private communications.
7. PROFIO, A. E., Methods of investigating neutron moderation and absorption using a pulsed source, Massachusetts Institute of Technology (November 1962).
8. GROSSHÖG, G., CTH-RF-4, internal report (February 1963).
9. CROUCH, M. F., Experimental measurement of the slowing-down time distribution for neutrons in water, Nuclear Sci. Eng. *2*, 631 (1957).
10. KRIEGER, T. J., and FEDERIGHI, F. D., Neutron slowing-down times and chemical binding, Trans. Am. Nuclear Soc. *2*, 102 (November 1959).
11. HAYNAM, G. E., and CROUCH, M. F., Monte Carlo calculation of the slowing-down time distribution for neutrons in hydrogen, Nuclear Sci. Eng. *2*, 626 (1957).

Tryckt den 10 juni 1964

Uppsala 1964. Almqvist & Wiksells Boktryckeri AB

B

CHALMERS UNIVERSITY OF TECHNOLOGY

DEPARTMENT OF REACTOR PHYSICS

CTH-RF-10 Jan. 1967

A SYSTEM FOR SIMULTANEOUS MEASUREMENT OF THE AMPLITUDE AND TIME DISTRIBUTION FOR PULSES FROM UP TO FOUR DETECTORS.

by

GUDMAR GROSSHÖG

1. Purpose

The purpose of the system is to determine the time dependence of a neutron flux with glass detectors. The background is assumed to be rather high and it is therefore necessary to have it under control. This can be done by measuring the time dependent amplitude distribution for the pulses from the photomultipliers, since the amplitude distribution for the background and the neutrons have very different shapes. The main part of the background comes from gammas which in the crystal have a long range compared to the dimensions. The amplitude distribution for the gammas will therefore be a continuously decreasing function of the amplitude. On the other hand the neutrons will give a very peaked distribution, since the reaction products of the neutron sensing reaction (neutrons against lithium - 6) have a short range in the crystal.

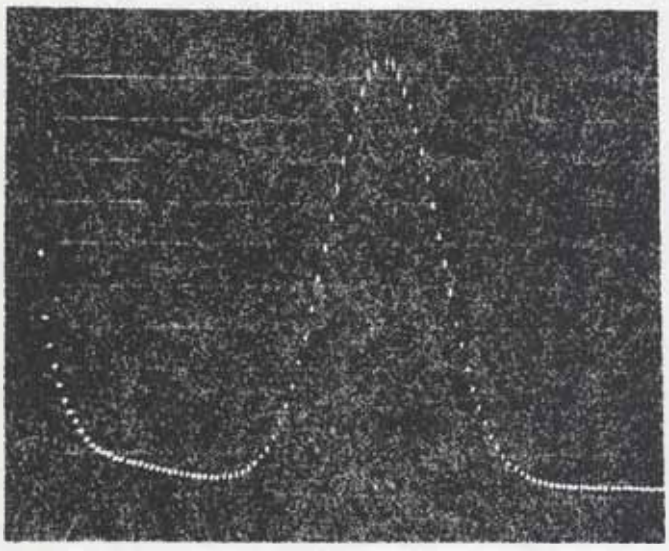

Fig. 1 The amplitude distribution of a Li-6 glass-scintillator. Linear intensity scale 10000 counts/division.

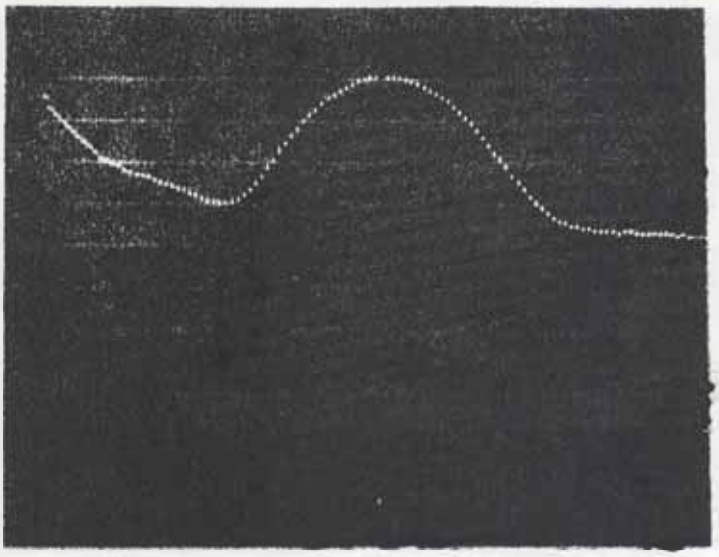

Fig. 2 The amplitude distribution of a Li-6 glass-scintillator. Logarithmic intensity scale 1 decade/2 divisions.

These effects can be seen i figures 1 and 2. Here only the distribution in the neighbourhood of the neutron peak is shown. The spot on the bottom of the figures should be read as 100.000 counts. It is one more than the capacity of the memory and was in this experiment the stop condition for the system.

One possibility to determine the neutron intensity is to extrapolate the background through the neutron peak. The neutron intensity is then determined as the area between the extrapolated and the measured curve. This can be done manually or with the help of a computer. Also other methods, which will be reported elsewhere can be used.

The advantage with this way of measuring the neutron intensity is that it is independent of the stability of amplifiers, discriminators and high voltages.

2. Description of the units.

We will give a short presentation of the different parts of the system. The units (See fig. 3) were constructed and built by

Intertechnique	Amplification unit (AP 17)
	Time measuring unit (HC 24)
	Amplitude measuring unit (CA 13)
	Memory block (BM 24)
	Converters for in- and output to the memoryblock
Oltronix	High voltage unit
	Low voltage units for some of the transistor circuits
Institute of Reactor Physics	Detectors
	Buffer register
	High voltage dividing unit
	Multiinput scaler
	Programming unit
	Amplification and pulsforming units

The details of the units from Oltronix and Intertechnique may be found in their manuals. We will here only present the most important features bearing upon this case and some of the modifications done.

THE AMPLIFICATION UNIT contains four linear amplifiers, one linear adding circuit and some logical circuits. The amplifiers have a maximum gain of 400, a rise time of 0.3 μs and a maximum output pulse - height of about 8 V. The adding circuit provides an analog summing of the signals from all of the amplifiers.

The logic circuits give a blocking signal if two or more pulses from different detectors are separated in time less than 2 μs. For each amplifier the logic circuit gives a standard pulse of 10 volts and 4.5 μs if an incoming pulse is followed by an enable pulse. The leading edge of this pulse is used to activate the time measuring unit.

THE TIME MEASURING UNIT measures the time with the help of a freerunning oscillator of 4 MHz, giving a time jitter of 1/4μs. The channel width can be chosen to 1, 2, 4, 8, 16 or 64 μs. The measuring cycle is activated by a zero time signal. There are four separate detector lines and each of them can be given a separate measuring range delayed according to the zero time signal in steps of 32 times the channel width. The deadtime is modified from originally 20 to 4 μs. During the deadtime the time register is stopped, the content is transferred, the register is corrected for elapsed time during the stop. At the end of the deadtime the register is put into operation again. A logical output signal defines the time of interest as the time during which any of the detector lines is operating. The number of channels is 256 per detector line.

THE AMPLITUDE MEASURING UNIT uses as input a bipolar pulse. The amplitude is 0.1 to 10 volt. Conversion from analogue to binary information is established with the help of a 20 MHz oscillator giving a conversion time of $3 + 0.05N$ μs where N is the channel number. The capacity of the address is 32 to 2048 and the gain of the conversion can be set to 64 - 2048 channels per 10 volt. The integral and differential linearity is for 1024 channels 0.05 and 1 per cent respectively. There is however larger deviations in some channels. These are systematic and can be corrected for during the data handling.

A time signal, with a jitter of less than 0.3 μs is sent out for every accepted input pulse. This time signal is used as an enable pulse for the amplification unit. There are a lot of blocking possibilities for coincidences and anticoincidences. We have used delayed anticoincidence for the blocking from the amplification unit and direct anticoincidence for synchronization of the deadtimes of the different units.

THE BUFFER REGISTER is a 20 stage binary register with a deadtime of 2.5μs. It collects the information from the units above and transfers it to the memory block.

THE MEMORY BLOCK has 1024 channels and a program time for storing 16μs. We use the parallel input for the information and a pulse at the end of the program as a signal to the system that the memory block is ready to take care of a new storing. For each storing one is added to the content of the actual channel.

THE HIGH VOLTAGE UNIT can give up to 3400 volt and 25 mA. Line stabilisation is 0.3 V per 10 per cent line voltage change and 0.3 V per 50 to 100 per cent load change.

THE HIGH VOLTAGE DIVIDING UNIT separates the four detectors. The voltage to each detector can be individually set by a ten turns potentiometer.

THE MULTIINPUT SCALER is constructed to meet the need of several scalers of different capacity. It contains 24 stages which can be divided into at most 6 parts. Every part can contain arbitrarily many stages with the limitation, of course, that the sum of them is 24. Each input is gated so that the scalers can be controlled separately. The deadtime is about 2 μs.

THE PROGRAMMING UNIT is principally a scaler which shifts a bistable circuit after a predetermined number of counts. The output of the bistable circuit is connected to the on-off function of the storing in the memory block and also to the gates of the multiinput scaler. The unit is fed with pulses either from outside or from a triggering circuit using the line frequency as time signal source.

THE AMPLIFICATION AND PULSE FORMING UNIT contains 5 amplifiers of the same type as those in the amplification unit and 5 discriminators.

3. Principle of Operation

The working principle of the system is sketched in fig. 3. The pulses from the preamplifiers are fed into the amplification unit. This gives an analogue signal which is the sum of the amplified input signals. Before entering the amplitude measuring unit this pulse is differentiated and amplified in the pulsforming unit. At the zero crossing time of the differentiated analogue pulse the amplitude measuring unit tests the system in order to see if it is still working with an earlier pulse. If that is not the case a pulse triggers the logical circuits in the amplification unit and a logical time signal for the actual detector is sent over to the time measuring unit.

The capacity of the time measuring unit is 4 times 256 time channels. The groups of 256 channels can be placed anywhere in the time scale and as a special case it can handle four detectors of 256 time channels. The zero time in a repetitive measurement is defined by the zero time pulse. After the zero time there can be a time delay before the region of interest during which the unit is working. The time from the beginning of the region of interest is measured and the information is sent over to the buffer register in form of a 10 bits binary coded word. The two last bits ($2^8, 2^9$) are in the four detector case used to determine the detector.

During the same time as the time measuring unit is determining the time, the amplitude measuring unit is converting the amplitude of the pulse into another binary word. This can contain up to 11 bits, of which we ordinarily only use 10, and is sent over to the buffer register as soon as the conversion is completed.

The purpose of the buffer register is to collect the information from the amplitude measuring unit and the time measuring unit. A predetermined part of this information is sent over to the memory block at a time when this is not engaged with possible earlier storing. We will explain this in more detail later on. For the time being it is enough to point out that the memory block can not handle a larger word than 10 bits (1024 channels). We therefore have to select as output a 10 bits information from the 20 bits input.

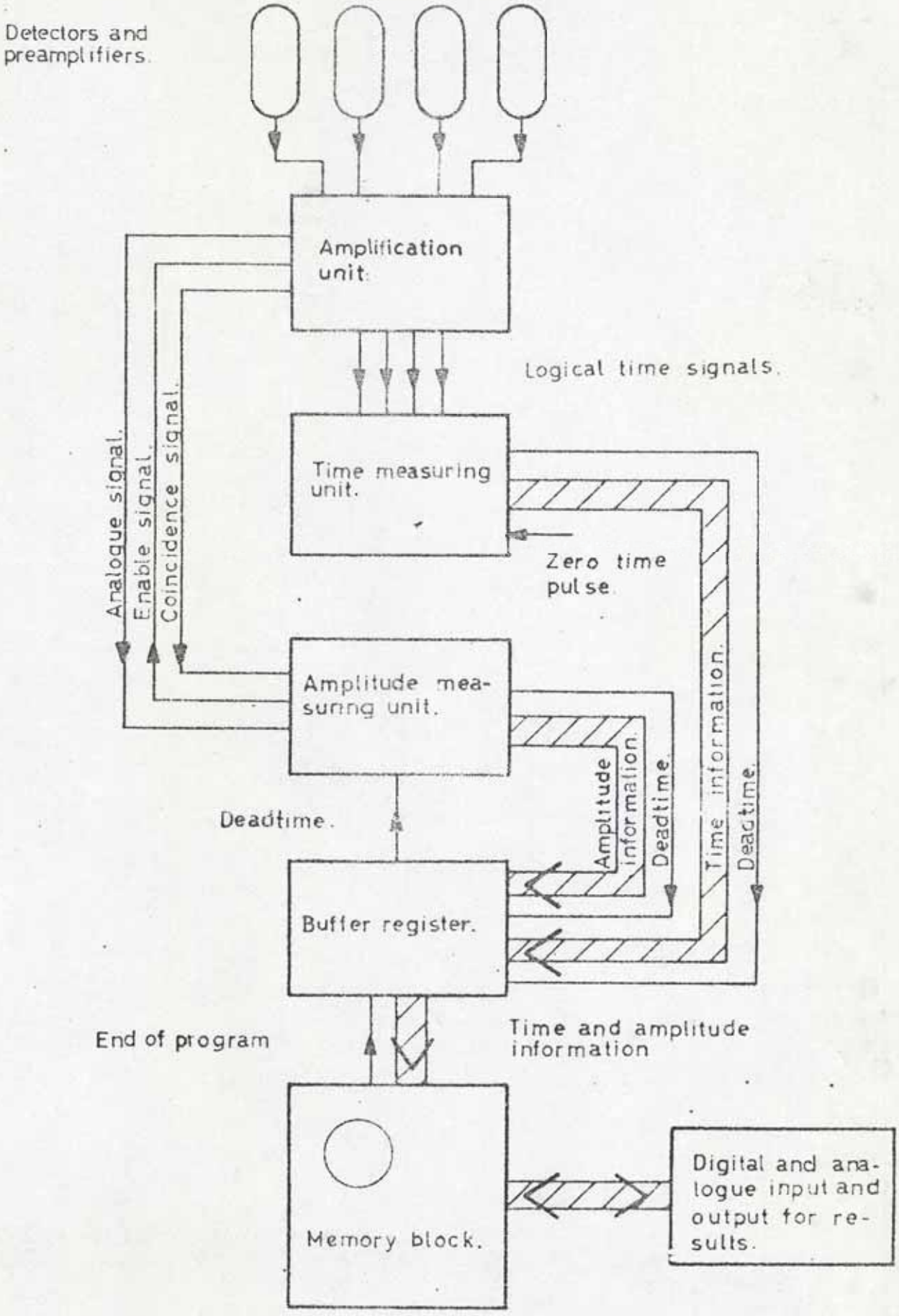

Fig. 3. Working principle of a four detector time and amplitude measuring system.

4. Dead Time Considerations.

There are three types of events during which the system can not take care of incoming information.

1. Coincidence between two or more detectors is recognized.
2. The system time (defined by the time measuring unit) is outside the region of interest.
3. Any of the time measuring unit, the amplitude measuring unit or the buffer register is engaged.

Coincidences between the detectors are detected in the logics of the amplification unit. In the case of coincidence a blocking signal is sent down to the amplitude measuring unit and the converting is not executed. The time measuring unit is supplied with a circuit that cancels the transfer if coincidences are recognized.

The deadtime signals are logically added in a circuit in the buffer register. The output of this circuit blocks the analogue input if any of the measuring units or the buffer register is engaged. The different deadtimes are 4 μs + a waiting time (< the channel width) for the time measuring unit, 3 + 0.05 • (channel number) for the amplitude measuring unit and 2.5 μs + the waiting time of the storing of an earlier pulse in the memory block. The maximum deadtime will occur if an information has been transferred immediately before the actual pulse. In this case the deadtime of the buffer register can be 18.5 μs.

As the deadtime is a complicated funtion of both intensity and amplitude, of which the first one is time dependent, it is rather difficult to calculate the deadtime corrections. There is, however, a simple way to measure it if one can afford to use one detector line for this purpose. Assume that this detector is irradiated with a time independent source giving a pulse rate of r counts/sec For this detector there will then be stored in the memory block

$$P_4(t) = G(t) \cdot r \cdot t \cdot N$$

pulses, where

t = channel width

N = the number of measuring cycles

G(t) = the transfer function, i.e. the probability that an incoming pulse will be stored.

For another detector we now have

$$P_i(t) = G(t) \cdot r_i(t) \cdot t \cdot N$$

from which

$$r_i(t) = r \cdot \frac{P_i(t)}{P_4(t)} \qquad i = 1, 2, 3$$

where $r_i(t)$ is the corrected counting rate of the i:th detector line.

This method has the advantage that it also corrects for differences in the channel widths if these are equal in the different detector lines. It can, however, only be used if the detector lines are parallel in time.

5. The Buffer Register.

The buffer register is the brain in the system and we will therefore describe it a little more in detail.

The function is illustrated in figure 4.

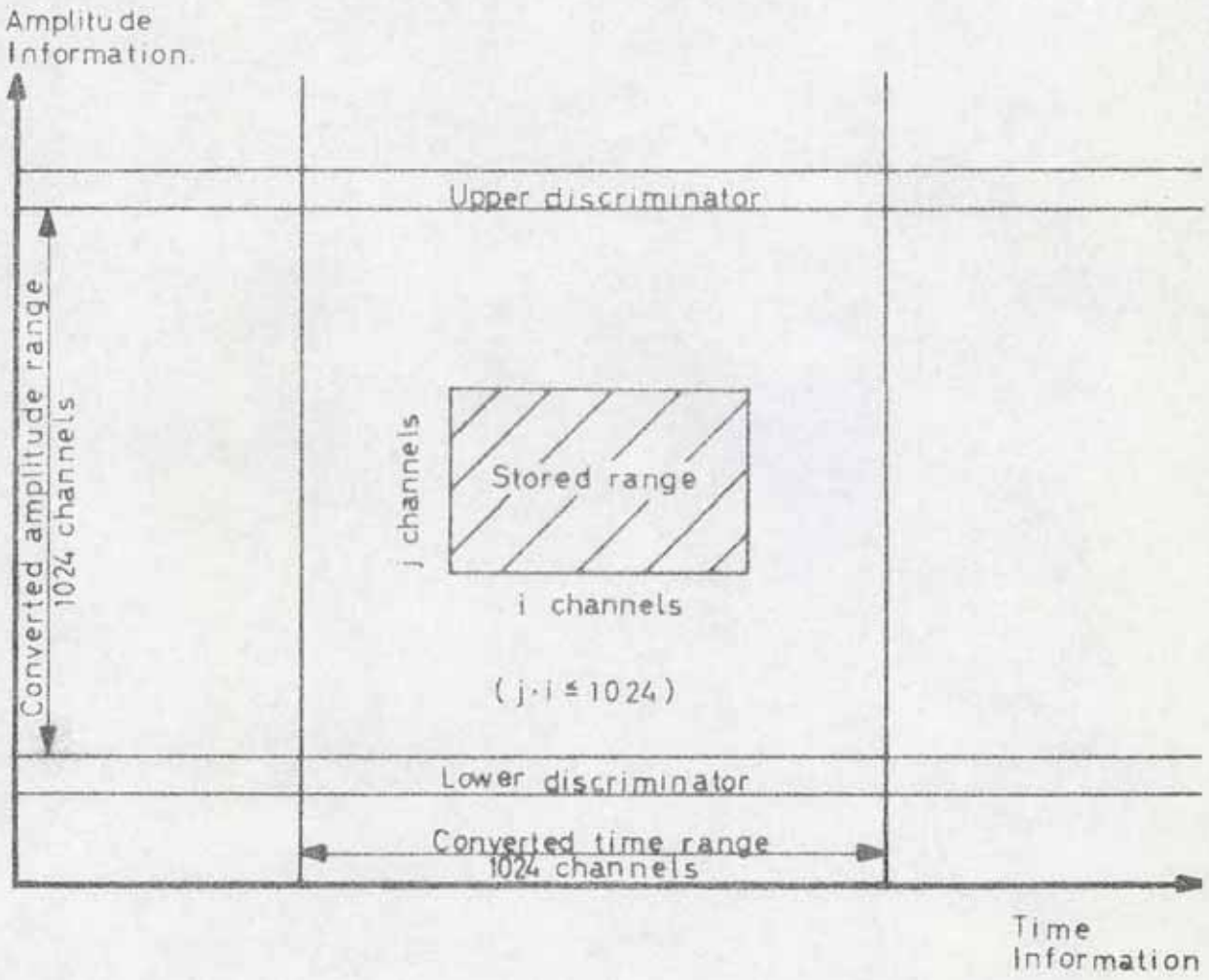

Fig. 4 Information map of the system.

The information field is here illustrated as an area built up by the time on the abscissa and the amplitude on the ordinata. The incoming information covers the whole area with positive amplitudes and times. The upper and lower discriminator and the region of interest are those functions of the system which determine the part of the total field which will be rejected in the first instance.

The measuring units now convert everything lying inside the region of interest in time and the converting range in amplitude. This information is fed into a 20 bits register in the buffer register unit.

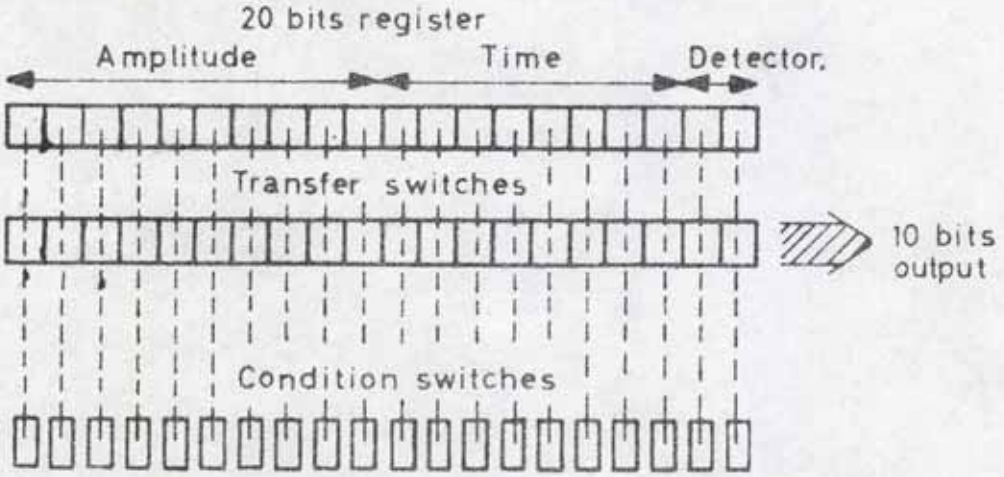

Fig. 5 The buffer register.

As is illustrated in figure 5 ten transfer circuits can be connected to ten of the bistable circuits with the help of switches. This switching system is constructed so that the only restriction is that the bistable circuits must be in the same order as the transfer circuits.

A condition for transfer can also be put in for every bistable. The condition circuit is a logical and - circuit into which one of the sides of the bistables may be connected. The condition for one of the bistables can therefore be on, off or independent. The condition circuit will inhibit the transfer if the condition is false.

By using the condition for all bistables not used for transfer, any part of the measured range can be transferred. It is therefore possible to use the full resolution of the measuring units but, of course, on the expense of the dimensions of the stored range.

6. The Logarithmic Time Scale Converter.

In the field of the pulsed neutron source one is faced with the problem of accurate measurements of the logarithmic decay of a counting rate. In order to get a correct value of the lowest decay constant even if the measured values are influenced by higher modes it is necessary to have a good resolution at the same time as one measures on a very long time scale. We have also the problem that if e.g. 32 channels are used for the amplitude and we have four detectors there are only 8 channels for the time. In order to meet these requirements the buffer register contains a possibility to shift the time scale into a logarithmic one. The principle is shown in figure 6.

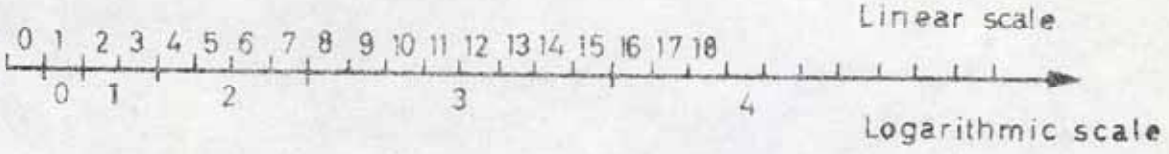

Fig. 6. Comparison between the linear and the logarithmic time scales.

The channel 0 is not used. Channel 1 is converted into channel 0, channels 2 and 3 into 1, channels 4, 5, 6, 7 into 2 and so on. This corresponds to the truth table in table 1.

linear scale								logarithmic scale		
2^0	2^1	2^2	2^3	2^4	2^5	2^6	2^7	2^0	2^1	2^2
(0	0	0	0	0	0	0	0	0	0	0)
(1	0	0	0	0	0	0	0	0	0	0)
X	1	0	0	0	0	0	0	1	0	0
X	X	1	0	0	0	0	0	0	1	0
X	X	X	1	0	0	0	0	1	1	0
X	X	X	X	1	0	0	0	0	0	1
X	X	X	X	X	1	0	0	1	0	1
X	X	X	X	X	X	1	0	0	1	1
X	X	X	X	X	X	X	1	1	1	1
a	b	c	d	e	f	g	h	A	B	C

Table 1. Numerical comparison between the linear and the logarithmic time scales. X = 1 or 0.

If we use the notations of the table, we can get the following logical expressions:

$$A = b.\bar{c}.\bar{d}.\bar{e}.\bar{f}.\bar{g}.\bar{h} + d.\bar{e}.\bar{f}.\bar{g}.\bar{h} + f.\bar{g}.\bar{h} + h$$

$$B = c.\bar{d}.\bar{e}.\bar{f}.\bar{g}.\bar{h} + d.\bar{e}.\bar{f}.\bar{g}.\bar{h} + g.\bar{h} + h$$

$$C = e.\bar{f}.\bar{g}.\bar{h} + f.\bar{g}.\bar{h} + g.\bar{h} + h$$

which are very simple to convert into a logical circuit. Above we have not taken into account the differences between the linear channels 0 and 1. This depends on the fact that the time measuring unit gives wrong results in the first two channels. We can therefore not use the logarithmic channel number 0 without doing a correction. The complication of taking the difference of the channels into account is therefore of rather little importance.

7. The Detectors

The detectors are composed of four parts:

a Glass scintillator
b Neutron absorber
c Light pipe
d Multiplier tube (RCA 4441)

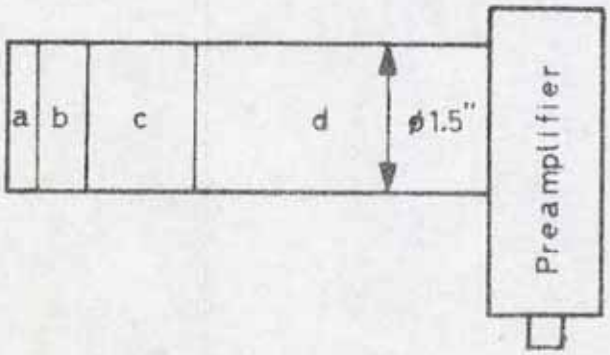

Fig. 7. Neutron detector.

We have two types of neutron sensing glass scintillators. One of them contains 7.8 % Li enriched to 96 % Li-6 and the other contains 2.7 % natural Li. As a neutron detector the last one will be transparent and measures therefore the neutron density, the other one is " black " and measures the neutron flux. The thickness of the scintillators is 1/8", which will give a very low time of flight effect in the detector.

The neutron absorber shall protect the scintillator for neutrons coming from the backward direction. It has the thickness 1/4" and is made of glass mixed with 8 % Li-6.

The need of light pipe can be seen in figures 8 and 9. The amplitude spectrum of a detector without any light pipe contains at least two peaks caused by the neutrons.

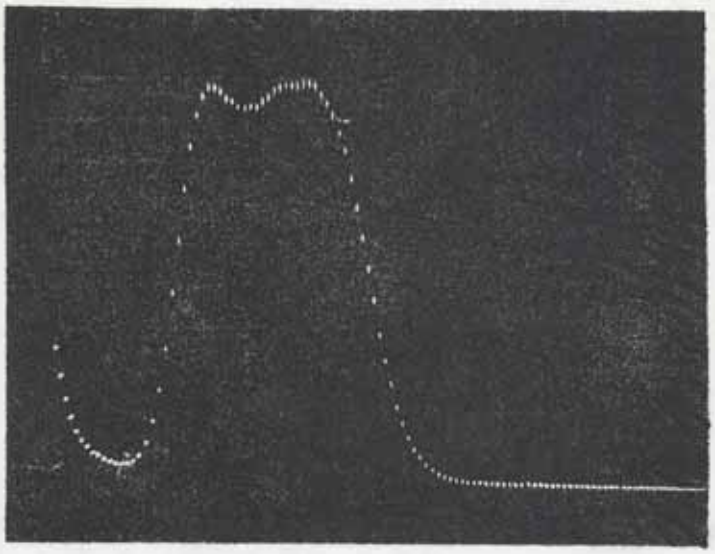

Fig. 8. Amplitude distribution for a detector without any lightpipe.

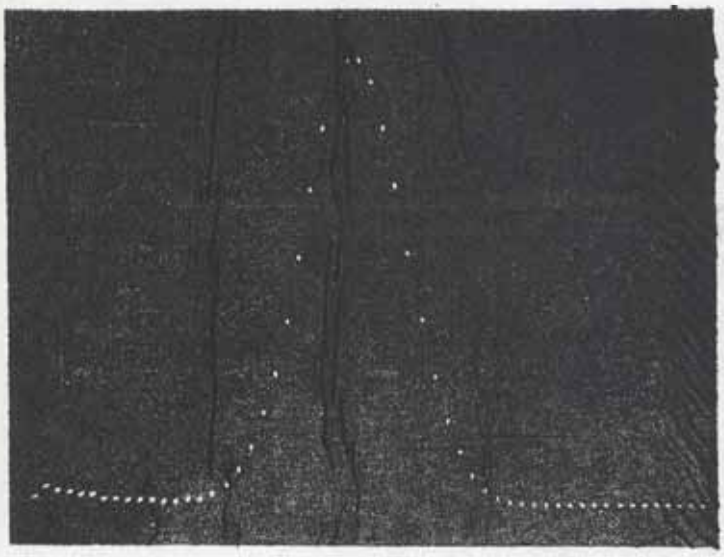

Fig.9. Amplitude distribution for a detector with lightpipe.

This depends on the fact that the photo cathode of the photomultiplier does not sense the light equally over the whole area. By using a lightpipe the light will be distributed approximately in the same way over the photo cathode for every scintillation.

In figure 9 we have used a lightpipe of 2 cm acryl plastic together with the neutron absorber mentioned above. The effect of double peaks has disappeared here. The acryl plastic was chosen because it has about the same properties as glass and is rather easy to work with.

8. Conclusions.

The system is built to handle glass scintillators as neutron detectors. Another use of it could of course be the measurement of short lived isotopes. In the latter case one should, however, wish to have better amplifiers and avoid the complexity of more than one detector. Owing to the design of the adding circuit not only the signals are added but also the noise. As an example of the use of the equipment we will give an very short presentation of measurement of decaying neutron field in a moderator. The moderator is a polyethylene cube with the side 4 cm. A burst of neutrons is injected into the medium during 32 μs. The region of interest begins 32 μs after the end of the pulse. The time channel width is 1 μs and the logarithmic converter has been used. At the medium there are three detectors, two black and one transparent. Detector number four is a NaI-crystal counting a constant source of gammas from Cs-137.

The results are shown in figure 10 and 11. In figure 10 there is a three dimensional representation of detectors 2 and 3. The intensity is on the ordinata, the amplitude on the abscissa and the time is advancing in the direction into the paper. Some lines for constant amplitude and the curve showing the last time interval are enlighted. In figure 11 we have all the detectors in another representation. The time is on the ordinata and the amplitude together with the detector number on the abscissa. The lighting up of the spots is proportional to the logarithm of the intensity.

Acknowledgements

We wish to thank the technicians of the department of reactor physics, who have built and tested the system, and the people at Intertechnique for their cooperation. The work has been supported by the Swedish Atomic Research Council.

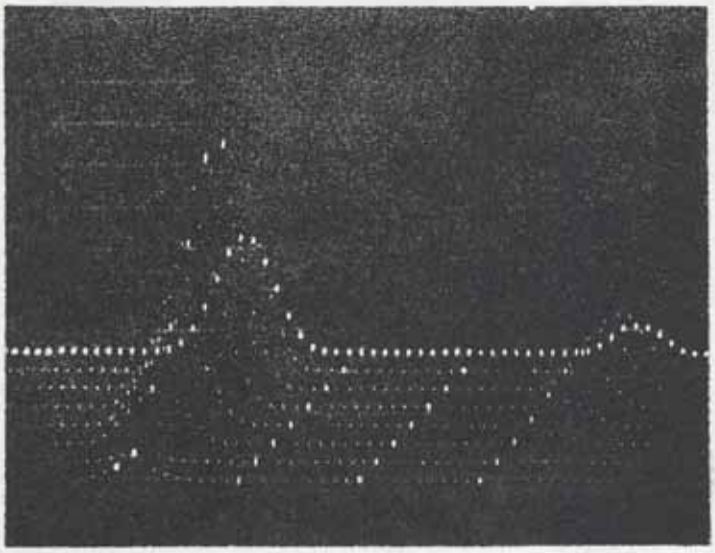

Fig. 10. The amplitude distribution for detector 2 and 3.

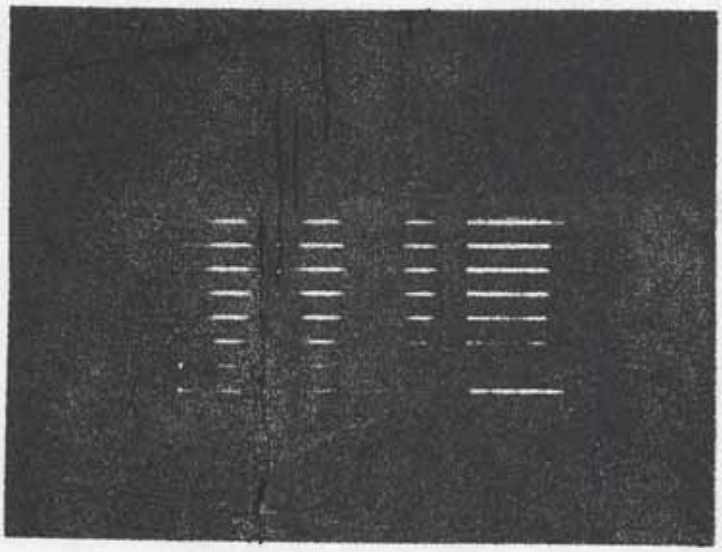

Fig. 11. Time - amplitude distribution for four detectors.

C

CHALMERS UNIVERSITY OF TECHNOLOGY

DEPARTMENT OF REACTOR PHYSICS

CTH-RF-16 DEC. 1968

DETERMINATION OF NEUTRON DECAY CONSTANTS USING SIMULTANEOUS PULSE HEIGHT AND TIME ANALYSIS

by

GUDMAR GROSSHÖG

CTH-RF-16

CHALMERS UNIVERSITY OF TECHNOLOGY
Department of Reactor Physics
Göteborg

DETERMINATION OF NEUTRON DECAY CONSTANTS USING SIMULTANEOUS PULSE HEIGHT AND TIME ANALYSIS

by
Gudmar Grosshög

December 1968

CONTENTS

1. INTRODUCTION.

The main problems when one wants to determine fundamental decay constants with the pulsed neutron method are higher modes and background. These two problems are also conflicting in the sense that the higher modes call for long waiting times but the background calls for short.

In this work we have tried to find a method to solve this problem for an experiment with detectors placed outside the moderator and using a low intensity neutron source. The main features of the method are:

a. Logarithmic time scale.
b. Rotating moderator.
c. Amplitude analysis for background subtraction.
d. More than one detector in the same experiment.
e. Auto correlation of the time distributions.

The method is applied to a cylindrical polyethylene moderator, earlier measured by SJÖSTRAND et al. [1]. The reason for choosing this is that it gives the possibility of a direct comparison with an independent experiment on the very same moderator. Some recent calculations made by GRIFFING [2] make a remeasurement of these assemblies interesting.

2. EXPERIMENTAL ARRANGEMENT.

A sketch of the experimental arrangement is given in figure 2.1. The moderator is composed of up to eight 2.2 cm thick polyethylene discs with a diameter of 18 cm. This gives an experimental series of cylinders with heights from 2.2 to 17.6 cm in steps of 2.2 cm. The corresponding bucklings go from 1.48 to 0.098 cm^{-2}. The moderator is contained in an aluminium box and is shielded by boron carbide. Three detectors are placed close to the moderator, the first and third at positions where the second mode of the cylindrical functions is zero, and the second at the maximum point of the fundamental mode.

The whole arrangement is rotated around the axis of symmetry in order to keep the contribution of the higher modes low. Owing to the cables the direction of rotation is shifted after every revolution. The height of the table is adjusted so that the target always is at half the height of the moderator.

Two series of experiments have been done. In the first we have crystals " black " to thermal neutrons in detector 1 and 2 and a background crystal in detector 3. In the second series detector number 1 contains a black, 2 a transparent, and 3 a background crystal.

The crystals are glass-scintillators with Li-6 as the neutron sensing nuclide. The black contains 7.8 % Li enriched to 96 % in Li-6, the transparent contains 2.7 % natural Li and the background crystal contains 7.8 % Li enriched to 99.999 % in Li-7. The black crystal then gives a pulsrate proportional to the thermal neutron flux while the pulse rate of the transparent is proportional to the neutron density.

It could be seen during the experiment that the background detector did not give correct information about the background. Two reasons for this have been found. First, the baseline shift makes it very difficult to find the correct setting of the high voltage, second, there is an influence from the traces of Li-6. Therefore, the background subtraction has been done by the method outlined in chapter 5, and the results from the background detector have only been used for comparisons.

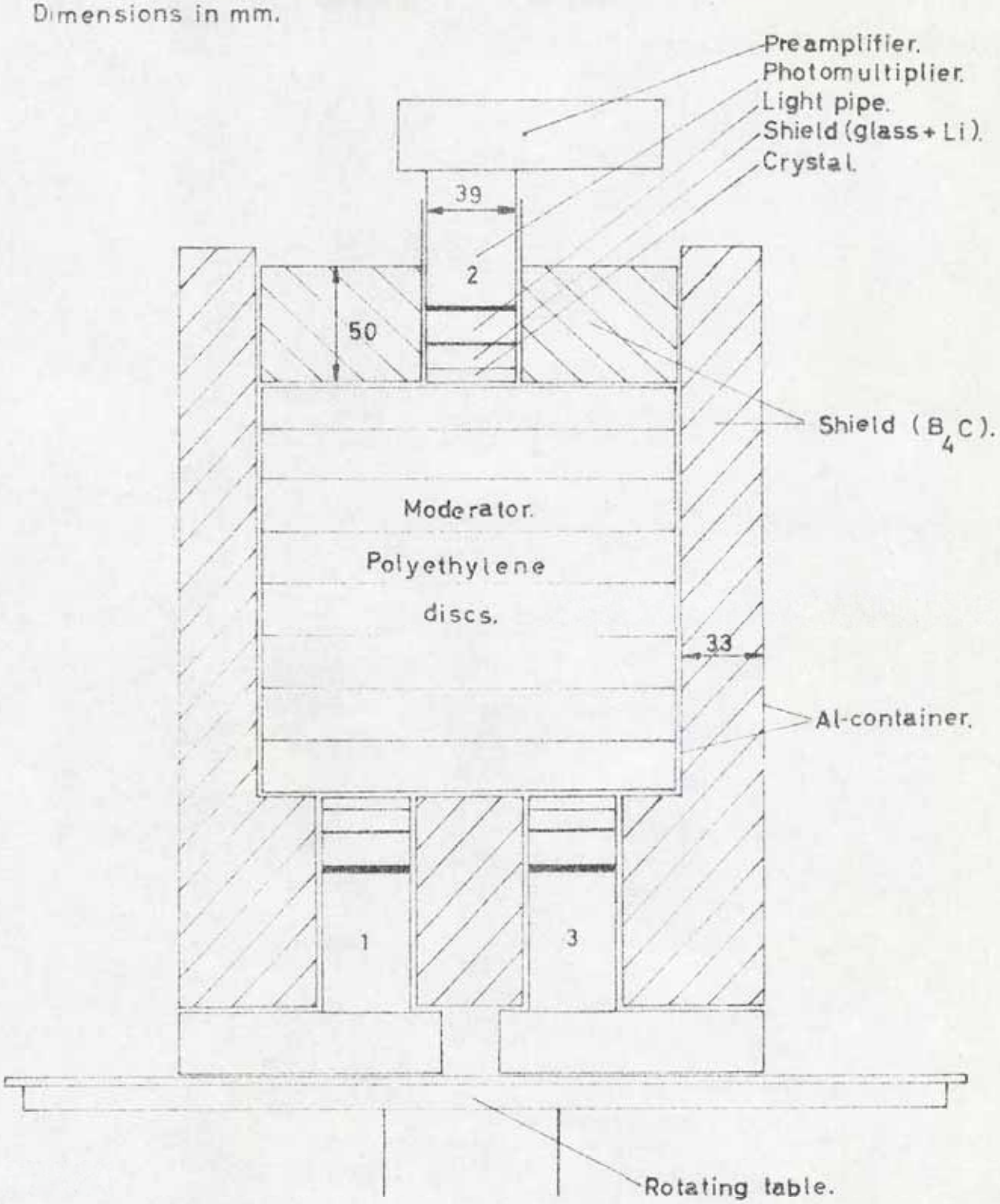

Fig. 2.1. Experimental arrangement.

3. THE ELECTRONIC SYSTEM.

The electronic system is composed of eight head units:

1. 150 kV neutrongenerator (SAMES)
2. Neutron detectors and preamplifiers
3. Amplifying and mixing unit (INTERTECHNIQUE AP 17)
4. Analog-to-digital converter (INTERTECHNIQUE CA 13)
5. Time-to-digital converter (INTERTECHNIQUE HC24)
6. Buffer memory
7. Memory block (INTERTECHNIQUE BM24)
8. Programming unit

Moreover, it contains amplifiers, baseline restorer, linear gate and discriminator from ORTEC and HV supply from OLTRONIX. Some scalers and a ratemeter are used to measure certain quantities and to give an external check on the system during the experiment. The principles of the system are sketched in figure 3.1.

The neutron generator is a 150 kV accelerator with an ion current of maximum 1 mA. During the whole experiment it has worked with the D-D reaction. We use this reaction for two reasons. First, the 2 MeV neutrons give less gammareactions than the 14 MeV neutrons from the D-T reaction. Second, the number of neutrons captured by the moderator in relation to those going into the surroundings is higher for the 2 MeV neutrons.

The accelerator is controlled by a multivibrator, so that the width of the neutron burst is continuously variable down to 2 microseconds. The rise and decay times are approximately 1.5 microseconds. In order to have low neutron production between the bursts the beam is swept and the ion source is keyed synchronously.

The measuring cycle is started at the end of the neutron burst by the condition that the end of the ion current is in coincidence with a signal from the multivibrator. This signal is the end of the control signal, delayed 3 microseconds in order to take into account the drift time of the ions and the propagation times in cables and amplifiers. As the coincidence time is short, spurious starts are kept to a minimum.

The start pulse (T_0) passes a programming unit, which controls the measuring time. It is switched on manually and off either by the condition that it has reached a preset number of measuring cycles or by the condition that there is an overflow in any of the channels in the memory block.

The purpose of the system is to measure the time and amplitude distribution from four detectors simultaneously. The capacity of the memory block is 1024 channels, which can be arbitrarily subgrouped in binary steps for the three parameters: number of detectors, amplitude channels and time channels. In this experiment we use the subgrouping (4x32x8), which means 4 detectors, 32 amplitude intervals and 8 time intervals. The division in amplitude is linear but in time it is logarithmic.

The pulses from the detectors are amplified and added in the amplifier unit (FA). The signal from the addition circuit is fed into an amplifier (AMP, Ortec 440 A), which has two outputs,one direct and one delayed. The delayed output is over a base line restorer connected to the direct current input of the analog-to-digital converter (ADC). If the system is not busy the pulse from the direct output passes a linear gate and activates a discriminator, which triggers the ADC and the logic circuits in FA. From these a signal in the actual detector line starts the time-to-digital converter (TC). From now on the conversion proceeds in both ADC and TC. The conversion time is fixed to 4 microseconds in TC but depends on the amplitude in ADC. The result of the conversions is loaded into the buffer memory, where it is kept until both the conversions are ready and the memory block has completed a possible preceding storing cycle. TC gives the time information in a linear scale. A conversion to the logarithmic time scale is realized during the transfer of the information to the memory block.

The system busy signal to the linear gate is calculated in the buffer memory. It signals busy if ADC or TC or the buffer memory is engaged or if the time is outside the actual time interval. The overall deadtime of the system is depending on the amplitude, the time channel width and the intensity. The minimum deadtime for a stored pulse is 8 microseconds.

Six scalers are incorporated in the system. They are counting different parameters chosen so that a direct check on the system can be done. The

scalers are gated either with the programming unit or with the signal marking the time period during which the system is active (RI). The purpose of the different scalers are given in table 3.2.

TABLE 3.1 Abbreviations used in text and fig. 3.1.

MV	Multivibrator
ACC	Accelerator
Exp	Experimental assembly
DL	Delay line
Sn	Scaler number n
Dn	Detector number n
PG	Pulse generator
FA	Amplifiers and mixing circuits
AMP	Head amplifier
Dir	Direct output
Del	Delayed output
BR	Baseline restorer
LG	Linear gate
DI	Head diskriminator
ADC	Analog-to-digital converter
TC	Time-to-digital converter
BM	Buffer memory
PU	Programming unit
MB	Memory block
BT	Blocking signal from the time converter
BA	Blocking signal from the amplitude converter
RI	Signal giving the actual time interval
BS	Blocking signal for the whole system
BMB	Blocking signal from the memory block
COI	Coincidence unit

TABLE 3.2 Scalers.

Scaler	Purpose	Gate
S1	Test pulses to 4 :h detector	RI
S2	Coincidences between detectors	RI
S3	Multivibrator pulses	PU
S4	Monitor pulses from BF_3 counter	PU
S5	Measuring time	PU
S6	Active measuring time	RI

4. DEADTIME CORRECTIONS

As a counting equipment grows in complexity, the problem of doing an exact correction for the pulse losses will be more and more difficult. One has therefore reasons to keep the correction as low as possible by having short conversion times and using a buffer memory before the often slow memory block. The consequence of this is, however, that the losses will depend not only on the intensities but also on the time and amplitude distribution of the stored pulses. Although it is difficult, it is quite possible to correct for these effects, since all information about them is contained in the measured distributions. There are, however, other effects that we know nothing about. These arise from those parts of the spectrum which are rejected in different places of the equipment by discriminators or by the buffer memory. So we are forced into some method by which we can measure at least the main part of the correction.

A schematic picture of the equipment from the view of deadtime losses is given in figure 4.1. Through a summing amplifier the pulses from the detectors are presented to a unit containing a discriminator and a gate. This unit will put the system into action, if the amplitude of the incoming pulse is above the threshold of the discriminator and if the system is not working with a preceding signal. In the block marked " system " in the figure we have collected all parts that have the same influence on the dead time for all of the detectors.

In order to give the system information about which of the detectors that is responsible for the actual signal, all amplifiers are followed by a one bit memory (monostables marked MS1 to MS4 in the figure). One of the first actions taken by the system after the arrival of the pulse is to read this information. As every monostable is controlled directly by its own detector, this part of the equipment will have a deadtime that depends on the pulse rate in the respective detector.

For these reasons the deadtime correction is divided into two parts and can be written

$$P_i(a,t) = G_i(R_i) \cdot H\left(\sum_{i=1}^{4} R_i\right) \cdot R_i(a,t) \qquad (4.1)$$

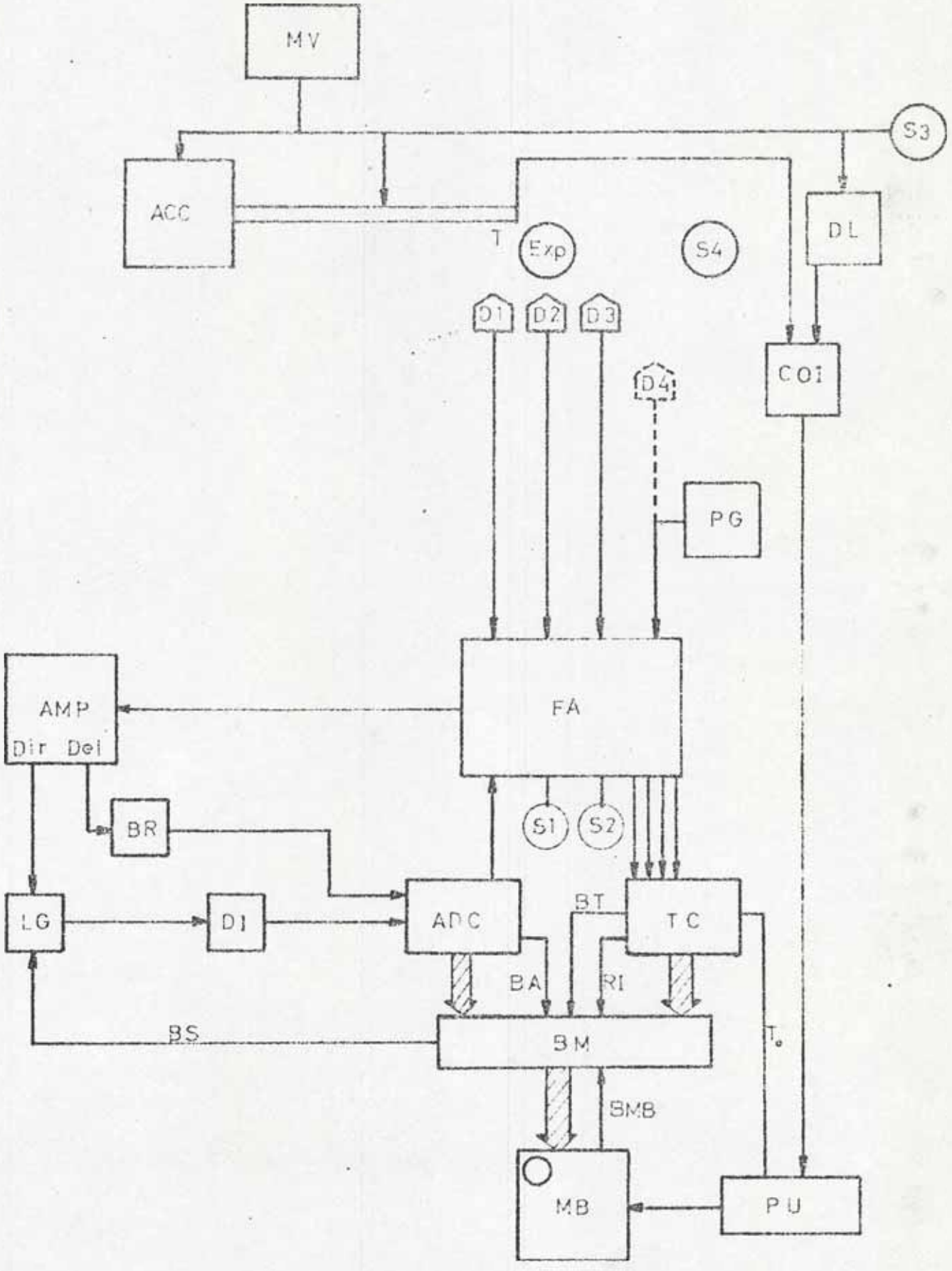

Fig.3.1. Working principle of the equipment.

where

P_i = stored number of pulses for detector i

R_i = incoming number of pulses for detector i

H = system transfer function

G_i = transfer function for detector line i

t = time

a = amplitude

Suppose now that we have a known distribution of well separated pulses in one detector line (e.g. 4). In that case $G_4 = 1$ and

$$P_4 (a,t) = H \cdot R_4 (a,t) \tag{4.2}$$

from which

$$H(t) = \frac{\int_{a_l}^{a_u} P_4 (a,t) da}{\int_{a_l}^{a_u} R_4 (a,t)\, da} \tag{4.3}$$

where a_l and a_u are the amplitude limits.

The functions G_i are the probabilities that a pulse, which arrives during a time period when the system is not busy, will be stored. The contrary might happen for two different reasons. In figure 4.2 the monostable and the system blocking signal after the arrival of a pulse are presented. τ is the on-time for the monostable and d is the time delay between the two signals. It is quite clear that a pulse arriving during the time d in the same detector line will not be stored and will not affect the system blocking signal.

The other reason is that the sensing point of the monostables and the head discriminator is not the same (see figure 4.3). That means that pulses between these two limits will turn the monostable on but will not start the system. Moreover, if such a pulse has arrived in a period τ before the actual pulse, then none of them will be recorded. Therefore we get the individual corrections

$$G_i = \exp \{ - (\tau \int_{a_{MS}}^{a_{HD}} R(a) da - d \int_{a_{HD}}^{\infty} R(a) da) \frac{i}{T} \} \tag{4.4}$$

where

a_{HD} = amplitude limit for the head discriminator

a_{MS} = amplitude limit for the monostable

T = total measuring time

In this connection it should be pointed out that a coincidence between pulses from any of the detectors during the time period d will have the result that none of them is stored. This is, however, taken care of by the system and contained in the function H.

We do not know the number of pulses with amplitude lower than a_{HD} (R_l) and must therefore estimate it. We assume that R_l is proportional to P_b, where P_b is the number of pulses stored in a representative amplitude channel, and that the proportionality constant K is the same for all of the detectors. This means that they have the same discriminator setting.

The number of coincidences during the whole experiment (C) is then approximately given by

$$C = \frac{1}{2} \sum_{\substack{i,j=1 \\ i \neq j}}^{4} (R_{si} + K \cdot P_{li}) (R_{sj} + K \cdot P_{lj}) \frac{\tau}{T} \qquad (4.5)$$

where

$$R_s = \int_{a_{HD}}^{\infty} R(a)\, da$$

τ = the coincidence time

T = the total measuring time.

The coincidences between more than two detectors are neglected. As the number of coincidences is counted we can calculate K from equation 4.5 and then get an estimate of R_l.

The test pulses needed for the measurement of H according to equation 4.3 are generated by a free running pulse generator. If the measuring time is long the errors involved will depend mainly on the total number of collected pulses. We can approximately write

$$H = 1 - \frac{\tau_m \cdot P_t}{t_c \cdot N} \qquad (4.6)$$

where

τ_m = mean deadtime

P_t = stored number of pulses

t_c = channel width

N = number of repetitions

If P_t is Poisson distributed we have

$$\mathrm{Var}\{H\} = \left(\frac{\tau_m}{t_c \cdot N}\right)^2 \cdot P_t$$

and the standard deviation

$$\sigma_H = \frac{(1-H)}{\sqrt{P_t}} \approx (1-H)\,\frac{\sigma_{R_t}}{R_t} \qquad (4.7)$$

where σ_{R_t} is the standard deviation of the total number of incoming pulses (R_t). From this equation we can conclude that the error from the correction can be neglected if H is not far from 1.

The above method has been checked with a rather simple numerical model. This model uses the fact that if the channel width is small, the effects from the amplitude converter will predominate. We assume also that the transfer time between the buffer register and the memory block is zero. The deadtime can now be separated into two parts. The first is the sum of all constant waiting times (DT), the second is proportional to the converting time and therefore also to the amplitude. The relation between the deadtime calculated in number of channels after the arrival of the pulse (k) and the amplitude (a) can then be written

$$k = DT + c \cdot a \qquad (a \geq 0) \qquad (4.8)$$

where c is a proportionality constant that depends on the settings of the amplitude converter. The inversion of this equation is

$$a(k) = \frac{k - DT}{c} \qquad (k \geq DT)$$

$$a(k) = 0 \qquad (k < DT) \qquad (4.9)$$

The probability S(j) that a channel j is closed is then

$$S(j) = \sum_{i=1}^{j-1} \sum_{k=j-i}^{\infty} p\,(a\,(k), i) \qquad (j > 1)$$
$$S\,(j) = 0 \qquad (j = 1) \tag{4.10}$$

p (a,i) is the probability of a pulse in the linear time channel i and amplitude channel a. It can be calculated approximately from the stored distributions (P (a,i)) as

$$p\,(a,i) = \frac{P(a,i)}{N} \qquad (a, i \text{ inside the measured range})$$
$$p\,(a,i) = 0 \qquad \text{elsewhere} \tag{4.11}$$

where N is the number of repetitions. It is assumed that the system is open in the beginning of each cycle and that all pulses above the discriminator level are stored. The correction is finally

$$k_H\,(i) = \frac{1}{1 - S(i)} = \frac{1}{H(i)} \tag{4.12}$$

The result of a calculation with this method is shown in figure 4.4. The distributions are taken from an ordinary experiment with eight logarithmic time channels and 32 amplitude channels. The calculation is made in a linear time scale but the result is transferred back to the logarithmic scale. Time channel number one is zero, as the system always is considered to be open at that time, number two is constant because DT is larger than the channel width. The other curves show plateaus and transients. With 32 amplitude channels the deadtime variation is 1.6 microseconds, which gives transients in the channel limits that last over a period of 3.2 microseconds. The shapes of the transients are determined by the amplitude distribution.

We have also compared the model with experiments where the correction factor has been measured by the method mentioned in the beginning of the chapter. The result is shown in figure 4.5. The input to the experiment is a neutron and gamma field where the neutrons give a dominant peak in the actual experiment decreasing with a decay constant of approximately 8500 s^{-1}. The difference between the runs is that they have different starting times, which gives the different initial intensities noted in the figure. The

relative accuracy of the experimental points is better than 1 %. From the figure we conclude that there is satisfactory agreement between the model and the experiment in the intermediate part, but there are deviations both in the beginning and the end part of the curves. We shall, however, keep in mind that all common effects are included in the experimental values. In the beginning there are transients, which have not been accounted for in the model. The effects in the end part are more difficult to explain. The corrections are, however, low and second orders corrections as channel jitter, buffering and storing times may come into the picture.

The result of this investigation is that a check of the experimental method has been obtained. The rather simple model gives correct results in the main part of the experiment but not in the limits. The model is also expensive by consuming rather long computing time. It is therefore not attractive to expand the model by putting more routines into the computer program. We will therefore in the following use the experimental method.

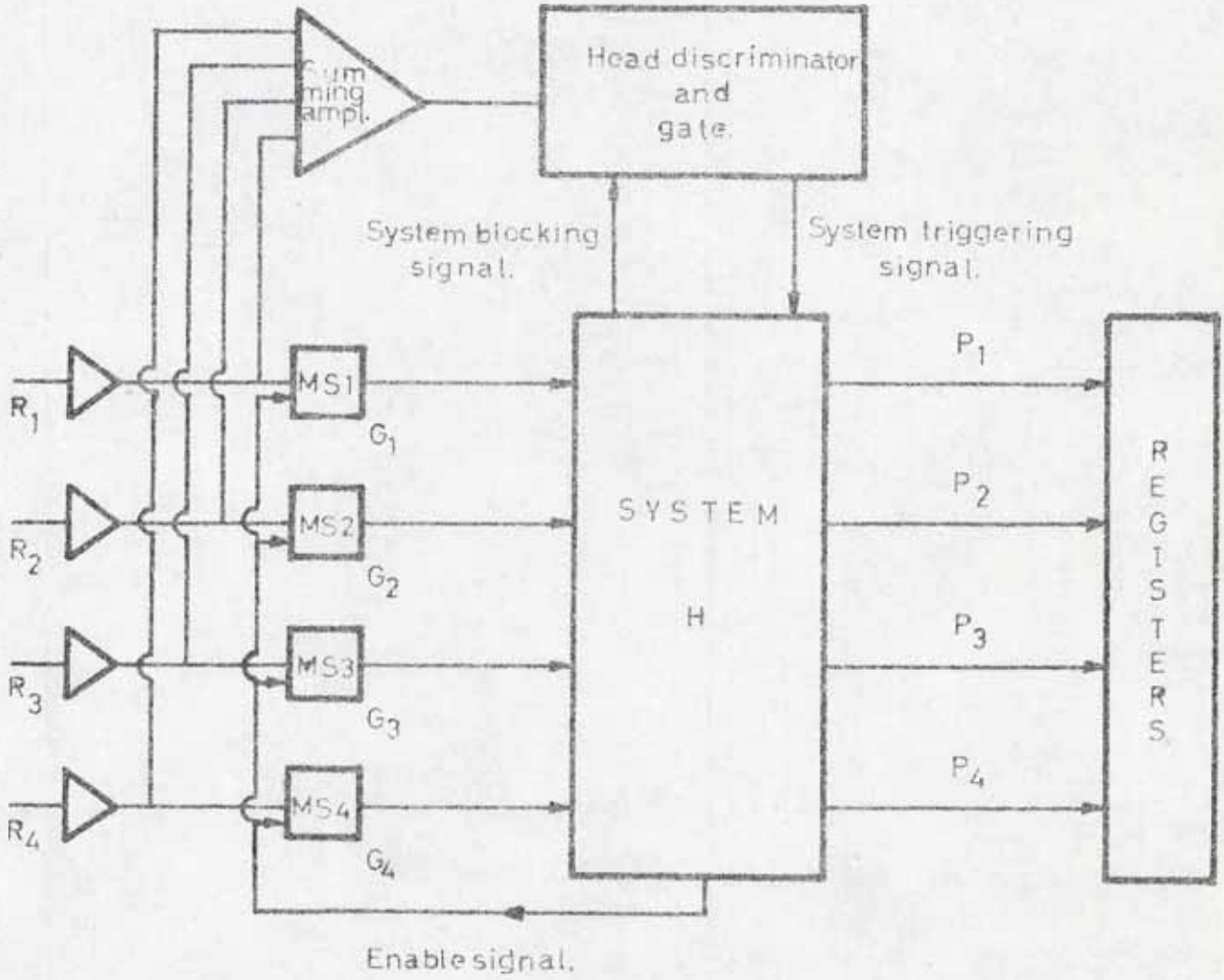

Fig. 4.1. Working principle for deadtime considerations.

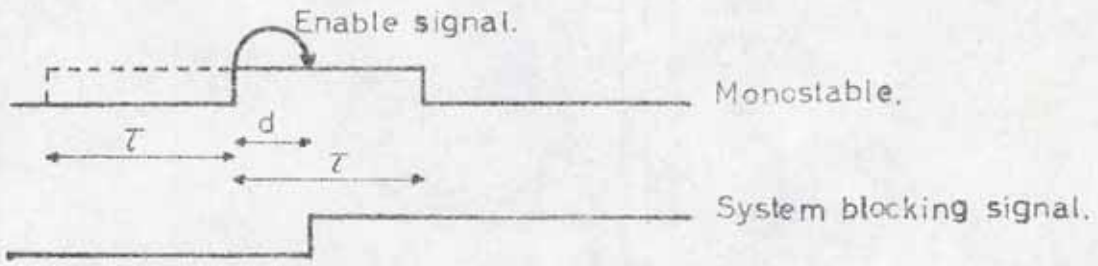

Fig.4.2. Blocking signals after arrival of a pulse.

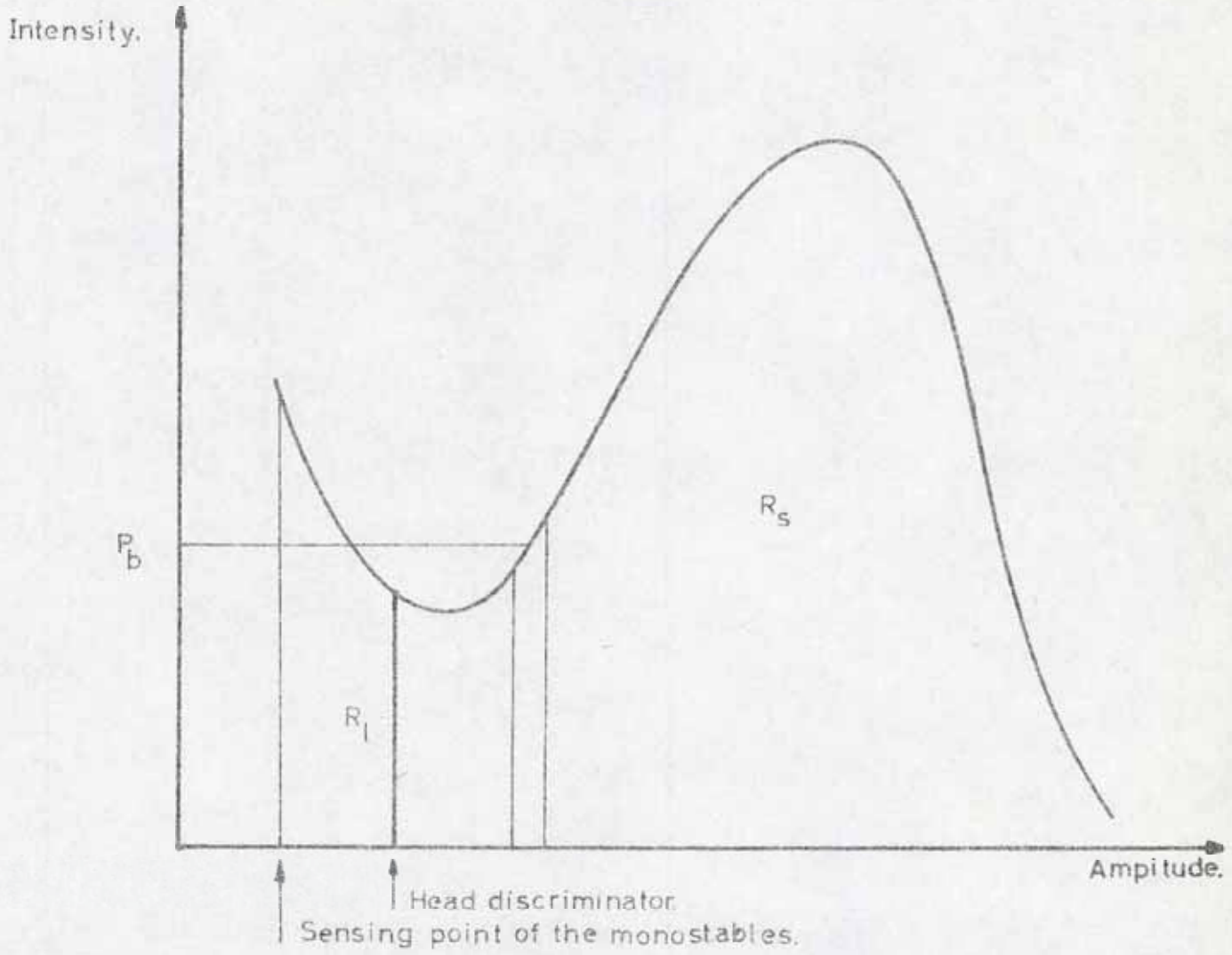

Fig 43. Amplitude distribution with discriminator settings.

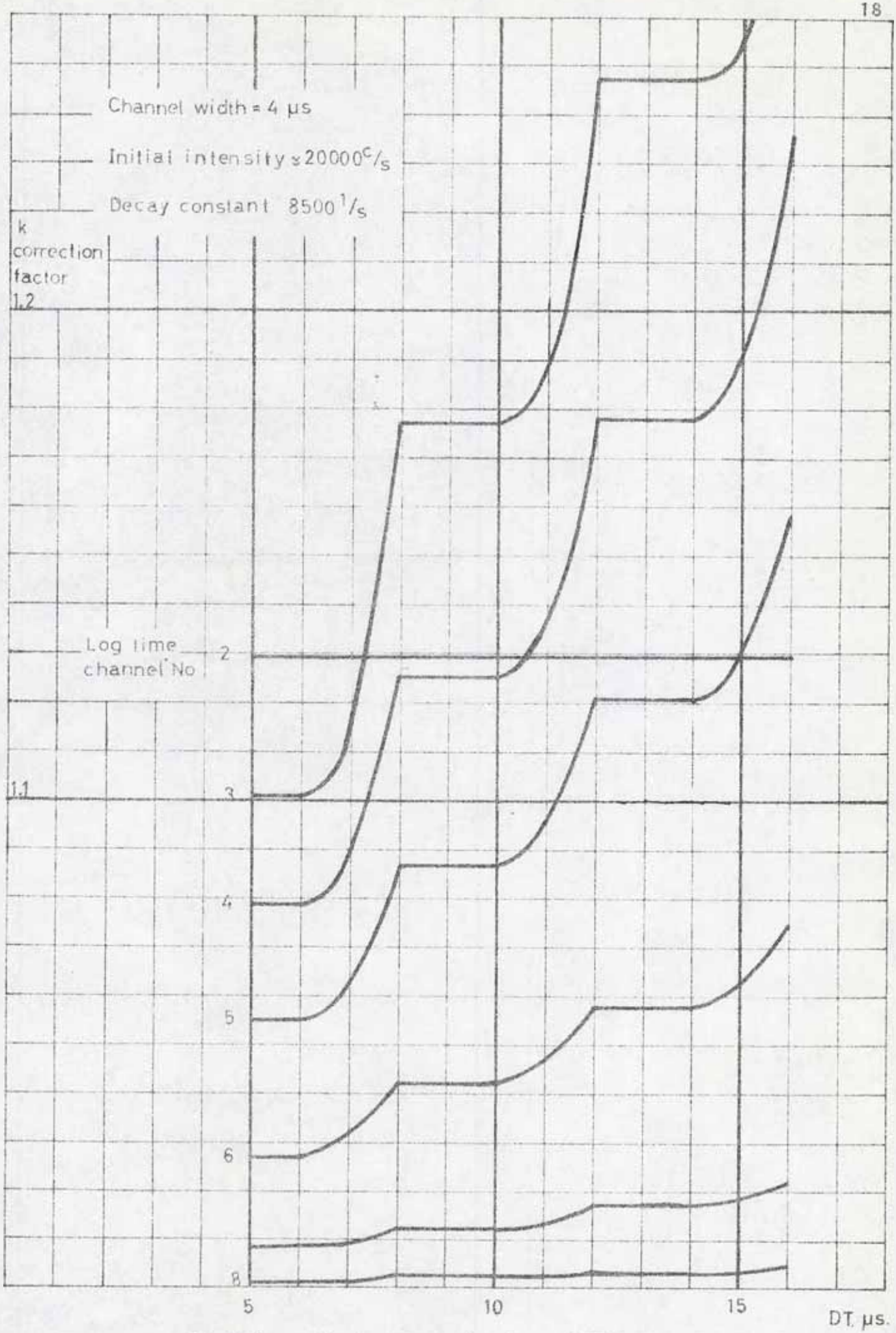

Fig 44 Correctionfactor as a function of DT.

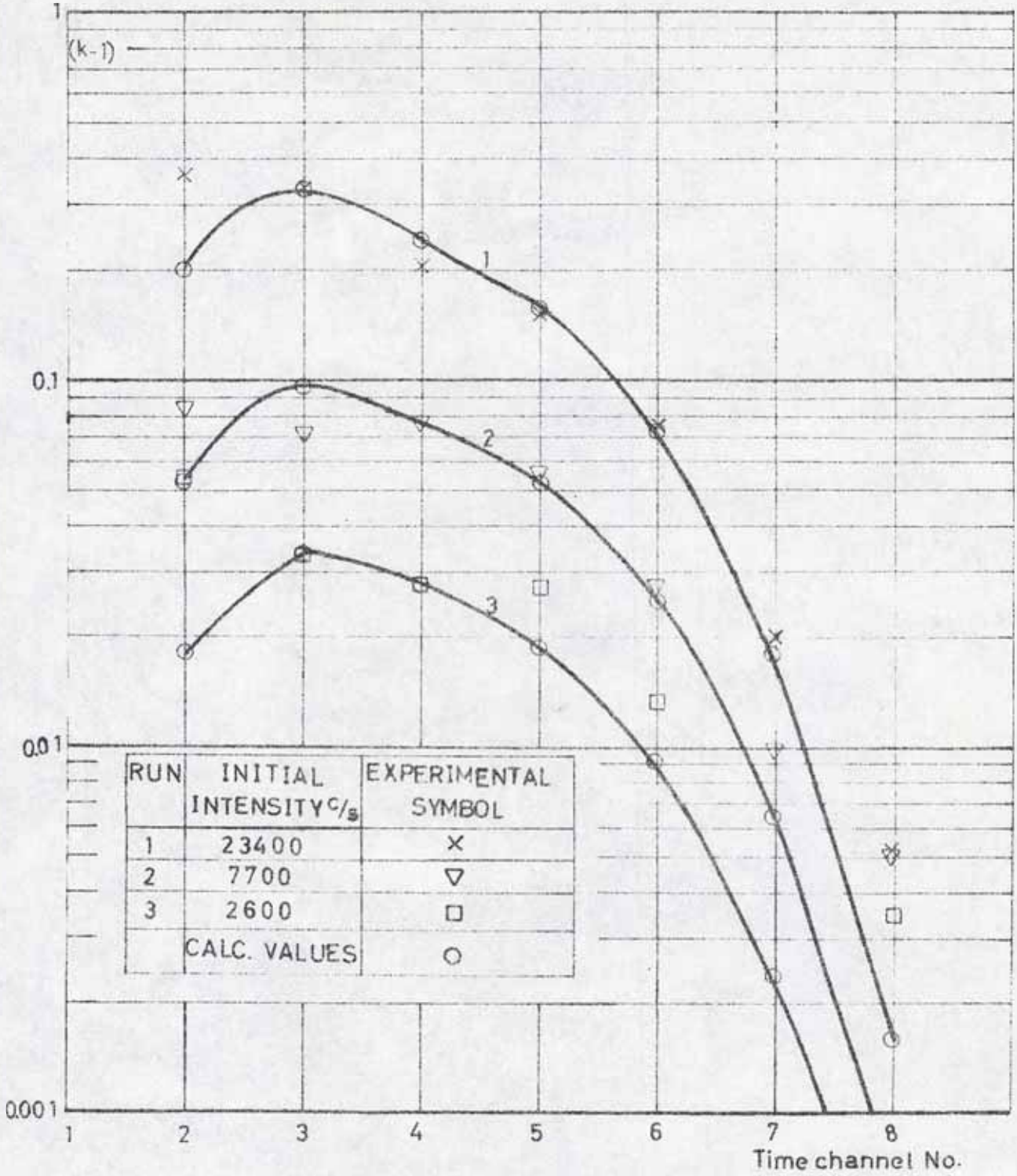

Fig. 45. Check of the deadtime correction.

5. BACKGROUND SUBTRACTION

The detectors are thin glass-scintillators (1/8"x 1 1/4") loaded with Li-6 as the neutron sensing part. We have chosen these detectors in order to compensate the low intensity of the neutron source with high sensitivity of the detectors. As a drawback we have that the scintillators have a sensitivity of gamma radiation, which can not be neglected. We have therefore tried to keep the gamma intensity as low as possible. Thus, the neutron shield is made of boron carbide, and aluminium has been used as construction material through most of the experimental area.

An investigation on which materials contribute to the background radiation with large time constants has been done by two students (Lars Moberg and Kåre Olsson) and their result is summarized in table 5.1. Such a background will cause a variation during an experiment and during a series of experiments. The time of one experiment is some hours and a series takes weeks. It gives, however, no measurable variation during the measuring cycle which is in the order of milliseconds.

There is also a faster variation. In figure 5.1 and 5.2 the amplitude and time distributions of a representative experiment is shown. Only the most interesting channels have been plotted. The time dependence of the background can be seen in figure 5.2, since the main part of the time variation of amplitude 3 origins from the background. If we compare this with amplitude channel 13, which mainly comes from the neutron distribution, we find that the background has a time dependence, not constant and not proportional to the neutron distribution. It is therefore not correct to assume, which often is done, that the background is constant.

The main contributions to the background shown in the figures can be divided into four groups:

1. Capture gamma in the experiment (mainly 2.3 MeV from hydrogen).
2. Capture gamma in the shielding.
3. Capture and decay gamma in construction materials and in the surroundings.
4. Noise in the system.

The first point is no problem if we are interested only in the fundamental mode. The second contains one part proportional to the outgoing neutron stream from the experiment and one part depending on neutrons scattered back from the surroundings. The third contains all energies, has rather low intensity, but will give a limit on how far we can follow the neutron decay. The fourth, where we include noise from the crystal and all electronic phenomena, contributes in the low part of the amplitude distribution, partly because it overlaps the other effects and partly because it is added from all of the detectors in the analog summing amplifier.

The ordinarily used methods to avoid background are to discriminate either directly on the amplitude distribution or on some quantity related to the shape of the pulse. The first of this is usable only if the ratio between the neutrons and the background is high for pulses above the threshold. The other will give a more complicated structure to every detector line. Another method is to measure the background with a scintillator that is insensitive to neutrons. There are two drawbacks of this method. Firstly, we must have the background detector in a position symmetric to the neutron detector close to the moderator, secondly this detector line must be adjusted to give exactly the same amplification as the neutron detector. This is not easy because at high intensities there will be baseline shifts, and at low intensities the statistics and the drift of the electronics come into the picture. For these reasons we have tried to do an analysis of the amplitude distribution in order to subtract the background directly.

Figure 5.3 is an experiment with no moderator but with all other parameters the same as in the other experiments. So, with the exception of backscattered neutrons that penetrate the shielding, this experiment contains only the background distributions. We conclude from the figure that the background can be divided into two parts, one transient in the lower part of the spectrum and one exponential, which covers the main part of the distribution. If this figure is compared to figure 5.1 one can see that within the neutron peak, an exponential is a good approximation to the background. The problem is now to determine the amplitude of this exponential. This could be done in those parts of the spectrum where the neutrons can be neglected, vz. in the high amplitude region. Two drawbacks make this method uncertain. Firstly, the accuracy will be low owing to the low pulserate in this region, secondly pile - up contributes.

We must therefore put some information about the neutrons into the picture. The amplitude distribution of the neutrons may, as can be seen in figure 5.1, be approximated by a gaussian distribution. A more careful investigation shows that a correction has to be incorporated in order to account for a small distortion in the distribution. We therefore approximate the distribution with

$$P(I) = A \exp\left\{\sigma \left(\frac{I - I_m}{x_o + k_c \cdot (I_m + 0.5)}\right)^2 + \gamma \left(\frac{I - I_m}{x_o + k_c \cdot (I_m + 0.5)}\right)^3\right\}$$

$$+ B \exp\{-\alpha I\} \qquad (5.1)$$

where A, B, σ, γ and α are constants and

x_o is the lower limit of the amplitude range converted (V).

k_c is the conversion factor (V/channel).

I is the amplitude in number of channels.

I_m is the amplitude where the neutron distribution reaches the maximum value.

We write the distribution in the form shown above in order to have constants that do not depend on baseline displacements. As x_o and k_c are determined by the settings of the converter we have six constants to determine. As we have only about 25 measured values to our disposal in one experiment, we cannot expect to get good estimates on all these constants from one amplitude distribution, so we divide the estimation into three steps:

1. α is determined from a series of background experiments.
2. σ and γ are calculated from a distribution with as low background as possible. Among a long series of experiments it is always possible to find a good distribution for this purpose.
3. Free to be determined are now only A, B and I_m. These are determined from the actual distribution with the other parameters fixed.

We have left I_m to be determined in the last step because we have found

that I_m has a variation through a high intensity experiment that cannot be neglected. In a low intensity experiment, however, this parameter is nearly constant. Forthis reason we have incorporated the possibility to determine I_m from that time channel which has the highest number of registrations and then keep it constant through this experiment. In this case we gain statistic accuracyby the fact that we estimate only two parameters. Through the whole calculation we use the leastsquares method to determine the parameters.

As an example of the results of a calculation, the maximum amplitude of the neutron distribution is plotted in figure 5.4 together with the corresponding value of the background distribution. The actual moderator is 8.8 cm high and the measured time range is delayed 0, 128, and 256 microseconds after the end of the neutron burst. From this figure we can see that the background is low in the main part of the experiment but that it reaches a value of about 0.8 times the maximum neutron amplitude at the endpoint. If we compare the neutron curves we find that they all have the same asymptotic shape and conclude that the method has worked well even in this case.

In these experiments we have also a detector that is loaded with Li enriched to 99.999 % Li-7 according to the manufactor. The result from this detector in the actual case is plotted in figure 5.5. Experiments 68051002 and 68051003 agree rather well with the results in 5.4. There is, however, a difference in experiment 68051001. This may be caused by the transient part of the background, since a comparison of the amplitude distributions shows that the agreement is bad in the transient part. The neutron intensity is, however, high in this region and the background is not so important. It should be pointed out that relations between the different experiments agree very well with those of figure 5.4 for the last channel.

Table 5.1 Dominating gamma radiation in the laboratory.

D-D neutrons			D-T neutrons		
Energy	Half-life	Material	Energy	Half-life	Material
MeV			MeV		
0.51	13 h	Cu	0.51	10 m 13 h	Cu
0.83	5.1 m	Cu	0.84	9.5 m	Al
0.84	291 d	Fe	0.85	2.6 h	Fe
1.04	5.1 m	Cu	1.02	9.5 m	Al
1.46	stable	K	1.37	15 h	Al
1.75	stable	(Bi)	1.73	3.5 h	(Fe)
1.78	2.3 m	Al	2.25	14 h	(Sn,Fe)
2.16	stable	(Sn)	2.75	15 h	Al
2.60	stable	(Bi)			

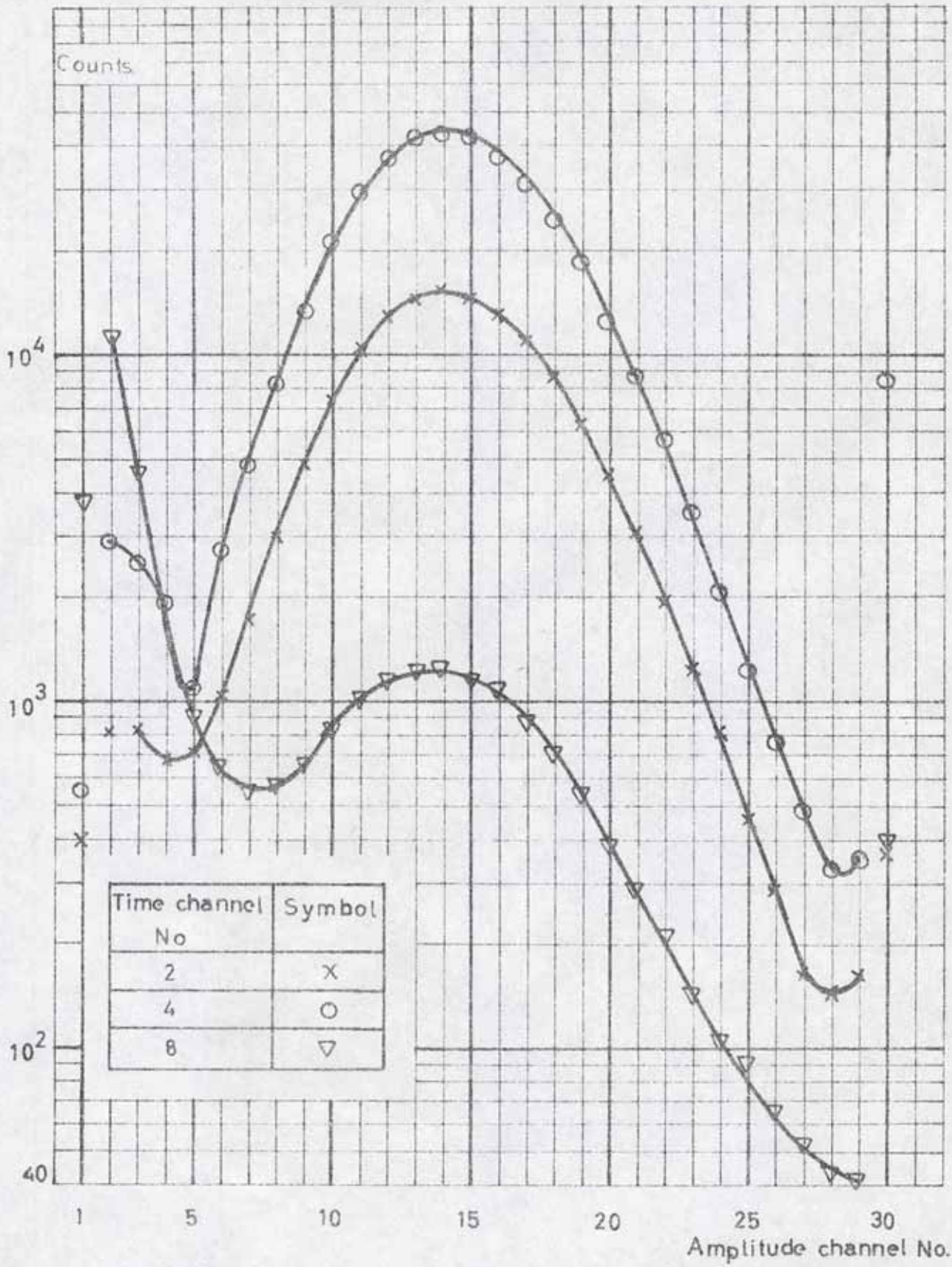

Fig. 5.1. Some amplitude distributions from experiment 68051002 det.1.

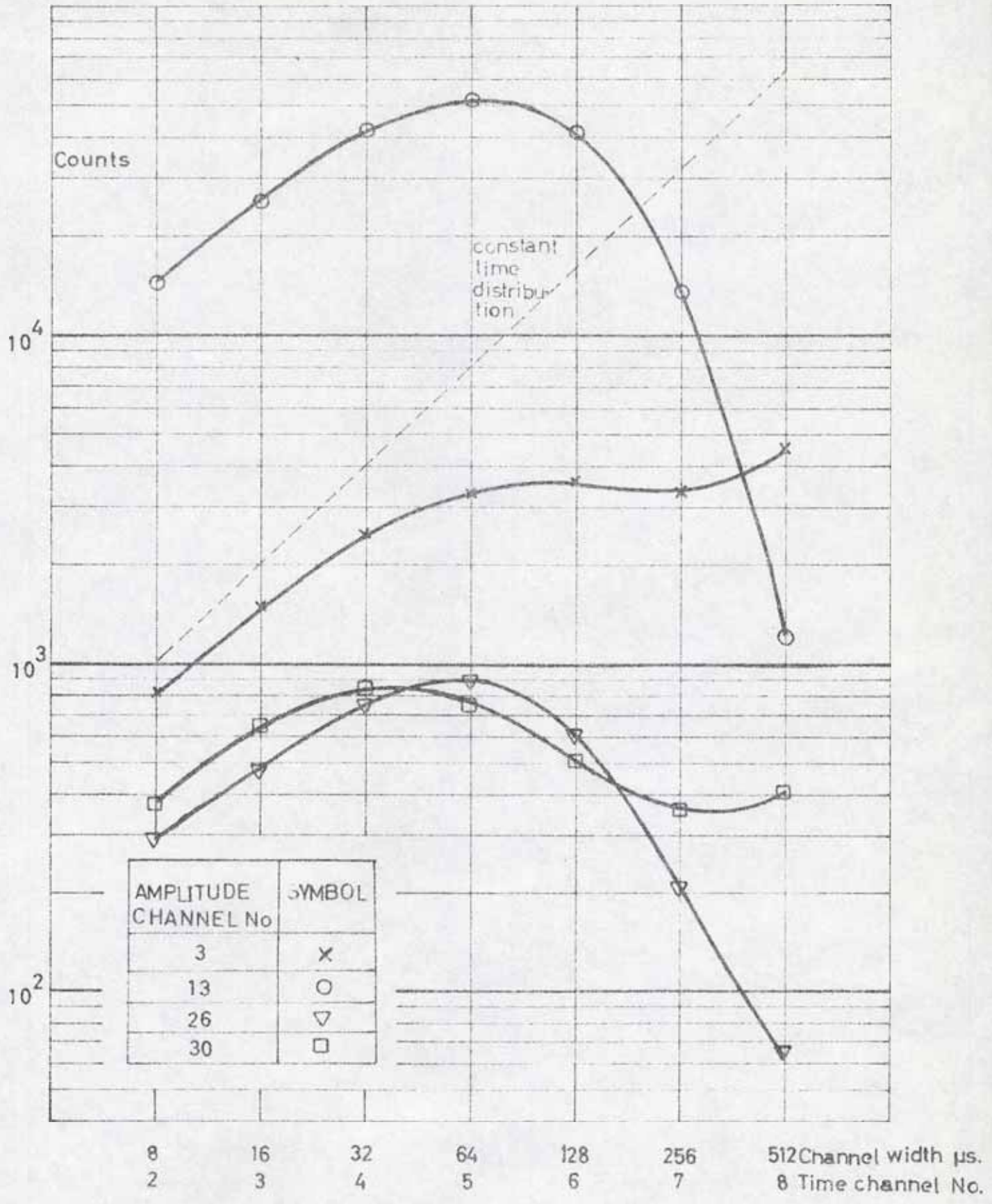

Fig. 5.2. Some time distributions from experiment 68051002 detector 1.

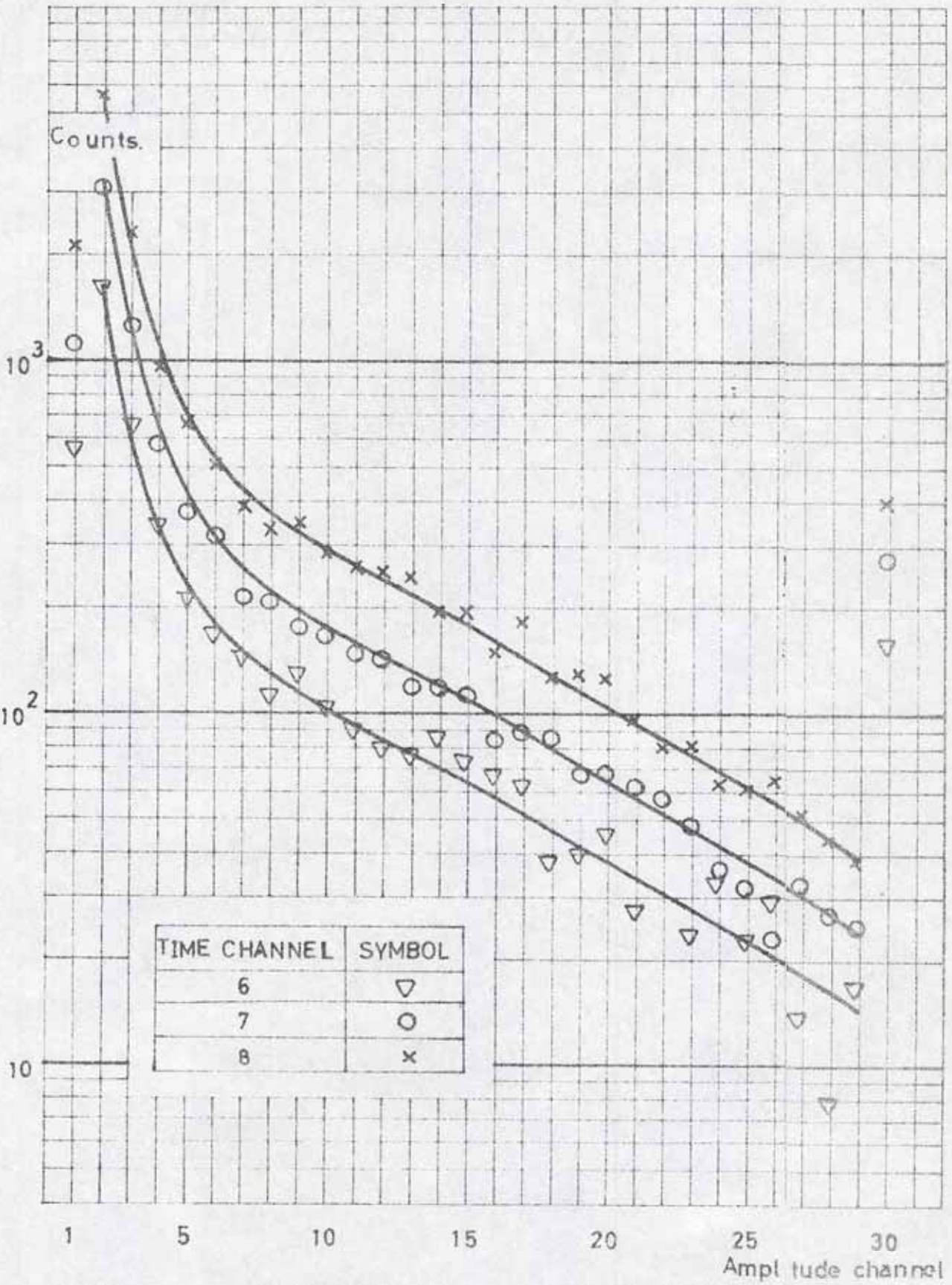

Fig.5.3. Background distributions from experiment 68051702 detector 1.

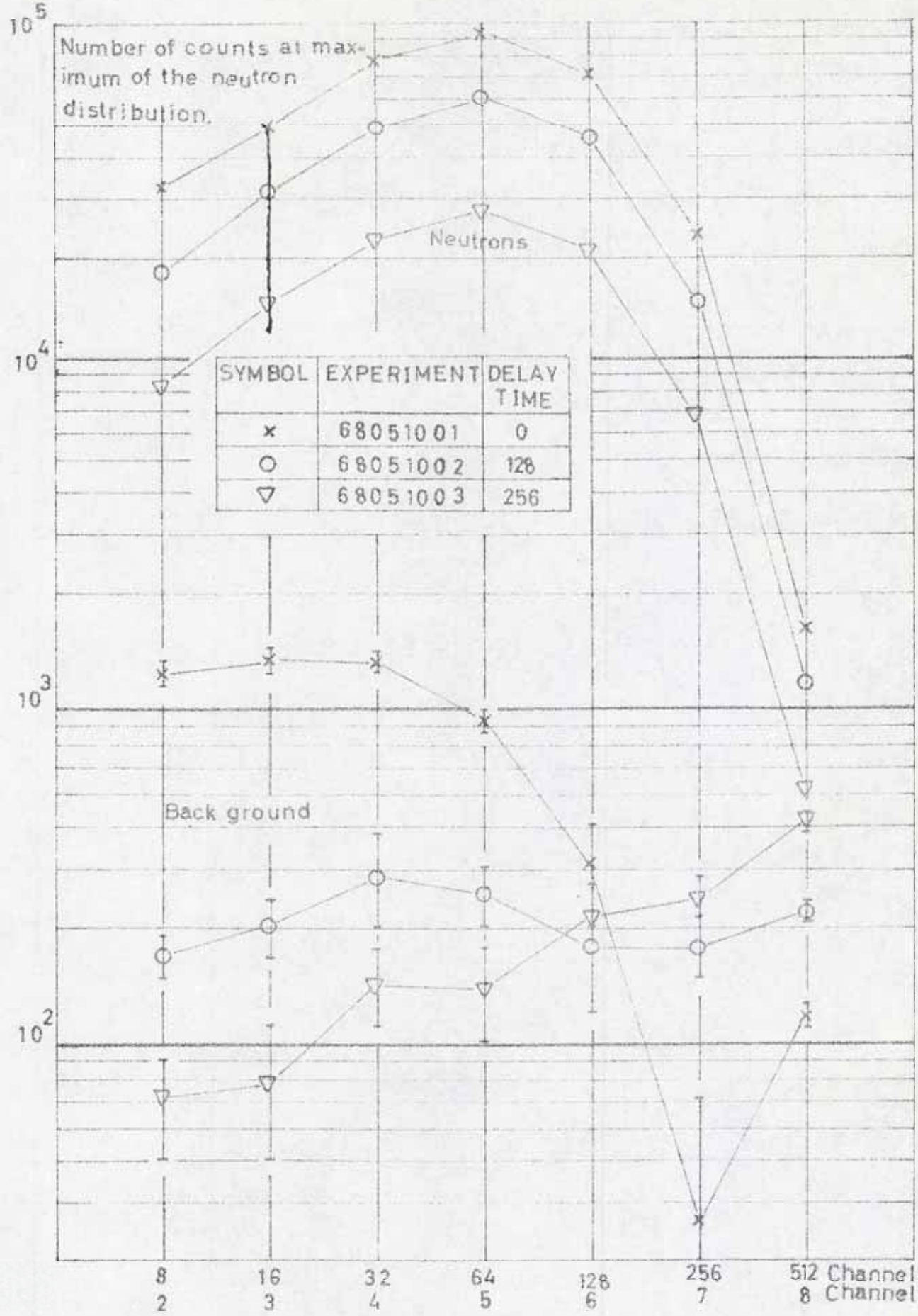

Fig.54. Maximum neutron pulsedistribution and corresponding number of background pulses for experiment 68051001-68051003 detector 1.

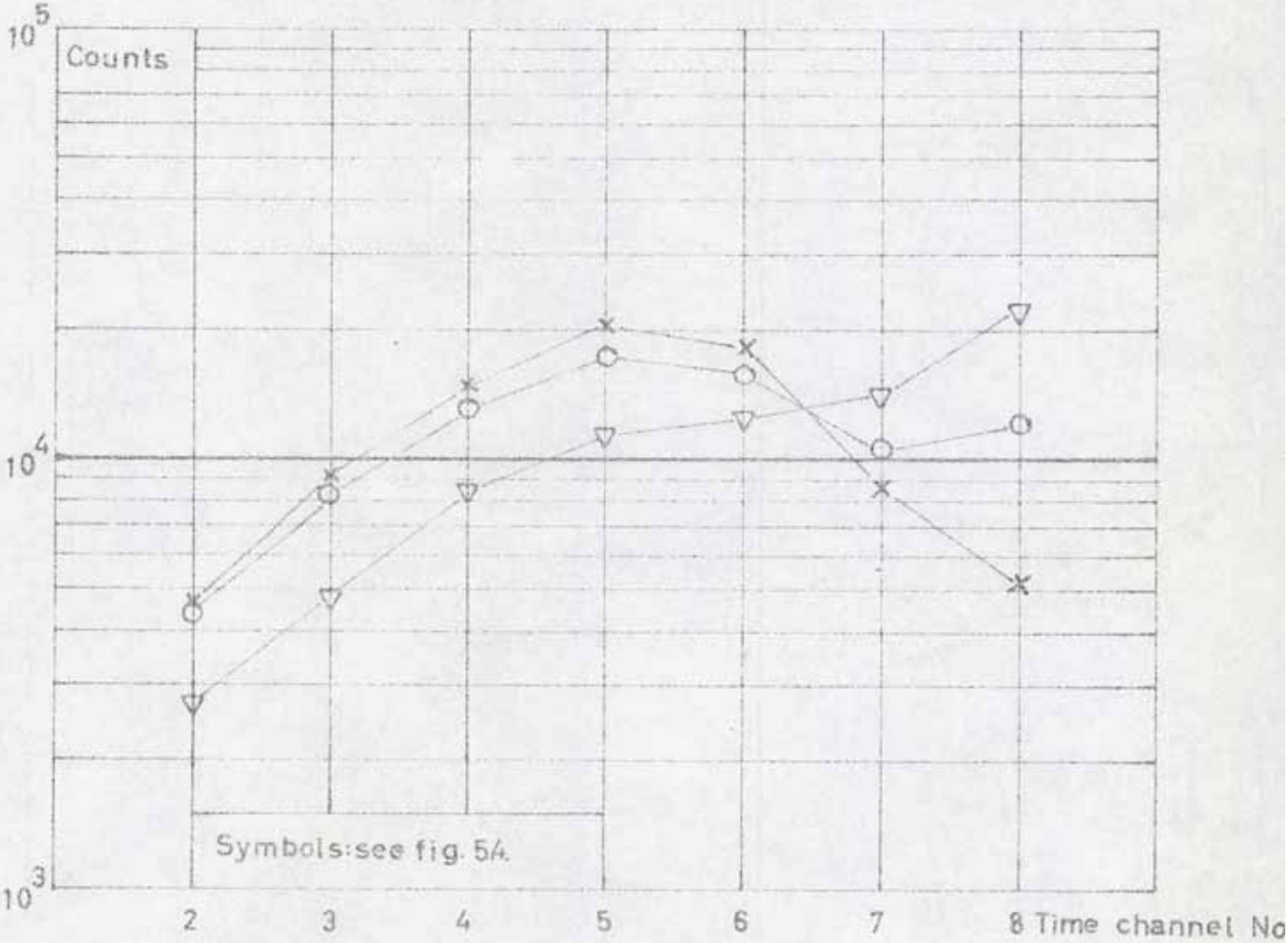

Fig. 55. Background according to detector 3.

6. THE DETERMINATION OF DECAY CONSTANTS.

The number of counts (P_i) in a channel i of a time analyser is, if the channel begins at time t_i and ends at time t_{i+1} and the input has a pure exponential time dependence with a decay constant λ and amplitude A:

$$P_i = \int_{t_i}^{t_{i+1}} A\, e^{-\lambda t}\, dt = \frac{A}{\lambda} \left(e^{-\lambda t_i} - e^{-\lambda t_{i+1}} \right) \qquad (6.1)$$

$$(i = 1, 2, \ldots)$$

Usually

$$t_{i+1} - t_i = t_c \qquad (6.2)$$

where t_c is a constant channel width. With the transformation

$$x = e^{-\lambda t_c} \qquad (0 \leqslant x \leqslant 1) \qquad (6.3)$$

we have

$$P_i = \frac{A}{\lambda}\, x^i \,(1 - x) \qquad (6.4)$$

Another alternative is to do a transform to logarithmic time scale

$$t_i = t_c \cdot 2^{i-1} \qquad (6.5)$$

from which

$$P_i = \frac{A}{\lambda}\, f_i$$

$$f_i = x^{2^{i-1}} \left(1 - x^{2^{i-1}} \right) \qquad (6.6)$$

For small values of the exponent we have

$$P_i = A\, t_c\, 2^{i-1} \qquad (6.7)$$

A sketch of the function f_i is given in figure 6.1.

The problem of measuring fundamental decay constants is that in the beginning we have a time distribution containing higher modes. In the end we have background and problems with low intensity. The advantage of using equation 6.6 instead of 6.4 is then that we more effectively cover the whole range of decay constants with few time channels.

The transformation of equation 6.5 can be done directly in the time analyser but in order to avoid a modification of this we have put a converting matrix in the buffer memory. With the transformation chosen as equation 6.5 the logics of the matrix are rather simple. We then look upon it as a data reduction, and the merits of it are that we can reduce 256 linear channels to 8 logarithmic without losing any important information.

We are now faced with the problem to determine λ or x from the distribution given by the experiment. We will here report three methods, two with differential and one with integral structure.

The first method is simply to divide two adjacent channels with each other. We then have

$$\lambda_i = \frac{1}{t_i} \log \left\{ \frac{1}{2} \left(\sqrt{1 + 4 R_i} - 1 \right) \right\} \qquad (6.8)$$

and if the information in each channel is Poisson distributed

$$\sigma_{\lambda_i} = \frac{1}{t_i \sqrt{P_i}} \cdot \frac{2 \sqrt{R_i (1 + R_i)}}{\sqrt{1 + 4 R_i} \left(\sqrt{1 + 4 R_i} - 1 \right)} \qquad (6.9)$$

where $R_i = \dfrac{P_{i+1}}{P_i}$

σ = the standard deviation

$t_i = t_c \cdot 2^{i-1}$

The relative standard deviation is shown in figure 6.2. The ordinate is chosen to make the standard deviation of Peierl's method equal to 1. The standard deviation is rather high and the only merit of this method is that there is no corre-

lation between every second channel.

The second method is the summation method. If we sum the equation 6.6 from i to N we get

$$S_i = \frac{A}{\lambda} \left(g_i - g_{N+1} \right)$$

$$g_i = \sum_{j=i}^{N} f_j + g_{N+1} = x^{2^{i-1}} \tag{6.10}$$

$$S_{N+1} = x^{2^N}$$

From these we have

$$\lambda_{i,j} = -\frac{2}{(2^i - 2^j)\, t_c} \log \left\{ \frac{S_i + E}{S_j + E} \right\} \qquad (j < i) \tag{6.11}$$

where $E = \frac{A}{\lambda} g_{N+1}$

and if we can neglect E

$$\sigma_{\lambda_{i,j}} = \frac{2}{t_c (2^i - 2^j)} \sqrt{\frac{1}{S_j} - \frac{1}{S_i}} \tag{6.12}$$

The standard deviation for i=1 is drawn in figure 6.3. We have used the same normalization as in figure 6.2. We find that the standard deviation is low and that the available channels can be chosen to give accurate information from all channels. The drawback is that the different values of lambda are not independent, and higher modes and background may, in a systematic way, have an influence on all of the lambda values.

The endterm E is small and can easily be taken into account by solving 6.11 iteratively. Higher modes are studied in figure 6.4, from which

the shift in the calculated λ, ($\Delta \lambda$) can be found.
The number of counts coming from the higher mode (m_o) and those coming from the lower one (n_o) together with the corresponding decay constants (λ_2 and λ_1) are supposed to be known. The formula given in the figure is correct only for small values of m_0/n_0. It can be seen from the figure that the shift can be high and that it has an influence on all the calculated values of λ.

The third method uses a correlation between two experiments 1 and 2, which are different in respect to the amplitudes of the joining modes. If we assume that two modes are included in the experiments, we can write

$$R_{1,i} = a_{11} f_{1,i} + a_{12} f_{2,i} + \delta_{1,i}$$

$$R_{2,i} = a_{21} f_{1,i} + a_{22} f_{2,i} + \delta_{2,i} \qquad (6.13)$$

where R = the number of pulses stored in the actual experiment and time channel

a_{ij} = the j:th amplitude of the i:th experiment

f = the corresponding functions as defined in eq. 6.6

δ = the deviations from the measured values.

We can easily transform equation 6.13 to 6.14

$$f_{1,i} = \alpha_{11} R_{1,i} + \alpha_{12} R_{2,i} - \varepsilon_{1,i}$$

$$f_{2,i} = \alpha_{21} R_{1,i} + \alpha_{22} R_{2,i} - \varepsilon_{2,i} \qquad (6.14)$$

where the matrix of α is the inverse of a and ε is the deviation from the functions f_i. ε and δ are connected by the transform α. We multiply now this equation with $f_{1,i}$, $R_{1,i}$ and $R_{2,i}$. The equations for the sums are then

$$\Sigma f_{1,i}^2 - a_{11}\Sigma f_{1,i}R_{1,i} - a_{12}\Sigma f_{1,i}R_{2,i} = \Sigma \varepsilon_i^2$$

$$\Sigma f_{1,i}R_{1,i} - a_{11}\Sigma R_{1,i}^2 - a_{12}\Sigma R_{1,i}R_{2,i} = 0 \qquad (6.15)$$

$$\Sigma f_{1,i}R_{2,i} - a_{11}\Sigma R_{1,i}R_{2,i} - a_{12}\Sigma R_{2,i}^2 = 0$$

We have here assumed that the correlations between ε and the R_j:s are zero. We can write an identical system of equations for the second equation in 6.14 and will therefore in the following drop the first index of f. We normalize the elements of 6.15 by introducing the following quantities

$$D_{12} = \frac{\sum_i R_{1,i}R_{2,i}}{\sqrt{(\sum_i R_{1,i}^2)(\sum_i R_{2,i}^2)}}$$

$$D_j = \frac{\sum_i f_i R_{j,i}}{\sqrt{(\sum_i R_{j,i}^2)(\sum_i f_i^2)}} \qquad (6.16)$$

$$d = \frac{\sum_i \varepsilon_i^2}{\sqrt{\sum f_i^2}}$$

We shall now seek for solutions where d is minimum. If the determinant

$$\begin{vmatrix} 1 & D_{12} \\ D_{12} & 1 \end{vmatrix} \neq 0$$

there will always be a solution for d (x) which can be calculated from

$$\begin{vmatrix} 1-d & D_1 & D_2 \\ D_1 & 1 & D_{12} \\ D_2 & D_{12} & 1 \end{vmatrix} \qquad (6.17)$$

This is a conic section from which we explicitly can get d as

$$d = 1 - \frac{(D_1 + D_2)^2}{2(1 + D_{12})} - \frac{(D_1 - D_2)^2}{2(1 - D_{12})} \qquad (6.18)$$

As D_1 and D_2 are functions of x we can with a computer calculate d (x) and seek the maxima. It should be pointed out that the quantities D_{12}, D_1, D_2 and d are close to 1 in a practical case. d must therefore be calculated with great numerical care.

As soon as the two values of x are determined, we can easily go back, calculate the a :s from 6.15, and do an inversion in order to get the amplitudes (a_{ij}). The resulting quantities are therefore the two lambda values and the four amplitude values.

We have only treated the case of two lambdas, because in the main part of our experiment we have a strong fundamental mode mixed with a rather small part of the higher modes. The latter is in our case more or less a correction. It is, however, rather simple to extend the method by introducing more experiments into the analysis in order to get more lambda values and a more correct fundamental mode. The result of a calculation with this method will be found in chapter 8.

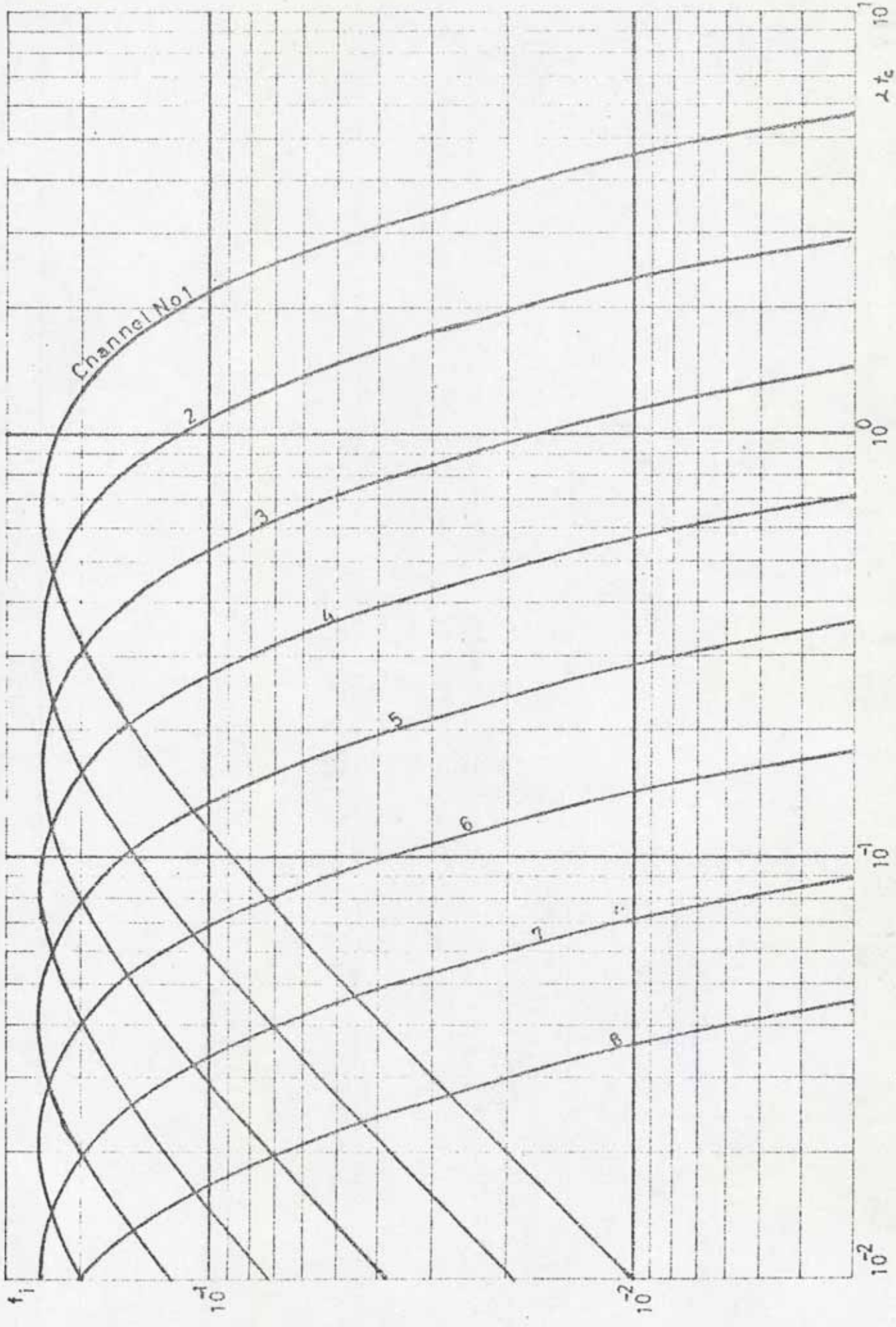

Fig. 6.1. The functions f_j.

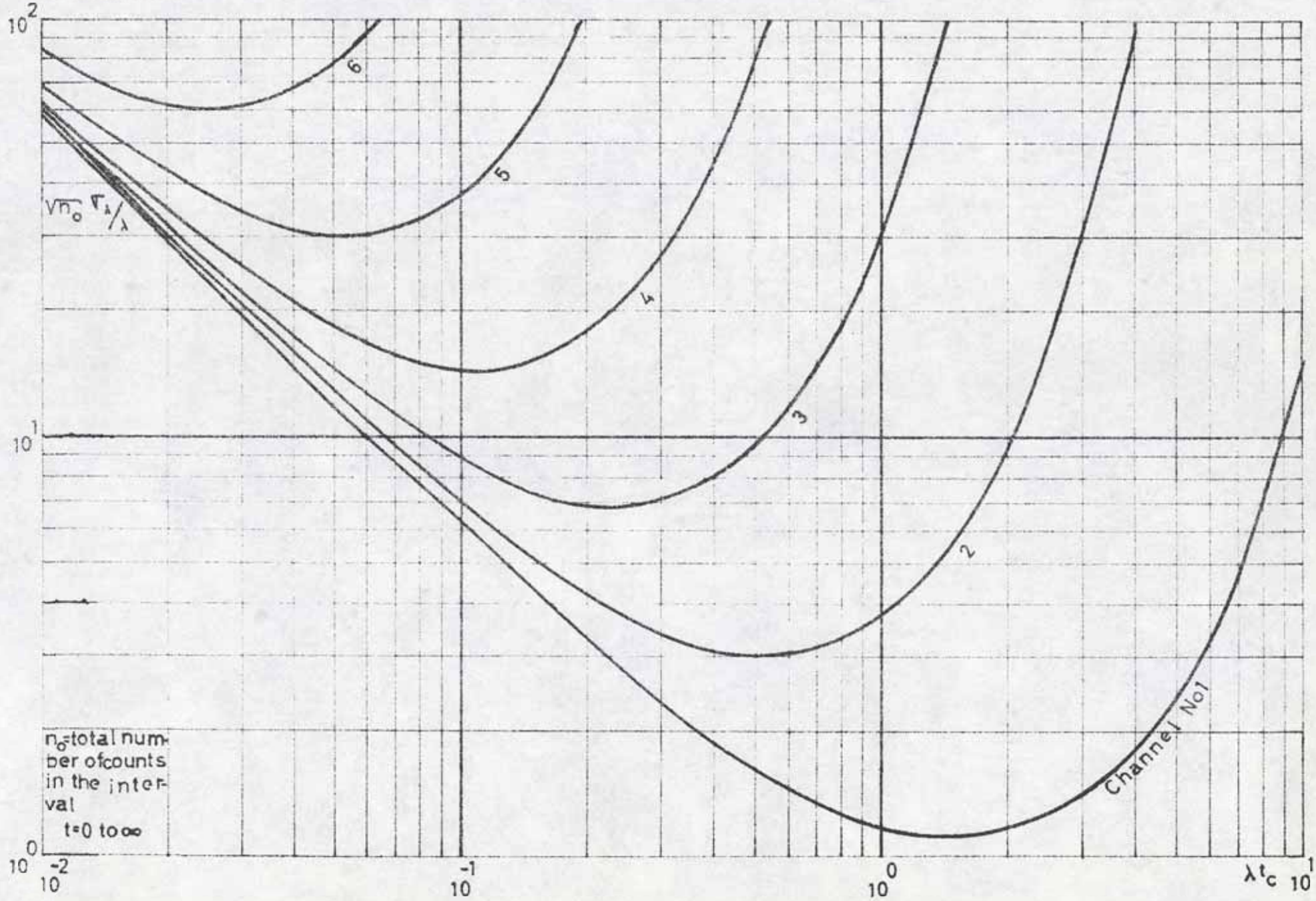

Fig.6.2. The standard deviation of the first method.

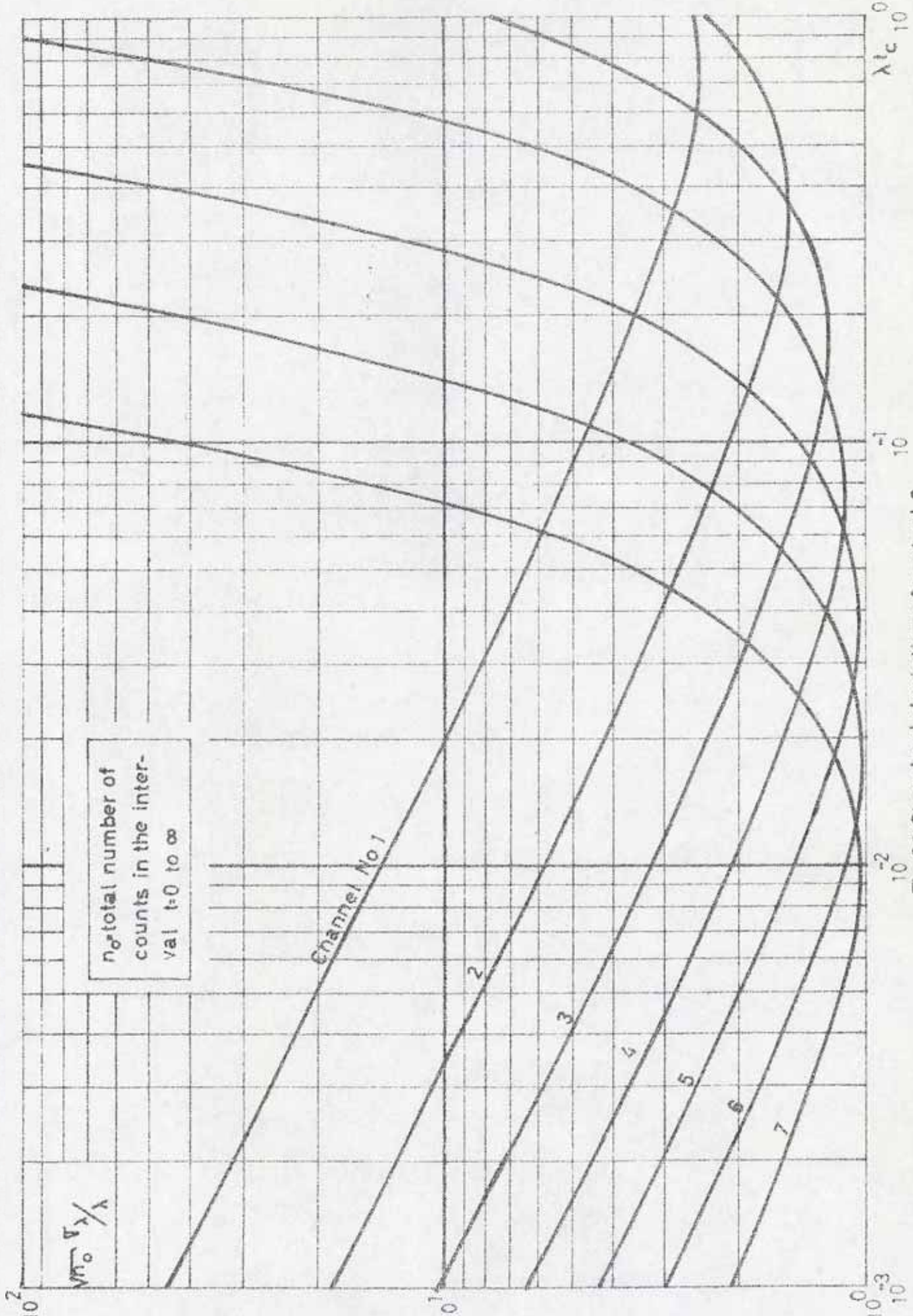

Fig.6.3.Standard deviation of method 2.

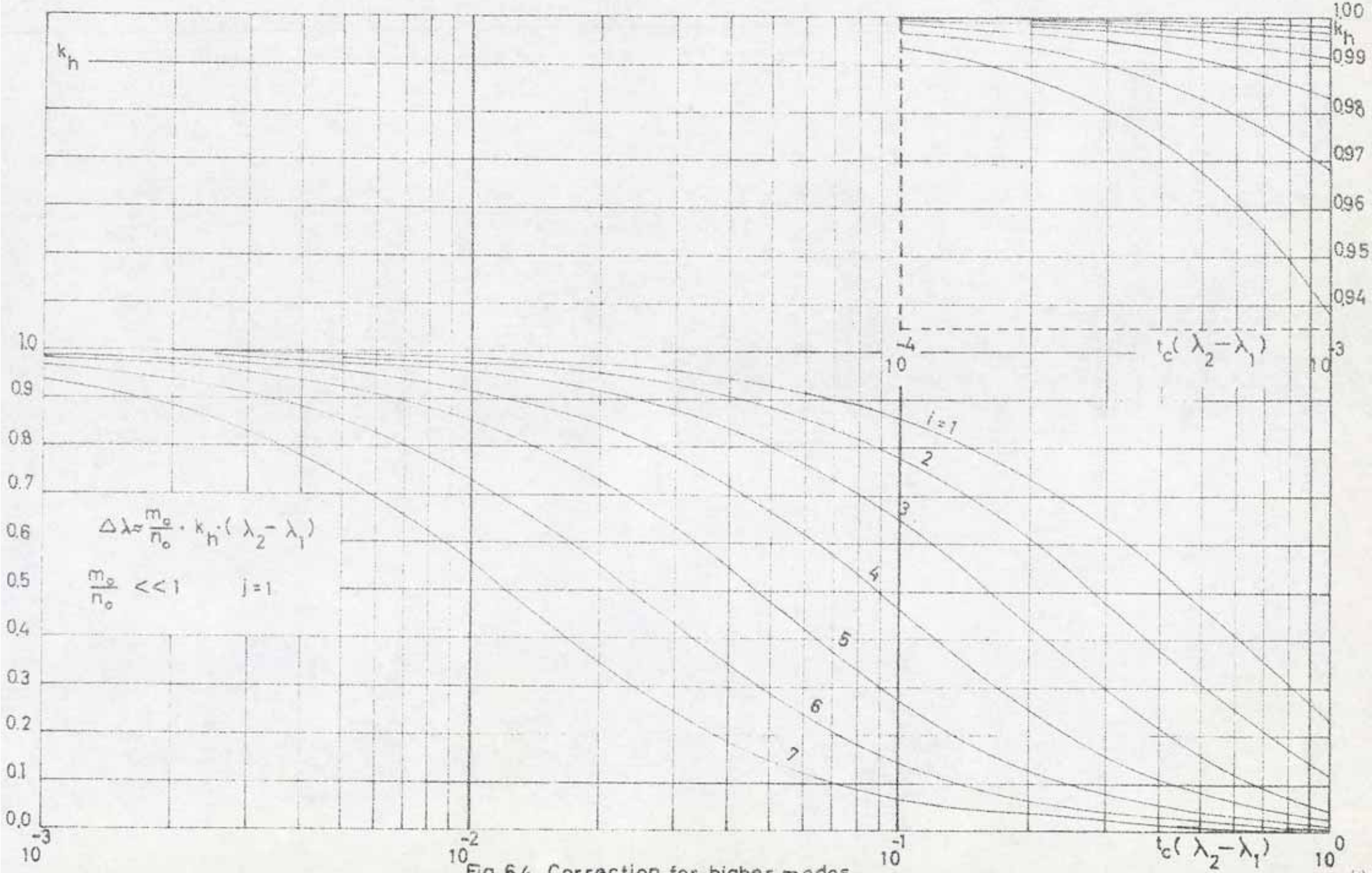

Fig. 6.4. Correction for higher modes.

7. DATA HANDLING.

The output from each experiment is a paper tape containing 1024 values and approximately 40 manually read parameter values. The analysis of these data is done on an IBM computer (system 360 model 50 H). The actual programs are listed in table 7.1. The philosophy in the organization of the programs and the files has been to achieve a system with comparable small parts independent of each other. The merit of this is that different parts of the analysis can be tested separately, which is valuable both during the test period of the program and during the actual analysis. Moreover, some parts of the analysis can easily be exchanged in order to take into account developments in methods and equipment.

The drawback is that the result has to be stored between the programs and that every job step in the computer has a rather long initial time lag before the control is transferred to the actual program.

The intermediate results are stored with the direct access method. The files are listed in table 7.2. This method is very valuable because we can stop the analysis at a predetermined point, check the results and recompute only those parts where changes have to be done. Files 10 and 11 are parameter files used through the whole sequence of programs, 13 and 14 are files for the entire spectrum, 12 contains the time distribution after background subtraction, 15 and 16 are result files.

The first program, REMSINP, checks the tape very carefully and reads the information. We do not have any parity check on the tape and have therefore chosen a code where the punching sequence can be checked before and during every number. PARIN reads the parameters from punched cards. The maximum number of counts in a channel is 99, 999. Sometimes it is necessary to have a higher number in some channels. With OWCO we can correct for this. The rest of the programs are directly related to the methods outlined in this report. In table 7.1 references are given to those equations which form the main part of the respective program. The program language is mainly PL/1 and in some cases FORTRAN.

Table 7.1 Programs.

Program	Method	Input file	Output file
REMSINP	Experiment input	-	10, 13
PARIN	Parameter input	-	10, 11
OWCO	Owerflow correction	13	13
DTFAKT	eq. 4.3	13	11
DECORR	eq. 4.3	11, 13	14
COAPCO	eq. 4.4 eq. 4.5	14	14
BAGMSU	eq. 5.1	14	12
SIMLAM	eq. 6.8	12	15
SUMLAM	eq. 6.11	12	15
CORLAM	eq. 6.18	12	16

Table 7.2 Data files.

File no.	Number of records	Records per exp.	Variables per record	Attributes
10	32	1	32	Bin fixed (31)
11	32	1	32	Bin float(single)
12	128	4	16	"
13	128	4	256	Bin fixed (31)
14	128	4	256	Bin float(single)
15	128	4	16	"
16	128	4	16	"

8. RESULTS.

The differential evaluating methods mentioned in chapter 6 have been used through the whole experiment in order to check it for systematic errors. The outcome from it is the same as from the correlation method but because this has better accuracy and gives better possibilities to survey the whole experimental series, we will limit the discussion to the results from this method.

The main input features of the series are collected in table 8.1. The channel widths are chosen to match the different decay constants in order to get the lowest possible standard deviation as given by figure 6.3. The neutron burst is long compared to the half-life in order to get the fundamental mode developed as much as possible. The ratio between the fundamental and the higher modes increases with increasing burst length, but the ratio between the fundamental mode and the background from outside neutrons and gammas goes in the opposite direction. The waiting times can be altered in steps of 32 times the channel width. Owing to the low intensity of the neutron source, we are limited to a few of the lowest settings.

The results of a time correlation on this experimental series are collected in figure 8.1. We observe that the scale of the ordinate is altered for each experiment. We can first conclude that the agreement between the points for each detector is good. We have also plotted the result of the smoothing effect of a three parameter fit for each detector and can see from these that the consistency through the series is good.

The most striking effect is, however, the difference between the detectors. Detector 1 was placed in a position where the contribution from the second radial mode should be minimal. Detector 2 was placed at the maximum of the first fundamental mode. One would therefore expect that detector 2 is more influenced by higher modes than detector 1. This seems also to be true. There are more variations in the values of detector 2.

The difference between the values of the detectors is plotted in figure 8.3. Here we can establish that the main trend is that the difference goes towards zero with increasing waiting time and that the relative difference increases

with buckling. The reasons for this can be that the higher modes are more lumped together in a flat system. This means that longer waiting times are necessary to get the fundamental decay constant. From the trend of the points we can see that this time must be considerable if we intend to use the result from detector 2. There are exceptions from this main rule. One may ask why the 1-3 correlation through the whole experimental series gives a lower difference than the 2-3 correlation. From the second series and the calculations of Griffing [2] we have learned that energy modes cannot come into the picture. The answer must then be a mixed set of positive and negative modes, some kind of continuum or a systematic error.

In figure 8.1 the values of Sjöstrand et al. [1] are also plotted. Although their values are a little more scattered, the overall agreement with detector 1 is good and we can conclude that this work is a confirmation of their measurement.

The theoretical values of Griffing show a rather small but systematic deviation. From the figure and the discussion above we can conclude that the correct value should be close to the result of detector 1 but between the result of the two detectors. However, it is in this case better to do the comparison in buckling instead of decay constants. The difference has therefore been transformed to a buckling difference and is plotted in figure 8.2 for the mean values of detector 1 and 2 (the mean value is calculated from all correlations but the 1 - 2, in experiment 680516 the only available value is taken) and the values of Sjöstrand et al. The difference, which with the values of Sjöstrand is rather scattered, is in our case more stabilized around a value of approximately 2 %. As the relative deviation in buckling is proportional to the relative deviation in the extrapolated height, the difference can, at least for the smaller moderators, easily be explained as an error in the extrapolated distance. The points indicate, however, a dependence between the height and the extrapolation distance.

The diffusion parameters are listed in table 8.2. The values of detector 1 should be taken as the result of this work. The deviations are those given by the least-squares method and therefore no systematic errors are taken into account. The result of detector 2 is listed only to underline how sensitive all the parameters are for higher modes in the experiment.

Table 8.1 Characteristics of the experimental series.

Experiment no.	Moderator height cm	Channel width μs	Neutron burst length μs	Waiting time μs
68050601	17,6	4	200	0
68050602				128
68050603				256
68050701	15,4	4	200	0
68050702				128
68050703				256
68050801	13,2	4	200	0
68050802				128
68050803				256
68050901	11,0	4	200	0
68050902				128
68050903				256
68051001	8,8	4	200	0
68051002				128
68051003				256
68051401	6,6	2	100	0
68051402				64
68051403				128
68051404				192
68051501	4,4	2	100	0
68051502				64
68051503				128
68051504				192
68051601	2,2	1	50	0
68051602				32

Table 8.2 Diffusion parameters.

	λ_o s^{-1}	D_o cm^2/s	C cm^4/s
Detector 1	5818	26830	2152
Standard dev.	13	179	186
Detector 2	6008	24603	1471
Standard dev.	27	216	191
GRIFFING	5761	27799	2368
SJÖSTRAND	5900	26500	2600
Standard dev.	90	600	800

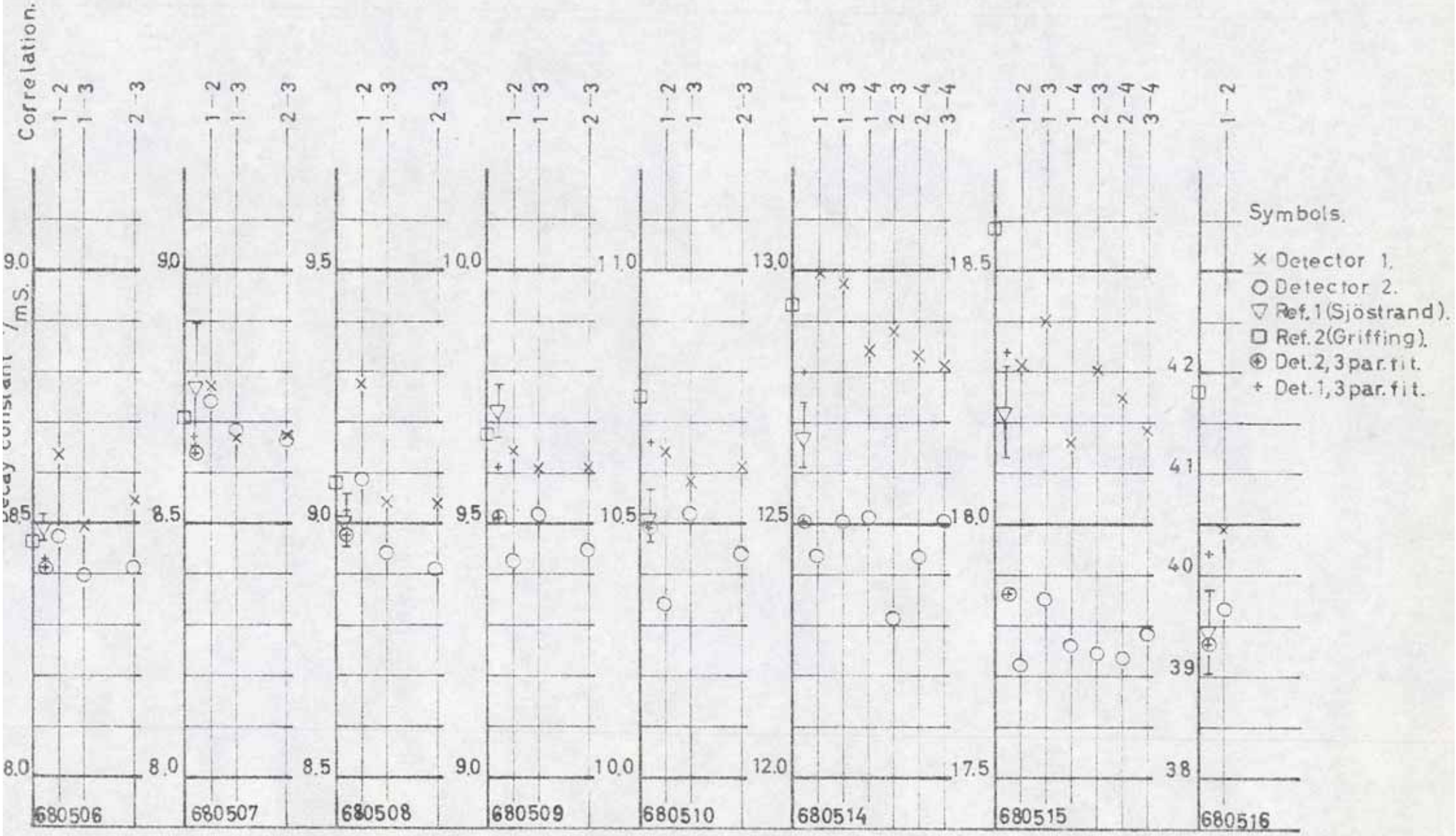

Fig. 8.1. Decay constants from autocorrelations.

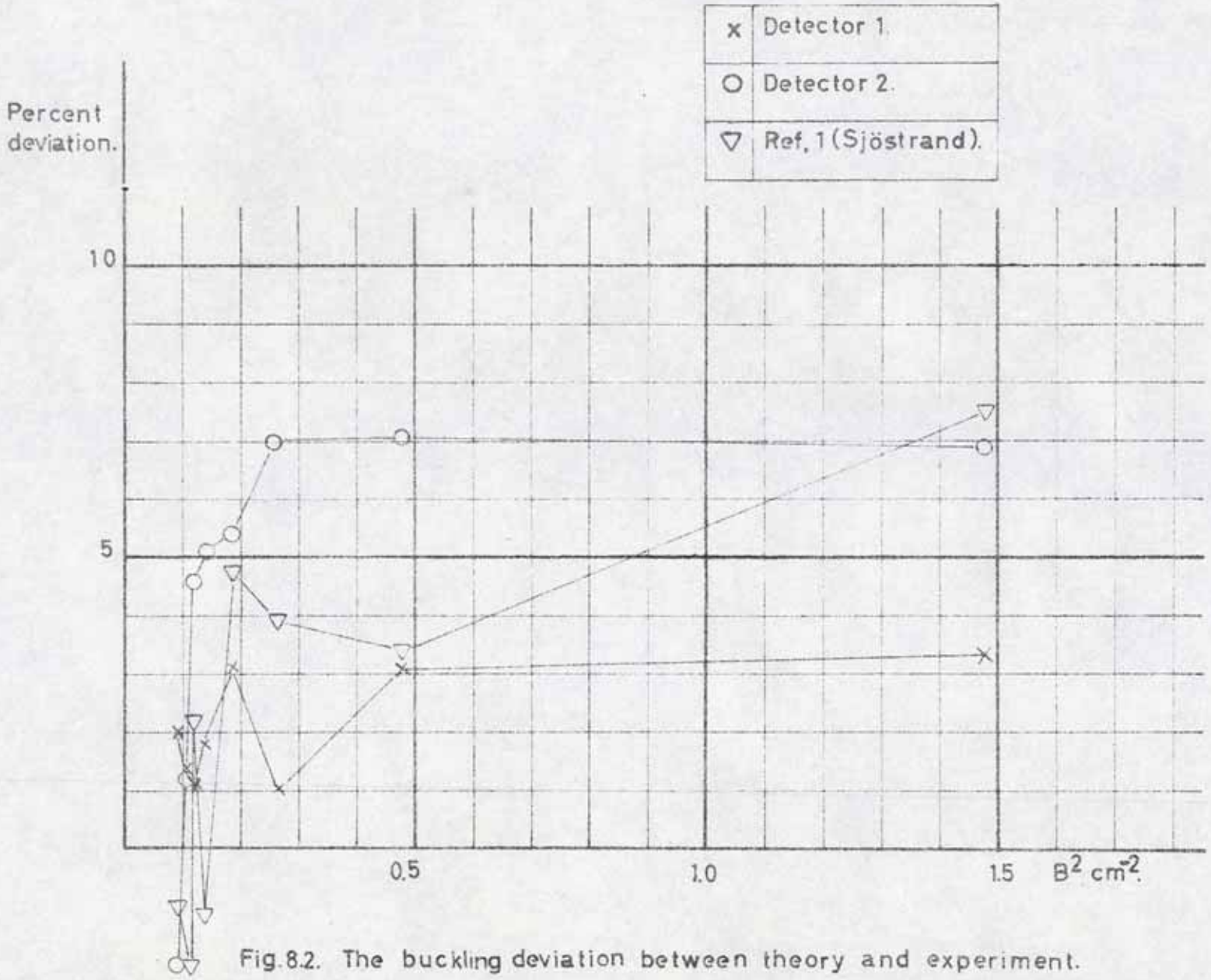

Fig. 8.2. The buckling deviation between theory and experiment.

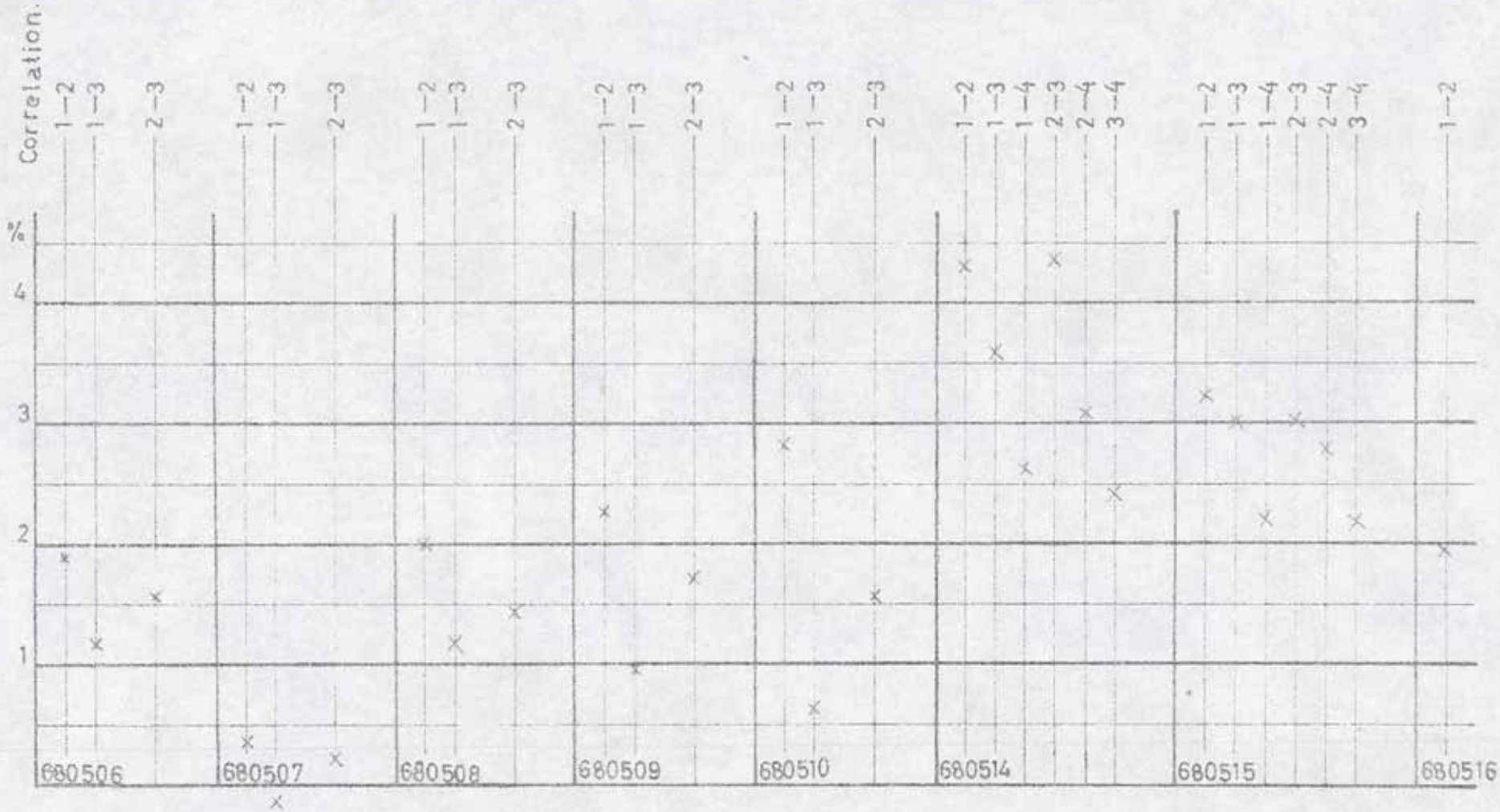

Fig. 8.3 Differences between detector 1 and 2.

ACKNOWLEDGEMENTS

The author is grateful to professor N.G. Sjöstrand and the members of his institution for help and valuable discussions during this work. The work has been supported by the Swedish Atomic Research Council.

REFERENCES.

1. Sjöstrand N.G., Mednis J., Nilsson T., Geometric buckling measurements using the pulsed neutron source method. Arkiv för fysik 15, 471 (1959).

2. Griffing G.W., Calculations on the fundamental time-decay constant of water and polyethylene, Neutron thermalization and reactor spectra, Vol I, Vienna 1968.

D

Reprinted from the proceedings

Ispra Nuclear Electronics Symposium

6-9.5.1969

Report EUR 4289 e

DEADTIME CORRECTIONS IN A TWO-PARAMETER SYSTEM CONTAINING FOUR DETECTORS

Gudmar Grosshög
Department of Reactor Physics
Chalmers University of Technology
Gothenburg, Sweden

Summary

A study of the deadtime correction in a complicated counting system is performed. It is shown how the transfer of information can be divided into extrinsic and intrinsic transfer. The intrinsic transfer depends on the total information flow from all detectors and has been treated with an experimental method, which is compared to a numerical model. The extrinsic transfer depends on the information flow in each detector line. It is shown that this effect can be studied through pile-up.

Introduction

As a counting equipment grows in complexity, the problem of doing an exact correction for the pulse losses will be more and more difficult[1-6]. One has therefore reasons to keep the correction as low as possible by having short conversion times and using a buffer memory before the often slow memory block. The consequence of this is, however, that the losses will depend not only on the intensities but also on the time and amplitude distribution of the stored pulses. Although it is difficult, it is quite possible to correct for these effects, since all information about them is contained in the measured distributions. There are, however, other effects that we know nothing about. They arise from those parts of the pulse spectrum, which are rejected in different places of the equipment by analog or digital data reduction. So we are forced into some method by which we can measure at least the main part of the correction.

The system

The purpose of the system is to measure the time and amplitude distribution from four detectors simultaneously. The capacity of the memory block is 1024 channels, which can be arbitrarily subgrouped in binary steps for the three parameters: number of detectors, amplitude channels and time channels. The method is applicable to different combinations of these parameters. Results are given for the subgrouping 4 detectors, 32 amplitude intervals and 8 time intervals. The division in amplitude is linear but in time it is logarithmic [7,8].

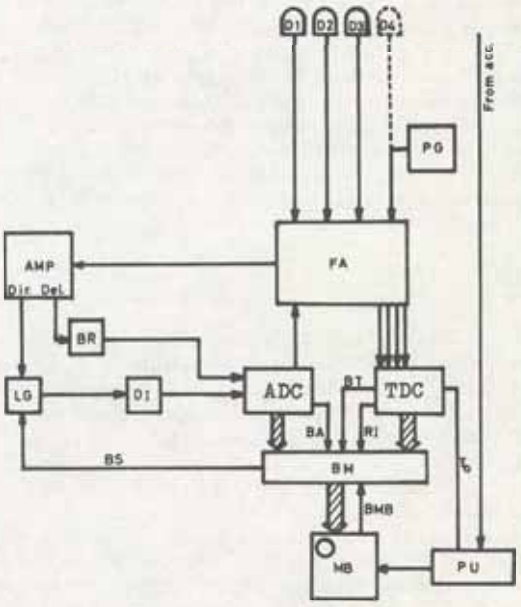

Fig. 1. Principles of the equipment.

The principles of the system are sketched in figure 1. A repetitive start pulse (T_0) passes a programming unit, which controls the measuring time. It is switched on manually and off either by the condition that it has reached a preset number of measuring cycles or by the condition that there is an overflow in any of the channels in the memory block.

The pulses from the detectors (Dn) are amplified and added by an summing amplifier in the amplifier unit (FA). The signal from the addition circuit is fed into an amplifier (AMP) with two outputs, one direct and one delayed. The delayed output is over a base line restorer (BR) connected to the direct current input of the analog-to-digital converter (ADC). If the system is not busy, the pulse from the direct output passes a linear gate (LG) and activates a discriminator (DI), which triggers the ADC and the logic circuits in FA. From these a signal in the actual detector line starts the time-to-digital converter (TDC).

From now on the conversion proceeds in both ADC and TDC. The conversion time is fixed to 4 microseconds in TDC but depends on the amplitude in ADC. The result of the conversion is loaded into the buffer memory (BM), where it is kept until both the conversions are ready and the memory block (MB) has completed a possible preceding storing cycle. TDC gives the time information in a linear scale. A conversion to the logarithmic time scale[7] is realized during the transfer of the information to the memory block.

The system busy signal (BS) to the linear gate is evaluated in the buffer memory from the signals BA, BT, RI and BMB. It signals busy if ADC or TDC or the buffer memory is engaged or if the time is outside the actual time interval. The overall deadtime of the system depending on the amplitude, the time channel width and the intensity. The minimum deadtime for a stored pulse is about 8 microseconds.

Deadtime losses

A schematic picture of the equipment from the view of deadtime losses is given in figure 2. In the block marked " system " we have collected all parts that have the same influence on the deadtime for all of the detectors.

In order to give the system information about which of the detectors that is responsible for the actual signal, all amplifiers are followed by a one bit memory (monostables marked MS1 to MS4 in the figure). One of the first actions taken by the system after the arrival of the pulse is to read this information. As every monostable is controlled directly by its own detector, this part of the equipment will have a deadtime that depends on the pulse rate of the detector in question.

So we see that two different types of deadtime appear in the system. The first depends on the pulse rate in each detector line, the second depends on the summed pulse rate and the pulse amplitude distribution from all detector lines. We will in the continuation use the attributes extrinsic and intrinsic for these effects.

We can now write

$$P_i(a,t) = G_i(R_i) \cdot H\left(\sum_{i=1}^{4} R_i\right) \cdot R_i(a,t) \qquad (1)$$

where

- P_i = stored number of pulses for detector i
- R_i = incoming number of pulses for detector i
- H = intrinsic transfer function
- G_i = extrinsic transfer function for detector line i
- t = time
- a = amplitude

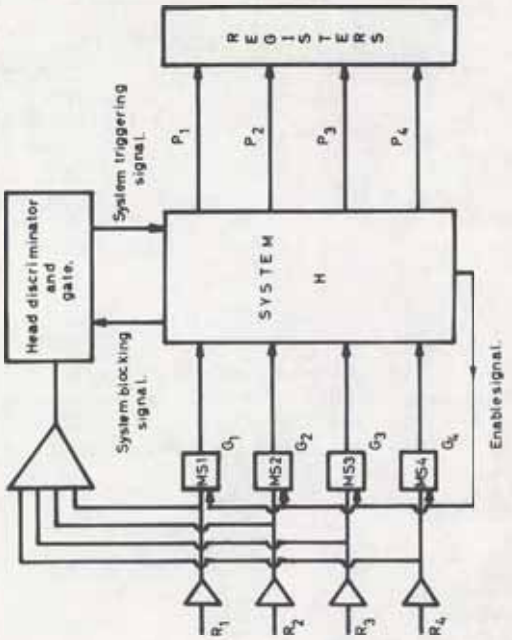

Fig. 2. Working principle for deadtime considerations.

In this equation we have assumed that the intrinsic and extrinsic transfer functions are independent of each other. Owing to the effects of overlapping this is generally not true. The equation is, however, a good approximation if, for a given i, any of the functions is not far from 1.

Intrinsic transfer.

Experimental method

Suppose that we have a known distribution of well separated pulses in one detector line i.g. 4. In that case $G_4 = 1$ and

$$P_4(a,t) = H \cdot R_4(a,t) \qquad (2)$$

from which

$$H(t) = \frac{\int_{a_l}^{a_u} P_4(a,t)\,da}{\int_{a_l}^{a_u} R_4(a,t)\,da} \qquad (3)$$

where a_l and a_u are the amplitude limits.

The transfer function given by this method contains the effects of all the detector lines but the test line. This depends on the fact that the test pulses are well separated and not Poisson distributed. We use this method in order to have G_4 equal to one and because the test pulses can in this case easily be generated by an ordinary pulse generator. With a constant pulse rate of 72 pulses per second in the test channel the influence of this is approximately one per mille.

So, we can measure the intrinsic transfer function simply by exchanging the detector in one detector line with a pulse generator. The numerator of equation 3 is then recorded in the analyser and the denominator can be counted in a scaler gated by a signal, which gives information about the time of interest.

Error analysis

The statistical errors of the method depends primarly on the variations of the recorded number of counts from the test line. In order to investigate this variation a series of runs was made with $H(t) \equiv 0$ and the number of input pulses going from 15 to $65 \cdot 10^6$. It was found that the standard deviation varied in the some way as that of a Poisson distribution. In 75 % of the runs the difference was less than 3 %. As an example the distribution of the channel contents for one run with $5.8 \cdot 10^6$ pulses is given in figure 3.

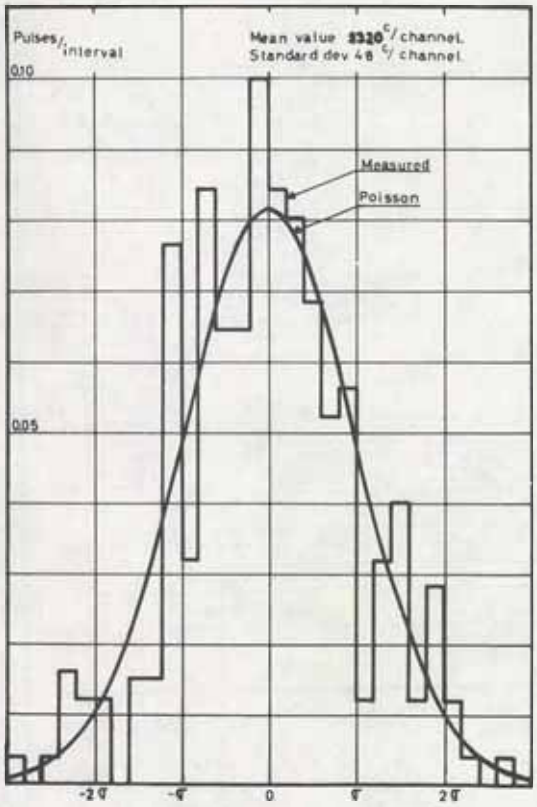

Fig. 3. Probability density function of the test line.

Numerical model

The method has been checked with a rather simple numerical model. This model uses the fact that if the channel width is small, the effects from the amplitude converter will predominate. We assume also that the transfer time between the buffer register and the memory block is zero. The deadtime can now be separated into two parts. The first is the sum of all constant waiting times (t_w), the second is proportional to the converting time and therefore also to the amplitude. The relation between the deadtime calculated in number of channels after the arrival of the pulse (k) and the amplitude (a) can then be written

$$k = t_w + c \cdot a \qquad (a \geq 0) \qquad (4)$$

where c is a proportionality constant that depends on the settings of the amplitude converter. The inversion of this equation is

$$a(k) = \frac{k - t_w}{c} \qquad (k \geq t_w)$$
$$a(k) = 0 \qquad (k < t_w) \qquad (5)$$

The probability that a channel j is closed is then

$$S(j) = \sum_{i=1}^{j-1} \sum_{k=j-i}^{\infty} p(a(k), i) \quad (j>1) \qquad (6)$$
$$S(j) = 0 \qquad (j=1)$$

$p(a,i)$ is the probability of a pulse in the linear time channel i and amplitude channel a. It can be calculated approximately from the stored distribution $P(a,i)$ as

$$p(a,i) = -\frac{P(a,i)}{N} \qquad \text{(a, i inside the measured range)}$$
$$p(a,i) = 0 \qquad \text{(elsewhere)} \qquad (7)$$

where N is the number of repetitions. It is assumed that the system is open in the beginning of each cycle and that all pulses above the discriminator level are stored. The intrinsic transfer function is finally

$$H(i) = 1 - S(i) \qquad (8)$$

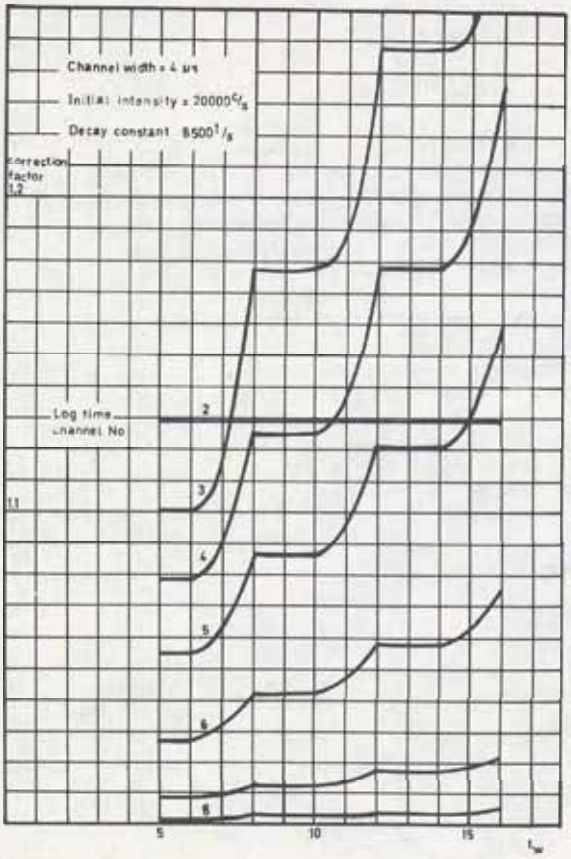

Fig. 4. Calculated correction factor as a function of the deadtime t_w.

The result of a calculation with this method is shown in figure 4. The distributions are taken from an ordinary experiment with eight logarithmic time channels and 32 amplitude channels. The calculation is made in a linear time scale but the result is transferred back to the logarithmic scale. Time channel number one is zero, as the system always is considered to the open at that time, number two is constant because t_w is larger than the channel width. The other curves show plateaus and transients. With 32 amplitude channels the deadtime variation is 1.6 microseconds, which gives transients in the channel limits that last over a period of 3.2 microseconds. The shapes of the transients are determined by the amplitude distribution.

We have also compared the model to the correction factor obtained from measurements using the above method. The result is shown in figure 5. The input to the experiment is a neutron and gamma field, where the neutrons give a dominant peak decreasing with a decay constant of approximately 8500 1/s. The difference between the runs is that they have different starting times, which gives the different initial intensities noted in the figure. The relative accuracy of the experimental points is also indicated in the figure.

From the figure we conclude that there is satisfactory agreement between the model and the experiment in the intermediate part, but there are deviations both in the beginning and the end part of the curves. We shall, however, keep in mind that all common effects are included in the experimental values. In the beginning there are transients, which have not been accounted for in the model. The effects in the end part may depend on uncertainties in the gating signal to the scaler needed for the denominator in equation 3. The correction is, however, low and second orders corrections may also come into the picture.

The result of this investigation is that a check of the experimental method has been obtained. The rather simple model gives correct results in the main part of the experiment but not in the limits. The model is also expensive by consuming rather long computing time. It is therefore not attractive to expand the model by putting more routines into the computer program.

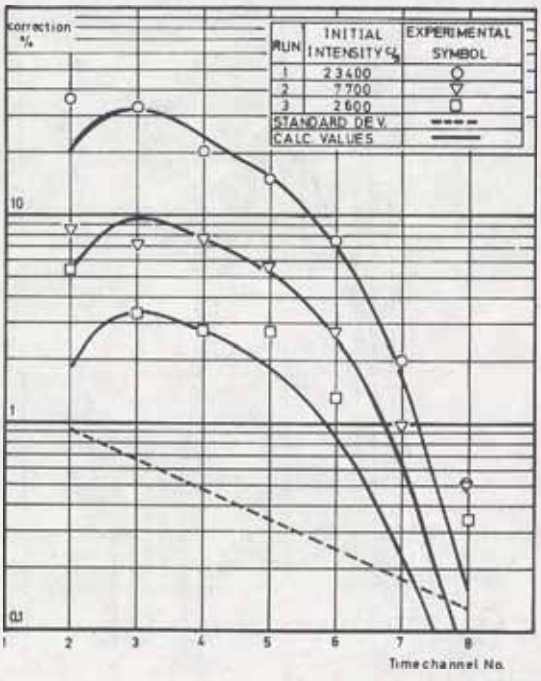

Fig. 5. Comparison between measured and calculated values of the intrinsic deadtime correction.

Extrinsic transfer

In the detector lines we have to take two effects into account. Firstly, there is the effect of pile-up in the amplifier chain, secondly, the monostables have a time period during which they can not be reactivated. So, the system we have to study here is two serial connected blocks If the deadtimes of these are t_1 and t_2, we can state the following about the resulting deadtime t_m.

a. If $t_1 \geq t_2$ then $t_m = t_1$

b. If $t_1 < t_2$ then $t_1 + t_2 > t_m > t_2$
(t_m depends on intensity)

c. If $t_1 << t_2$ then $t_m \approx t_2$

From these statements it is clear that it is favourable to have the largest deadtime in the beginning of the chain. This presupposes that all irrelevant information can be sorted out at this early stage, which often is not possible. One is therefore left with a compromise and must try to sort out as much irrelevant information as possible to the lowest price in deadtime.

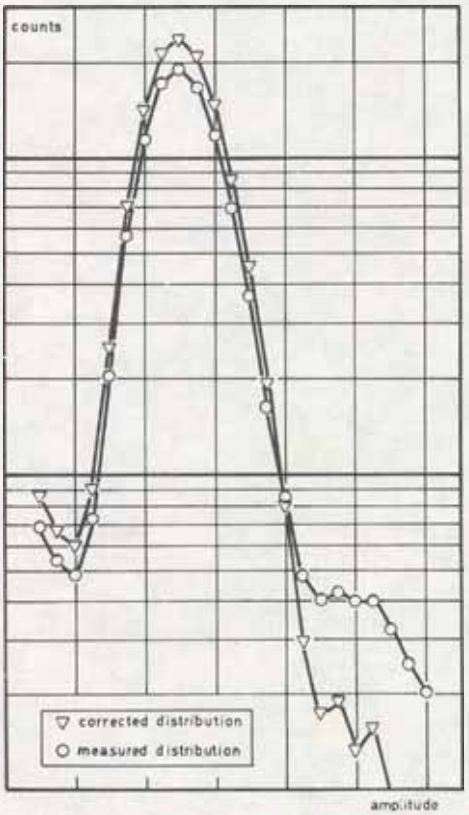

Fig. 6. Comparison between a measured and a corrected amplitude distribution.

In our case the deadtime of the monostables is of the same order as that of the pile-up effects. As the pile-up effects are reflected on the amplitude distributions, we will use them to study the extrinsic deadtime effects.

Pile-up is a coincidence in the analog parts of the system between two different pulses. The result is an analog addition between the two pulses, which gives a pulse with strange shape[9]. If we can assume that the resulting pulse has a definite length (τ) we can write

$$p_m(a)\,da = p(a)\,da + \tau (I_1 - I_2)\,da$$

$$I_1 = \int_0^\infty \int_0^\infty g(a_1, a_2, a)\, p(a_1)\, p(a_2)\, da_1\, da_2 \qquad (9)$$

$$I_2 = p(a) \int_0^\infty p(a)\, da$$

where

$p_m(a)$ = the measured distribution in counts per second and amplitude interval.

$p(a)$ = the corrected distribution

$g(a_1, a_2, a)$ = the probability that a pulse with the amplitude a_1 and a pulse with the amplitude a_2 is stored as a pulse with the amplitude a.

The function g depends on the pulse shape and on how the ADC treats strange pulse shapes. As a simple model we assume that the undisturbed pulse has a rectangular shape with amplitude a and length $\tau/2$. Then we can write

$$g(a_1, a_2, a) = \delta (a - ea_1 - ea_2) \qquad (10)$$

where δ is the Kronecker delta function and e is a parameter to be determined.

Equation 9 can easily be solved by iteration, starting with $p_m(a)$ as the first approximation for $p(a)$. For ordinary values of the pulse rate the iteration converges in few steps.

Errors in the parameters e and τ give distortions in the resulting amplitude distribution. The parameters can therefore be determined by trial and error with the condition that the distortions shall be out. In our case we have found $e = 0.9$ and $\tau = 3$ microseconds.

Another problem is the low part of the amplitude distribution, which is not measured. In order to take this into account we have to extrapolate the distributions down to zero.

It should be pointed out that pile-up caused by pulses from different detector lines is sorted out by a coincidence circuit. The result of this operation is a blocking of the whole system. Therefore, the deadtime caused will be contained in the intrinsic deadtime.

As an example the amplitude distribution before and after correction is given in figure 6. The intrinsic correction is 20 % and the local intensity is 40, 000 counts per second.

Acknowledgements

The author is grateful to professor N.G. Sjöstrand and the members of his institution for help and valuable discussions during this work. Particularly I want to thank Gunnar Rönnberg for his work with the computer programs.
The work has been supported by the Swedish Atomic Research Council.

References

1. F. Rau und G. H. Wolf, Nucl. Instr. and Meth. 27 (1963) 321.
2. Kerstin Löw, Nucl. Instr. and Meth. 26 (1964) 216.
3. H. Seufert, Nucl. Instr. and Meth. 44 (1966) 335.
4. P. Paatero and K. Eskola, Nucl. Instr. and Meth. 44 (1966) 357.
5. C. E. Cohn, Nucl. Instr. and Meth. 41 (1966) 338.
6. J. Harms, Nucl. Instr. and Meth. 53 (1967) 192.
7. G. Grosshög, CTH-RF-10 (1967) (internal report).
8. G. Grosshög, CTH-RF-16 (1968) (internal report).
9. A. M. R. Ferrari and E. Fairstein, Nucl. Instr. and Meth. 63 (1968) 218.

E

[redacted]

CHALMERS UNIVERSITY OF TECHNOLOGY

DEPARTMENT OF REACTOR PHYSICS

CTH-RF-17 JULY 1969

THE PULSED NEUTRON METHOD APPLIED TO THE INTERACTION BETWEEN TWO MODERATORS.

by

GUDMAR GROSSHÖG

CONTENTS

SUMMARY

The possibility to use the pulsed neutron method in the study of two interacting moderators has been investigated. It is found both through theory and experiment that transport effects have a dominant influence on the decay constants.

The decay constants have been measured in a system consisting of two polyethylene discs separated along the symmetry axis. The discs had a diameter of 18 cm. Two series were measured. In the first the discs had a height of 2.2 cm. They were separated by a distance that was varied up to 13.2 cm in steps of 2.2 cm. In the second the height of the discs was 4.4 cm, the maximum separation distance was 8.8 cm, and the step length was the same as in the first series. The experiments cover a range in decay constants that goes from 10.000 to 40.000 s^{-1}. The reliability of the measurement is checked in the limit of zero separation distance and in the limit of no interaction.

It is found that in all of the experiments, with the exception of those in the limits, the decay constants are drifting in time. Therefore they cannot, within the scope of the experiments in this report, be looked upon as reliable pseudomodes.

The result found can be extended to include all experiments with the pulsed neutron method applied to moderators containing cavities or having concave boundaries. A method to eliminate the drifting effect through the incorporation of absorbers in the cavities is suggested.

1. INTRODUCTION

The ordinary way to calculate the neutronic interaction between assemblies is to define an interaction parameter ρ as the fraction of the outgoing neutrons from one of the assemblies that reaches the other one. If the interaction takes place between two plane surfaces we can write

$$\rho = \frac{\iint J(S_1)\, f(\Psi,\theta)\, dS_1\, dS_2 \cos\theta / s^2}{\int J(S_1)\, dS_1} \qquad (1.1)$$

where $J(S_1)\, dS_1$ = the total outward current at dS_1

s = the distance between dS_1 and dS_2

S_1, S_2 = the plane surfaces

$f(\Psi,\theta)$ = the angular distribution of the neutrons at the surface normalized in the range $\left[(0,2\pi)\,(0,\frac{\pi}{2})\right]$

Ψ, θ = the spherical polar angle coordinates of dS_2 relative to dS_1

$f(\Psi,\theta)$ may be expressed by a Legendre series. If it is independent of Ψ we can write

$$f(\Psi,\theta) = \sum_{l=o}^{\infty} a_l P_l(\cos\theta) \qquad (1.2)$$

In the diffusion approximation this takes the form

$$f(\Psi,\theta) = \frac{1}{A}\left(1 + \frac{3}{2}\eta\cos\theta\right)$$

$$A = 2\pi\left(1 + \frac{3}{4}\eta\right) \qquad (1.3)$$

where $\eta = \frac{2D}{\bar{v}\phi}\,\frac{\delta\phi}{\delta x}$ at the surface

D = the diffusion constant (cm^2/s)

$\bar{v}$ = the neutron mean velocity (cm/s)

The ordinary way to evaluate ρ is to use a cosine angular distribution corresponding to the second term of the expansions 1.2 or 1.3. The result of such a

calculation is shown in figure 1.1, which gives ρ as a function of the separation distance (d) between two identical cylindrical discs with the diameter 18 cm. In the lower curve the variation of the neutron current over the surface of the discs has been approximated with a constant, in the upper with a parabola. Explicit expressions for the two cases can be found in reference 1.

In order to give a correct picture of the neutron angular distribution at a free surface many terms are generally needed in the series expansion. Most of these are, however, required in order to take into account the fact that there are no incoming neutrons. Therefore, if we are interested in only the outgoing part, the first two terms give a rather good estimate of the angular dependence [2 fig. 9.6].

In figure 1.2 the result of a calculation for the first two terms is shown. Expression 1.1 has here been evaluated numerically on a computer. As the radial distribution a zeroth order Bessel function has been used. The agreement between the curve for the second term approximation in figure 1.2 and the upper curve in figure 1.1 is excellent, which shows that the difference in the radial distribution is not so important.

If one now does an experiment in order to measure ρ as a function of the separation distance d for two identical discs one would expect ρ (d) to be somewhere beetween the curves for the first and second term in figure 1.2. It should be close to the first term for low d where the backscattered neutrons create rather symmetrical angular distribution and more close to the second term for high values of the separation distance d. This behaviour is confirmed by measurements on subcritical assemblies [3]. There is one exception in the material presented by Clark and that is in the limits of very small separation distances. However, the magnitude of the difference is small and may be explained by the influence of epithermal neutrons or by some systematic error in the comparisons between experimental and calculated values.

Kiyose et al. [1] have suggested that the pulsed neutron method could be used in order to measure the interaction parameter. They have also made an experiment with graphite discs (diameter 150 and thickness 50 cm). The result of this measurement is, however, very puzzling. For separation distance up to 30 cm they have got good agreement with the approximation

that has a parabola as current distribution and uses the second term in equation 1.2 as angular distribution. For larger separations the measurement gives higher values than the mentioned approximation. These results are in direct contradiction to the material of Clark. Although higher terms in the angular expansion (1.2) can explain the high values at large d, the behaviour is unexpected.

As we could not find any resonable explanation of the discrepancy, we suspected that there might be something wrong in the application of the pulsed neutron method to this case. Therefore, we have made a careful study of the method and a measurement with polyethylene discs and thus checked the experiment with another material and another set-up.

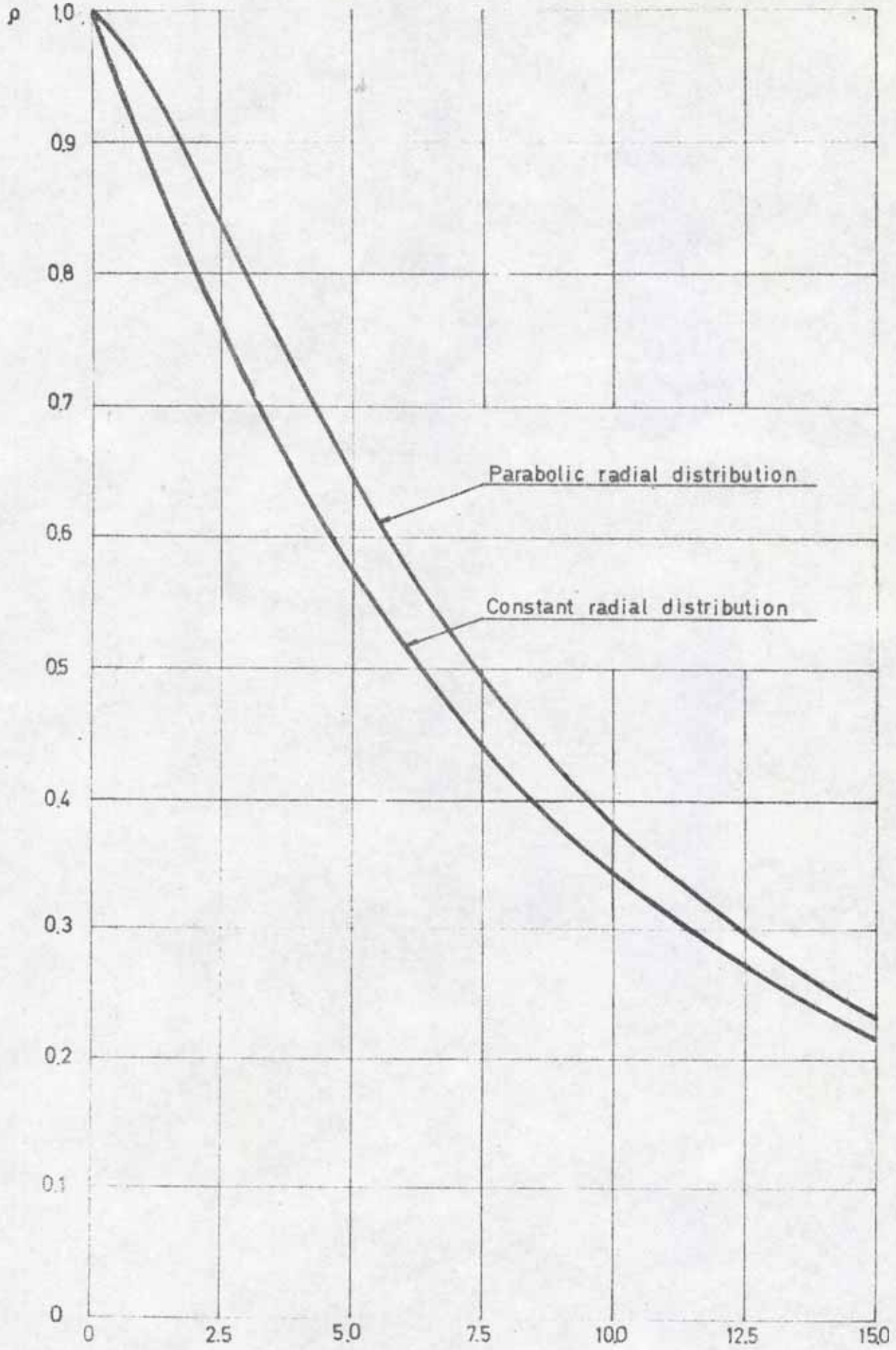

Fig.1.1. The interaction parameter ρ.

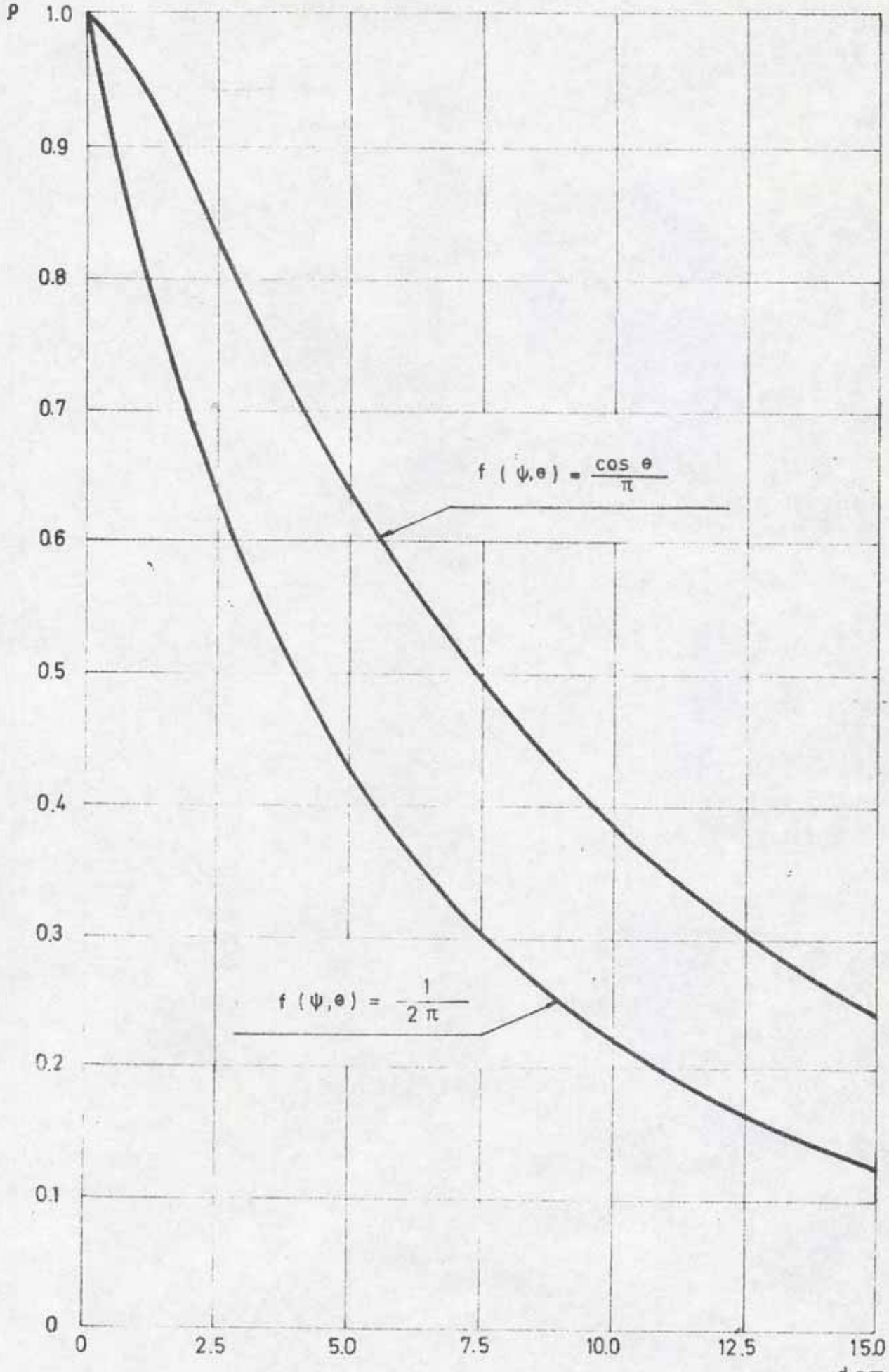

Fig.1.2. ρ at isotropic and cosinus angular distribution.

2. THEORY

We consider first the stationary diffusion approximation. With the geometrical parameters as given by figure 2.1 the neutron flux for the positive part of z can be written

$$\phi = A_{,} \left(\sin(\gamma z) - \mathrm{tg}(\gamma e) \cos(\gamma z) \right) \qquad (2.1)$$

where we have used the boundary condition $\phi = 0$ at $z = e$.
Following diffusion theory we have the input and output currents at $z=d/2$

$$J_{+} = \frac{\phi}{4} - \frac{D}{2\bar{v}} \left(\frac{\delta\phi}{\delta z}\right)$$

$$J_{-} = \frac{\phi}{4} \quad \frac{D}{2\bar{v}} \left(\frac{\delta\phi}{\delta z}\right) \qquad (2.2)$$

As the problem is symmetric with respect to $z = 0$ we have by definition

$$\rho = \frac{J_{+}}{J_{-}} \qquad (2.3)$$

from which

$$\frac{1-\rho}{1+\rho} = \frac{2D}{\bar{v}\,\phi} \left(\frac{\delta\phi}{\delta z}\right)_{z = d/2} = \eta \qquad (2.4)$$

If we check this expression in the limits we find that $\rho = 0$ gives $\eta = 1$, which is correct within the limits of diffusion theory. A better value at this limit is, however,

$$\eta = \frac{2}{3\Gamma_o}, \quad \Gamma_o = 0,7104 \qquad (2.5)$$

In order to correct for this we rewrite equation 2.4

$$\frac{1-\rho}{1+\rho} = \frac{3\Gamma_o}{2}\eta = \eta' \qquad (2.6)$$

We then have an expression, which in the limits is consistent with an ordinary measurement with one and two discs respectively.
η can be calculated from equation 2.1, which gives

$$\eta = \frac{2D\gamma}{\bar{v} \cdot \mathrm{tg}(\pi - \gamma(b+\delta))} \qquad (2.7)$$

We can now outline a method to determine ρ. Lambda is measured. From the inversion of the buckling expansion

$$\lambda = \lambda_o + DB^2 - CB^4 \qquad (2.8)$$

we get the buckling

$$B^2 = \frac{2(\lambda - \lambda_o)}{D\left(1 + \sqrt{1 - \frac{4C(\lambda - \lambda_o)}{D^2}}\right)} \qquad (2.9)$$

γ is then determined by

$$\gamma = \sqrt{B^2 - a^2} \qquad (2.10)$$

where

$$a^2 = \left(\frac{2.405}{r + \delta}\right)^2$$

Finally we have

$$\rho = \frac{1 - \eta'}{1 + \eta'} \qquad (2.11)$$

We can interpret ρ as the albedo of the other disc. η and η' may be considered as loss coefficients. The method outlined is the same as that used by Kiyose et al. [1] with the exception of the correction for the boundary effect. Equations 2.7 to 2.11 are illustrated in figure 2.2 for the interaction of two 2.2 cm thick polyethylene discs and in figure 2.3 for two 4.4 cm discs. The radius of the discs is 9 cm. The standard deviations of ρ relative to the deviations of lambda are shown in figure 2.4 and 2.5. As lambda can be measured with an accuracy within a few per cent, the curves show that from these considerations the experiment should give accurate values on ρ for all values of d with the exception of very large separation distances.

So far we have considered only the stationary interaction between the discs. In an ordinary pulsed experiment this is the usual method. However, an inspection of the Boltzmann equation for the region between the discs shows that the wave properties plays an important role. Therefore, we must reconsider the transfer between the discs and take the time lag into account.

We first assume that all neutrons have same velocity and a direction parallell to the symmetry axis of the discs. Taking into account the fact that the incoming neutrons were transmitted a time earlier we can write

$$\rho = \frac{J_+\left(t - \frac{d}{v}\right)}{J_-(t)} \qquad (2.12)$$

If both of the moderators have an exponential time dependence this gives

$$\rho = \frac{J_+(t)}{J_-(t)} e^{\lambda \frac{d}{v}} = \rho_{st} \cdot \rho_p \qquad (2.13)$$

where ρ_{st} is the stationary transfer coefficient as calculated before and ρ_p is a coefficient taking into account the exponential decay of the neutron field.

From equation 2.13 we find that ρ_p depends on the velocity. Therefore, we must do a more careful investigation and take the velocity distribution into account. We will consider exponential decay and can write with M (v) as the velocity distribution.

$$J_{out}(t) = J_o \, e^{-\lambda t} \int_0^\infty M(v)\, dv$$

$$J_{in}(t) = J_o \, e^{-\lambda t} \int_{v=\frac{d}{t}}^\infty M(v)\, e^{\frac{\lambda d}{v}} \rho_{st}\, dv \qquad (2.14)$$

from which

$$\rho_p = \frac{\int_{v=d/t}^\infty M(v)\, e^{\frac{\lambda d}{v}} dv}{\int_0^\infty M(v)\, dv} \qquad (2.15)$$

With a Maxwell velocity distribution this gives

$$\rho_p = \frac{4}{v_T \cdot \sqrt{\pi}} \int_{v=d/t}^\infty e^{\left(\xi \left(\frac{v_T}{v}\right) - \left(\frac{v}{v_T}\right)^2\right)} \left(\frac{v}{v_T}\right)^2 dv \qquad (2.16)$$

where

v_T = the most probable velocity

$\xi = \frac{\lambda d}{v_T}$

The velocity distribution of the incoming neutrons is shown in figure 2.6 and ρ_p is drawn in figure 2.7.

From equation 2.16 we realize that ρ_p depends on the time. Moreover it is singular for infinite times. Therefore, the measured lambda value will also be time dependent and a fundamental mode does not exist. The same conclusion can be drawn from any reasonable velocity distribution.

We can compare this with the results of Corngold [4]. He has found that above a certain limit, $(v\Sigma)_{min}$ for λ, a fundamental mode does not exist. In our case we have a domain inside the experimental assembly where this limit is equal to zero. Therefore, also from this aspect we may expect that a fundamental mode does not exist.

We must, however, be careful here. If we are going with the separation distance into an interatomic range we could also conclude that a fundamental mode never exists, which obviously is wrong. Our model is, however, a three region macroscopic model with transport theory in one and diffusion theory in two of the regions. Therefore, it should not be used to draw conclusions in the interatomic range.

Measurements on graphite and beryllium have been done above the Corngold limit [5], and experimentally welldefined fundamental modes have been established. The explanation of this is the appearance of pseudomodes in the continuum [4, 6]. Therefore, the question about the existence of pseudomodes is natural also in this case. An inspection of figures 2.6 and 2.7 gives the result that one can expect pseudomodes for small values of d where the distortion of the spectrum is not so tremendous.

The definition of pseudomodes is not quite clear. From a theoretical standpoint they are caused by discrete exponentials embedded in a continuum or by the fact that the continuum has peaks. The experimentalist measures the time dependence of the decaying neutron field. The appearance of a pseudomode causes here an exponential decay, that lasts for some period. The strength of the pseudomode is reflected in the time during which the logarithmic time derivative can be looked upon as a constant. In order to have an experimentally well defined pseudomode this time period must be of the same order as for a discrete mode mixed with higher modes and background. So it is in the measurements on beryllium and in order to accept pseudomodes we require the same here.

We have treated ρ_p more or less as a correction. However, as can be seen from figure 2.7, it is an essential parameter. As it is difficult to calculate we have to realize that it will introduce a large error in the resulting ρ_{st}. The problem is, however, interesting in itself and therefore we will concentrate the experimental analysis to the appearing lambda values.

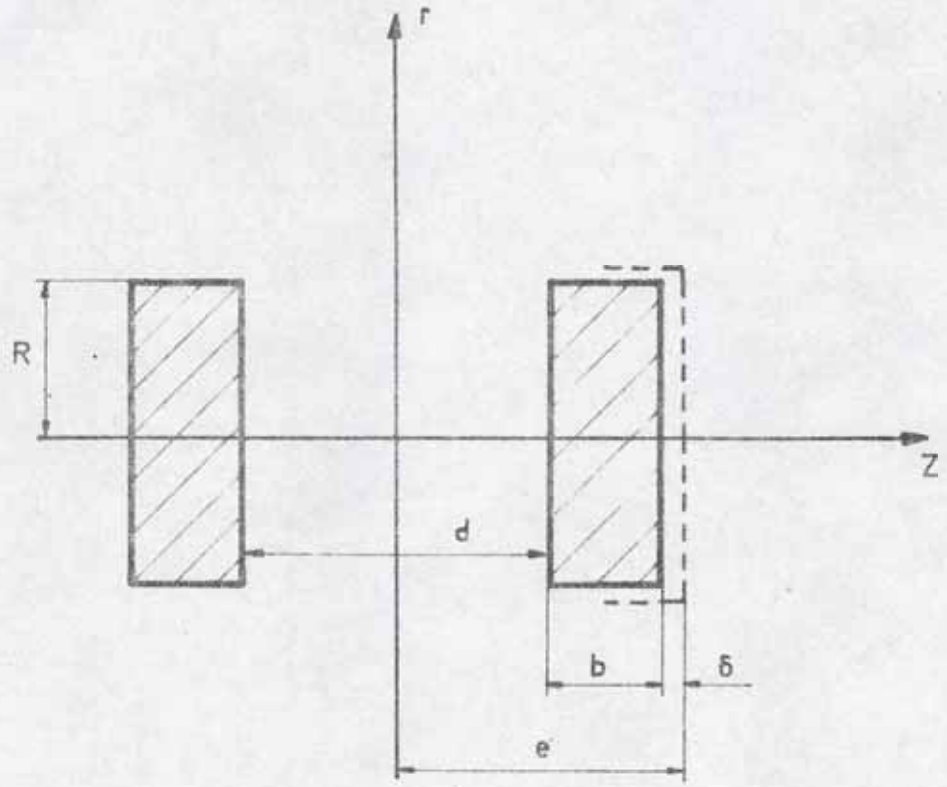

Fig. 2.1. Space parameters

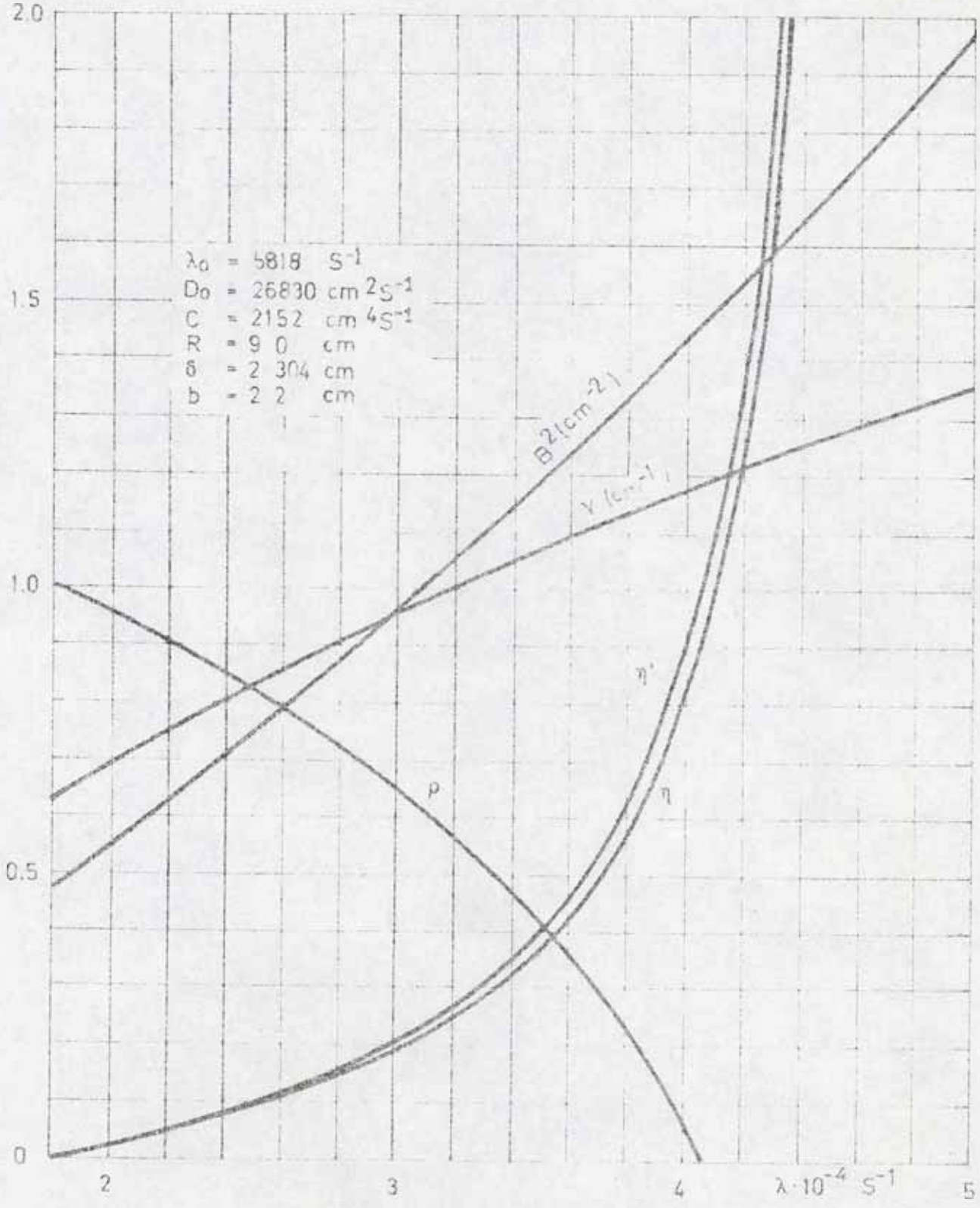

Fig.2.2 Parameters in the interaction of two 2.2 cm polyethylene discs.

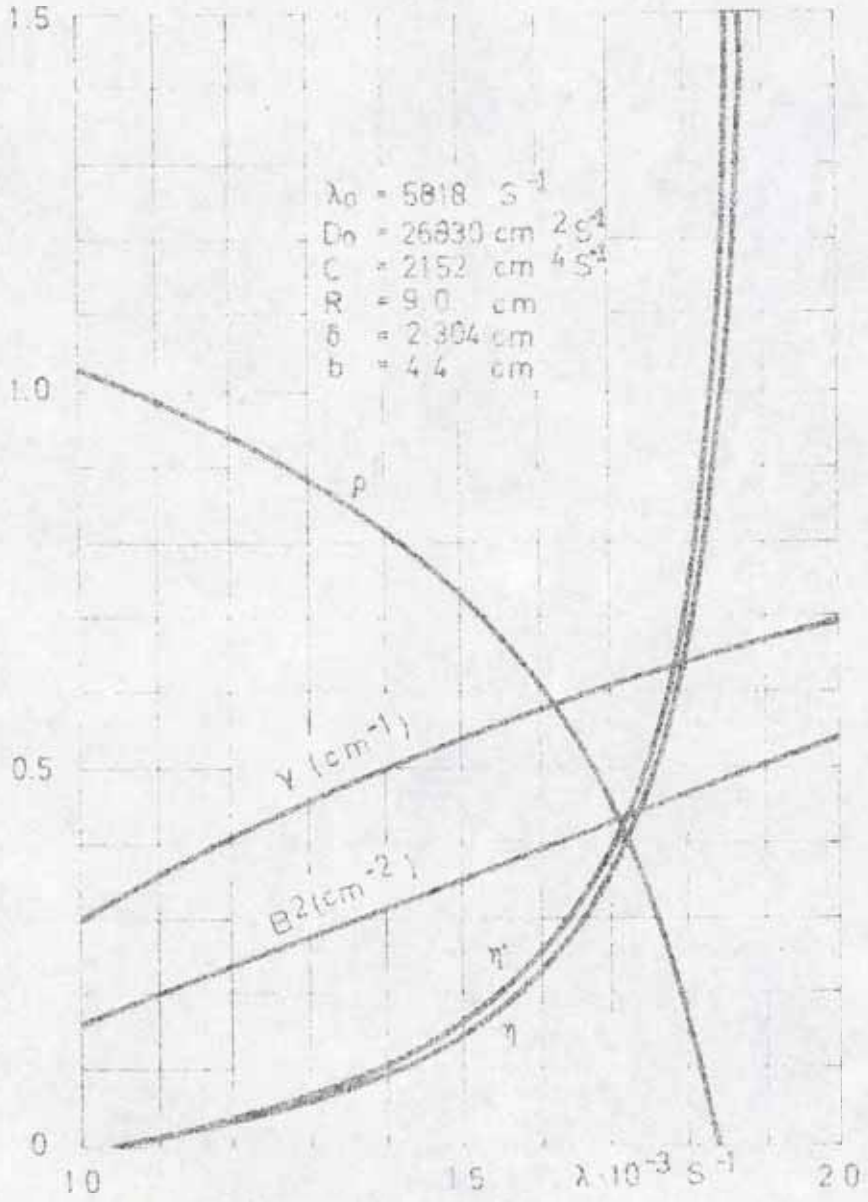

Fig. 2.3. Parameters in the interaction of two 4.4 cm polyethylene discs.

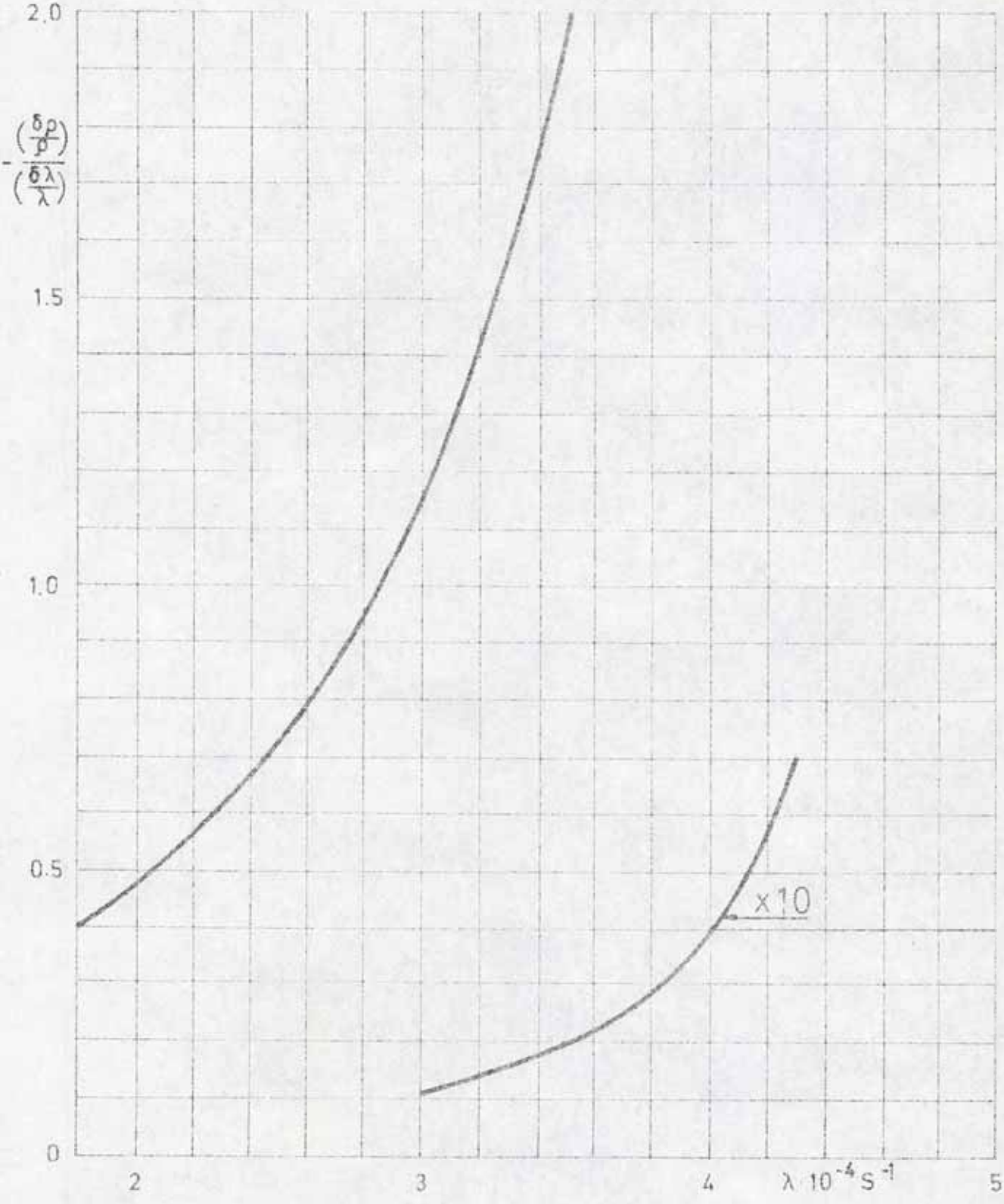

Fig.2.4. The relative error of ρ. 2.2 cm. discs.

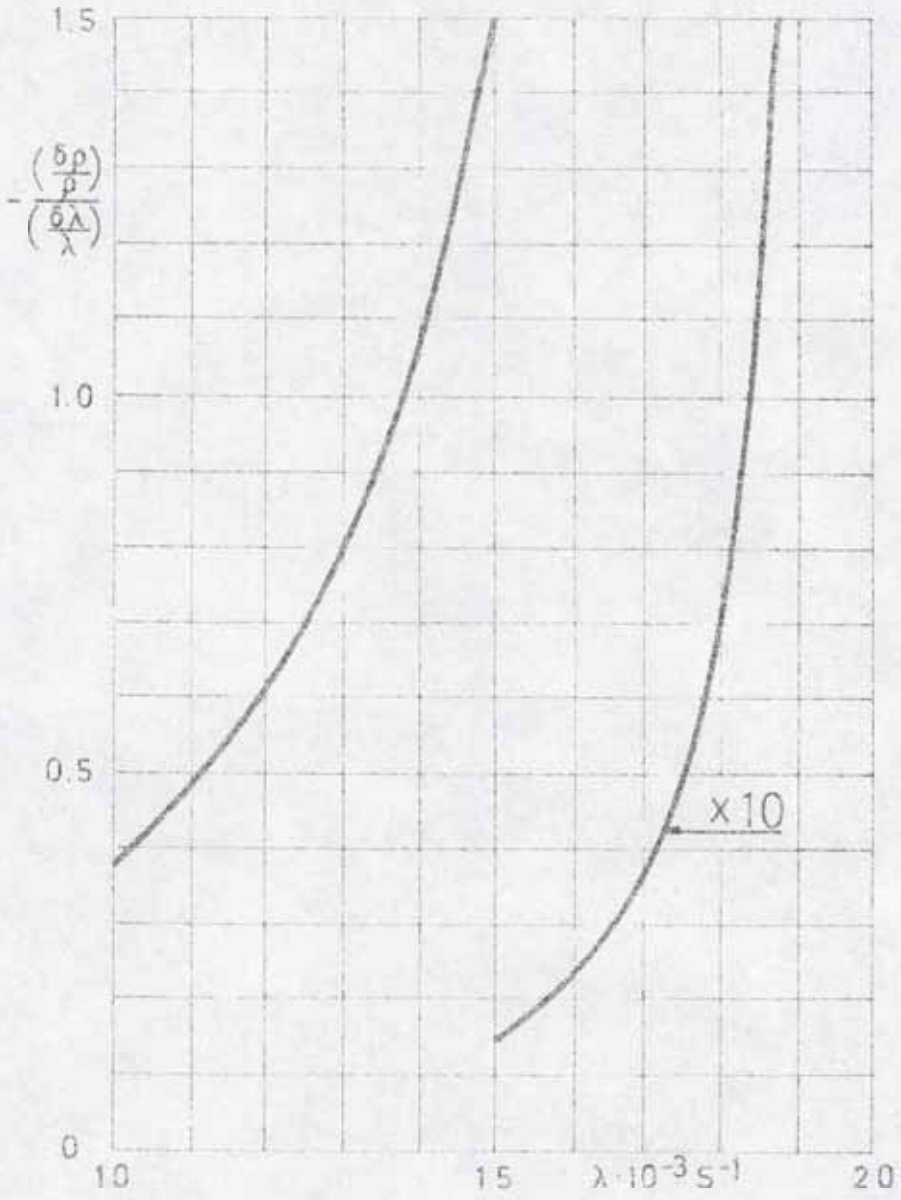

Fig. 2.5. The relative error of ρ. 44cm discs.

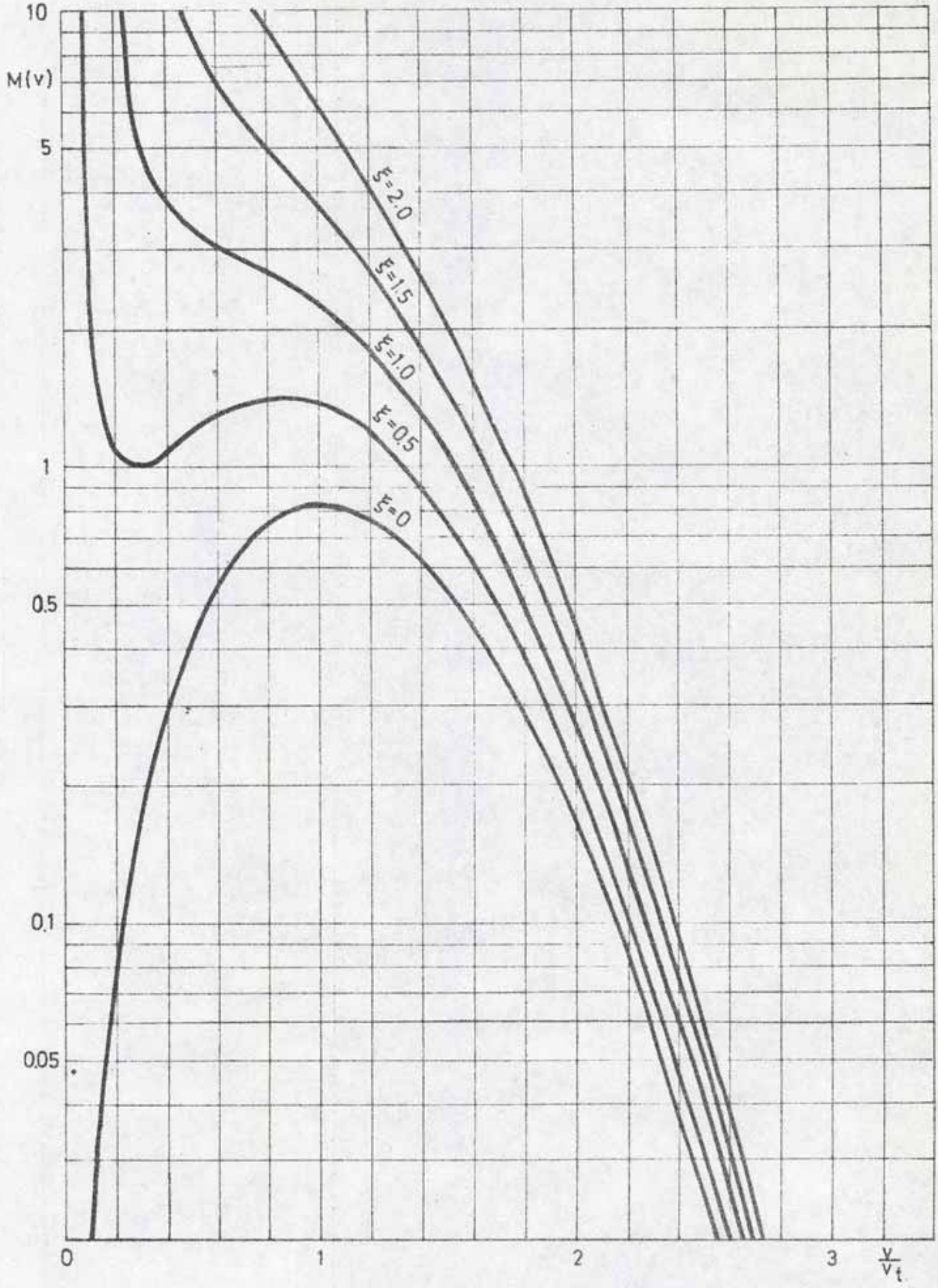

Fig. 2.6. The incoming velocity distribution.

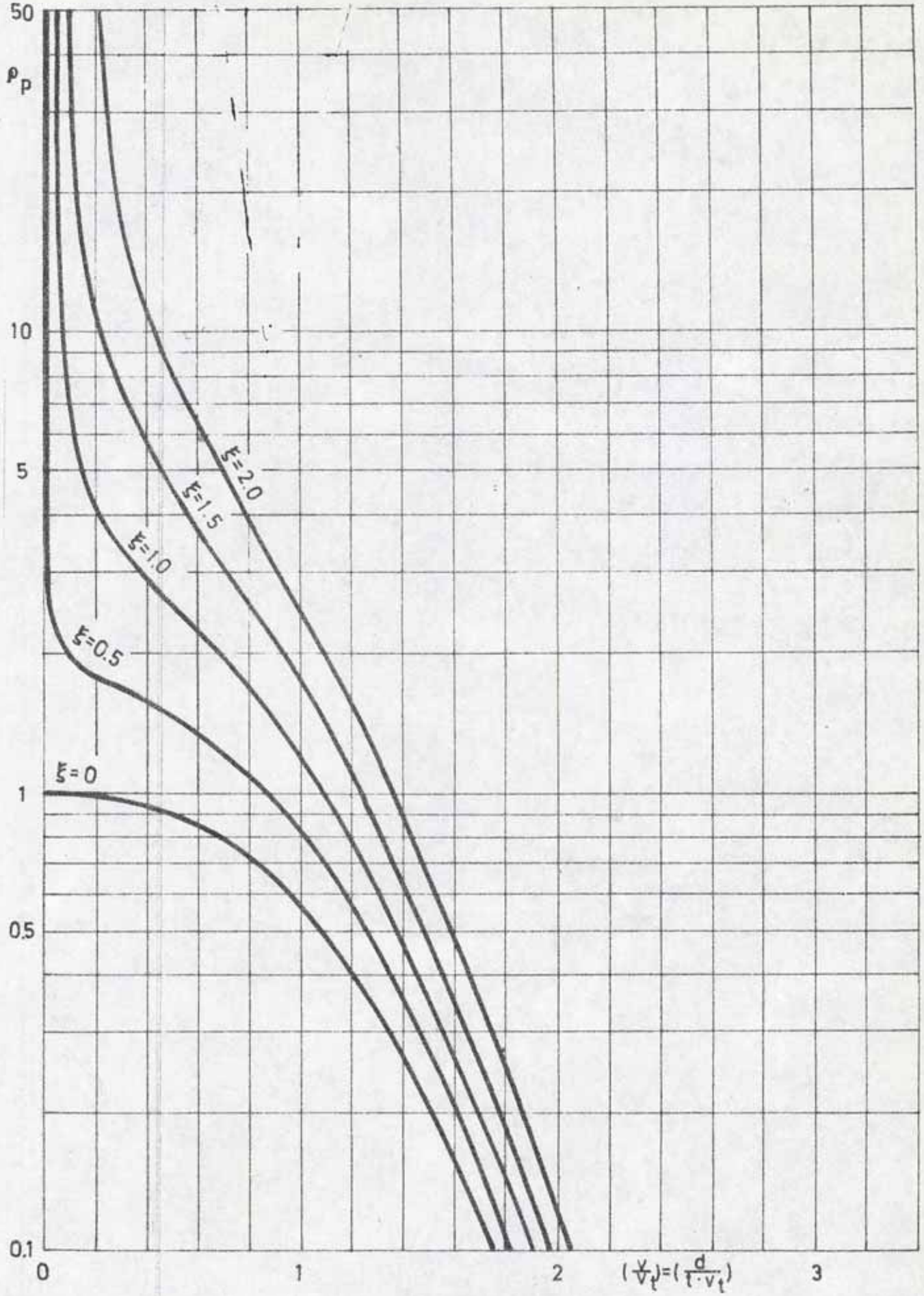

Fig.2.7. The dynamic transfer function.

3. THE MEASUREMENT

The experimental arrangement is shown in figur 3.1. As moderators we used polyethylene discs, which were separated by three thin aluminium bars and shielded by boron carbide. Three glass scintillators were used as neutron detectors. The first detector had 1/v response, the other ones were black.

The tritium target was placed at the symmetry plane ($z = 0$ in fig. 2.1) and the assembly was rotated around the cylindrical symmetry axis.

A description on the headpart of the electronics can be found in reference 7. One part of the system has, however, been reconstructed, namely that which controls the information about which of the detectors is responsible for an incoming pulse. In analogy to the digital converter (ADC) we name this unit detector to digital converter (DDC). In the old version pulses could be cut off by the blocking signals, coincidences between different detectors blocked the whole system during 10 microseconds and the noise from different detectors was added in the summing amplifier. The new unit was constructed in order to avoid these drawbacks.

The block diagram of the new unit is shown in figure 3.2. The principle can be used for any number of detectors. In the figure only one of the detector lines is sketched. The interconnections with other detector lines are indicated with empty arrows.

The input signal turns on a Schmitt trigger. The front of the signal gives a 50 nanosecond trigger signal, which tries to shift on a corresponding bistable circuit. It will succeed if the bistable is not blocked by an external signal or if any of the other lines contains an on-condition in either the Schmitt trigger or the bistable circuit. If the bistable circuit goes on it opens a linear gate in order to send a delayed linear pulse into the summing amplifier.

The important features of the circuit are that during the same time more than one gate is never opened and that the opening always occurs so that the pulses are not cut. If two pulses arrive with the leading edges in coincidence within

50 nanoseconds, no gate will be opened. If they are separated by more than 50 nanoseconds but less than the deadtime of the system, the first one arrived will be treated, and if they are separated by more than the deadtime of the system, both of them will be taken care of.

Two series of measurements were done, the first one (D series) with 2.2 cm thick polyethylene discs and a separation distance going from 13.2 to 0 in steps of 2.2 cm. In the second (E series) we used 4.4 cm discs and the separation distance varied from 8.8 to 0 with the same step length. The diameter of the discs was 18 cm in both of the series. For each distance we made three measurements with different delay times between the end of the neutron burst and the beginning of the measurement. In the D series the delay time was 10, 30 and 50 microseconds, in the E series it was 20, 60 and 100 microseconds. The length of the neutron burst (D-T reaction in a 150 kV SAMES neutron generator) was adjusted so that the channel with the highest intensity was nearly filled during a measurement of 80 minutes. The length of the neutron burst was varied up to 20 microseconds in the E series and up to 50 microseconds in the D series.

The measured distributions were corrected for deadtime and background. The decay constants were then calculated with a correlation method. The programs used were REMSINP, PARIN, OWCO, DTFAKT, DECORR, PILEUP, BAGMSU and CORLAM. The methods used by the programs are described in the references 7 and 8.

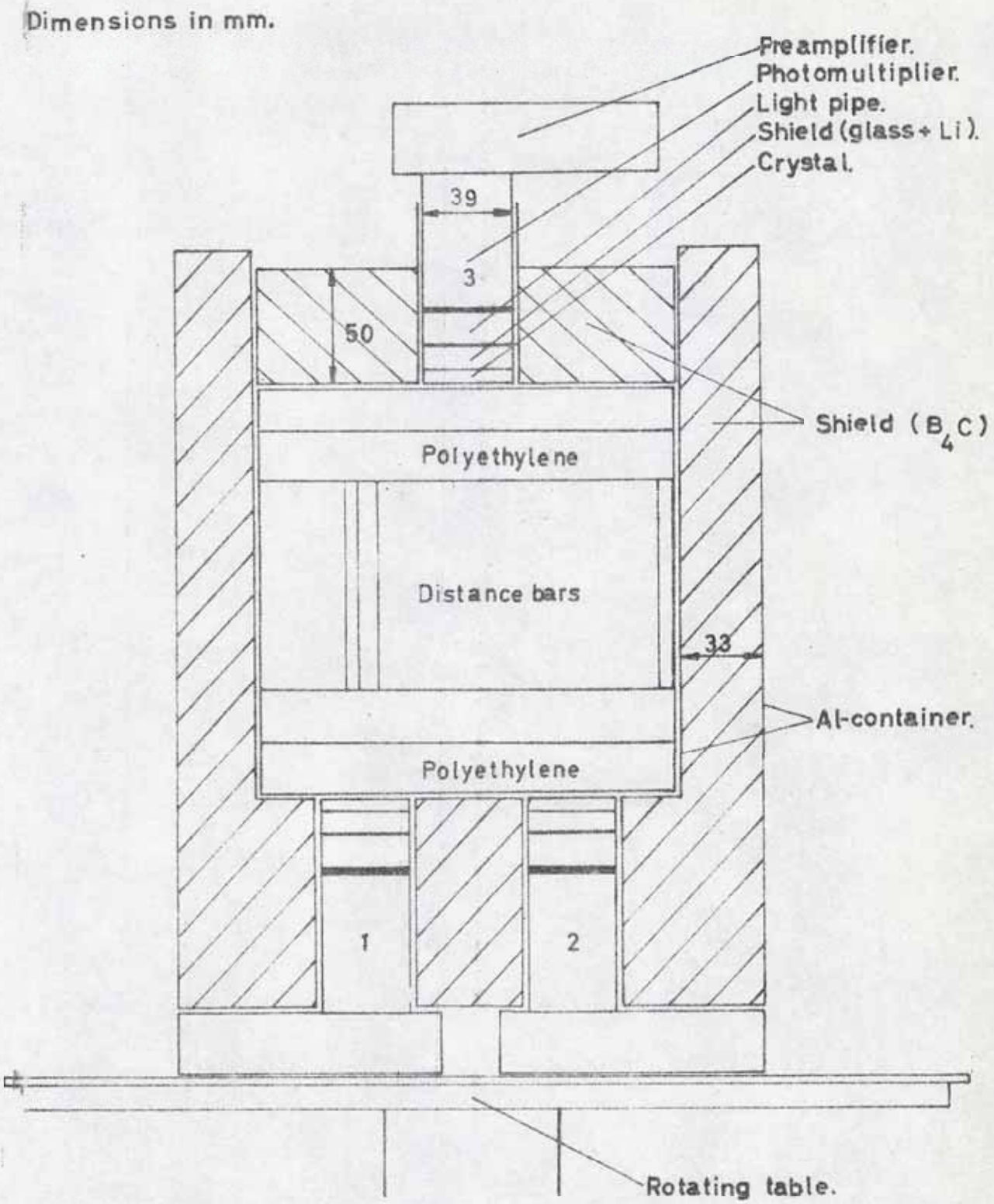

Fig. 3.1. Experimental arrangement.

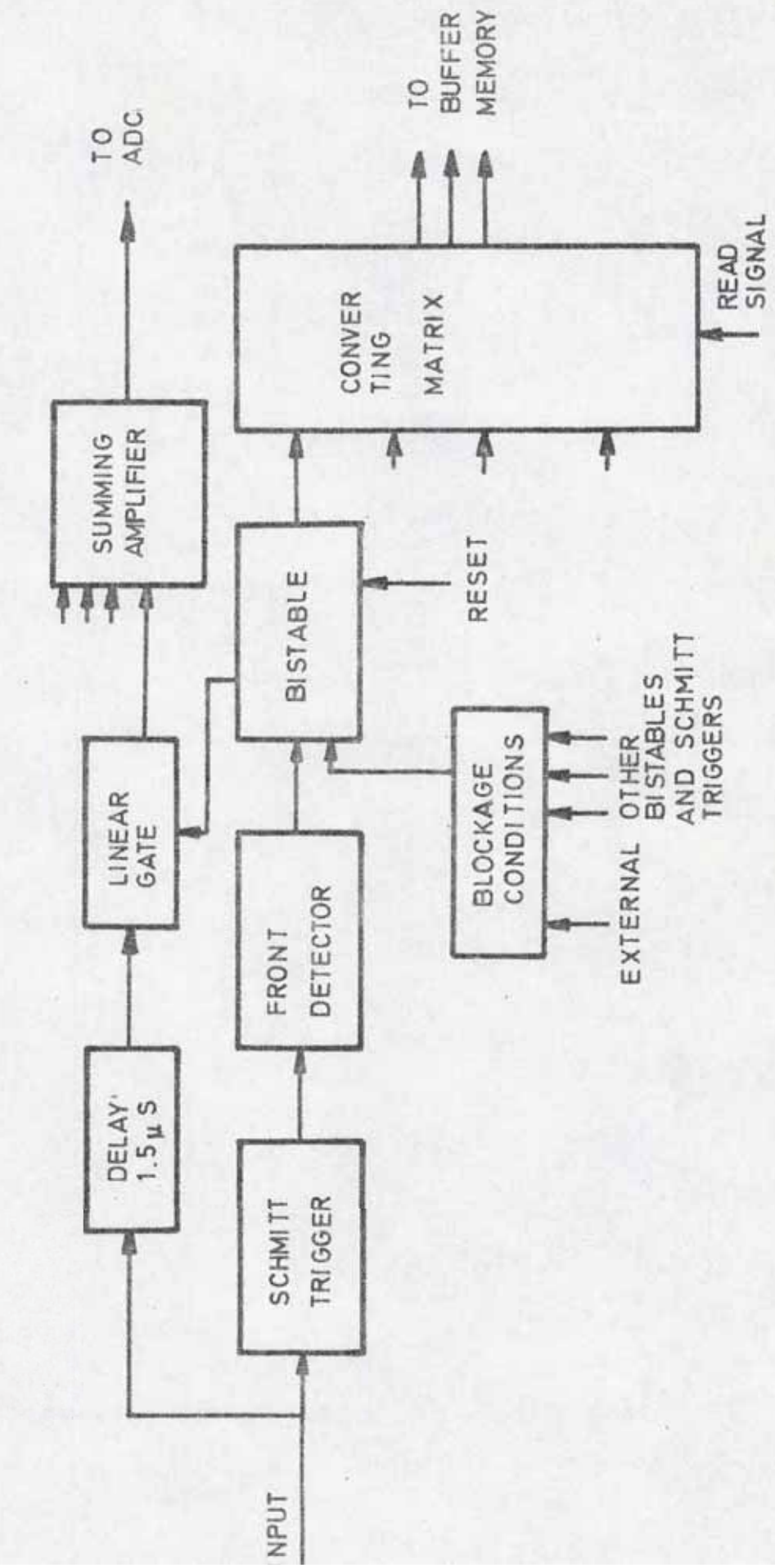

Fig. 3.2. Working principle of the Detector to Digital Converter (DDC).

4. RESULTS

The results given by the program CORLAM contain information about amplitudes, correlation coefficients, decay constants and standard deviations. We will here mainly use the information about the decay constants and their error limits.

Some remarks must be done about the principles and limitations of CORLAM. As input we use two different measurements on the decaying neutron intensity. These measurements are done with a channel width that varies in the sequence 1, 2, 4, 8 .... in order to cover the entire measurable part of decay with few channels. The program correlates two measurements against each other and tries to determine two decay constants. If the modes are sharp the program will find both of them. No information is, however, given whether the first found or the second is the fundamental one. This decision must be done manually from the amplitude values or other indications.

During this experiment the program has always found a first mode. It is difficult for the program to find the second mode if it is close to the first, if it has low intensity, if it is not sharp, or if the two series are nearly proportional to each other. In these cases the program does an estimate on the second mode. It has been found by experience that these estimates often are rather good. The amplitudes calculated are, however, often bad. This depends on an inversion of a matrix that tends to be singular in these cases.

It can be seen from the equations in reference 7 that if the two series are proportional to each other only one decay constant can be found. The estimate of this is then equivalent to the least-squares method. Therefore, the abscence of a second mode may be caused either by the fact that the two experiments are too close in time or space or by the lack of a second mode.

The error limits calculated by the program will be the statistical standard deviation if the modes are sharp. If the modes are drifting (the logarithmic time derivate of the neutron distribution is not constant in time), the effect of this will be included in the error limits.

The experimental series E and D contain for each separation distance three measurements with different delay times between the end of the neutron burst and the beginning of the measurement. This gives three correlations, which we will name the 1-2, 1-3, and 2-3 time correlations. During the whole experiment we used three detectors. A correlation between detector 1 and 2 gives

information about energy transients because they are symmetrically placed but have different energy sensitivity. Therefore, we call this an energy correlation. The last correlation is a correlation between detector one and three. As these two detectors have different space positions, the first at the zero place of the second radial mode and the third at the symmetry axis, they give information about the changes in the space distribution. Therefore, this correlation is called a space correlation.

The result of the experiment is presented in figure 4.1 to 4.18. The first mode found by the program is marked by a cross, the second by a circle. In most of the cases the first one is also the fundamental one. An estimate of the second mode is marked by parantheses and no marking is done in the cases when the program has failed to find the second mode. The standard deviations are only marked in those places where they are of special interest. The standard deviation of the fundamental mode is in the logarithmic diagrams less than the symbols. The lines drawn are only inter-connections between the measured values.

The Eseries contains 6 measurements, the D series 8. We will in the following refer to the different measurements with serial letter D and E and experimental number 1 to 8 and 1 to 6 respectively.

E6 and D8 are measured with one of the interacting media removed. This means that D1 is identical to E6. They represent, however, two different measurements and serve as a link between the two series.

Figures 4.1 and 4.2 give the energy correlation. If we compare the checkpoints E6 and D1 we find that the latter one is more stable in time. The reasons for this may be that D1 contains a sharper second mode, which has been included in the fundamental in E6. The same reason may be behind the drifting in the limit E1. The most striking feature of this correlation is, however, the second mode found in the D series at the shortest delay. With the exception of D2 and D3 it is rather independent of the separation distance. It must be identified as the thermalization time constant and gives a thermalization time of 4.8 microseconds. As a comparison, the Nelkin model gives for water 4 microseconds [9 page 228].

The thermalization effect appears only at delays of 10 microseconds. This depends on the high decay rate of this mode and therefore it may be neglected for all correlations that do not include the 10 microseconds delay.

The space correlations are plotted in figure 4.3 and 4.4. The checkpoints are not so stable here as in the energy correlation. Especially the modes lower than the fundamental in D1 give reasons to suspect some influence of background.

During the measurement there was a slow but rather serious drift in the amplification factor of the third detector. It was manually compensated by changes in the high tension to the photomultiplier, but as a matter of the fact the program of background subtraction had a more complicated case to handle than normal. One of the results of this is that D4 with delay 30 microseconds is missing. A comparison between E6 and D1 shows that there really is a difference that does not depend on the experimental set up. Although we shall have this defect in mind, it will have no influence on the general conclusions drawn from the experiment.

Space modes are more difficult to handle than energy modes. This is underlined by the results of this correlation. Two bands of decay constants are formed. The higher can be identified as the second radial mode. The drift of the decay constant must be explained by the mixing of modes in the direction of the symmetry axis. With the exception of one case (D5) the energy effects are removed. The point D5 indicates, however, that there may be some influence in the cases of 10 microseconds delay.

The time correlations are plotted in figure 4.5 to 4.16. The space and energy correlations separated some special effects. The characteristic of the time correlations is that they give information about the local effects of each detector.

Therefore, we have to expect that slow local transients which cannot be accounted for by the crude model of two decay constants, give a drifting effect. This effect is seen in the third detector. As we irradiate the cylinder through the curved boundary this detector is the last one that reaches the equilibrium decay. From the measurements E1, E6, D1 and D8 we find that considerable time is needed. The dominating higher mode has negative amplitude, a fact that has been found earlier [7]. As the transparant detector has rather low sensitivity, the best asymptotic values are measured by detector two. The agreement with earlier measurements is good for the values from this detector. This fact verifies the reproducibility of the methods and the equipment.

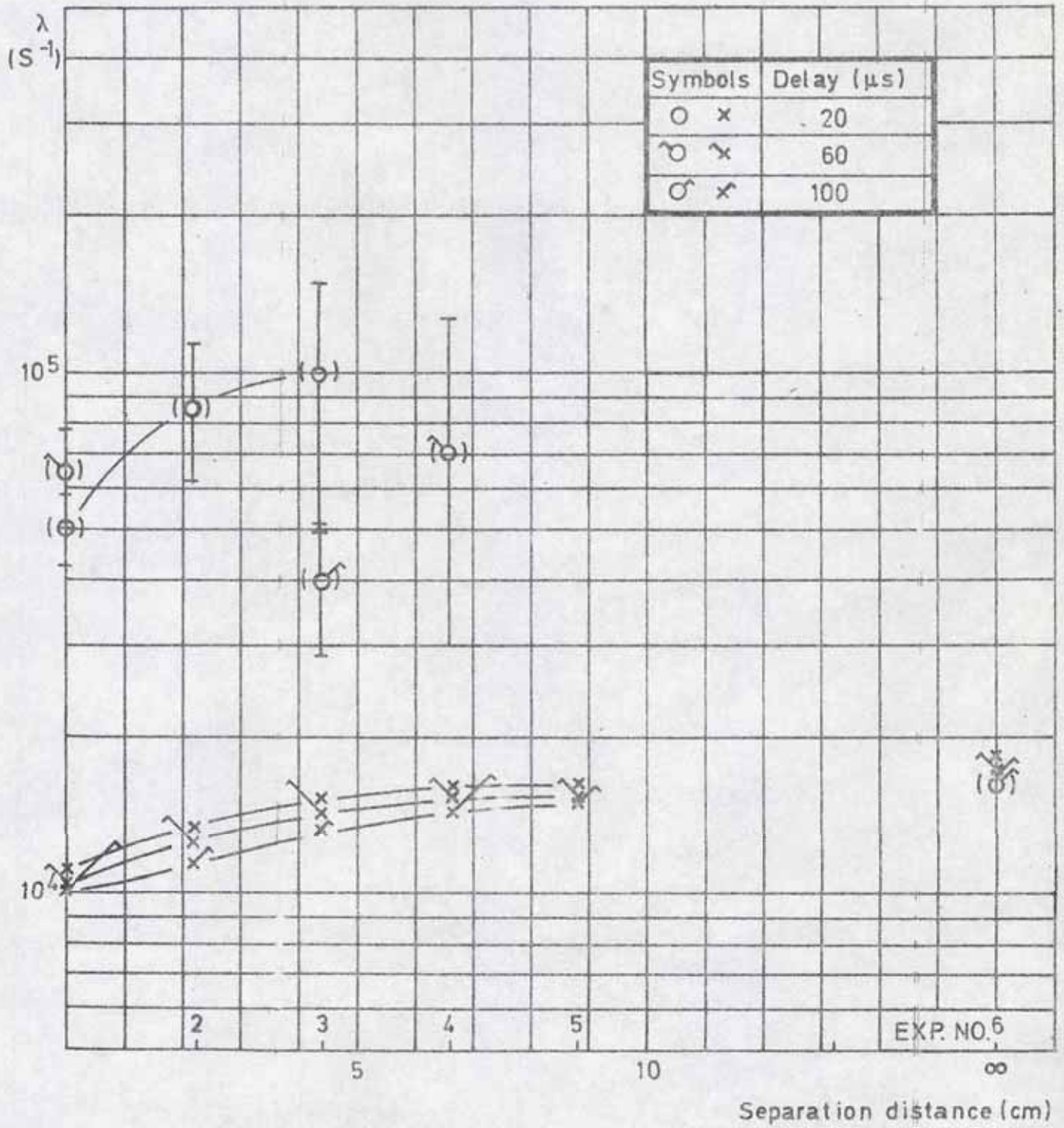

Fig. 4.1. Energy correlation Series E

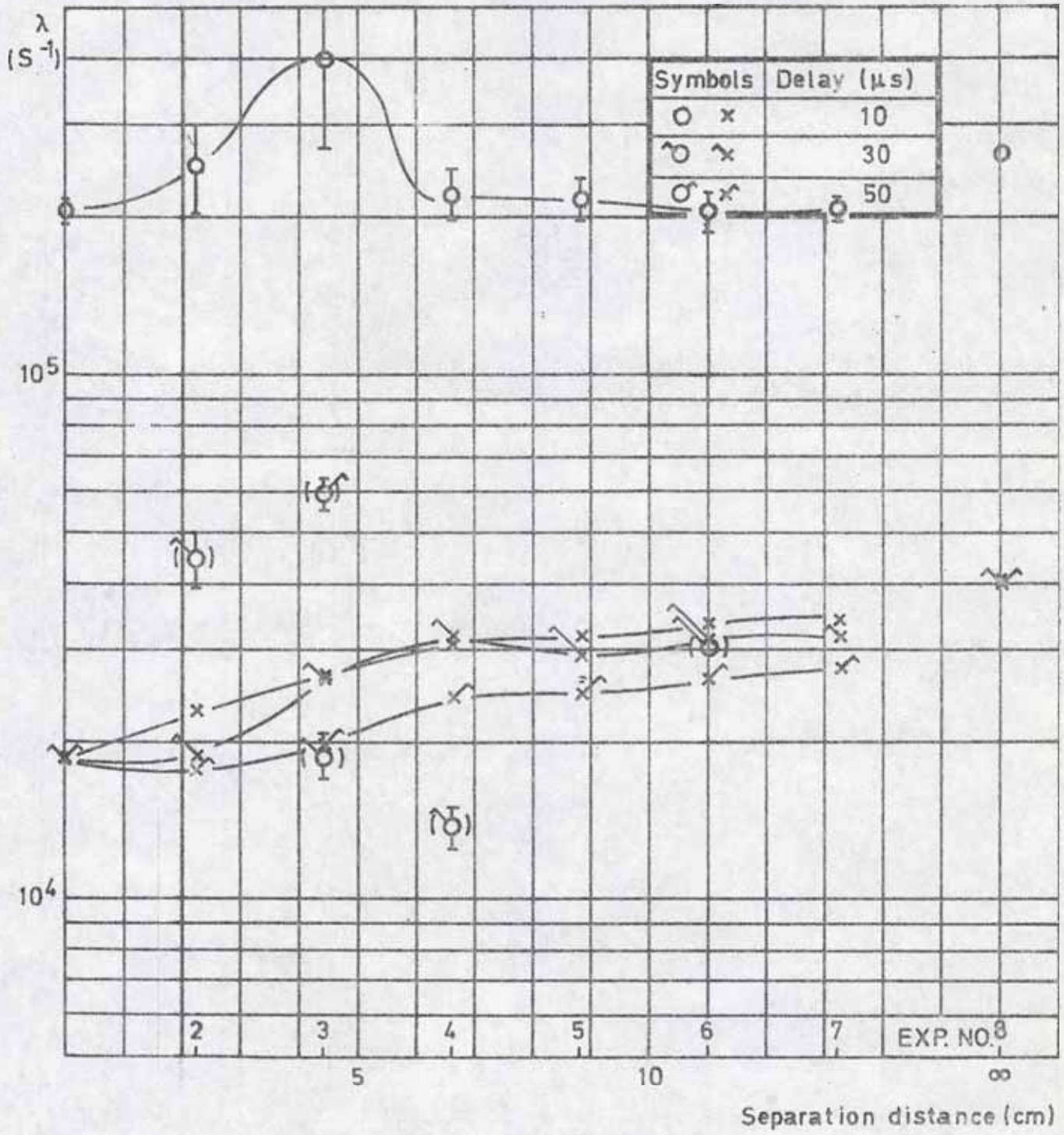

Fig. 4.2 Energy correlation Series D

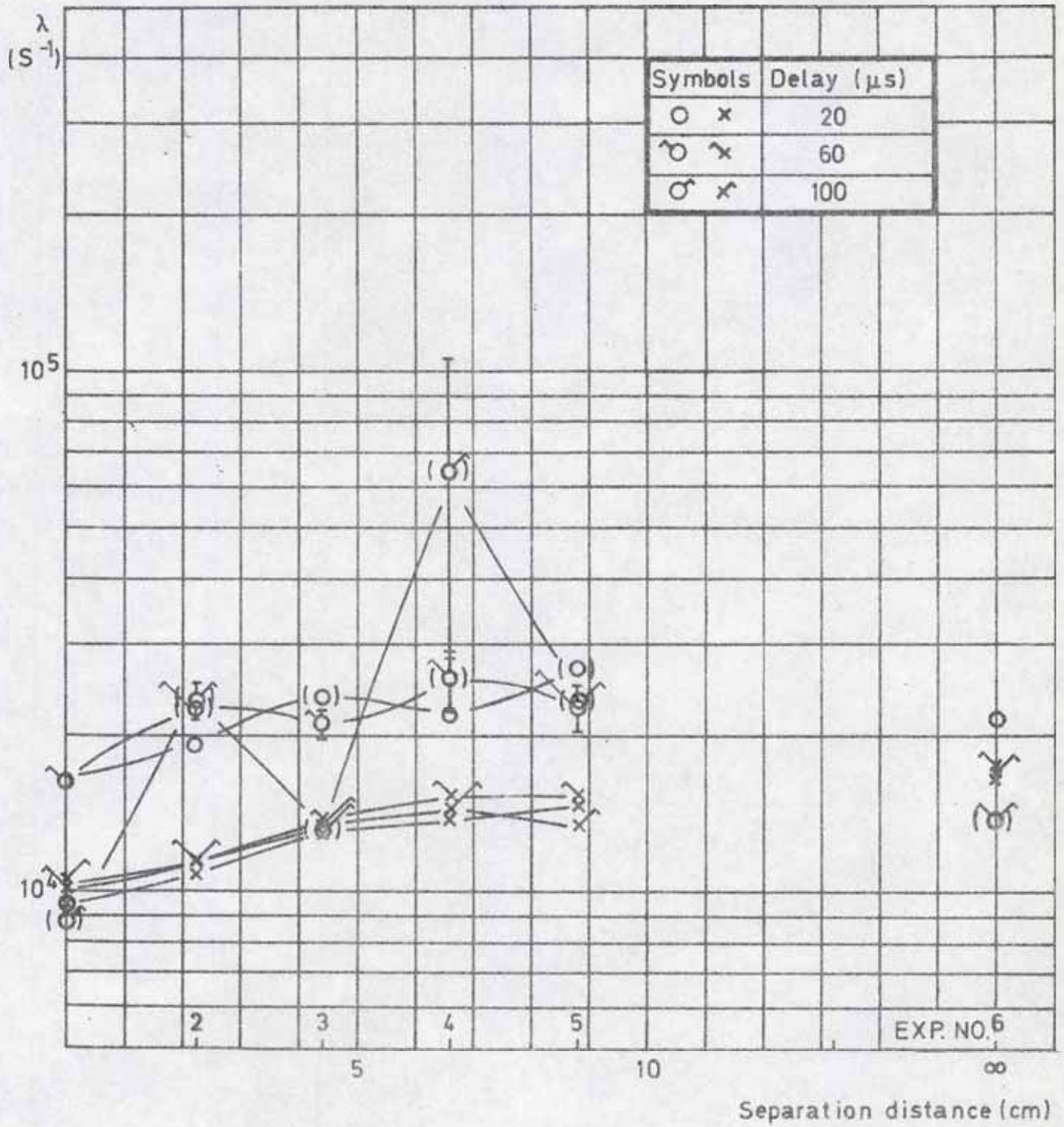

Fig. 4.3 Space correlation Series E

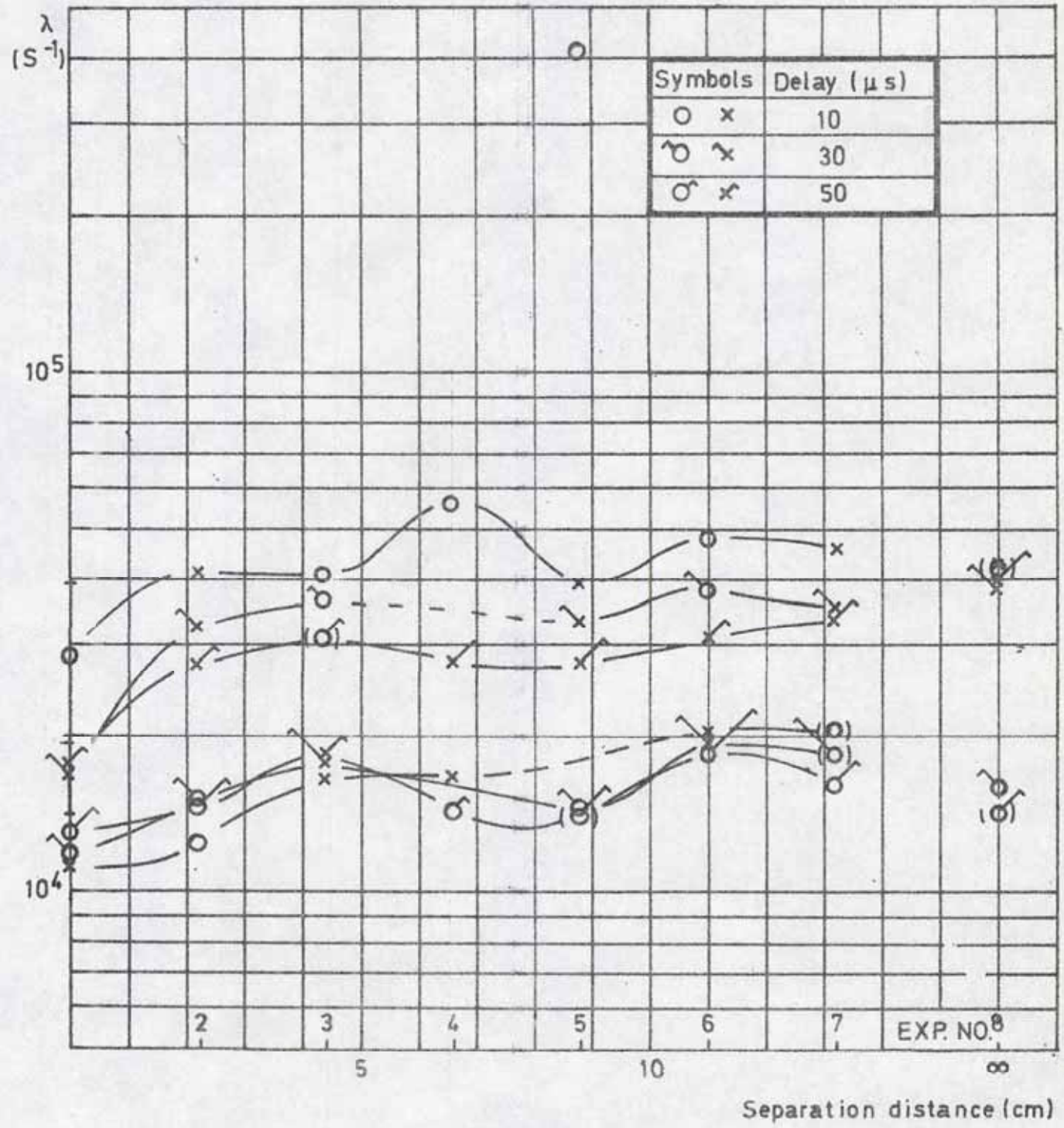

Fig. 4.4 Space correlation Series D

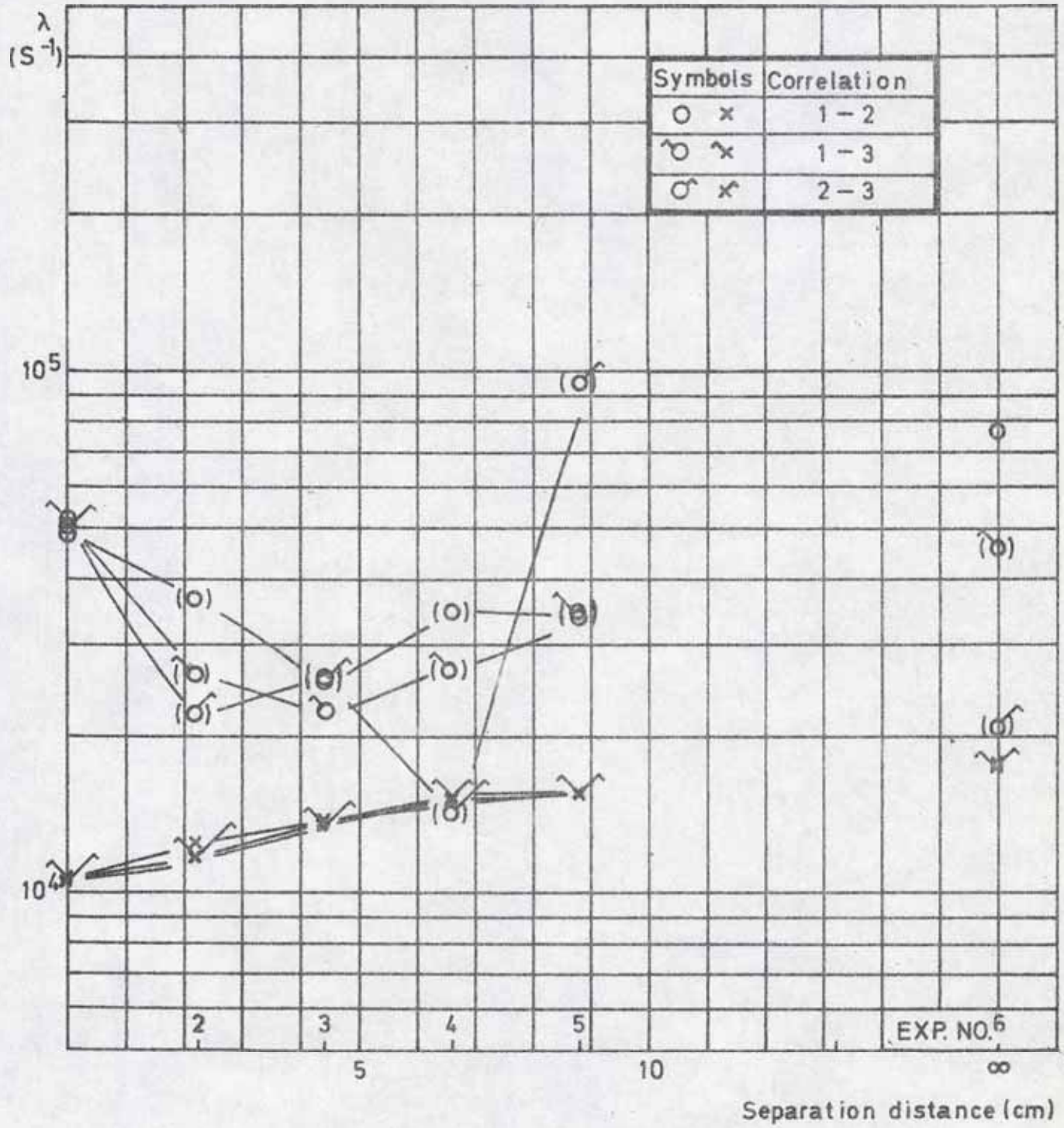

Fig. 4.5. Time correlation Series E. Detector 1.

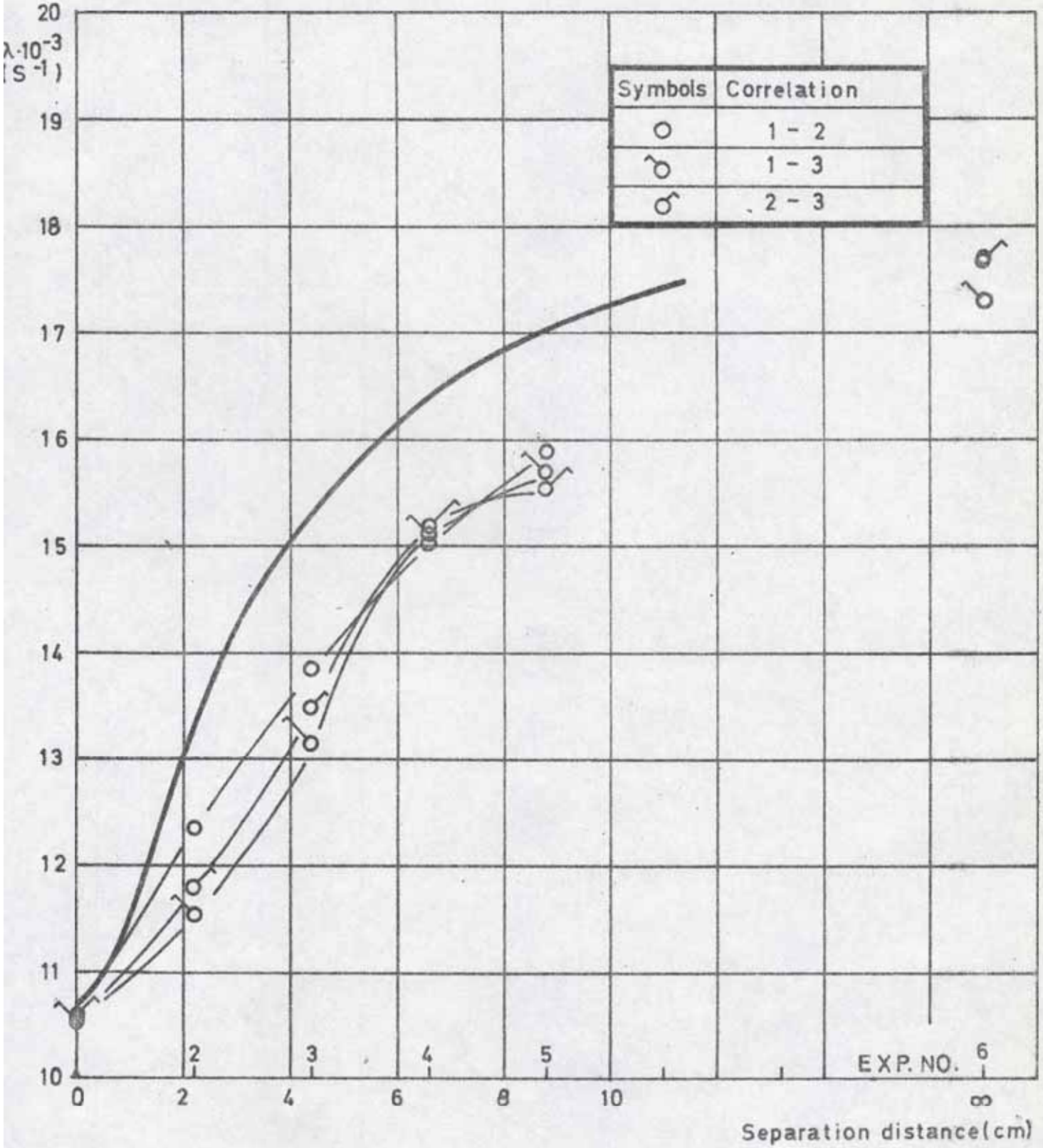

Fig.4.6. Time correlation. Series E. Detector 1.

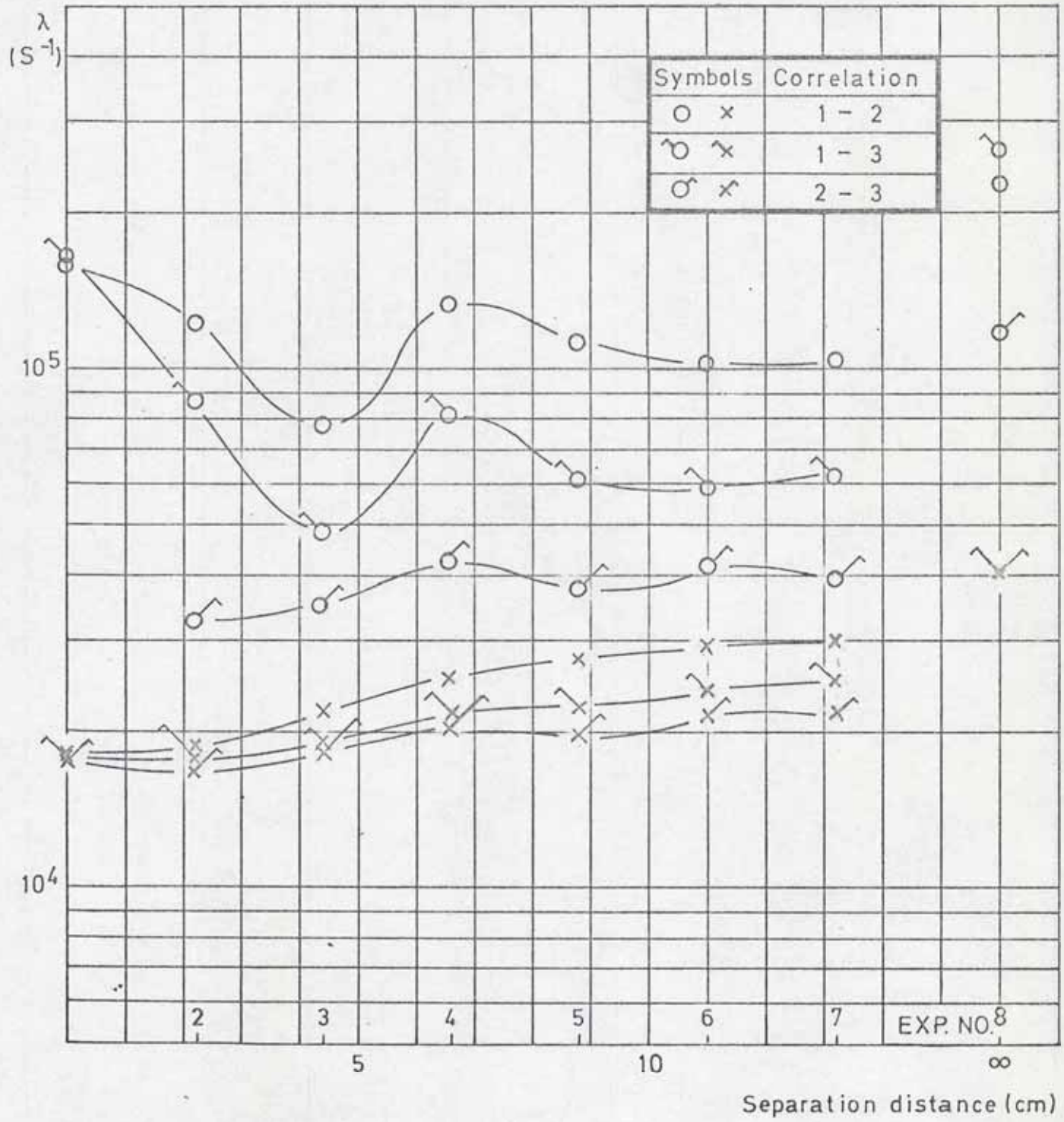

Fig. 4.7. Time correlation Series D . Detector 1.

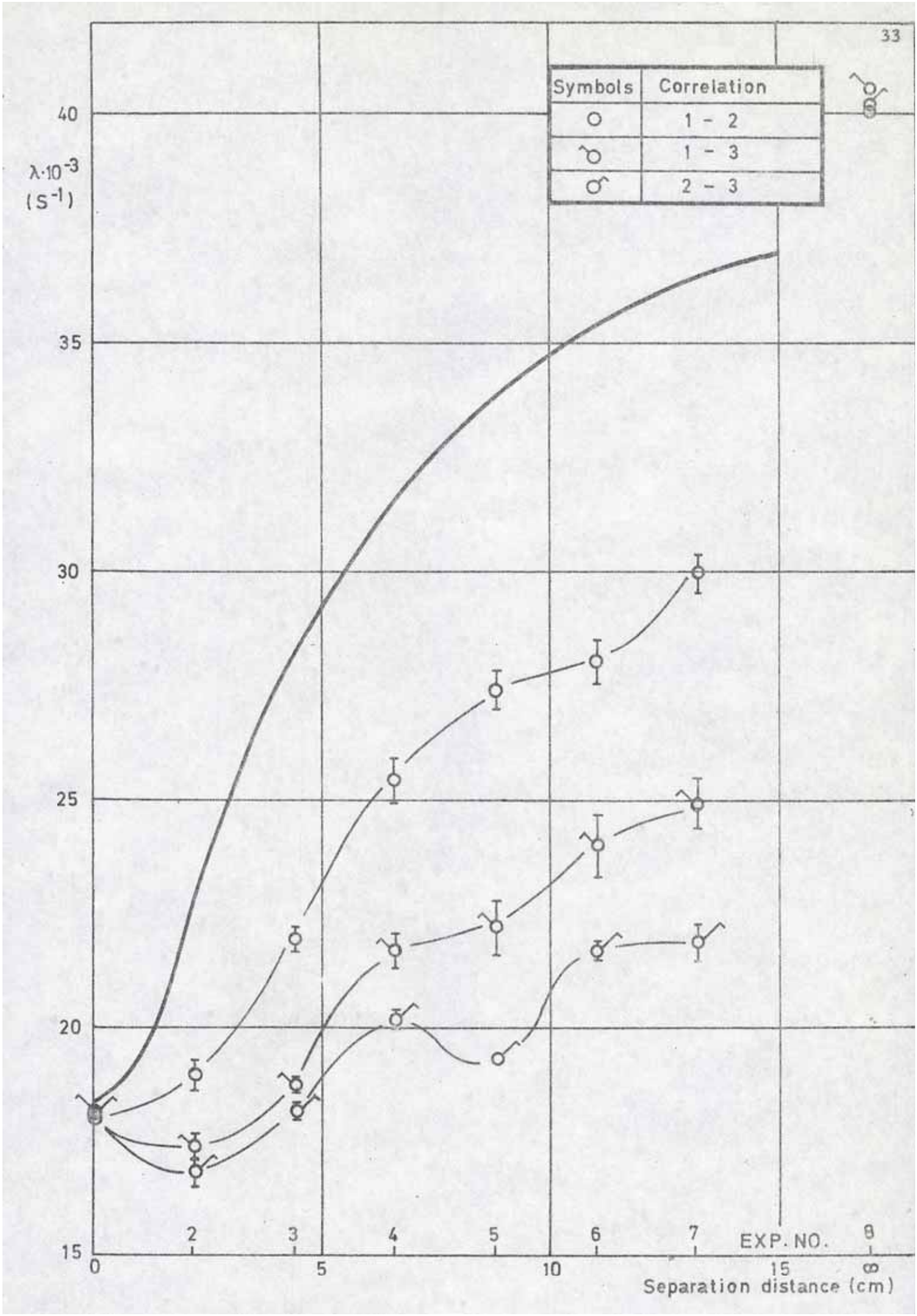
Symbols
Correlation
1 - 2
1 - 3
2 - 3
λ·10⁻³ (S⁻¹)
40
35
30
25
20
15
0
5
10
15
∞
Separation distance (cm)
2
3
4
5
6
7
8
EXP. NO.

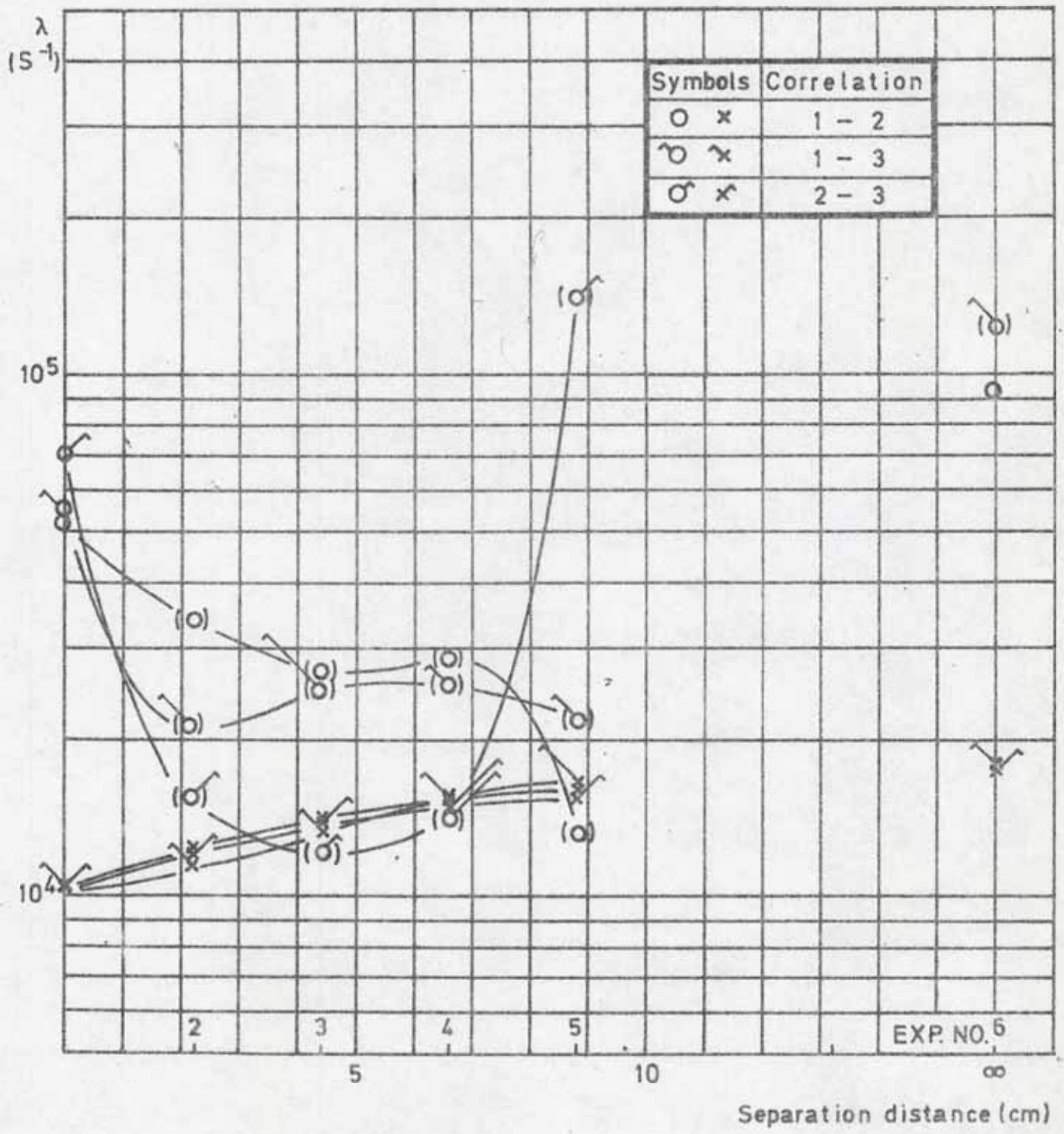

Fig. 4.9. Time correlation Series E . Detector 2.

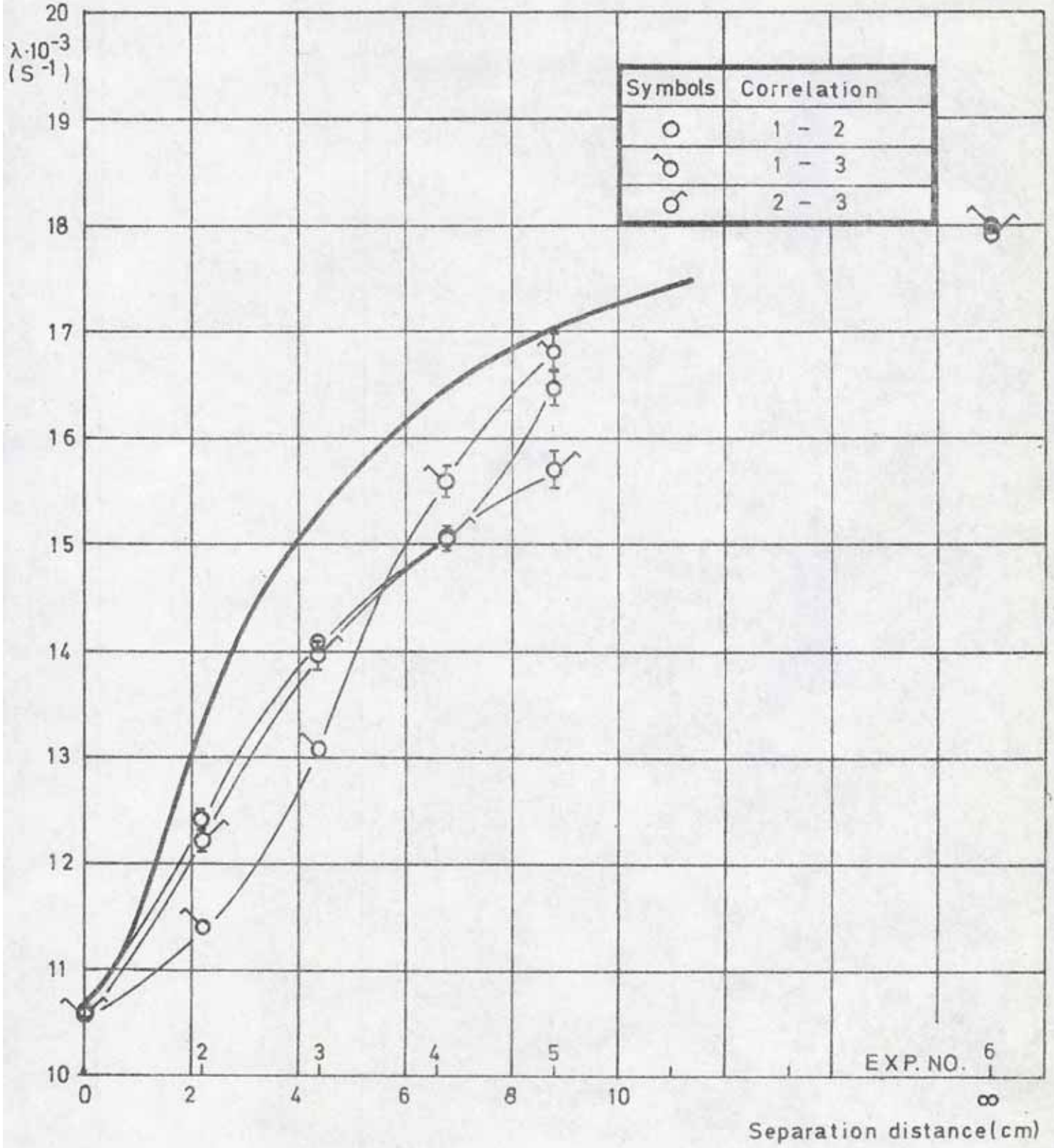

Fig.410 Time correlation. Series E. Detector 2

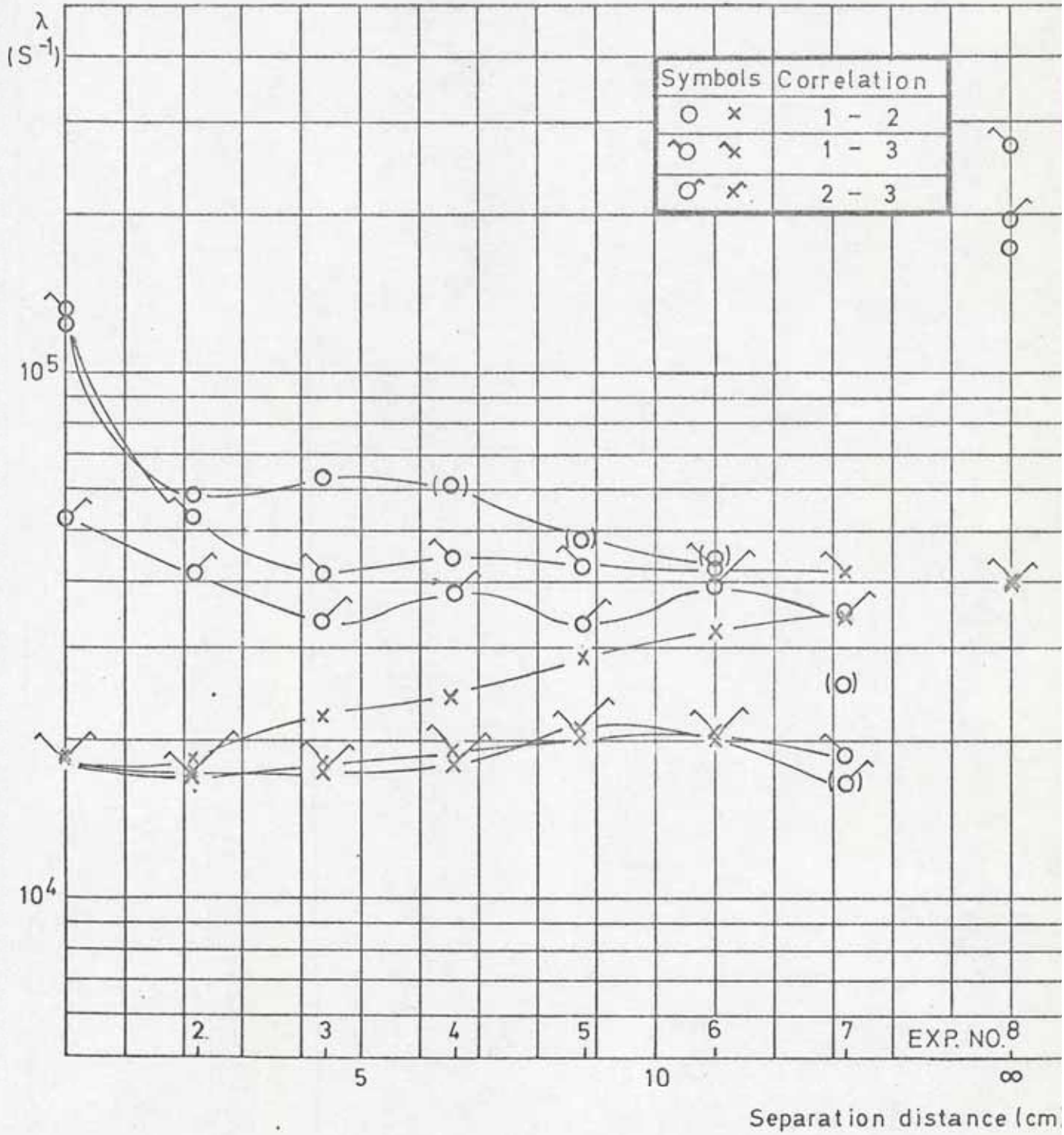

Fig. 4.11 Time correlation Series D. Detector 2

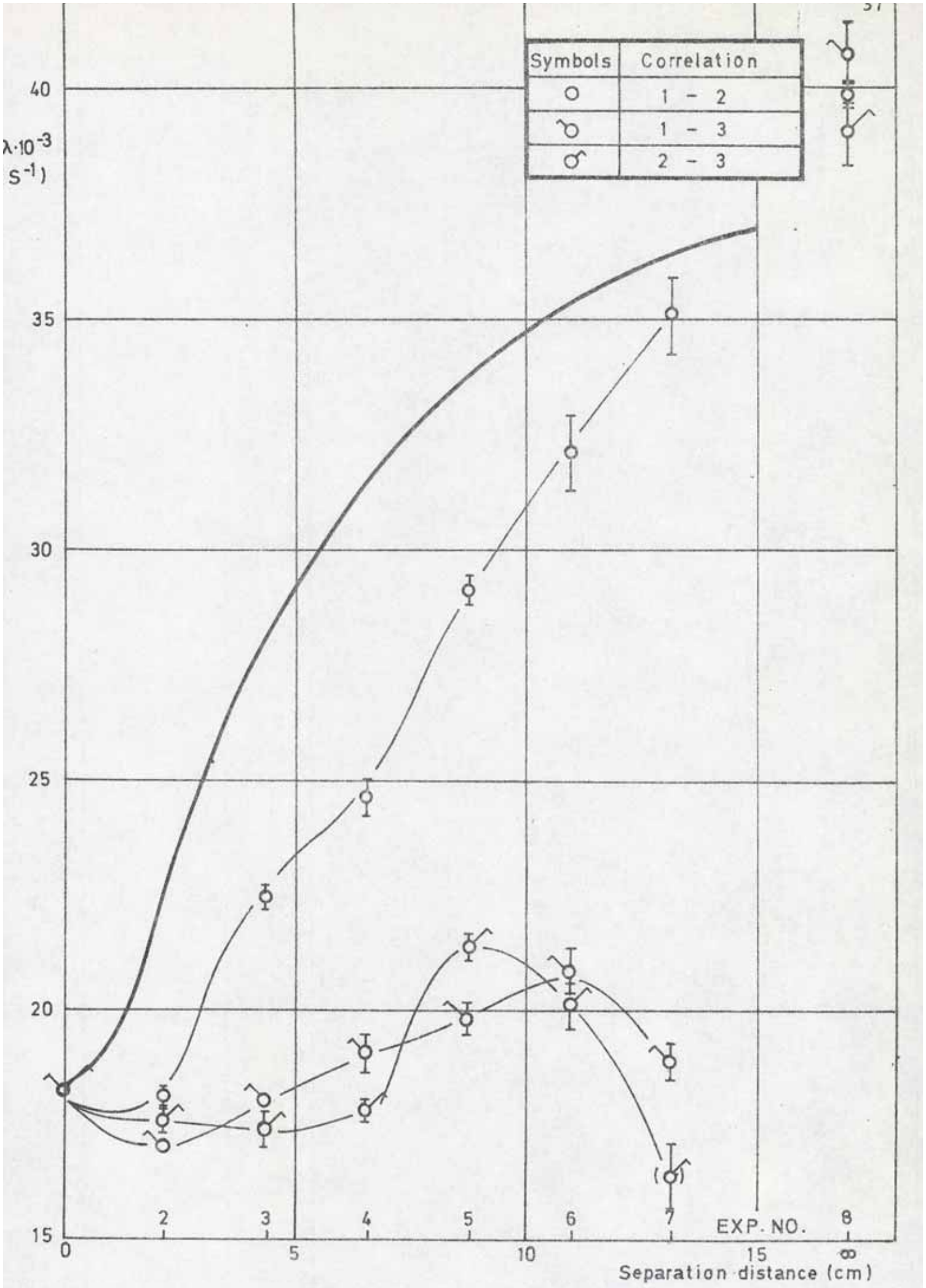

Fig.412. Time correlation Series D. Detector. 2.

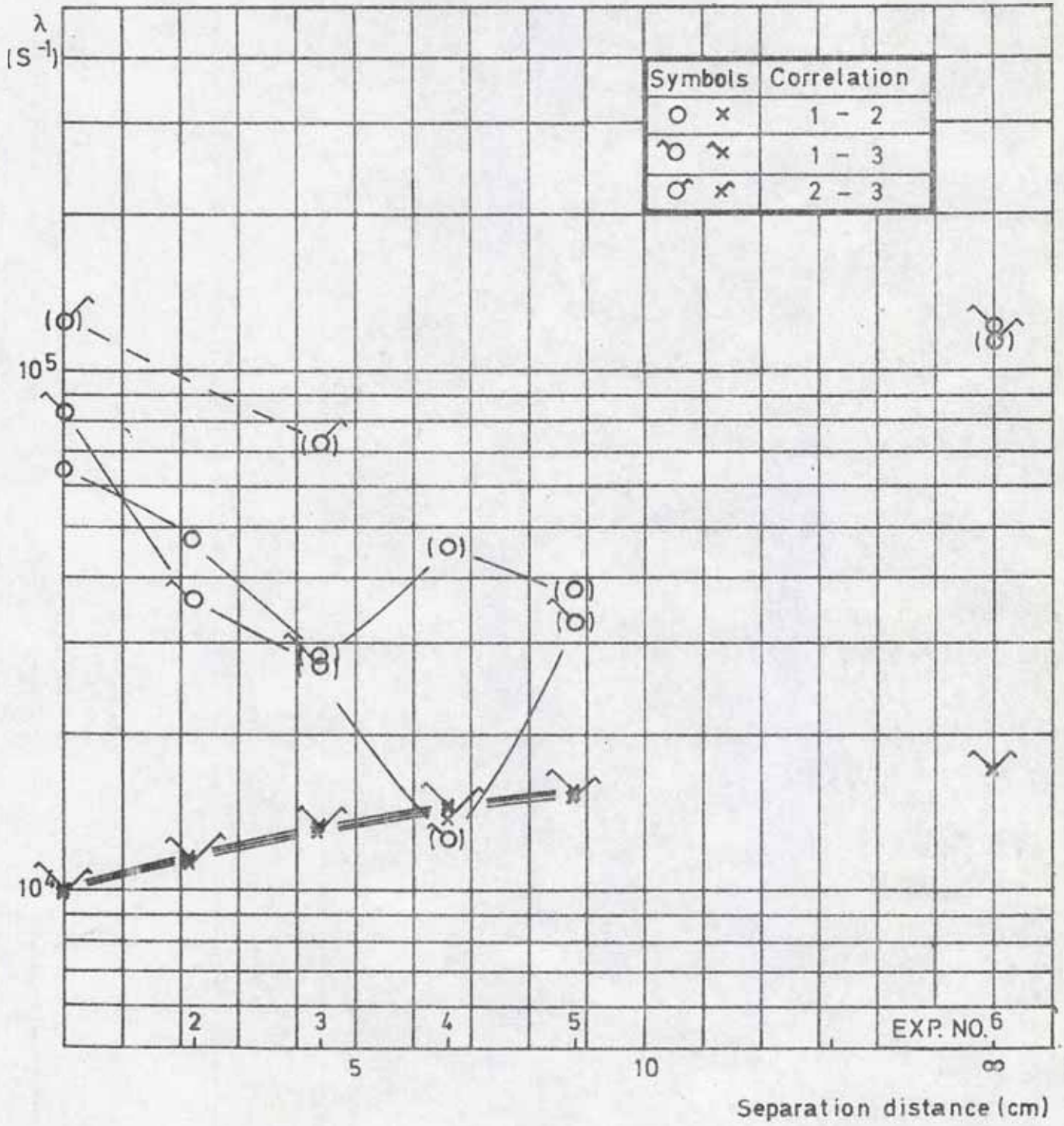

Fig. 4.13. Time correlation Series E Detector 3

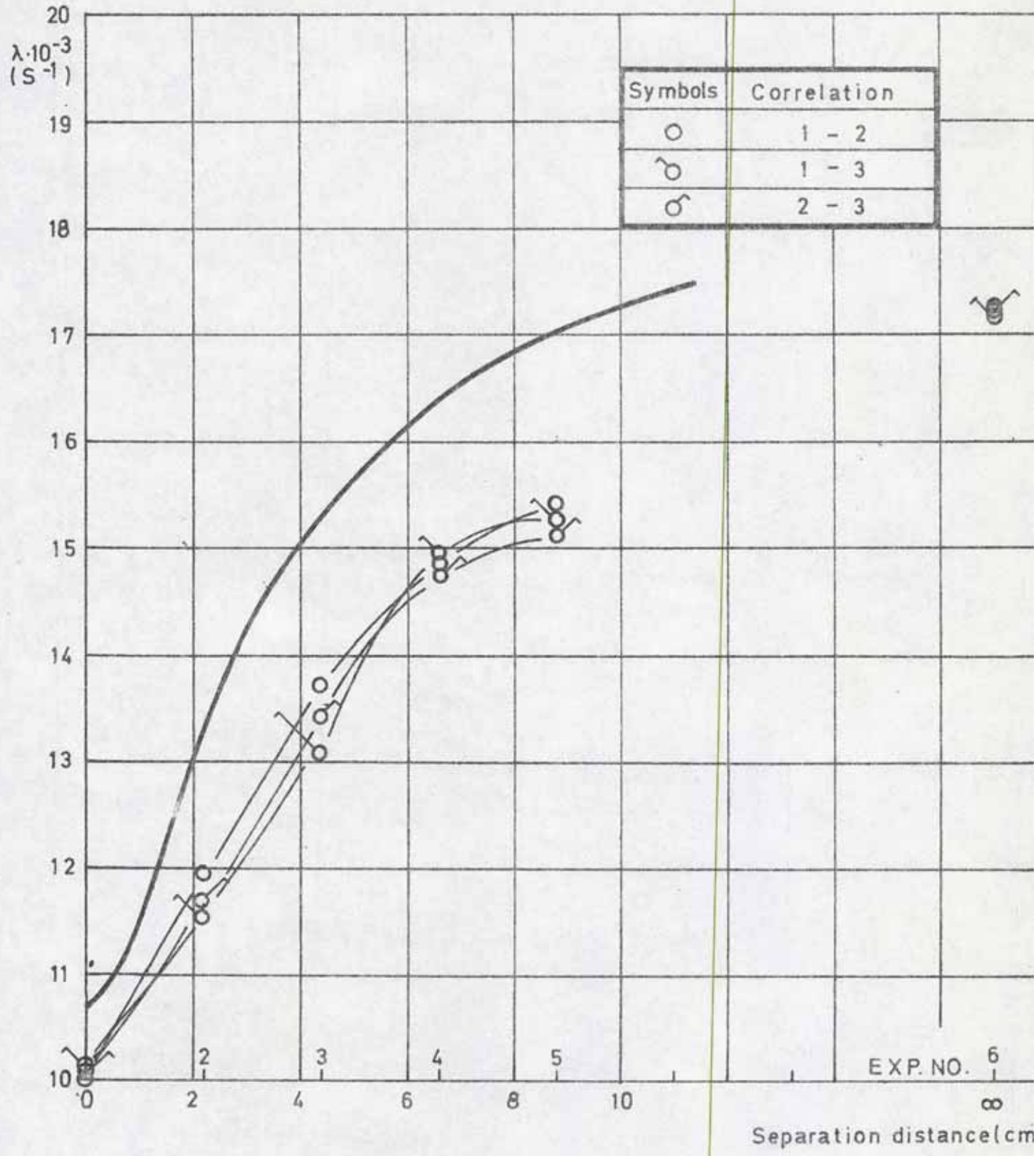

Fig.4.14 Time correlation. Series E. Detector 3

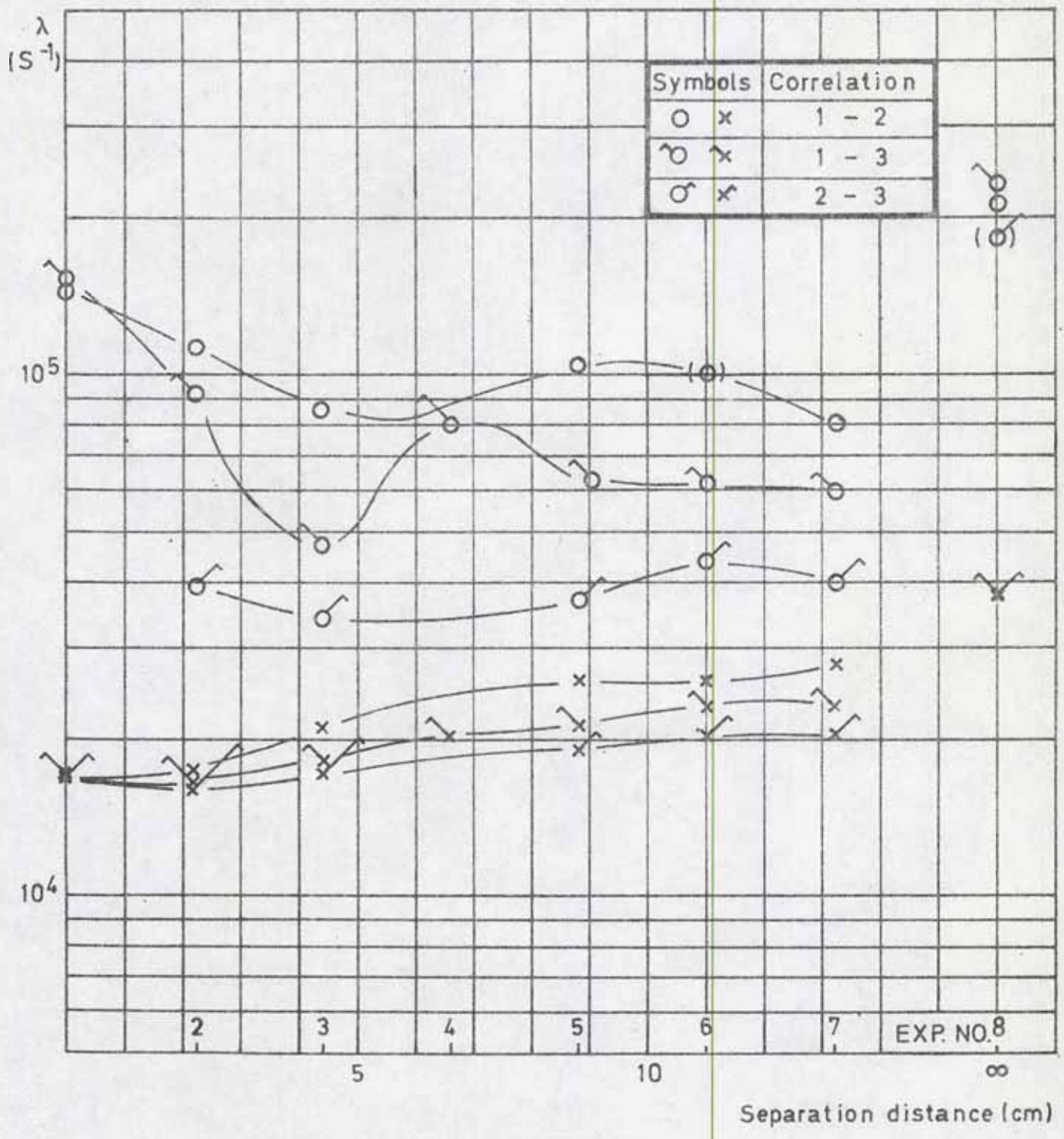

Fig. 4.15 Time correlation Series D Detector 3

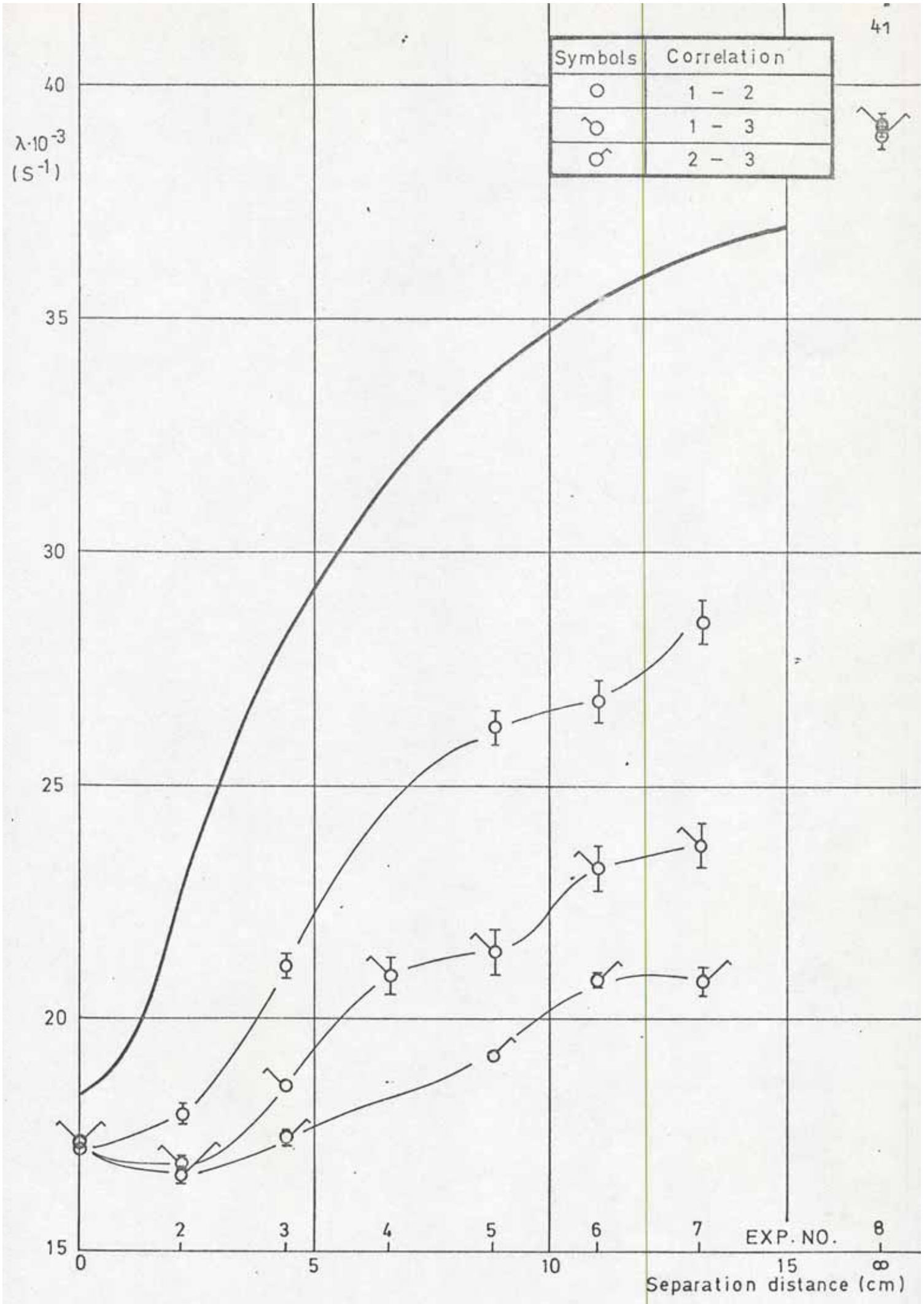

Fig 4.16 Time correlation, Series D, Detector 3

5. DISCUSSION

Figures 5.1 and 5.2 give the lambda values calculated by the method outlined in chapter 2. The constant used are the same as in figure 2.2. The time dependent transport effect has not been accounted for. The lower curves have also been drawn in some earlier figures. A comparison with the experimental values gives immediately the result that the mentioned effect exists. The comparison also shows that the effect is different in series E and D, and we can conclude that it depends on the decay constants.

In a stationary system an increasing separation distance will give a deteriorated neutron economy of the system. It is interesting to note that the dynamic effect is so heavy that it sometimes gives an improved neutron economy. This can be seen in measuring point D2 which has lower lambda values than D1. During a time period the neutrons are "stored" in the space between the two discs.

The next question is the existence of the suggested pseudomodes. It is in this case more difficult to get good experimental evidence, partly because there is no stringent definition on these modes. They are, however, reflected in the stability of the obtained decay constants. Therefore, we will use this concept in the following discussion. We must, however, keep in mind that instabilities are also created by mixed modes with nearly equal decay constants.

The energy correlation gives converging decay constants in the checkpoints but not in the rest of the experiment. We can compare this with the time correlations for the actual detectors. We find that none of them is stable. The highest drift occurs in detector 1. The lowest separation distance shows in some cases a somewhat better converging tendency than the other distances (figure 4.8 and 4.14) but the convergence is also here rather bad as compared to the check points.

The space correlation shows rather scattered values. The upper mode is rather well defined in series E but clearly drifting in series D. A comparison of the time correlations for detectors 2 and 3 shows more drifting effects in detector 3 for the D series, but the contrary conclusion can be drawn from the E series.

The fundamental mode as seen by the experiment varies rather much. There is, however, a systematic tendency that goes through the whole material. The decay constant has a trend against low values in D2 and E2 and high values in D4 and E4. As this trend does not depend on the series it is difficult to explain. It may be caused by the variations instroduced by the adjustments of the neutron burst length and amplified through the instability of the decay constants. One can, however, not completely remove the suspicion of some kind of resonance effect.

As a summary on the question of pseudomodes, we conclude, that within the scope of this experiment there are no useable pseudomodes. The drift of the modes is systematic in energy for low values of the separation distance but elusive in space.

As we found that this method can not be used to determine the stationary interaction we seek for a method to cancel the dynamic influence. The integral Boltzmann equation can be written [2 eq. 9.8 a]

$$f(\bar{x}, E, \bar{\Omega}, t) = \int_0^\infty ds \left[\exp\left\{ - \int_0^\infty \Sigma(\bar{x} - s\bar{\Omega}, E)\, ds'\right\}\right] q(\bar{x} - s\bar{\Omega}, E, \bar{\Omega}, t - s/v \quad (5.1$$

where the symbols used are defined in reference 2. A necessary condition for an exponentially decaying field is that the integral is bounded. This means that the condition

$$\frac{\lambda s}{v} \leqslant \int_0^s \Sigma(x - s'\Omega, E)\, ds' \qquad (5.2)$$

must hold for all transfers within the convex boundary of the system, that is for all $\bar{x}$, E and $\bar{\Omega}$. In our case the condition is met within the two discs but not for all transfers between them. However, if an absorbing disc is placed between the moderators the condition 5.2 is fulfilled if the following condition holds.

$$\frac{\lambda d}{v} \leqslant \Sigma_a \cdot d_a \qquad (5.3)$$

where d_a is the thickness and Σ_a the absorption coefficient of the absorber. Equation 5.3 shall be fulfilled for all values on v. Attractive is the case of an 1/v absorber. We then have

$$d_a > \frac{\lambda \cdot d}{\Sigma_{ao} \cdot v_o}$$

where Σ_{ao} is the absorption cross section at the velocity v_o. The case of equality gives then equivalence to the stationary case. This can be achieved through an iterative process. The remaining problem is then the waiting time, which must be long enough to guarantee equilibrium and the oscillations, which must be damped down to a magnitude that can be neglected.

The delay effect in a pulsed neutron experiment has been studied with graphite slabs by Dance [11]. It has also been mentioned in the connection of channels in graphite blocks in an article by Deniz et al. [12].

Dance finds that he can use the concept of pseudomodes and has calculated correction factors in order to get the stationary interaction. The strength of the delay effect is directly connected to the parameter ξ defined in equation 2.16. The highest value of ξ in the experiment of Dance is 0.1, which is approximately the same as our lowest value (experiment E2). So, our results in connection with those of Dance confirm the general trend that can be found trough inspection of figure 2.6, namely that the decay curves at low values of ξ can be interpreted as pseudomodes, which, however, lose their significance at higher values of ξ.

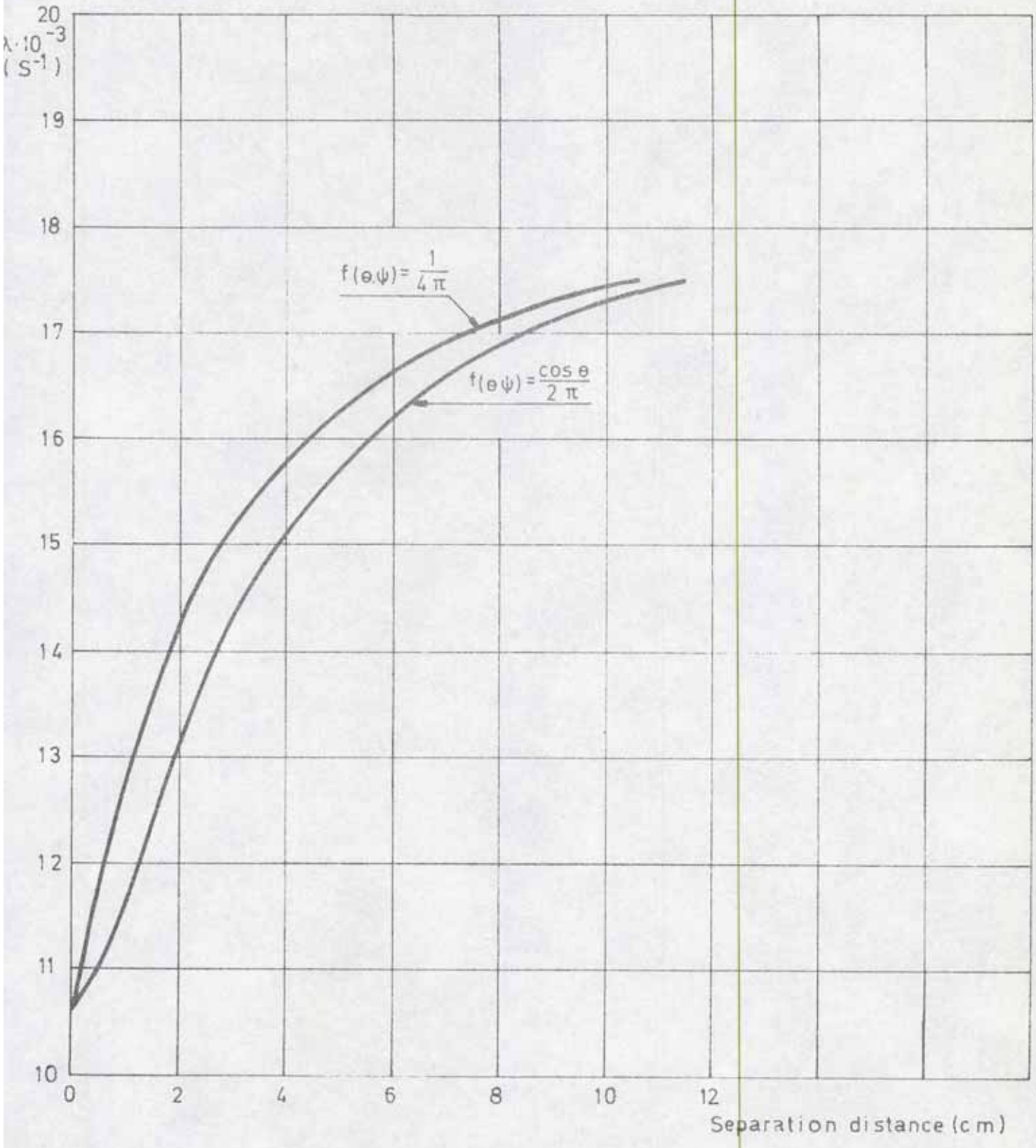

Fig 5.1. Calculated decay constants. ($\rho_p = 1$). Series E.

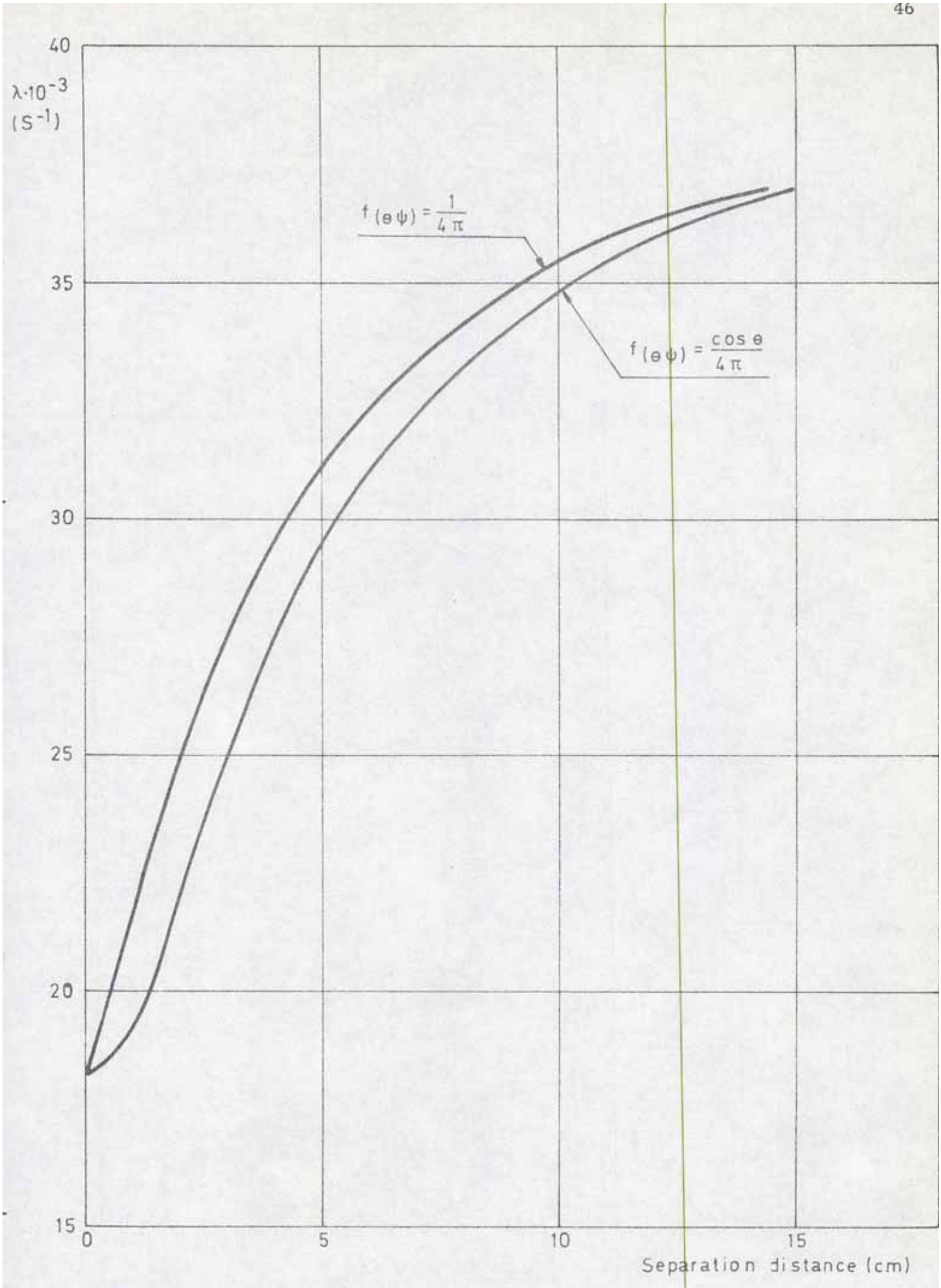

Fig. 5.2. Calculated decay constants ($\rho_p = 1$). Series D.

6. CONCLUSIONS

The conclusions from this work is that the pulsed neutron method cannot be directly applied to the case of two interacting moderators and that within the scope of this experiment the apparent decay constant is not enough stable in time to give relevant information about the stationary interaction.

As the dynamic transport effects appear already at rather small distances it follows that in all applications of the pulsed neutron method on systems containing concave boundaries or cavities the result must be corrected for these effects.

From the preceeding discussions and the work of Corngold [4] we can formulate the following general rule for the application of the pulsed neutron method: "The dynamic transfer kernel shall be bounded for all interactions between all subdomains of the system ". The dynamic transfer kernel is here defined to include the delay effect in q of equation 5.1.

It has been shown that an absorber may be used to cancel the transport effect. Solid absorbers may be used but in the case of cavities one may also use a gas.

ACKNOWLEDGEMENTS

The author is grateful to professor N.G. Sjöstrand and the members of his institution for help and valuable discussions. K. Mandorf served as operator during two sunny weekends. C. Varenius typed the report. The work has been supported by the Swedish Atomic Research Council.

REFERENCES

(1) R. Kiyose, Y. Shimazaki, S. Enomoto, A study on interaction of subcritical assemblies. - Symposium on criticality control of fissile materials, Stockholm 1965. Proceedings, p. 337-345.

(2) A.M. Weinberg & E.P. Wigner, The physical theory of neutron chain reactors, The University of Chicago Press, 1958.

(3) H.K. Clark, A simple practical method for calculating interaction. - Symposium on criticality control of fissile materials, Stockholm 1965. Proceedings, p. 87 - 102.

(4) N. Corngold, Some transient phenomena in thermalization, - Nucl. Sci. Eng. 19 (1964) p. 80.

(5) W.M. Andrews, Measurement of the temperature dependence of neutron diffusion properties in beryllium using a pulsed neutron technique. 1960. (UCRL 6083).

(6) N. Corngold, Decay constant of a neutron pulse. - Nucl. Sci. Eng. 23 (1965) p. 403.

(7) G. Grosshög, Determination of neutron decay constants using simultaneous pulse height and time analysis. 1968. (CTH-RF-16).

(8) G. Grosshög, Deadtime corrections in a two parameter system containing four detectors. - Ispra nuclear electronics symposium, Ispra 1969.

(9) K.H. Beckurts & K. Wirtz, Neutron physics. Springer, 1964.

(10) N.G. Sjöstrand, J. Mednis, T. Nilsson, Geometric buckling measurements using the pulsed neutron sources method. - Arkiv för fysik 15 (1959) p. 471.

(11) K.D. Dance, Pulsed-source investigation of the effect of transverse gaps on neutron transport in a diffusing medium. Stanford, Stanford Univ., 1968. 210 p.

(12) V. Deniz, J.G. Le Ho, M. Sagot, Study of lattices of graphite with empty channels by means of the pulsed source technique. - Nucl. Sci. Eng. 32 (1968) p. 201.

F

CHALMERS UNIVERSITY OF TECHNOLOGY

DEPARTMENT OF REACTOR PHYSICS

CTH-RF-18 Nov. 1969

MEASUREMENT OF THE NEUTRONIC INTERACTION BETWEEN TWO CYLINDRICAL MODERATORS

by

GUDMAR GROSSHÖG

CONTENTS

SUMMARY.

The stationary interaction parameter between the plane surfaces of two identical, cylindrical, polyethylene discs has been measured with the pulsed neutron method. It was shown possible to overcome the delay effect caused by the flight of the neutrons in the gap between the moderators by means of the insertion of absorbers. In the measurements the ratio of separation distance to diameter was varied between 0,06 and 0.77, and the corresponding interaction parameter went from 0.93 to 0.24. Using two different thicknesses of the discs two series of measurements were performed, one covering decay constants between 10,000 and 17,000 s^{-1} and the other the range 17,000 to 40,000 s^{-1}. Although full equilibrium of the neutron distribution was not reached in all cases in the last series, the resulting values of the two series show a general agreement. A calculation based on a zeroth order Bessel function as radial distribution and $(\cos\theta)/\pi$ as angular distribution of the neutrons leaving the interact ng surfaces gives too large interaction parameter for all separation distances. However, the overestimate seems to be small when the surfaces are close together.

1. INTRODUCTION.

An essential parameter in the criticality control of fissile materials is the interaction parameter ϑ (1). For an assembly of bodies, which interact through the interchange of neutrons, the interaction parameter is defined as the probability that a neutron coming from one body hit another one.

The interaction parameter depends on the shape and position of the interacting surfaces, on the angular distribution and on the velocity distribution of the outgoing neutrons. For simple systems approximate expressions for the interaction parameter are available (1, 2). These expressions are often conservative in the sense that they give an overestimate of the interaction. For more complex assemblies it is difficult to calculate the interaction parameter and therefore experimental determinations are needed.

One method often used to measure the interaction relies on determination of the reactivity of a multiplying assembly (1). Another course of action is to use the pulsed neutron method (3). We have earlier shown that this method can be used only at small values of a parameter ξ defined as

$$\xi = \frac{\lambda s}{v} \tag{1.1}$$

where

λ = the decay constant
s = the length of the flight path of a neutron between the interacting surfaces
v = the velocity of the neutron

and then only if a correction is incorporated, which takes into account the time the neutrons spend in the space between the interacting media (4). We have also shown experimentally that this delay effect is so strong that it at large values of ξ affects the basic concept of the pulsed neutron method, which means that no stable asymptotic decay can be found.

The breakdown of the classical pulsed neutron method is caused by two effects. At finite voids it is caused by a singularity, which appears at the low energy part in the energy distribution of the transferred neutrons. One can explain this through the fact that a memory cycle that tends to be infinite

at zero energy has been incorporated into the system. This means that the spectrum of decay constants contains a continuum that goes down to zero. A theoretical study starting directly from the Boltzmann equation is needed in order to get a complete understanding of this phenomenon.

The same ideas can be applied to infinite channels or plane infinite spacings. A singularity appears here for all energies when the angle of the flight path tends to be parallel to the channels or the surface of the plane spacing (5).

There is a close analogy between this type of measurements and a stationary experiment. PALMEDO et al. (6) have recently shown that a measurement in an assembly of Al-H_2O plates does not give an exponential decay in the direction parallel to the plates. This is in agreement with numerical predictions by CLANCY et al.(7) and theoretical by WILLIAMS (8). In this case the limit of the appearing continuum is determined by the properties of aluminium.

Another way to look upon the effect is to establish that the flight of neutrons creates an energy and space dependent importance function, which favours the low energy part of the energy distribution of the transferred neutrons. The delay effect can then be cancelled if we introduce a medium, which has such properties that it, together with the delay effect. gives an importance function identically equal to 1.

The purpose of this work is to apply these ideas to an assembly constructed of two circular polyethylene discs separated along the symmetry axis, and to determine the stationary interaction parameter for the transfer between the plane surfaces of the discs.

2. THE METHOD

The stationary interaction parameter for two interacting surfaces can be written

$$\rho_{st} = \frac{\int\int dS_1 dS_2 \, J(S_1) \, f(\Psi,\theta) \, (\cos\theta) / s^2}{\int dS_1 \, J(S_1)} \qquad (2.1)$$

where

$J(S_1)\, dS_1$ = the total outward current at dS_1

s = the distance between dS_1 and dS_2

$S_1 S_2$ = coordinates in the surface

$f(\Psi,\theta)$ = the angular distribution of the outgoing neutrons, normalized over all outward directions

Ψ, θ = the spherical polar angle coordinates of dS_2 relative to dS_1

In a pulsed system the interaction parameter depends not only on the angular distribution of the outgoing neutrons but also on the velocity distribution and the time the neutrons spend in the space between the moderators. Thus we write

$$\rho_d = \frac{\int\int\int dS_1 \, dS_2 \, J(S_1) \, f(\Psi,\theta) \, M(v) \, g(t_d) \, (\cos\theta) / s^2}{\int dS_1 \; J(S_1)} \qquad (2.2)$$

where

ρ_d = the dynamic interaction parameter

$M(v)$ = the velocity distribution of the outgoing neutrons

$g(t_d)$ = the importance of the neutrons when they arrive at a surface in relation to the importance when they left the other one

t_d = the time a transferred neutron spends in the space between the intracting surfaces.

If the neutron population in the bodies decreases exponentially the importance

function is given by

$$g = \exp(\lambda s / v) \qquad (2.3)$$

where

λ = the decay constant
v = the velocity

It is easily seen that the integral over the velocity in equation 2.2 will be unlimited with this importance function for any reasonable velocity distribution. However, if an absorbing filter is placed between the two surfaces we get

$$g = \exp(\lambda s / v - \Sigma_a s_a) \qquad (2.4)$$

where

s_a = the flight path in the absorber
Σ_a = the absorption cross section

If we assume that the absorber has a $1/v$ - cross section, we can transform equation 2.4 and thus we get

$$g = \exp(-\alpha_T v_T / (v \cos\theta)) \qquad (2.5)$$

$$\alpha_T = d_a \Sigma_{aT} - \lambda d / v_T \qquad (2.6)$$

where

v_T = the most probable velocity
Σ_{aT} = the absorption cross section at the most probable velocity
d_a = the thickness of the absorber
d = the separation distance.

Through the incorporation of the absorber we have got a possibility to control the importance function. If we put g from equation 2.5 into 2.2 we see that the velocity integration in 2.2 will give a limited value for $\alpha_T \geq 0$ and that $\alpha_T = 0$ makes equation 2.2 identical to 2.1.

As α_T depends on λ, it can only be approximately estimated prior to the measurement. Therefore, we measure the dynamic interaction parameter $\rho_d(\alpha_T)$ for some points in the neighbourhood of $\alpha_T = 0$ and interpolate or extrapolate in

order to determine the stationary interaction.

$$\rho_{st} = \rho_d(0) \tag{2.7}$$

The method used to determine ρ_d is based on the knowledge of the diffusion parameters and the validity of the diffusion theory. The details are described in reference 4 and 9, so we only reproduce the formulae.

$$\frac{1-\rho}{1+\rho} = \frac{2\,k\,D\gamma}{\bar{v}\,tg\,(\pi - \gamma\,(H+\delta))} \tag{2.8}$$

$$\gamma = \sqrt{B^2 - \left(\frac{2.405}{R+\delta}\right)^2} \tag{2.9}$$

$$B^2 = \frac{2\,(\lambda - \lambda_o)}{D\left(1+\sqrt{1 - 4\,C\,(\lambda-\lambda_o)/D^2}\right)} \tag{2.10}$$

where

ρ	=	the interaction parameter
k	=	a correction factor
D	=	the diffusion constant
$\bar{v}$	=	the mean velocity
H	=	the thickness of the discs
δ	=	the extrapolation distance
γ^2	=	the buckling along the symmetry axis
B^2	=	the total buckling
R	=	the radius of the discs
λ_o	=	the decay constant at zero buckling
C	=	the diffusion cooling constant

3. THE MEASUREMENT.

The experimental arrangement is shown in figure 3.1. The same assembly was used as in the work described in reference 4. The moderators were polyethylene discs with diameter 18 cm and height 2.2 cm. They were separated along the symmetry axis by three aluminium bars. The detectors were glass scintillators loaded with Li. One was placed at the symmetry axis and the other two at the zero of the second order radial mode. As the latter give the best representation of the asymptotic decay, the result of the first has only been used to check the measurement. The assembly was shielded by boron carbide. The assembly was irradiated with neutrons from the D-T reaction in an 150 keV neutron generator and rotated during the measurement around the symmetry axis.

The filter was made of fine grade silver plates. In order to have as low delay effect as possible from the backscattering in silver, the filter was divided into two equal parts placed one at each surface. Each filter was composed of up tofour plates. The thickness of these was varied in powers of two. Therefore, we got 16 combinations with an approximately linear dependence between filter combination and absorption. Owing to the symmetric arrangement the step length was determined by twice the thinnest plate. The thickness of this, in turn, was fixed by the manufacturer, who couldn't roll thinner than 0.25 millimeters.

The thickness and effective absorption are listed in table 3.1. The filter combination is given as a four bit binary word where a bit equal to one denotes that the respective plate is included. The significance of the bits is associated to the thickness of the plates. The effective absorption given in the table is the thickness of the absorber times the macroscopic absorption cross section at 2200 m/s. The values are corrected for the scattering of neutrons. The scattering cross section of silver at 2200 m/s is approximately 10 per cent of the absorption cross section. In order to correct for this we assume that half the scattered neutrons go into the forward direction and half into the backward direction. This is a crude approximation but it gives sufficient accuracy for our purpose.

We have earlier shown that an experiment of this type without filters (4) depends very strongly on the decay constants involved. Therefore, we have made two series of measurements:

a) The D series with 2.2 cm polyethelene discs, which gives a range in the decay constant from approximately 17,000 to 40.000 s^{-1}.

b) The F series with 4.4 cm polyethylene discs, which gives a range in the decay constant from approximately 10,000 to 17,000 s^{-1}.

The delay time between the neutron burst and the beginning of the measurement is 64 microseconds for the D series and 192 microseconds for the F series. This shall be compared with the time spent by a 2200 m/s neutron in the gap between the moderators. The distances used are given in table 3.2 together with the number of possible flights between the surfaces for a 2200 m/s neutron. From the table we conclude that the delay time is sufficient to give a good exchange of neutrons between the discs in the F series. It is, however, too short in the last experiments of the D series. On the other hand, another step in the delay time will give a too low intensity.

In order to give support to the extrapolation in ρ_d (equation 2.7) at least three measurements with increasing filter thickness were made for each distance. The lowest filter combinations used are given in table 3.2.

The electronic equipment is described in references 9 and 10. The most important improvement since the completion of these works is that every detector line has got a baseline restorer of its own in order to get a better individual amplitude resolution. Also the data handling has been modified since the previous work(9, 10 and 11). Especially weighting factors proportional to the variance of the collected channel contents have been included in the program of background subtraction. The merits of this are that the program now is less sensitive to the amplitude limits chosen. The new version of the background program is named BAZI. A new program named SIFI has been written in order to calculate the interaction parameters. It is based on the equations 2.8, 2.9 and 2.10. The programs used in the data handling are then REMSIP, PARIN, OWCO, DTFAKT, DECORR, PILEUP, BAZI, CORLAM and SIFI.

Table 3.1

Combination	Effective absorption	Thickness (cm)
0000	0.000	0.000
0001	0.199	0.051
0010	0.392	0.101
0011	0.591	0.153
0100	0.765	0.198
0101	0.964	0.249
0110	1.158	0.299
0111	1.356	0.351
1000	1.537	0.397
1001	1.736	0.449
1010	1.930	0.499
1011	2.129	0.550
1100	2.302	0.595
1101	2.501	0.646
1110	2.695	0.696
1111	2.893	0.748

Table 3.2

Experiment number	Separation distance	Possible number of flights		Lowest filter combination
		before beginning of experiment	before end of experiment	
D1	2.2	6.4	32	0001
D2	4.4	3.2	16	0011
D3	6.6	2.1	11	0110
D4	8.8	1.6	8	1000
D5	11.0	1.3	6.4	1010
D6	13.2	1.1	5.3	1100
F1	1.1	38.4	140.8	0000
F2	2.2	19.2	70.4	0000
F3	4.4	9.6	35.2	0001
F4	6.6	6.4	23.4	0010
F5	8.8	4.8	17.6	0011

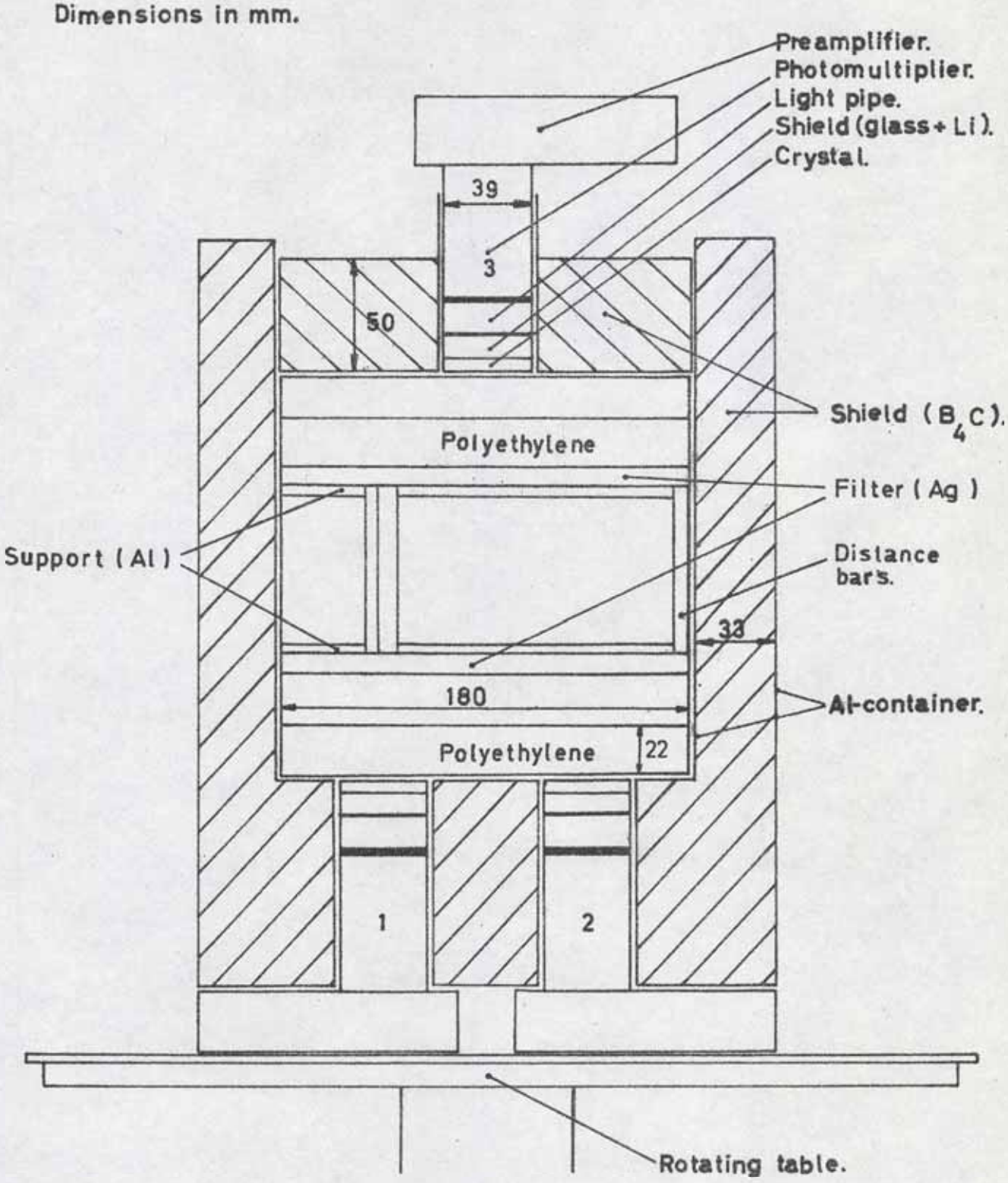

FIG. 3.1 EXPERIMENTAL ARRANGEMENT.

4. RESULTS.

The resulting decay constants from a correlation between detector 1 and 2 are plotted in figure 4.1. The different measurements are here represented by three characters. The first of these is a letter representing the series (F or D), the second and third are digits representing the experiment number and the measurement number. We will in the following use this notation. The last digit will be omitted when we refer to a whole experiment.

Experiment F0 and F6 are included in the F series in order to have comparisons at zero and infinite separation distance. In experiment F0 the discs were separated only by the filter, in experiment F6 we measured with one of the moderators removed. The figure shows that the decay constants increase with increasing filter thickness and that they at large thicknesses approach a limiting value, which agrees with the decay constant of a single moderator. The first experiments cover most of the available range but the last use only a small part in the neighbourhood of the upper limiting value. The figure shows only the F-series where we have most measurements for each separation distance. The D series contains only three measurements per experiment but gives a similar result.

In order to determine the interaction parameter we need the diffusion parameters for polyethylene. They have been calculated by GRIFFING (12) and measured by SJÖSTRAND et al. (13) and by GROSSHÖG (10) (marked RF 16 in the figure). The corresponding " dispersion curves " are drawn in figure 4.2. From the figure we realize that the different curves give rather different values within the actual range. Now, equation 2.8 is singular at

$$\gamma = \frac{\pi}{H+\delta}$$

that is, when the interaction parameter is small. Therefore, the determination of ρ_d will depend strongly on the chosen diffusion parameters.

In reference 10 we have found that for flat systems very long waiting times are needed in order to remove the influence of higher spatial modes. Also the choice of extrapolation distance and its buckling dependent variation comes into the picture.

From the above facts we find it necessary to have a very accurate relation between decay constant and buckling. So measurements were also performed corresponding to the limiting points $\rho = 0$ and $\rho = 1$ of the two series, i.e. the decay constant was determined for one single disc, and for two and four discs

close together and without filter. These results served as our main calibration points. In connecting them we could have used the curvature obtained from the earlier measurements given in figure 4.2. However, in the actual range the influence of the diffusion cooling is smaller than the difference between the curves in the figure. It is also doubtful whether the curvature should be the same for our open geometries. Therefore, we chose to approximate the dispersion curve with a straight line going through the two limiting values.

With this method and using eqs. (2.8-10) ρ_d was obtained from the measurements, and the results are shown in figure 4.3 for the F series and 4.4 for the D series. The error limits are based on those obtained by the program CORLAM, which evaluates the decay constants. The lines are only interconnections between different measurements in an experiment. The experiment number and, within parantheses, the distance between the innermost surfaces of the filter are given for each experiment.

In order to have a comparison material we have calculated the a_T dependent interaction parameter for the actual distances. We used equation 2.2 with M (v) as a Maxwell distribution and g (t_d) as given by equation 2.5. The angular dependence was (cos θ) /π and the radial distribution was assumed to be a zeroth order Bessel function. The numerical integration in velocity was carried out over 20 energy groups with an interval of 0.2 v_T. The number of intervals in angle was between 10 and 20 depending on the distance between the discs. The result of this calculation is shown in figure 4.5. As a comparison the result is also drawn for a one group calculation for the distance 2.2 cm. This shows that when the energy distribution is taken into account a lower interaction occurs at small values for a_T but a higher at larger ones. This is caused by the hardening of the spectrum in the absorber. The values for $a_T < 0$ depends strongly on the number of velocity groups owing to the singularity in the intergrand, and therefore the curves are dashed in this part of the figure.

A systematic difference between the curves in figure 4.5 and the experimental series is that the distance between the moderators is equal to the values given in figure 4.3 and 4.4 plus the thickness of the filter for the experimental values. The curves in figure 4.5 are, however, calculated for the indicated distance between the moderators. This will have a negligible effect on the results for all experiments except FO as the variation of the filter thickness is small in comparison to the separation distance.

The general trend of the result from the F series agrees rather well with the theoretical model. Deviations in the individual measurements can, however, be seen especially at large values on a_T. The result of the first measurement in the FO experiment is put equal to 1 as we have calibrated the series in this point. The decreasing trend of FO1 and FO2 can be explained by the increase in thickness of the filter, which in this experiment is equal to the separation distance, but FO3 and FO4 give unexpectedly low results. Experiment F1 agrees very well with the shape of the corresponding theoretical curve and so does experiment F2, although the values are somewhat more scattered in this case. A clear downward trend can be seen in F3 at large a_T values. F4 and F5 agree in general with the theory, but the last measurement of F5 gives a lower value than expected.

The error limits indicated in the figure 4.3 do not include the errors in the calibration points and errors due to the approximation of the dispersion curve. These errors can easily give an explanation to the behaviour shown in the figure. Another fact that may influence, mostly as an upscattering of the values, is differences in the piling of the assembly, which had to be done between all experiments in connection with the exchange of the filters.

Figure 4.3 gives a somewhat wrong impression owing to the fact that the above errors are amplified by the factor $\exp(a_T)$. As the errors come into the picture mostly at large values of a_T, we can expect that the values are rather good when a_T is in the neighbourhood of zero a fact which is confirmed by the behaviour of the experimental values in this range.

The stationary interaction is estimated by a manual interpolation of the experimental values in order to get the value at $a_T = 0$. The calculated behaviour of each experiment is then taken into account. The estimated values are marked with circles in figure 4.3. The error limits take into account the error limits of the individual measurements and the deviations in shape between the experimental values and the curves in figure 4.5.

The result of the D series is plotted in figure 4.4. The most striking feature of these values is that they do not behave as expected from the theoretical model. Two reasons for this will be stated. The first is that the dispersion curve is less well known in this range and the approximation with a straight line may be worse than in the F series. The second is that the neutrons have not reached

an asymptotic spatial distribution in all cases. The effect of this on the apparent decay constant can be positive or negative depending on whether the outflow or inflow of neutrons preponderates. However, as the mean energy of the neutrons first arrived is higher than the energy of the later ones a behaviour like that in figure 4.4 can be expected.

For these reasons the values estimated at $a_T = 0$ in the D series are extrapolated or interpolated from the measured values without taking the theoretical behaviour according to figure 4.4 into consideration. The difference between F and D series may then be connected to a difference in mean energy between the two series. As the values can not be considered as asymptotic as in the F series we have there a larger risk of systematic errors. This has not been included in the indicated errors limits.

The resulting values for the interaction parameter are plotted in figure 4.6. The different curves drawn as a comparison are calculated in the following way . ρ_o and ρ_1 are obtained from equation 2.1 with

$$f(\Psi,\theta) = 1 / 2\pi$$

respectively

$$f(\Psi,\theta) = (\cos\theta) / \pi$$

in diffusion theory we can write according to reference 9

$$f(\Psi,\theta) = (1 + 3\eta(\cos\theta)/2) / A \qquad (4.1)$$

$$A = 2\pi(1 + 3\eta/4)$$

where

$$\eta = \frac{1-\rho}{1+\rho} \qquad (4.2)$$

With this angular distribution equation 2.1 gives

$$\rho_{DIFF} = \frac{1-\eta}{1+\eta} = \frac{4\rho_o + 3\eta\rho_1}{4 + 3\eta} \qquad (4.3)$$

from which

$$\eta = \frac{2b}{a\left(1 + \sqrt{1 + 4b/a^2}\right)} \qquad (4.4)$$

where

$$a = \frac{4\rho_o + 3\rho_1 + 1}{3(1+\rho_1)}$$

$$b = \frac{4(1-\rho_o)}{3(1+\rho_1)}$$

Equation 4.3 with η from eq. 4.4 defines the curve ρ_{DIFF} in figure 4.6.

The experiment clearly indicates that the calculation with $(\cos\theta)/\pi$ as angular distribution gives an overestimate of the interaction through the whole measurement. On the other hand diffusion theory gives a slight underestimate and the $1/2\ \pi$ angular distribution gives a large underestimate. It is interesting to note that the value at 1.1 cm separation distance is close to the ρ_1 - curve. This type of behaviour can also be noted in stationary experiments (1). It is somewhat puzzling as one expects diffusion theory to be more accurate here than in the other part of the experiment. The explanation may be that already a small spacing gives a loss of neutrons with directions nearly parallel to the surface to such an extent that the angular distribution is better represented by a $(\cos\theta)$ - distribution than by the one given by diffusion theory. To this we can add the fact that diffusion cooling comes into the picture in such a way that the buckling concept is of limited validity in this case. That is, as the diffusion cooling takes place mostly in the neighbourhood of the free surfaces, it will not vary in the same way when we increase the buckling by decreasing the volume of the moderator as when we increase the buckling by the splitting of the moderator.

The agreement between the two series is excellent at 2.2 and 4.4 cm separation distance but not so good at 6.6 and 8.8 cm. The differences are probably caused by the systematic errors discussed above. Therefore, the results from the D series are more reliable in these cases. The trend towards the ρ_1 curve for the D series may be caused by the fact that we have not reached the asymptotic decay.

The above discussion shows that the method is sensitive to systematic errors. Therefore, we have considered it necessary to investigate this point more carefully. Systematic errors may be introduced through:

a) Uncertain diffusion parameters,
b) The fact that the asymptotic state is not reached
c) Backscattering of neutrons from the shielding, the detectors and the aluminium walls
d) Scattering in the filter
e) Different positions of the target in relation to one of the discs.

f) Leakage of neutrons through slits in the shielding
g) Systematic errors in the data handling

Item a and b have been discussed earlier. In order to check mainly item d but also to some extent the others, check runs were made in series D with the same conditions as in the main experiment but with one of the moderators removed. The resulting decay constants are plotted in figure 4.7. The calibration point DO is also included in the figure. It gives a somewhat higher value than the mean value of the check measurement but the difference is inside the error limits. As no systematic trend can be found in these measurements, we conclude that item a and b in the above list are the most serious sources of systematic errors. These errors influence both series at large values of the separation distance. One can expect that item a is most serious in the F series and b in the D series.

The resulting values of the interaction parameter are given in table 4.1 together with the extrapolated values of the distances between the moderators.

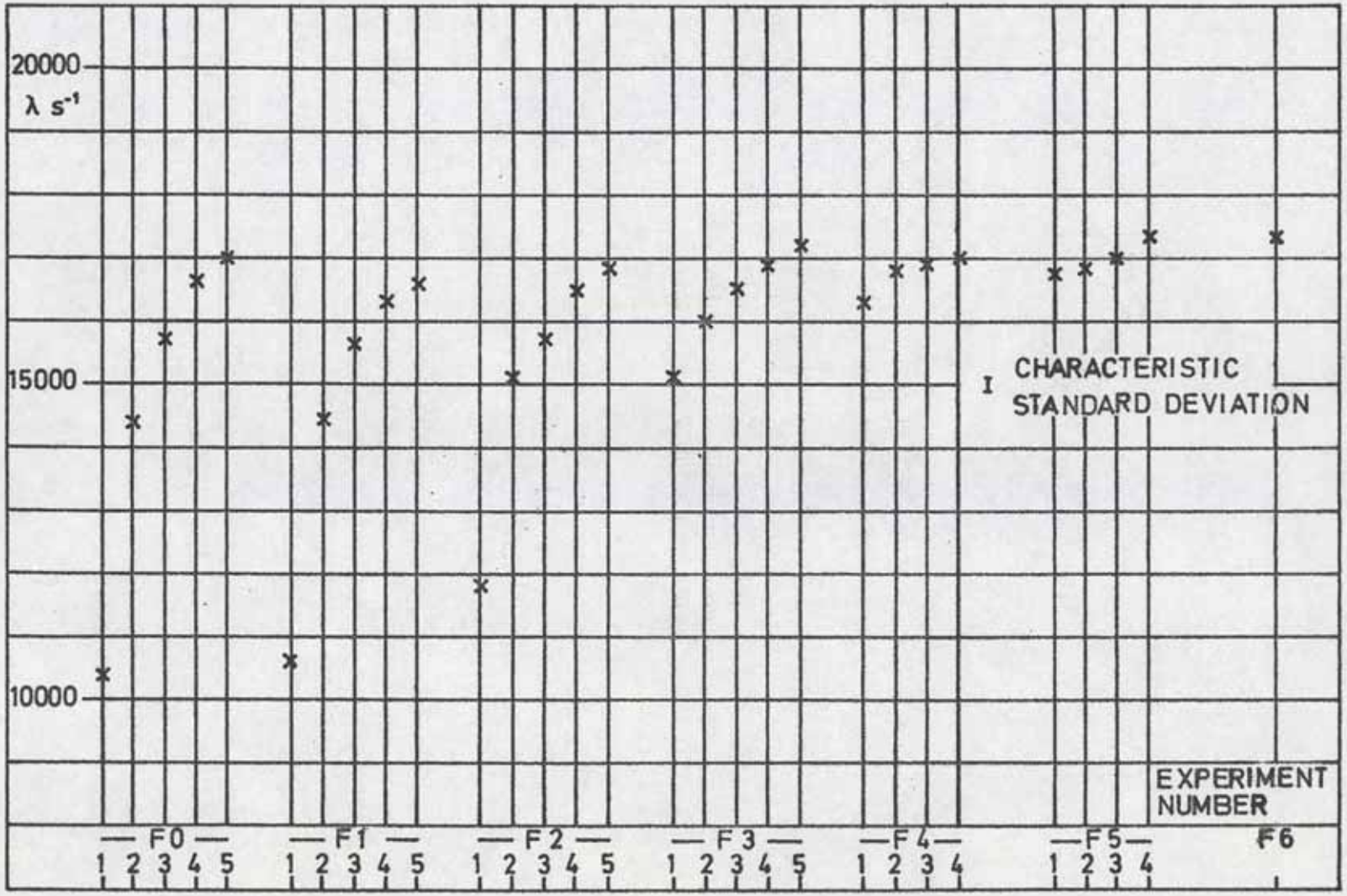

FIG. 4.1 DECAY CONSTANTS FROM A CORRELATION BETWEEN DETECTOR 1 AND 2. THE F SERIES.

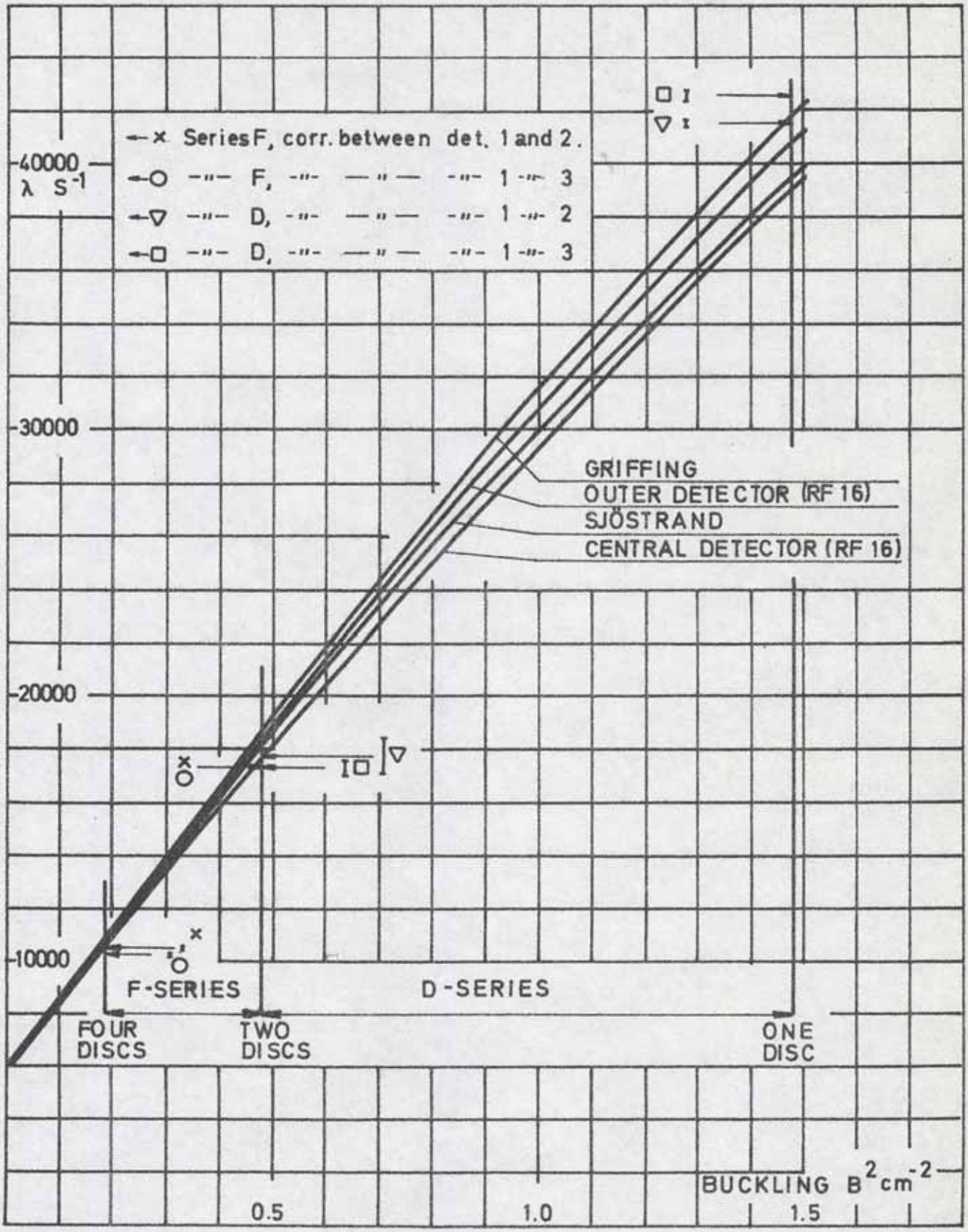

FIG. 4.2 DISPERSION CURVES FROM MEASURED AND CALCULATED DIFFUSION PARAMETERS.

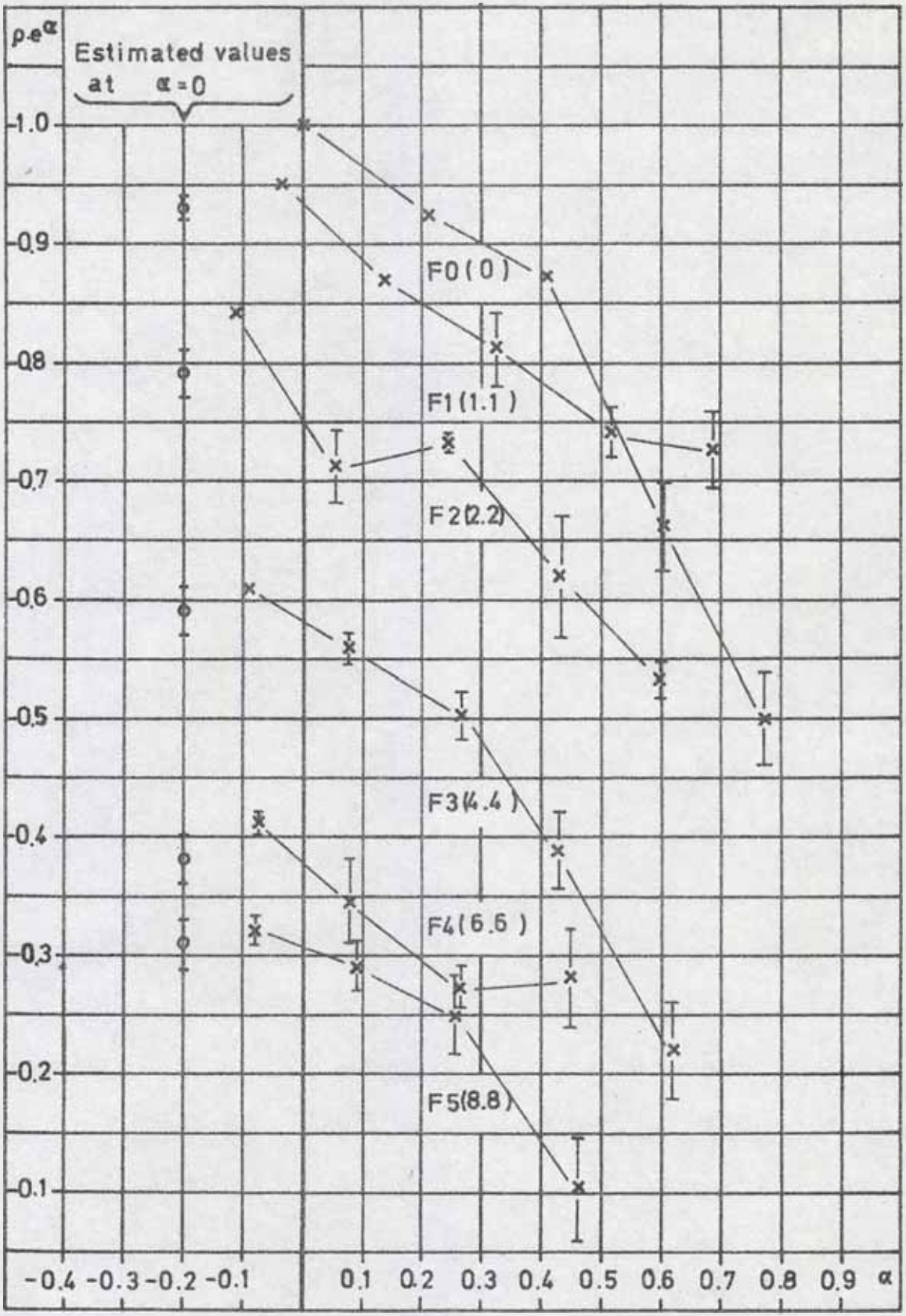

FIG. 4.3 THE TRANSFORMED INTERACTION PARAMETER. EXPERIMENTAL VALUES FROM THE F SERIES.

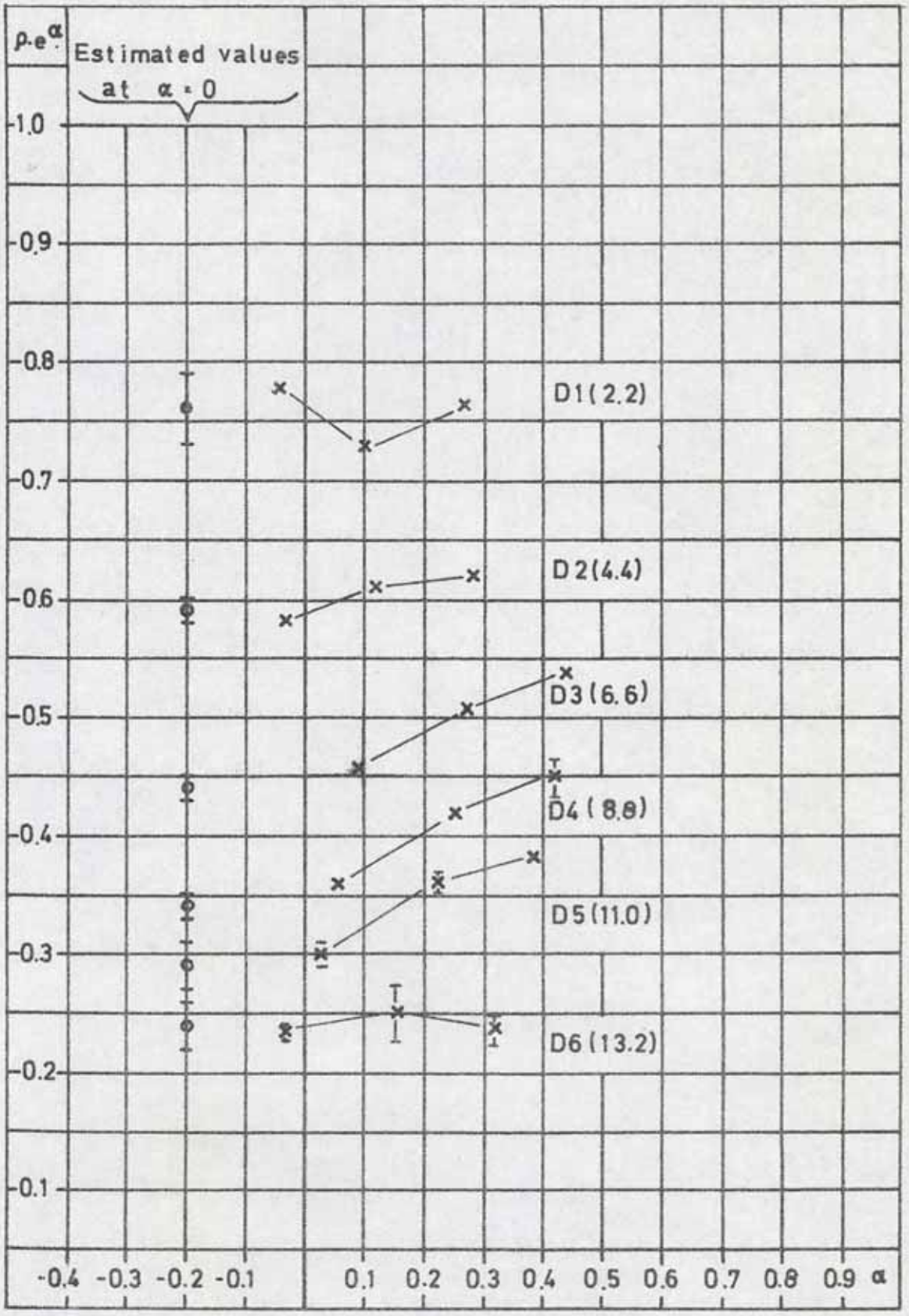

FIG. 4.4 THE TRANSFORMED INTERACTION PARAMETER. EXPERIMENTAL VALUES FROM THE D SERIES.

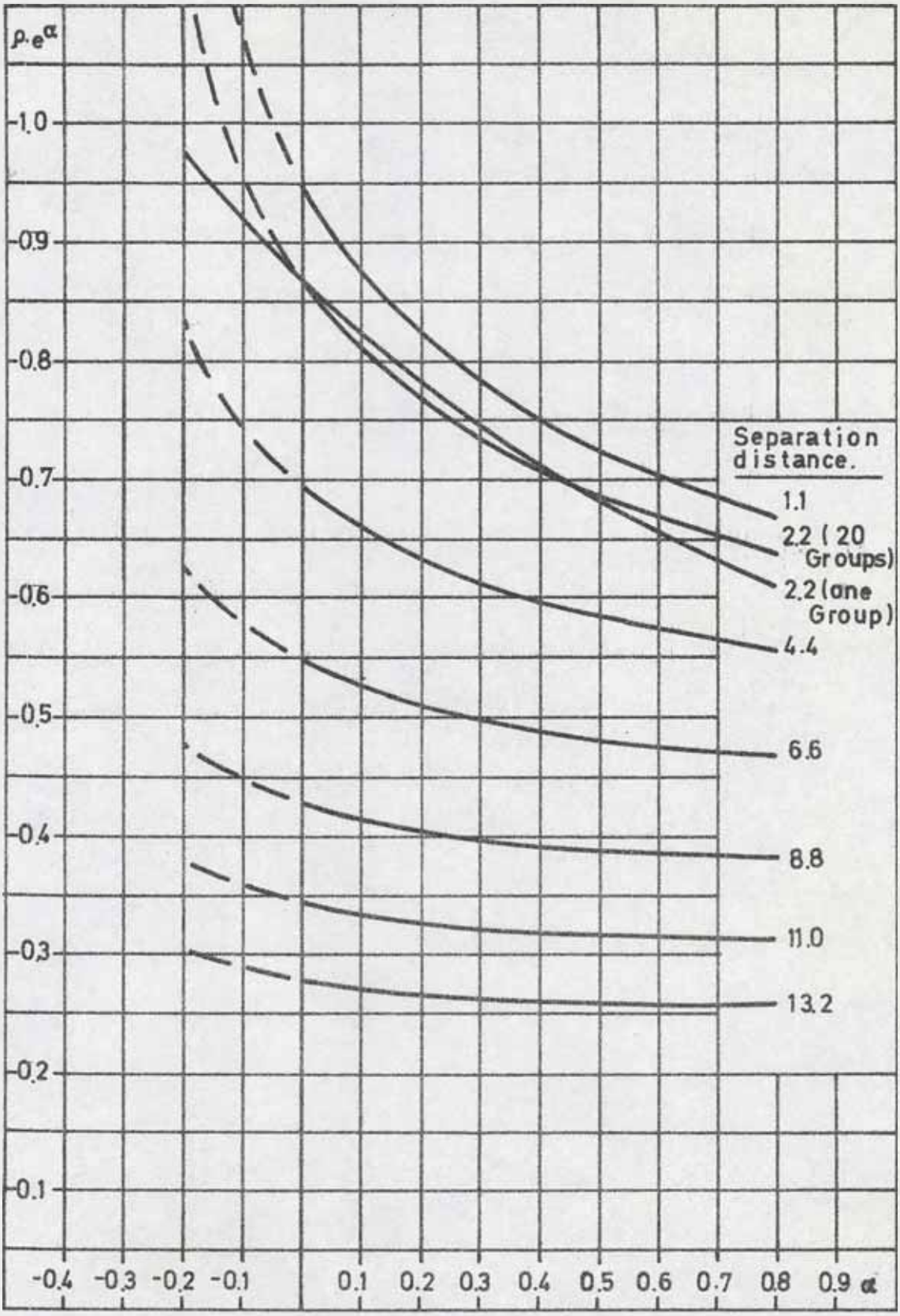

FIG. 4.5 CALCULATED VALUES ON THE TRANSFORMED INTERACTION PARAMETER.

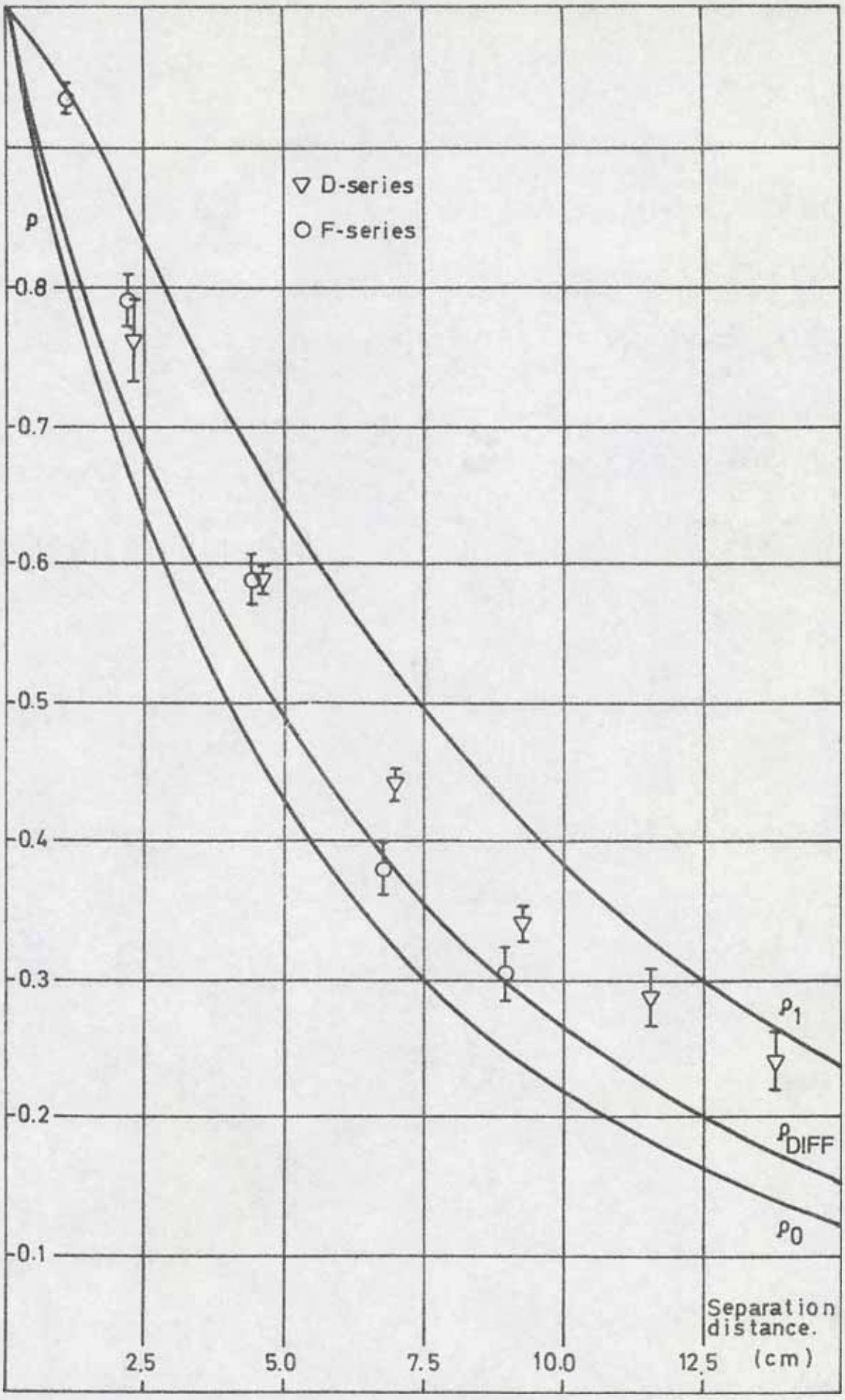

FIG. 4.6 THE STATIONARY INTERACTION PARAMETER.

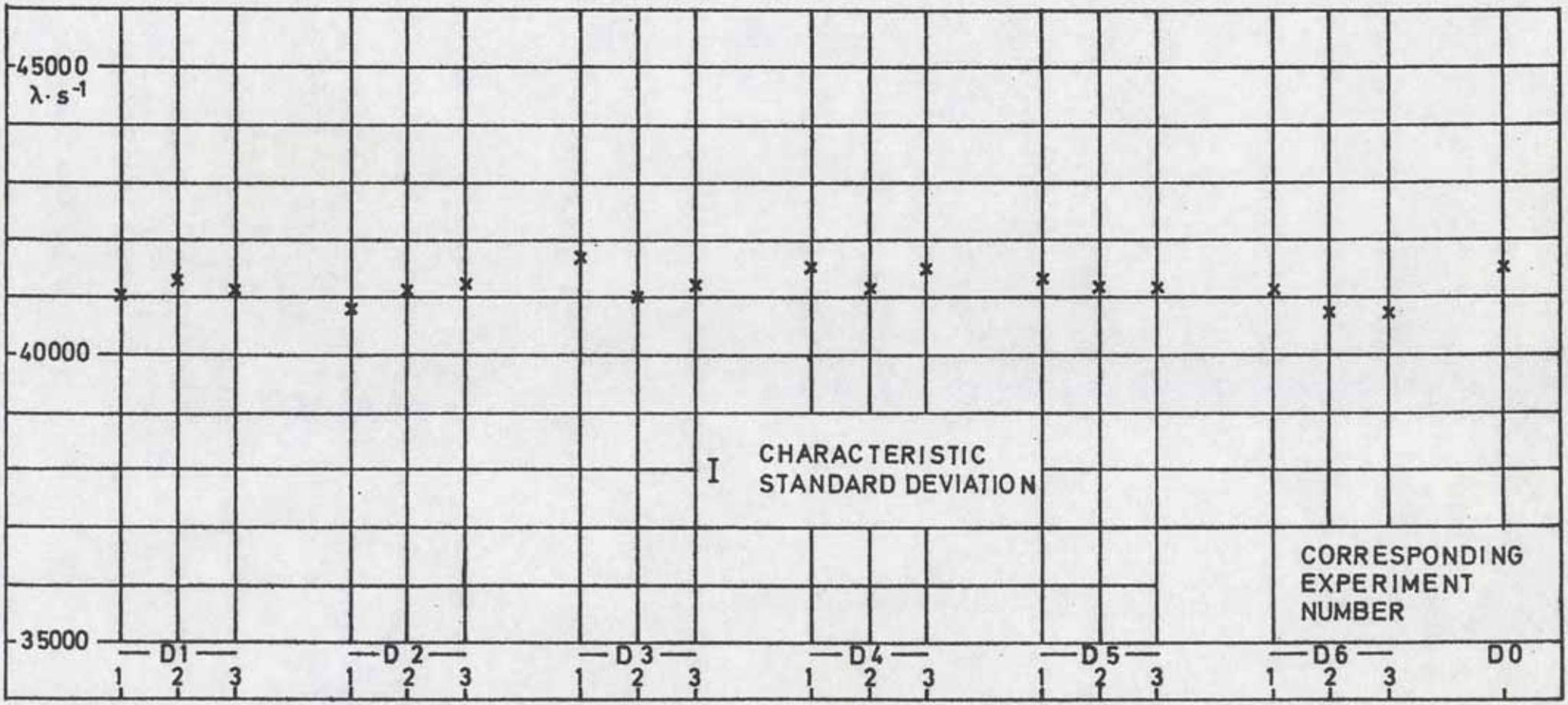

FIG. 4.7 DECAY CONSTANTS FROM A CHECK MEASUREMENT CORRESPONDING TO THE D SERIES.

Table 4.1 Resulting values of the interaction parameter.

Distance between filters (cm)	Series F		Series D	
	Distance between moderators (cm)	Interaction parameter	Distance between moderators (cm)	Interaction parameter
1.1	1.1	0.93 ± 0.01		
2.2	2.2	0.79 ± 0.02	2.3	0.76 ± 0.03
4.4	4.5	0.59 ± 0.02	4.6	0.59 ± 0.01
6.6	6.8	0.38 ± 0.02	7.0	0.44 ± 0.01
8.8	9.0	0.31 ± 0.02	9.2	0.34 ± 0.01
11.0			11.6	0.29 ± 0.02
13.2			13.9	0.24 ± 0.02

5. CONCLUSIONS.

The conclusions from this work are that the method of introducing absorbers in order to get an equivalence between pulsed systems and stationary systems works satisfactorily. The resulting interaction parameter for two circular surfaces shows that the ordinary approximation((cos θ) /π as the angular distribution (14)) gives a large overestimate in most of the measured range. The overestimate is, however, small at small separation distances, a fact that should be observed by those, who are concerned with the safety of interacting subcritical assemblies.

In this work the choice of dimensions and arrangements has been limited by the use of an already existing assembly. The experience from the work is that the measurement can be improved through:

a) A better knowledge of the diffusion parameters
b) A choise of the moderator dimensions so that the decay is slow enough to allow a complete interaction before the intensity is outside the measurable range.
c) The use of a mechanical construction that gives a better reproducibility of the separation distance, the filter position and the moderator dimensions.
d) The possibility to have higher intensity in the neutron bursts.

ACKNOWLEDGEMENTS.

The author is grateful to professor N.G. Sjöstrand and the members of his department for help and valuable discussions during this work. Gunnar Rönnberg made the program 'SIFI', the modifications in BAZI and he also calculated the curves in figure 4.5. Lennart Carlsson drew the figures and Christina Varenius typed the report. The work has been supported by the Swedish Atomic Research Council.

REFERENCES

1. Proc. IAEA Symposium on criticality control of fissile materials, Stockholm 1965.
2. H.K. Clark, An approximate method for calculating interaction. Proceedings of the Livermore array symposium, Livermore 1968. TID-4500, UC-46.
3. R.Kiyose, Y. Shimazaki, S. Enomoto, A study on interaction of subcritical assemblies. - Proc. IAEA Symposium on criticality control of fissile materials, Stockholm 1965.
4. G.Grosshög, The pulsed neutron method applied to the interaction between moderators (to be published in **J. Nucl. Energy**).
5. V.Deniz, J.G. Le Ho and M. Sagot, Study of lattices of graphite with empty channels by means of the pulsed neutron method. Nucl. Sci. Eng. 32, 201 (1968).
6. P.F. Palmedo and J.F. Conant, Neutron diffusion in aluminium-water lattices: measurement of anisotropy in the continuous eigenvalue region. Nucl. Sci. Eng. 36, 326 (1969).
7. B.E. Glancy, G. Durance and D.B.McGulloch, On the existence of discrete eigenvalues in slab lattice exponential experiments, J. Nucl. Energy 22, 445 (1968).
8. M.M.R. Williams, Diffusion lengths in hetergeneous, nonmultiplying assemblies. Nukleonik 12, 3, 129 (1969).
9. G.Grosshög, The pulsed neutron method applied to the interaction between two moderators. CTH-RF-17. (1969).
10. G.Grosshög, Determination of neutron decay constants using simultaneous pulse height and time analysis, CTH-RF-16 (1968).
11. G.Grosshög, Deadtime corrections in a two-parameter system containing four detectors. Proc. Ispra nuclear electronics symposium. Ispra 1969.
12. G.W. Griffing, Calculations on the fundamental time-decay constant of water and polyethylene. Proc. IAEA Symp. on Neutron thermalization and reactor spectra, Vol I, Ann Arbor 1967.
13. N.G. Sjöstrand, J. **Mednis** and T.Nilsson, Geometric buckling measurements using the pulsed neutron source method. Arkiv för fysik 15,471 (1959).
14. E.Fermi, Sul moto dei neutroni nelle sostanze idrogenate, Ric. Scientifica, 7,2, 13 (1936).

G

CHALMERS UNIVERSITY OF TECHNOLOGY

DEPARTMENT OF REACTOR PHYSICS

CTH-RF-19 FEBR. 1970

AN EXPERIMENTAL STUDY OF THE THERMAL NEUTRON FIELD DECAY IN A SPHERICAL MODERATOR WITH A CENTRAL CAVITY

by

GUDMAR GROSSHÖG

CONTENTS.

SUMMARY

The decay of a neutron field in a spherical light water moderator with a central cavity has been studied. Measurements were performed for two values on the moderator radius, 10.0 and 4.6 cm. The radius of the cavity was varied from 0 to 8.2 and from 0 to 4.1 cm respectively.

It was found that the cavity creates an instability in the logarithmic decay rate and that the instability increases with the cavity radius in an irregular way. A comparison with a simple diffusion model showed that the general trend could be explained for the larger moderator radius but not for the smaller one.

An important conclusion from the work is that measurements with the pulsed neutron method in heterogeneous media must be corrected for time dependent effects also if the ratio of the cavity to moderator volume is small.

1. INTRODUCTION.

An important property of the Boltzmann equation is that when time-dependent neutron transport problems are treated with a Laplace transform there results an equation which is identical with that of a corresponding stationary case. This equivalence is of great significance in the use of the pulsed neutron method, as was first pointed out by Sjöstrand (1). Thus, results from pulsed source measurements on homogeneous moderators can be directly applied to critical, stationary systems, e.g. reactors (2). However, for heterogeneous systems the situation is not so simple. It was recently observed by Bell (3), Dance (4), Denis et al. (5) and by the author (6) that in the case of a moderator containing cavities a delay effect appears, which depends on the logarithmic decay rate. This means that the analogy between the stationary and dynamic case is not complete and it also means that the pulsed assembly does not give a clean asymptotic decay constant.

The delay effect depends on the time the neutrons spend in the cavity. In open geometries, i.e. moderators containing gaps or channels penetrating the moderator, the neutrons may be trapped if they have directions nearly parallel to the surface of the cavity. We have earlier studied this effect (6) and found that the appearing logarithmic decay constants were unstable in time and very far from the values that could be expected from stationary diffusion theory. In a later work (7) we showed that the delay effect can be eliminated by introducing absorbers in the cavity.

The neutrons may also be trapped in the cavity if they enter it with velocities not far from zero. In an open geometry this effect is mixed with the effect mentioned above. In this work we have tried to isolate the velocity effect by the use of a spherical water moderator with a central cavity. This closed geometry offers also the benefit of no neutron losses through the cavity.

The spherical homogeneous light water moderator has in our laboratory been carefully studied by Eikert (8, 9). We have in the present experiment used the same technical arrangement for which the details can be found in his reports. It had been advantageous to use also his small BF_3 detectors, but their low sensitivity required a larger source strenght than could be accepted from the radioprotection point of view. Therefore we were forced into a measurement with glass-scintillators and had to accept a correspondingly higher background. A special technique was used in order to keep the

2. SOME REMARKS ABOUT THE ANALOGY BETWEEN HETEROGENEOUS STATIONARY AND DYNAMIC SYSTEMS.

A Laplace transform of the Boltzmann equation gives an equation for the Laplace transform of the flux that is identical to the stationary Boltzmann equation in the case of a homogeneous moderator with convex boundaries. The three parameter expansion of the " dispersion curve "

$$\lambda = \lambda_o + D_o B^2 - CB^4 \qquad (2.1)$$

where

λ_o = the absorption rate

D_o = the diffusion constant

C = the diffusion cooling coefficient

B^2 = the geometric buckling

implies then experiments for determining either the diffusion parameters or the buckling. The quantities so found are supposed to be used in stationary problems or compared with quantities received from stationary experiments. The purpose of this chapter is to underline that this course of action is not strictly correct if one is dealing with heterogeneous moderators.

The Boltzmann equation can be written

$$\frac{1}{v}\frac{\partial F}{\partial t} = -\underline{\Omega}\cdot\nabla F - \Sigma_a F - \Sigma_s F + KF + S \qquad (2.2)$$

where

v = the neutron velocity

$F = F(\underline{r}, \underline{\Omega}, E, t)$ = the neutron flux

$\Sigma_s = \Sigma_s(\underline{r}, E)$ = the scattering cross section

$\Sigma_a = \Sigma_a(\underline{r}, F)$ = the absorption cross section

K = the scattering operator

$S = S(\underline{r}, \underline{\Omega}, E, t)$ = the neutron source distribution

In a pulsed system we assume a zero source distribution and make the substitution

$$F(\underline{r}, \underline{\Omega}, E, t) = F_p(\underline{r}, \underline{\Omega}, E)\, e^{-\lambda t} \qquad (2.3)$$

This gives

$$\underline{\Omega}\cdot\nabla F_p + (\Sigma_s + \Sigma_a - \frac{\lambda}{v})F_p = KF_p \qquad (2.4)$$

Equation 2.4 is formally stationary and there is no problem before one tries to include the boundary conditions. However, the heterogeneities introduce time - dependent boundary conditions (11), and therefore the direct analogy with a stationary solution is lost. An excellent example on the experimental use of this behaviour was given by Arai and Küchle (10) when they measured the " imaginary "part of the dispersion curve ($\lambda>0, B^2<0$).

The term λ /v in equation 2.4 is often called time absorption. Because of its sign in the pulsed neutron method a better name would be " time multiplication ". Multiplied with the flux it acts as a source. But from the static point of view it is a very unusual source. It amplifies every incoming neutron with a factor proportional to λ /v but it does not change the direction of the neutron. In one-group diffusion theory there is a direct equivalence between λ /v and the multiplication but the analogy is only fictive which can be seen from the equation (2.4)

3. A ONE-GROUP DIFFUSION MODEL.

In spite of the remarks in the preceding chapter we will here solve the problem of the spherical symmetric assembly containing a central cavity with stationary diffusion theory. The delay effect of the cavity will be incorporated as a boundary condition. The model can then serve as a comparison material to the measured values of the logarithmic decay rate.

The solution of the spherical diffusion equation with zero neutron flux at the outer extrapolated boundary (R_o) is

$$\phi(r) = \frac{A}{r}\left(\sin(Br) - \mathrm{tg}(BR_o)\cos(Br) \right) \qquad (3.1)$$

At the inner surface ($r = R_i$) we write

$$\eta = \delta \left(\frac{1}{\phi} \frac{\partial \phi}{\partial r} \right)_{R_i} \qquad (3.2)$$

where δ is the extrapolation distance ($2D/\bar{v}$), and η is a loss coefficient defined by

$$\eta = (1 - \rho) / (1 + \rho) \qquad (3.3)$$

ρ is the interaction parameter, that is the number of incoming neutrons per outgoing neutron through an element of the surface between the moderator and the cavity. The eigenvalue equation for B is then

$$BR_i = (1 + \eta R_i/\delta)\ \mathrm{tg}\{ B(R_i - R_o) \} \qquad (3.4)$$

The interaction parameter depends on the logarithmic decay rate of the neutron field, the mean distance travelled by the neutrons in the cavity and the velocity of the neutrons. Using the mean cord length in the cavity (12) we can write

$$\rho = \exp\{ (4 p R_i \lambda) / (3 \bar{v}) \} \qquad (3.5)$$

where we have incorporated a free parameter p to be determined later. Insertion into equation 3.4 gives

$$BR_i = (1 - (R_i/\delta) \tanh\{ (4p R_i \lambda) / (3\bar{v}) \}) \cdot \mathrm{tg}\{ B(R_i - R_o) \} \qquad (3.6)$$

An interesting limit is small values of R_i . A power expansion of 3.6 with p = 1 gives

$$BR_o = \pi + (BR_i)^3 (1 - \lambda / (DB^2)) / 3 + 0((BR_i)^5) \qquad (3.7)$$

The expansion shows that the delay effect is present in the same order of approximation as the stationary effect. It depends on λ and must be accounted for not only at large but also at small cavities.

The primary solution is drawn for the actual geometries in figure 3.1. Inspecting equation 3.6 one finds that the buckling will be imaginary if

$$\frac{R_o - R_i}{R_i} \left(1 - \frac{R_i}{\delta} \tanh \{ (4 p R_i \lambda) / (3 \bar{v}) \}\right) < -1 \qquad (3.8)$$

The peak indicated for $p = 0$ but excluded for other values of p depends on the three term expansion of λ where we used the diffusion parameters given by Elkert (9). If λ is a continuously increasing function of B^2 the limiting values of B are

$$B \to \pi / (2 (R_o - R_i)) \quad \text{when } (R_i \to R_o,\ R_o \to \infty)$$

$$B \to \pi / R_o \quad \text{when } (R_i \to 0)$$

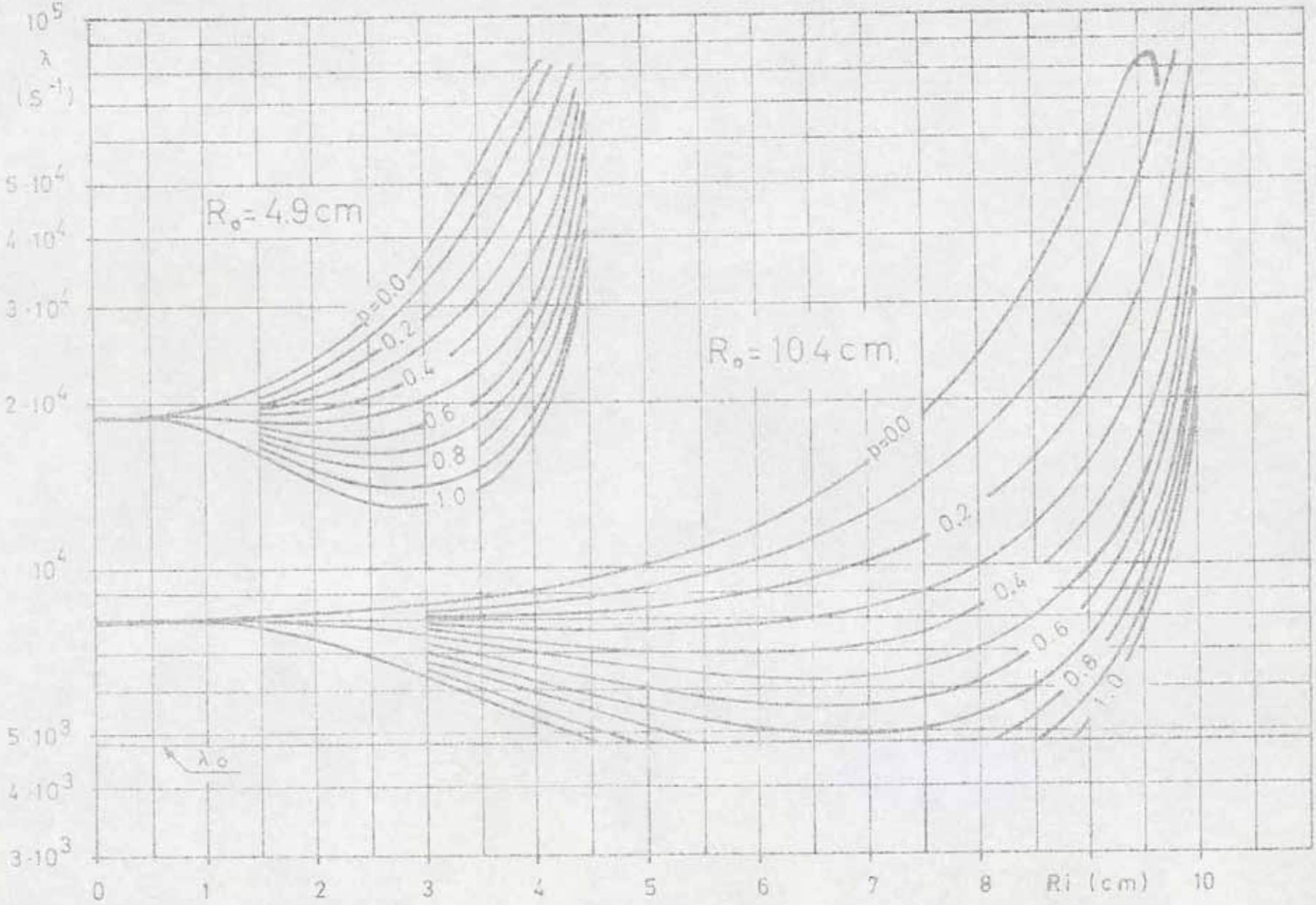

Fig. 3.1 The logarithmic decay rate as a function of cavity radius for the two measured geometries according to one-group theory.

4. EXPERIMENTAL ARRANGEMENTS.

In this work we have used the same mechanical support, the same spherical aluminium shells and the same shielding as in the measurement on diffusion parameters for light water in spherical geometries by Elkert (8,9). In order to arrange the central cavity the largest shell was cut into two equal halves, a smaller one was mounted on a screw and then the outer shell was repaired with tape. Finally, the space between the two shells was filled with distilled water.

As detector we used a Li-glass scintillator (13). We have earlier measured the decay in moderators with open cavities and found that the logarithmic decay rate was not stable (14). In those measurements we chose a logarithmic time scale, with which we were able to cover the entire measureable part of the decay with 8 time intervals. A very accurate background subtraction could then be done by the use of 32 channels for the measurement on the amplitude distribution of the detector pulses. This gave a good precision in the determination of the decay constant but the details of the decay curve was lost. In this experiment we were interested in the time variation of the logarithmic decay. Therefore, we wanted a linear time scale with as many time intervals as possible. This had to be done at the expense of the number of amplitude intervals. As the exchange of channels between amplitude, number of detectors and time only could be done in powers of two we chose: one detector, two amplitude intervals and 256 time intervals. The remaining part of the analyzer memory (512 channels) was used to measure the deadtime.

We have earlier found that the amplitude distribution can be approximated with a Gauss distribution for the neutrons and an exponential for the background (14). It is easily realized that the lowest background to neutron ratio in a one channel analyzer is achieved if a small window is placed at the maximum of the neutron distribution. Decreasing the window width will then cause both the neutron and background sensitivity to go to zero but the ratio between them will remain approximately constant. A necessary condition in a time dependent system is that the gain does not depend on the time or the intensity. In order to be able to check this we placed the limit between the two amplitude intervals on the maximum of the neutron peak. Our criterion on approved measurements was then that both the channels should have the very same time dependence. It was possible to fulfil this criterion during the whole measurement, thanks to the recently incorporated base line restorers.

5. THE MEASUREMENT.

The experiments were performed in three series. During the A and B series we used the largest shell to define the outer radius (10.0 cm). The inner radii were 8.2, 6.7, 5.6, 4.8, 4.1, 3.7, 3.4, 3.0, 2.6 and 0.0 cm. In the A series two measurements were performed with inner radius 8.2 cm, one in the beginning of the series and one at the end. This served as a check on the reproducibility of the measurements. In the A series the detector was placed on the outer shell in 90 degrees angle to the target, but in the B series it was placed opposite to the target. The time interval width was 8 microseconds and the measurement period started 10 microseconds before the 4 microseconds wide neutron burst.

The C series was performed with 4.6 cm as outer radius. The inner radii were 4.1, 3.7, 3.4, 3.0 and 2.6 cm. The time interval width was 4 microseconds and the detector was placed in the same position as in the A series.

In all the series a background measurement was included. It was identical to the other measurements in the series but no moderator was present.

6. CORRECTIONS.

The deadtime correction was made with the same basic method as described earlier (15). In order to adapt the method to the linear time scale some modifications were introduced. The procedure was as follows.

Two detector lines were used, the first for the neutron detector and the second for pulses from a pulse generator. First the sum of the two amplitude intervals was formed. This gave 256 channel contents for each of the detector lines. We denoted them $P_d(i)$ and $P_t(i)$ were i is the channel number running from 0 to 255. Then, the frequency of the testpulses (f_t) was determined from the 16 last channels. As the detector line frequency was low here we could write

$$f_t = \left(\sum_{i=240}^{255} P_t(i) \right) / 16 \qquad (6.1)$$

which gave the frequency in number of pulses per channel. The correction formula is then

$$P_{dc}(i) = (f_t \, P_d(i)) / (P_t(i) \, k_{tp}(i)) \qquad (6.2)$$

where $P_{dc}(i)$ is the corrected number of pulses in the detector line and k_{tp} a correction factor for the time spent by the test pulses in the system.

$$k_{tp}(i) = 1 - (P_t(i-1) \, t_m) / (N_s \, t_c) \qquad (6.3)$$

where

t_m = the time used to handle a test pulse
N_s = the number of neutron bursts
t_c = the channel width

This correction term was neglected in the earlier version of the deadtime correction because then we used a very low rate of test pulses. In the present measurements we increased the test pulse rate and therefore the correction had to be included.

The correction in eq. 6.2 corresponds to the intrinsic transfer discussed in reference 15. The extrinsic transfer could not be calculated with the method given in the reference owing to the few amplitude channels used. In

spite of the fact that it had some influence on the beginning of the decay we decided to neglect it.

The background measurements showed three typical parts. The first one was a reproduction of the neutron burst followed by a very fast decay, a typical thermalization process. The second was a decay, which unluckily enough had approximately the same logarithmic decay rate as that of series A and B. Therefore, it was carefully investigated by a measurement with several amplitude channels in the actual interval. It was found that within the accuracy of the measurement no sign of neutrons could be detected. Therefore we explain it as the capture gamma from the absorption of the thermal neutrons in the shielding.

The third part was constant in time but proportional to the neutron intensity. The main part of it was assumed to come from short lived activities. Taking the differences in intensity into account, the background was subtracted from the measurements.

The result from the background subtraction with the above method was also compared to a background subtraction with the assumption that the background was constant in time. Although a small difference could be noted, we found that the difference was small compared to the standard deviations of the resulting logarithmic decay rate and therefore it could not affect the general conclusions from this work.

The corrections were done by two computer programs LILA and BALA. The latter determined also the logarithmic decay rate. The mechanical structure, the screw that supports the inner Al-shell and the outer Al-walls have not been corrected for. The screw was kept in position during the measurement of the homogeneous moderator and it can be seen by a comparison with the values of Elkert that it gives a neglectable correction (fig. 7.4 - 7.10 , experiment 1). Elkert has shown that the correction for the outer wall is small (8). The inner wall may give an influence on the decay rate but only through the very low energy part of the neutron distribution, which penetrates the cavity.

7. RESULTS.

In this chapter the result of the measurements will be presented first in three diagrams, figure 7.1 to 7.3, where the most characteristic decay curves of the series A. B and C are plotted. We will then follow the time of the logarithmic decay rate for the series A and B in the figures 7.4 to 7.9. Finally the time variation of the C series is presented in figure 7.10.

During the measurement of each series the intensity of the accelerator was held as constant as possible. This gave an approximate normalization to the decay curves within the same series, and therefore we are able to compare not only the logarithmic decay rate but also the amplitudes. The three plotted decay curves in figure 7.1 correspond to experiment A1, A5 and A10. The inner radii are 0, 4.5 and 8.2 cm. The values are corrected for deadtime and background. Experiment A1 shows a decay with a rather well defined decay constant. A5 is worming around A1 and A10 shows how the moderator loses a lot of neutrons into the cavity during the first ten microseconds. These neutrons then cause the decay to be so slow that the intensity at 900 microseconds (about channel number 120) is comparable to that of the homogeneous moderator.

Series B (figure 7.2) gives a result not far from series A. A notable effect is the peak at channel number 6 in the experiment B10. An explanation for this can be found in the fact that the detector is placed in a position where the initial neutron flux is low. Therefore the thermal neutrons coming through the cavity will give a noticeable effect.The time lag of the peak is approximately 37 microseconds, which gives a thermal neutron distance of about 7 cm. As this value is low in comparison to the cavity diameter we conclude that the neutrons at this stage have not reached thermal equilibrium. There is a small sign of a repeated peak at channel number 15. However, an increased statistical accuracy is needed in order to get confirmation on the existence of this peak.

The three experiments plotted in figure 7.3 correspond to experiment C1 with 0, C2 with 2.6 and C6 with 4.1 cm inner diameter. As the moderator volume here is less than in the preceding experiments we get a higher influence of background. This causes the values to be more scattered, and approximations in the background subtraction are more serious. As in the B10 experiment we can recognize an indication of a peak, in this case at channel 9 in the C6 experiment, but the peak is too weak to give any relevant information

about the time lag.

The general conclusion so far is that the cavity introduces a very long damped oscillation. The decay might go over into a pure exponential decay but we do not reach that state within the experimental time range.

In figures 7.4 to 7.10 the decay constants from the A and B series are plotted as a function of the inner radius. The decay constants are calculated from the 16 consecutive time intervals beginning with the time interval noted in the figures. Some of the curves from the one-group model are included in the figures as a comparison material.

The figures show a general trend that can be interpreted as a convergence to the one group model with a p of about 0.6. The convergence is slow but this is also to some extent the case for the homogeneous moderator. Disregarding the general trend we can find some irregularities, which must be considered as systematic as they appear in both the independently measured series. Figure 7.4 (time 17) shows a convex structure for low values on R_i and a very low value at experiment 9. Figure 7.5 (time 33) gives an impression of a rather smouth relation between the decay constant and the inner radius. Figure 7.6 (time 49) contains peaks at experiment number 4 and 6 for both the series. In figure 7.7 there is a tendency of peaks at experiment 6 for both the series and at 4 for the B series but the A series contains here an indication of a minimum. In figure 7.8 and 7.9 the statistics is poor, but remarkable are the high values of the decay constants for both series at experiment number 4 in figure 7.8 and the low values at the same place in figure 7.9.

The significance of the deviations is poor, but combining these observations with those done in the study of two interacting moderators (6) leads to the conclusion that there exist effects which can not be explained by a simple theoretical model. The behaviour indicates an oscillating neutron wave that goes into resonance with special values of the inner radius.

If one follows the time development of the decay constant in experiment A10 one finds that it varies up and down. This behaviour is confirmed by the independent check measurement and gives support to the theory of oscillation or propagation effects.

The decay constants from series C are plotted in figure 7.10. Our diffusion model is here not at all able to represent the experimental values. A resonance effect, more pronounced than in the A and B series, is indicated.

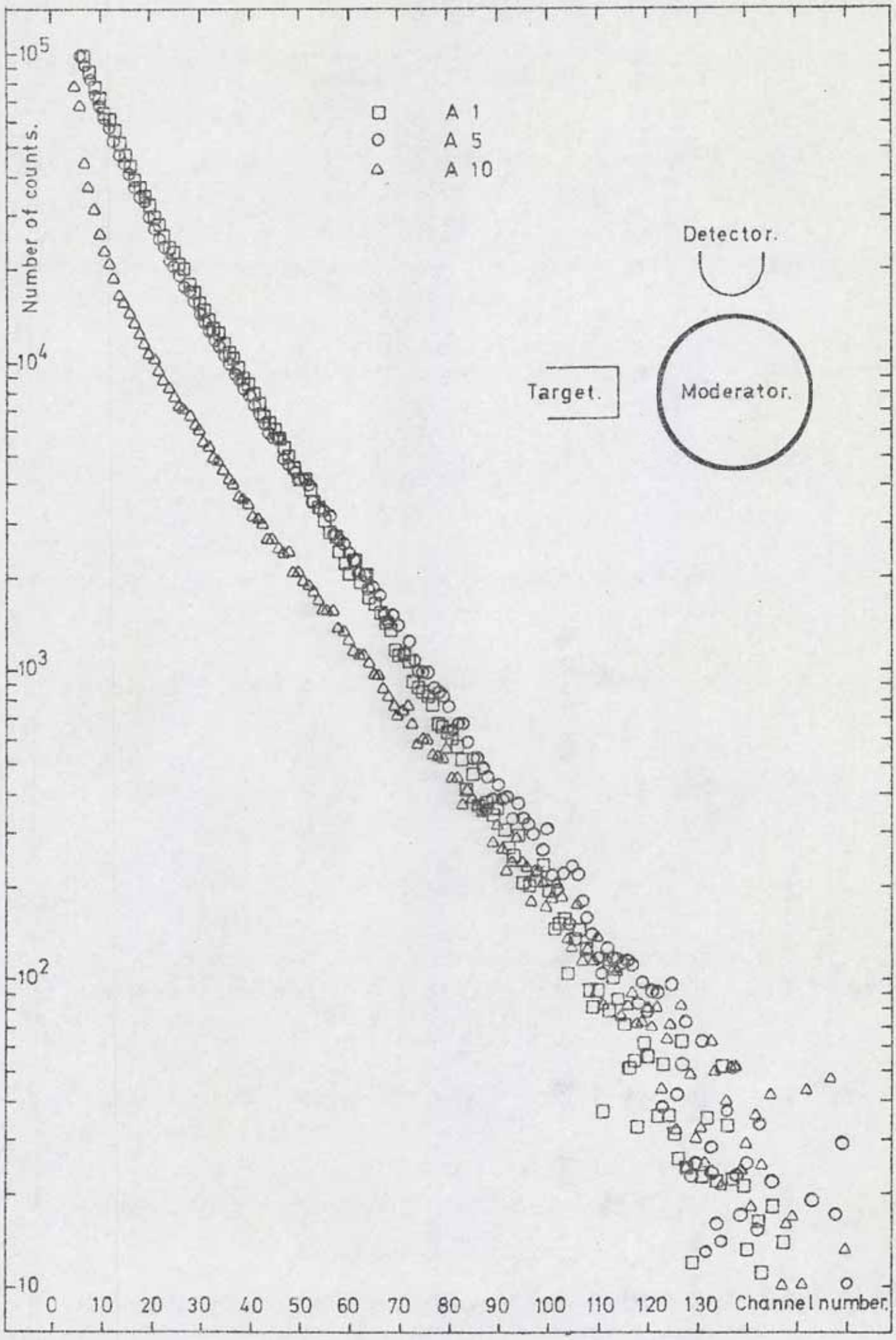
Number of counts.
10^5
10^4
10^3
10^2
10
A 1
A 5
A 10
Detector.
Target.
Moderator.
0 10 20 30 40 50 60 70 80 90 100 110 120 130 Channel number.

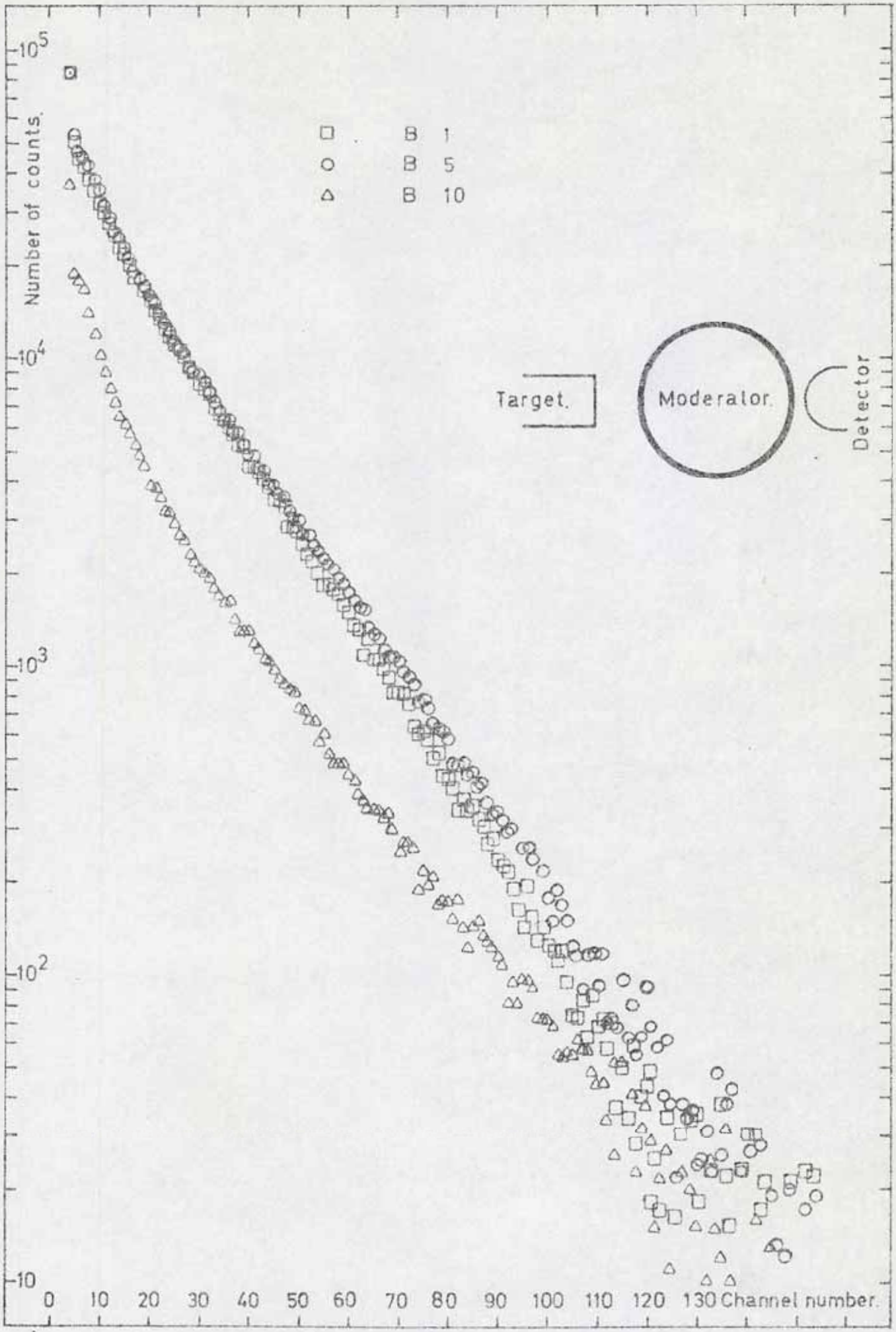

Fig. 7.3. Three decay curves from the B series.

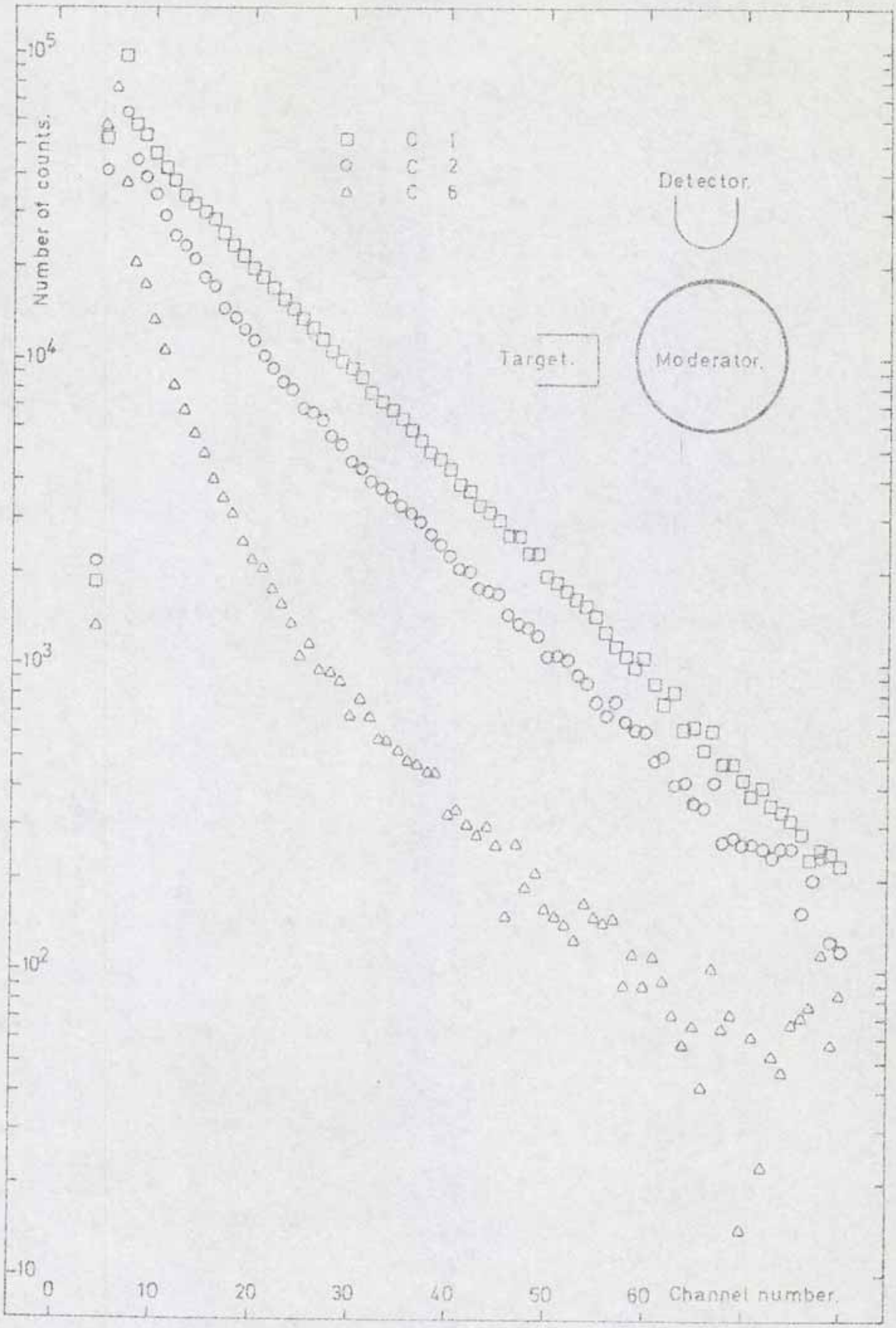

Fig. 7.3 Three decay curves from the C series.

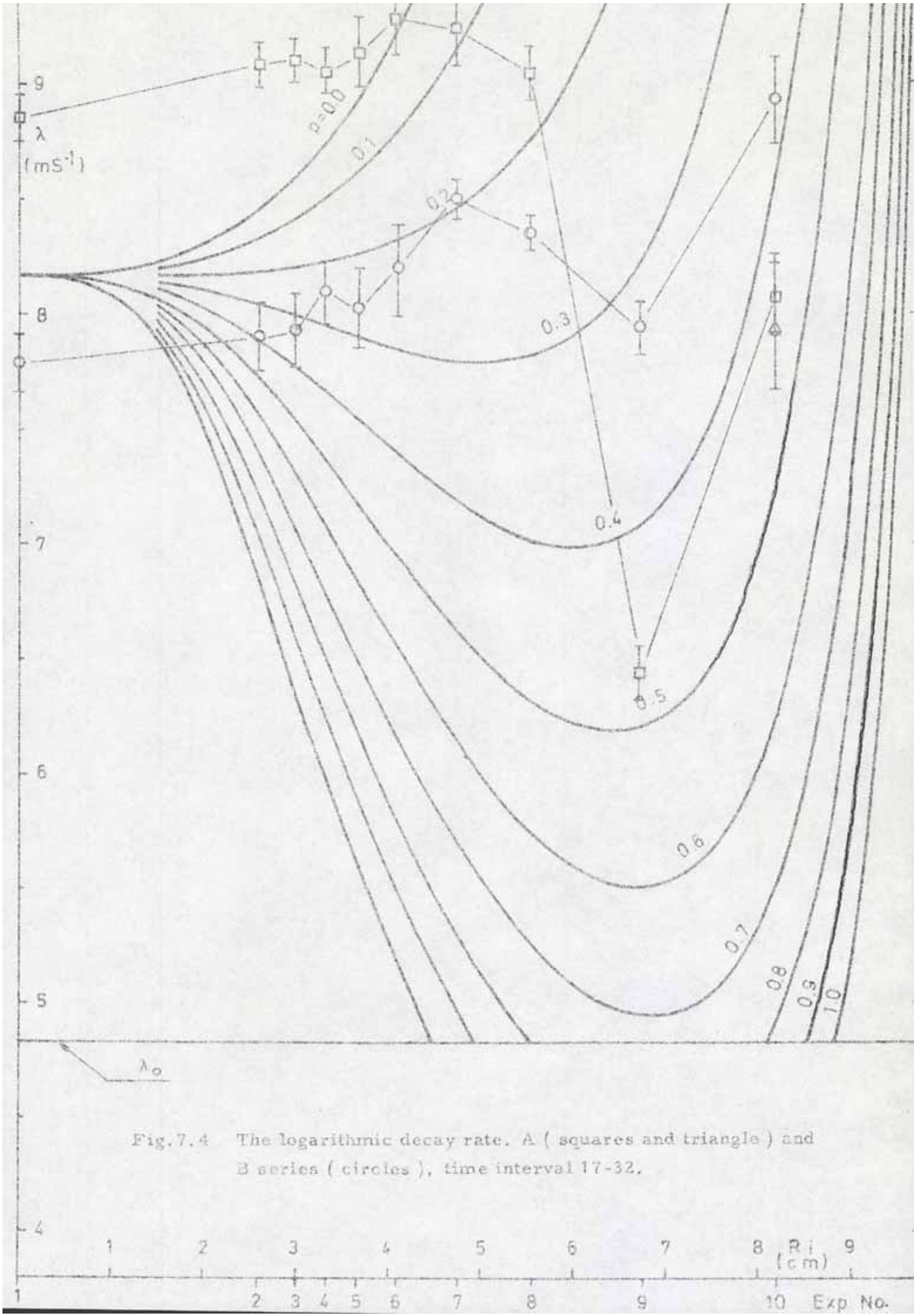

Fig. 7.4 The logarithmic decay rate. A (squares and triangle) and B series (circles), time interval 17-32.

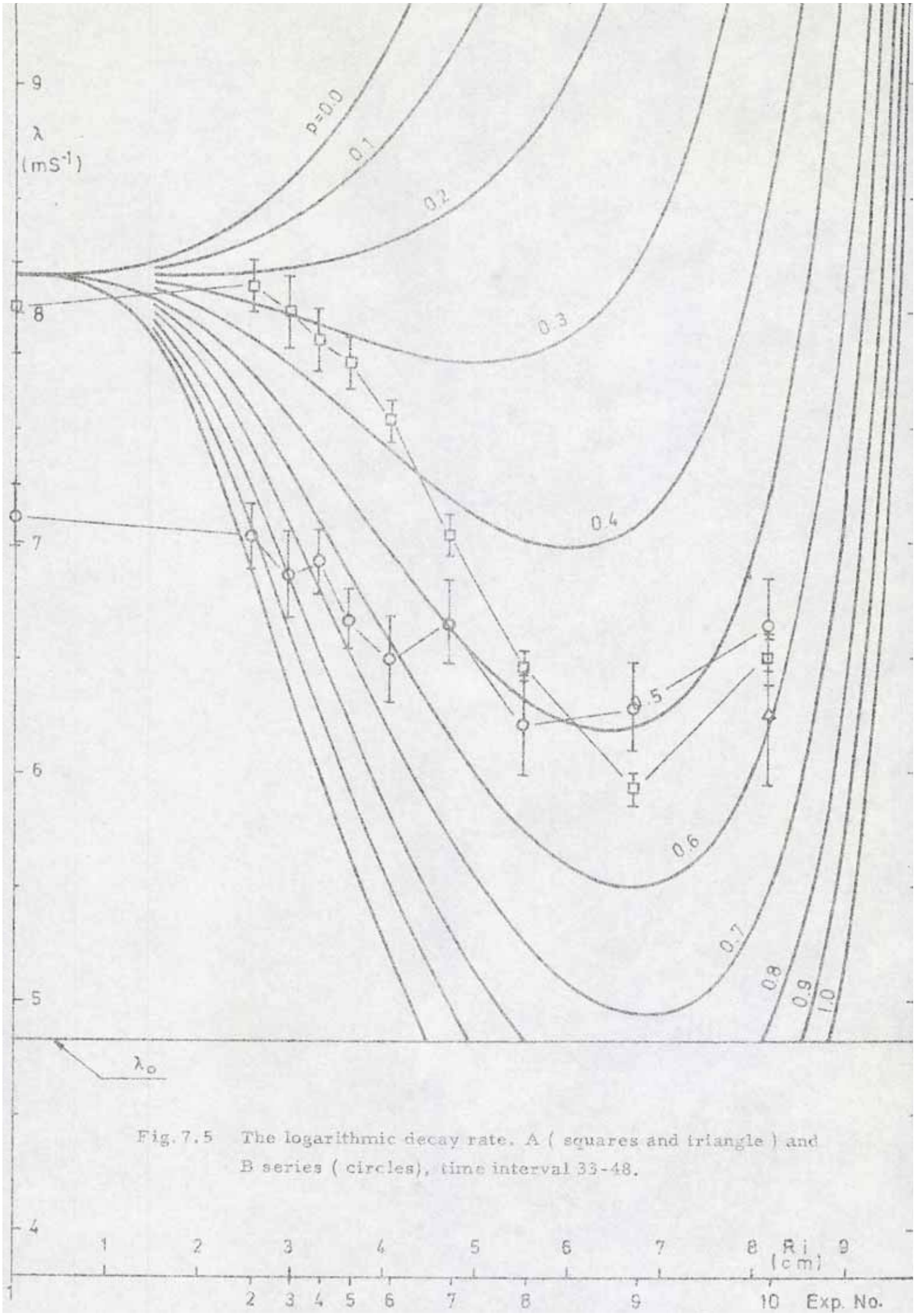

Fig. 7.5 The logarithmic decay rate. A (squares and triangle) and B series (circles), time interval 33-48.

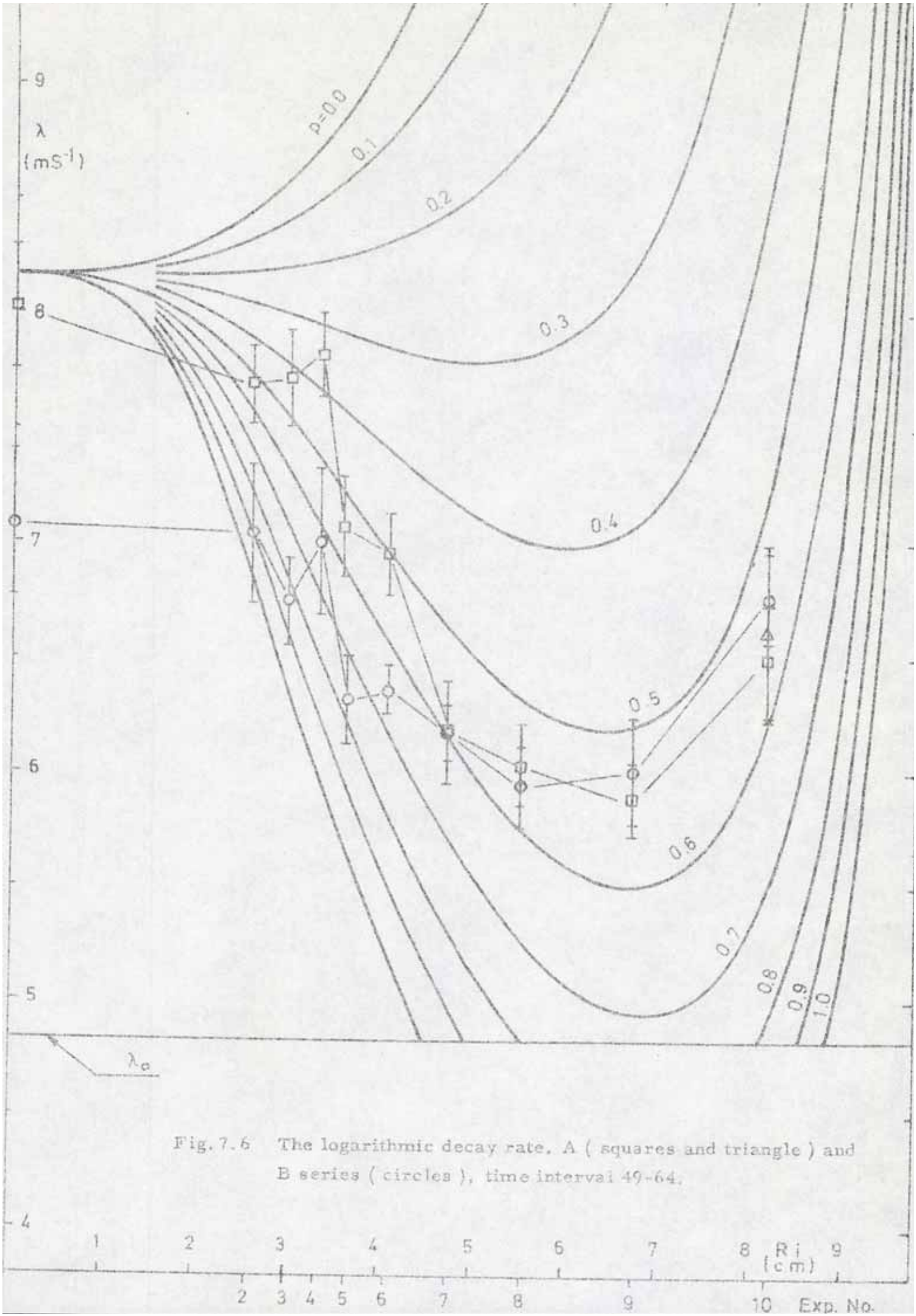

Fig. 7.6 The logarithmic decay rate. A (squares and triangle) and B series (circles), time interval 49-64.

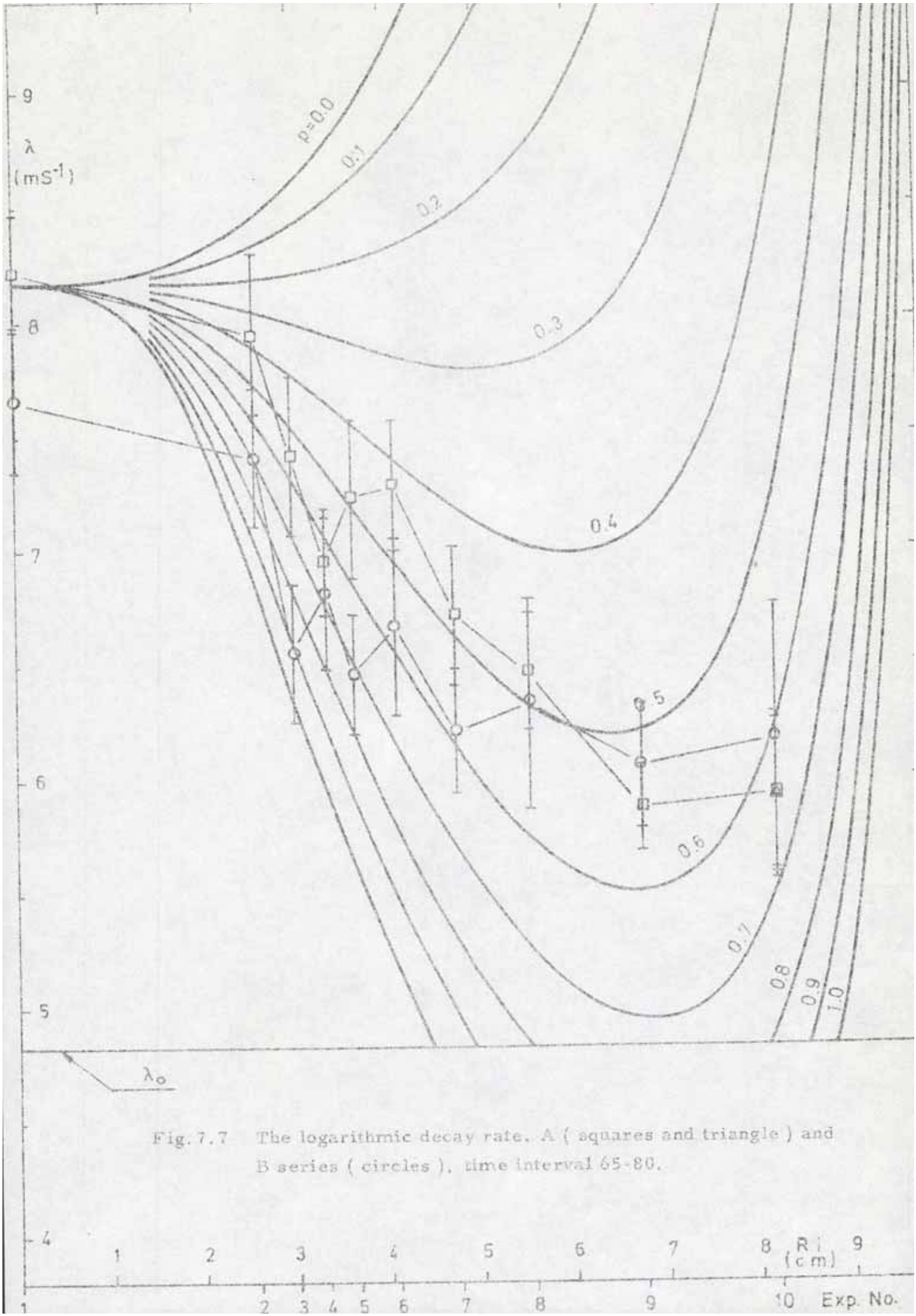

Fig. 7.7 The logarithmic decay rate. A (squares and triangle) and B series (circles), time interval 65-80.

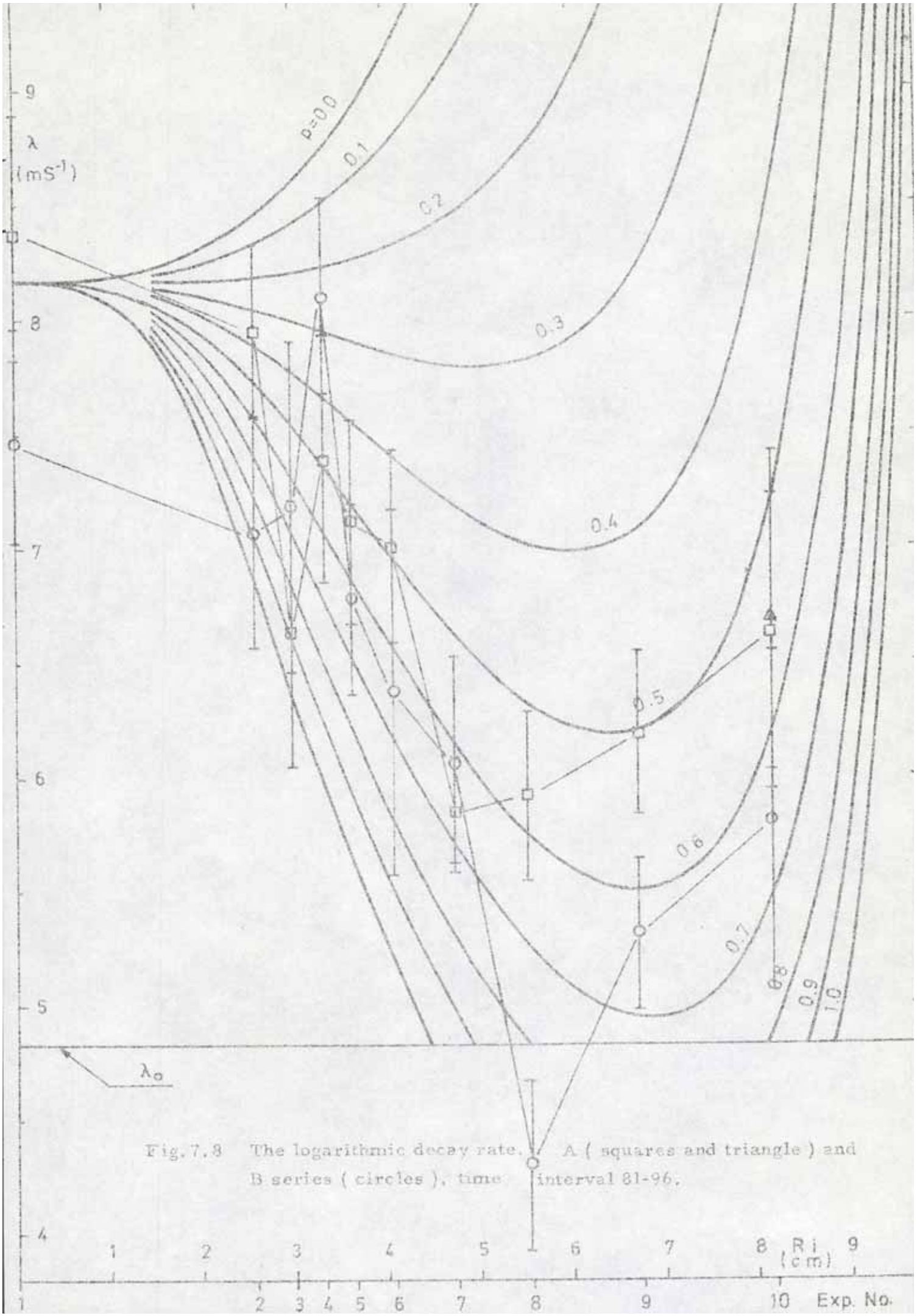

Fig. 7.8 The logarithmic decay rate. A (squares and triangle) and B series (circles), time interval 81-96.

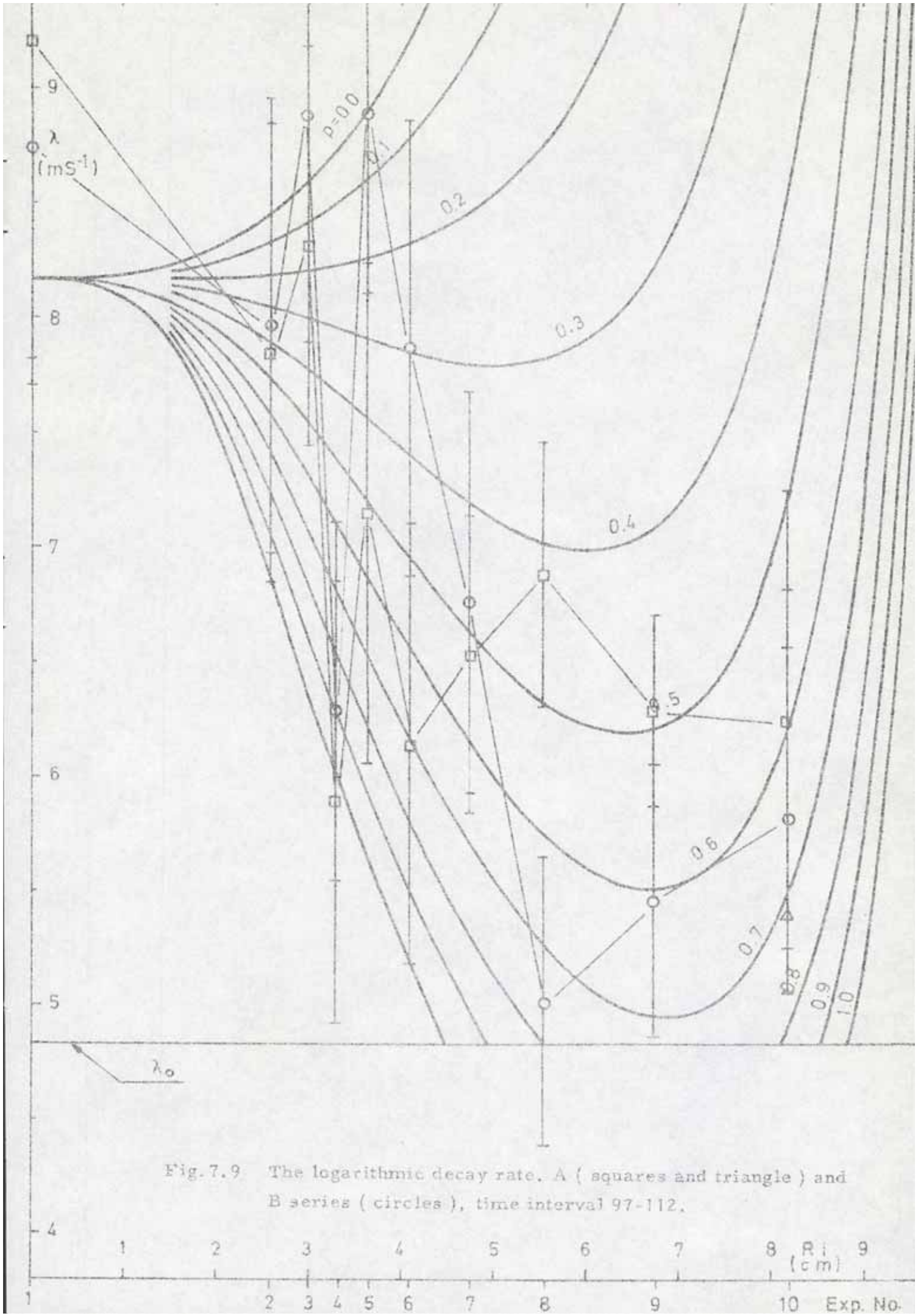

Fig. 7.9 The logarithmic decay rate. A (squares and triangle) and B series (circles), time interval 97-112.

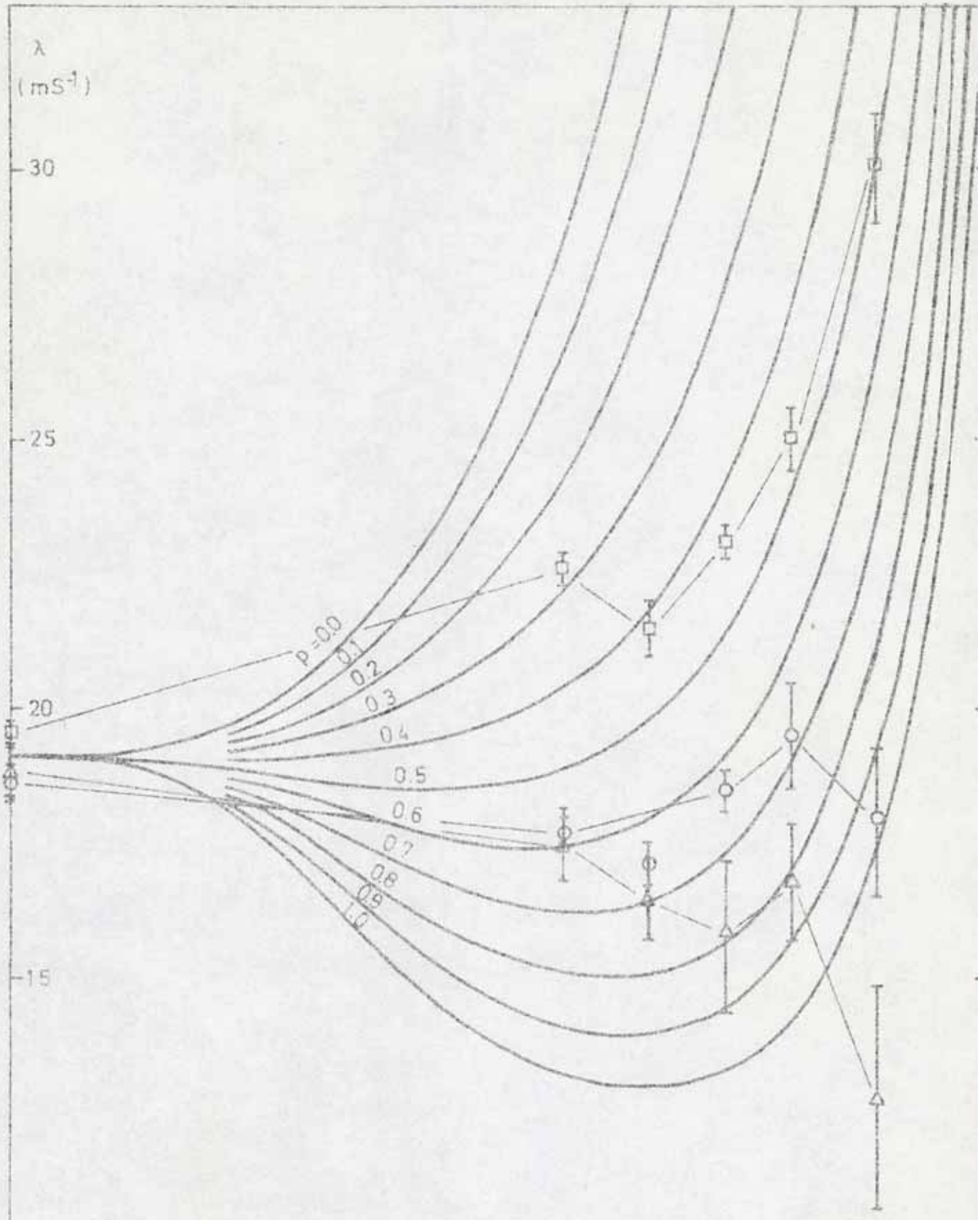

Fig. 7.10 The logarithmic decay rate. C series, Time interval 17-32 (squares), 33-48 (circles) and 49-64 (triangles).

8. DISCUSSION.

Summing the experiences from these measurements we can describe the decay process in a moderator with a closed cavity by the following items.

1. The thermalization period. The neutrons seem to behave almost as in a homogeneous moderator. However, our time intervals are too long to give detailed information on this process.

2. The filling period. The neutrons diffuse into the cavity, and the neutron distribution in the moderator decreases almost as if the cavity was an absorber.

3. The reentrant period. The first thermal neutrons have crossed the cavity and give a positive contribution to the neutron population in the moderator. The result may be a peak in the time dependent distribution.

4. The oscillation period. The process in item 2 and 3 is repeated. A damped oscillation may result. The oscillation seems in this experiment to be aperiodic at the 90 degree position of the detector but two periods can be observed at the 180 degree position. It should be pointed out that the detector only senses the outward flux from the moderator. The situation in the interior may be different.

5. The pre-"asymptotic" period. The decay constant varies slowly with time to an asymptotic value. This may be described as an aperiodic oscillation but it has a longer period than that of the oscillation period.

6. The " asymptotic" period. This is the period where the picture of pseudomodes (in analogy to the fundamental decay constant of a homogeneous moderator) may give a constant logarithmic decay rate. Evidently there are some long range oscillations also during this period. These oscillations depend very strongly on the radius of the cavity.

7. The post-"asymptotic" period. During this period the logarithmic decay is expected to decrease slowly to zero. Dance (4) asserts that he has found such a period in the case of open heterogeneous systems. We have looked for a corresponding effect here, but we can not get clear evidences for it. The problem is that this period is very sensitive to the background subtraction, and a too low amplitude on the background gives al-

ways a tendency towards low values on the logarithmic decay. As we do not have the possibility to separate the two effects unambiguously in this experiment the question about the existence of this period must be left open.

The different periods overlap in the experiment. The most interesting question is the existence of pseudomodes. We can directly from the figures conclude that they are not so well defined as in the case of a homogeneous moderator. The question of existence is then a matter of definition. The figures indicate a rather good stability in the A series, but it is not so good in the B series and bad at least for large cavities in the C series.

The comparison between the one-group model and the A and B series indicates a value on the parameter p of about 0.6. Accepting equation 3.5 we conclude that the assumed mean cord length is too high or the velocity is too low. The first of these alternatives is not probable. Regarding the second a velocity increase occurs at the boundary of a pulsed water moderator (16) but it can not explain the whole deviation unless it is amplified in the case of these interacting surfaces. Another explanation might be that we have not reached the asymptotic period, but in that case the logarithmic decay rate approaches the pseudomode so slowly that it is experimentally very difficult to measure.

9. CONCLUSIONS.

The conclusion from this work is that a closed cavity in a moderator creates a delay effect that depends on the decay rate of the system. The appearing logarithmic decay rate is drifting in time and reliable pseudo-modes can not be found for large values on the inner radius.

The decay rate for a given time varies with the inner radius in a way that can not be described by a simple theory. The irregularities are small but systematic and indicate a resonance effect or that the point spectrum of the decay constants is different for different values on the inner radius.

The experiment indicates that measurements in heterogeneous systems with the pulsed neutron method should not be interpreted from static diffusion theory, but that dynamic effects must be considered.

ACKNOWLEDGEMENTS.

The author is grateful to professor N.G. Sjöstrand and the members of his departmentfor help and valuable discussions during this work, Gunnar Rönnberg made the computer programs, Kent Mandorff operated the accelerator, Lennart Carlson drew the figures and Christina Varenius typed the report. The work has been supported by the Swedish Atomic Research Council.

REFERENCES.

1. N.G. Sjöstrand, On the theory underlying diffusion measurements with pulsed neutron sources. Arkiv för fysik 15,147 (1959).

2. N.G. Sjöstrand, J. Mednis and T. Nilsson, Geometric buckling measurements using the pulsed neutron source method. Arkiv för fysik 15,471 (1959).

3. S.R. Bull, A pulsed-source investigation of the effect of cylindrical void channels in a neutron diffusing medium. Thesis, Stanford Univ. (1967).

4. K. Dance, A pulsed-source investigation of the effect of tranverse gaps on neutron transport in a diffusing medium. Thesis, Stanford Univ. (1968).

5. V. Deniz, J.G. LeHo and M. Sagot, Study of lattices of graphite with empty channels by means of the pulsed source technique. Nucl. Sci. Eng. 32,201 (1968).

6. G. Grosshög, The pulsed neutron method applied to the interaction between two moderators. CTH-RF-17 (1969).

7. G. Grosshög, Measurement of the neutronic interaction between two cylindrical moderators. CTH-RF-18 (1969).

8. J. Elkert, Determination of the diffusion parameters for thermal neutrons in water using the pulsed method and spherical geometries. CTH-RF-12 (1967).

9. J. Elkert, Determination of the diffusion parameters for thermal neutrons in water using the pulsed method and spherical geometries. Nukleonik 11, 159 (1968).

10. E. Arai und M. Küchle, Messung der Diffusionslänge in zeitlich abklingenden Neutronfeldern. Nukleonik 7,416 (1965).

11. K. Case and P.F. Zweifel, Linear transport theory. Addison-Wesley 1967. (pp. 21 - 24).

12. K. Case, F. de Hoffman and G. Placzek, Introduction to the theory of neutron diffusion, Los Alamos Scientific Laboratory 1953. (p. 21).

13. G. Grosshög, A system for simultaneous measurement of the amplitude and time distribution for pulses from up to four detectors. CTH-RF-10 (1967).

14. G. Grosshög, Determination of neutron decay constants using simultaneous pulse height and time analysis. CTH-RF-16 (1968).

15. G.Grosshög, Deadtime corrections in a two parameter system containing four detectors. Proc. of Ispra Nuclear Electronics Symposium, Ispra (1969) p. 237.

16. J. Wood and M.M.R. Williams, The validity of the buckling concept and the importance of spatial transients in the pulsed neutron experiment. J.Nucl. Eng. 21,113 (1967).